DOKUZ EYLÜL UNIVERSITY
GRADUATE SCHOOL OF NATURAL AND APPLIED SCIENCES

PRODUCTION OF HYDROXYAPATITE COATING BY SOL-GEL TECHNIQUE ON 316L STAINLESS STEEL AND ITS CORROSION PROPERTIES

by
N. Funda AK AZEM

September, 2008
İZMİR

PRODUCTION OF HYDROXYAPATITE COATING BY SOL-GEL TECHNIQUE ON 316L STAINLESS STEEL AND ITS CORROSION PROPERTIES

A Thesis Submitted to the
Graduate School of Natural and Applied Sciences of Dokuz Eylül University
In Partial Fulfillment of the Requirements for the Degree of Doctor of Philosophy in Metallurgical and Materials Engineering,
Metallurgical and Materials Engineering Program

by
N. Funda AK AZEM

September, 2008
İZMİR

Ph.D. THESIS EXAMINATION RESULT FORM

We have read the thesis entitled "**PRODUCTION OF HYDROXYAPATITE COATING BY SOL-GEL TECHNIQUE ON 316L STAINLESS STEEL AND ITS CORROSION PROPERTIES**" completed by **N. FUNDA AK AZEM** under supervision of **PROF. DR. AHMET ÇAKIR** and we certify that in our opinion it is fully adequate, in scope and in quality, as a thesis for the degree of Doctor of Philosophy.

Prof. Dr. Ahmet ÇAKIR

Supervisor

Prof. Dr. Tevfik AKSOY	Assoc. Prof. Dr. Hüseyin YILDIRAN
Thesis Committee Member	Thesis Committee Member
Prof. Dr. Mehmet ERBİL	Assist. Prof. Dr. Aylin ALBAYRAK
Examining Committee Member	Examining Committee Member

Prof.Dr. Cahit HELVACI

Director

Graduate School of Natural and Applied Sciences

ACKNOWLEDGMENTS

First of all, I would like to express my deep sense of gratitude to my advisor Prof. Dr. Ahmet Çakır for his constructive ideas, constant support and guidance throughout the course of this work. I would also like to thank my committee members, Prof. Dr. Tevfik Aksoy, Assoc. Prof. Dr. Hüseyin Yıldıran, for reviewing my work and offering valuable suggestions and sharing their visions about the content of my thesis.

I wish to extend my sincere thanks to Prof. Dr. Mehmet Erbil, Assoc. Prof. Dr. Tunç Tüken and Süleyman Yalçınkaya for helping me in starting the impedance experiments and sharing their knowledge of this field. Thanks also to Assist. Prof. Dr. Aylin Ziylan Albayrak for helpful discussions and assistance. I am especially indebted to Işıl Birlik for all of the assistance that she provided me in the times of need. In addition, I would like to thank Esra Dokumacı, Bahadır Uyulgan, Çağrı Tekmen, Süleyman Akpınar, Osman Çulha and Faruk Ebeoğlugil for their invaluable assistance and kind friendship. I am also grateful to Metin Gemici and Dalyan Özkan for their technical assistance and help. I would also like to express my genuine gratitude to each of people, although it would be impossible for me to name all.

I gratefully acknowledge the financial assistance provided by The Scientific and Technological Research Council of Turkey (TUBITAK), under project number MISAG-259. Besides, I would like to thank to Sandvik Company for providing 316L stainless steel substrate materials.

A special thank goes to my family for their concern, confidence and support. Finally, I extend my greatest thanks to my husband Zafer who encouraged and unconditionally supported me. No word can do justice to my appreciation for him.

N. Funda AK AZEM

PRODUCTION OF HYDROXYAPATITE COATING BY SOL-GEL TECHNIQUE ON 316L STAINLESS STEEL AND ITS CORROSION PROPERTIES

ABSTRACT

Hydroxyapatite (HAP) coatings which are widely used for orthopedic and dental prosthesis were produced on 316L stainless steel substrates via sol-gel technique by using sol solution containing $Ca(NO_3)_2.4H_2O$ and $C_6H_{15}O_3P$ as calcium and phosphorus precursors, respectively. In the study, surface modifications processes named as alkali and acid treatment, and formation of CaP seed by the electrodeposition technique were applied to the substrate so as to establish and induce a bioactive HAP layer on the surface of substrates. Effect of aging time and pH of the sol solution on the properties of sol-gel coating were investigated and successfully optimized for HAP phase formation. Besides, effect of chemical additives to the sol solution on the coating morphology and phase structure was studied. Results revealed that surface modification via electrodeposition route has improved the coating quality and provided coating with a porous and crack free structure derived from the sol solution with pH adjusted to 2.25 and subjected to aging process for 24h. It was also observed that silica addition into the sol solution has provided affirmative effect on the coating quality. Corrosion efficiencies of the coatings produced were determined in the physiological saline solution (0.9 percent NaCl) by means of polarization and electrochemical impedance spectroscopy studies. Obtained HAP coatings were found to show better corrosion performance compared to the uncoated 316L stainless steel substrate. It was concluded that there was an inverse relation between corrosion performance of the coating and porosity, that is the lower corrosion performance of the coating corresponds to increasing porosity.

Keywords: hydroxyapatite coating, sol-gel technique, 316L stainless steel, corrosion

SOL-JEL YÖNTEMİYLE 316L PASLANMAZ ÇELİK ÜZERİNE HİDROKSİAPATİT KAPLAMANIN ÜRETİLMESİ VE KOROZYON ÖZELLİKLERİ

ÖZ

Ortopedik ve diş protezlerinde geniş bir kullanım alanına sahip olan hidroksiapatit (HAP) kaplamalar, sol-jel tekniği yardımıyla, kalsiyum ve fosfor başlangıç kimyasalı olarak sırasıyla $Ca(NO_3)_2.4H_2O$ ve $C_6H_{15}O_3P$ sol çözeltileri kullanılarak 316L paslanmaz çelik altlıklar üzerinde üretilmiştir. Çalışmada, altlık yüzeyine biyoaktif HAP tabakasının oluşumunu teşvik etmek için alkali ve asit işlemi ve electroçöktürme yöntemi ile CaP esaslı çekirdeklerle yüzeyin aşılanması olarak isimlendirilen yüzey işlemleri uygulanmıştır. Hazırlanan sol çözeltisinin yaşlanma zamanı ve pH etkisinin sol-jel kaplamaları özelliklerine etkisi incelenmiş ve HAP fazı üretimi için başarıyla optimize edilmiştir. Ayrıca, sol çözeltisine yapılan kimyasal katkıların kaplama faz yapısına ve morfolojisine etkisi incelenmiştir. Sonuçlar, elektroçöktürme yöntemi ile gerçekleştirilen yüzey modifikasyonunun kaplama kalitesini iyileştirdiğini çatlaksız ve gözenekli yapıya sahip kaplamanın, pH'ı 2,25 olarak ayarlanmış ve 24h yaşlandırma işlemine tabi tutulmuş sol çözeltisi kullanılarak elde edildiğini göstermiştir. Ayrıca, sol çözeltisine silika katkısı uygulamasının da kaplama kalitesinde olumlu bir etki gösterdiği görülmüştür. Üretilen kaplamaların etkinliği, yüzde 0,9 NaCl içeren fizyolojik tuzlu çözelti içerisinde polarizasyon ve elektrokimyasal empedans spektroskopisi çalışmaları ile belirlenmiştir. Elde edilen HAP kaplamaların, kaplanmamış 316L paslanmaz çelik altlığa göre daha iyi korozyon performansı gösterdiği bulunmuştur. Gözenekli yapıdaki kaplamanın düşük korozyon performansı göstermesinden kaplamanın korozyon performansı ile gözeneklilik arasında ters ilişki olduğu sonucuna varılmıştır.

Anahtar kelimeler: hidroksiapatit kaplama, sol-jel yöntemi, 316L paslanmaz çelik, korozyon

CONTENTS

Page

CHAPTER ONE

INTRODUCTION

Joint replacements with metallic prosthesis are very successful, reproducible procedure and excellent treatment to eliminate pain and restore in a diseased or fractured hip joint for both the short-term and long-term period. Cemented hip arthroplasty has been very successful in the short-term and intermediate-term results. However, there are significant problems with failure after long-term use, especially in younger, active patients due to aseptic loosening. For this reason, major issue of prosthesis design is the fixation between the implants (commonly metals) and their surrounding bones (Chang, Chen, Huang, & Wang, 2006; Goyenvalle, Aguado, Nguyen, Passuti, Guehennec, & Layrolle, 2006). Uncemented prostheses emerged as a new technology to biologically fix implants to bones without the use of cement. Recent clinical results show that uncemented prostheses reduce aseptic loosening rate and thigh pain in hip replacement. Usage of the uncemented prostheses allows bone ingrowth into the surrounding prostheses (Leea, Kim, & Kim, 2000; Mont & Hungerford, 1997). Research focuses on improving the strength of the implant-tissue interface. Thus, to improve bone ingrowth of uncemented prostheses the application of calcium phosphate (CaP) as coatings was performed.

The osteoconductive behaviour of CaP has been known for about 80 years. The benefits of CaP as a healing material can be summarized as follows: (a) lack of formation of fibrous tissue at the interface with the living bone, (b) formation of a strong binding (calcified tissue) between the implant and the bone tissue and (c) quick growth of the bone tissue reducing convalescence period (Piveteau, Gasser, & Schlapbach, 2000). Hard skeletal tissue is a complex composite consisting of cells embedded within mineralized organic matrix. Bone mineral is a CaP based compound with a structural similarity to hydroxyapatite (HAP). It has been well known that HAP is bioactive and biocompatible with human hard tissues (Jarcho, 1981; Geesink, 1990). Unfortunately, the mechanical strength of hydroxyapatite is fairly poor and not be used as implants in load bearing applications. Therefore,

load-bearing implants have been coated with HAP. For medical applications, bioactive hydroxyapatite films are of great importance due to the bioactive film coated metallic implants (titanium, cobalt and stainless steel alloys) can combine the mechanical advantages of the metal with biological affinity of apatite to natural tissue, consequently healing time can be shortened (Balamurugan, Balossier, Kannan, & Rajeswari, 2006; Weng et al., 2003). Type 316L stainless steel (316L SS) is widely used material for implant fabrication in orthopaedic applications due to reasonable corrosion resistance, its easy fabrication and inherent mechanical properties among metallic implants (Kannan, Balamurugan, & Rajeswari, 2002). Moreover, the need to reduce costs in public health services has compelled the use of stainless steel as the most economical alternative for implants.

Since Furlong and Osborn (1991) first began clinical trials using the HAP coated implants in 1985, it has been reported that HAP coatings can successfully enhance clinical success, and a less than 2% failure rate was reported during a mean follow-up study of 10 years (Geesink, 2002; Geesink, & Hoefnagels, 1995; Manally, Shepperd, Mann, & Walczak, 2000). Recently, many methods have been used to produce HAP coating on implant surfaces. The sol-gel process provides an attractive alternative because of the homogeneity due to atomic level mixing, easy formation of crystalline films at relatively low temperature, offering the possibility to tailor microstructures, its convenience for complex shape coatings and technical simplicity. In the sol-gel synthesis of HAP, alkoxides or metal salts are frequently used as either calcium or phosphorus precursors (Cameron, Chai, Gross, & Ben-Nissan, 1998; Liu, Yang, & Troczynski, 2002).

Morphology, solubility and adhesion of the hydroxyapatite coating synthesized by using sol-gel technique depend on the many factors. In this context, sol-gel method provides some benefits for the coating parameters that can be tailored easily by the sol preparation period and/or heat treatment process. Therefore, the surface morphology of the films can be controlled by sol-gel processing parameters such as different precursors, heat-treatment and addition of chemical additives (Weng et al., 2003).

Studies show that usage of stoichiometric HAP has a limited ability to form an interface with, and to stimulate the growing of new bone tissue. Also, stoichiometric HAP does not degrade significantly but rather remains as a permanent fixture susceptible to long-term failure (Furlong, & Osborn, 1991). In contrast, the mineral found in bone is not stoichiometric compound, but exhibits variable deficiencies in Ca, P and OH. The mineral phase of bone is a multi-substituted HAP. The type and amount of ionic substitution in the apatite phase varies from 8wt% in carbonate to minor concentrations in Mg, Na and trace elements of Si, Sr, Zn and Pb with the ppm level (Lventouri, Bunaciu, & Perdikatsis, 2003). These substitutions in the apatite structure play important roles in biological activity of bone mineral and CaP based implant materials that incorporate element substitutions, by influencing the solubility, surface chemistry and morphology of the mineral. Silica in particular has been found to be essential for normal bone and cartilage growth and development (Klein, Pratka, Vander, Wolke, & DeGroot, 1991). Furthermore, there have been many attempts in the direction of developing materials and techniques to impart suitable biological and mechanical properties to synthetic composites to be used in the replacement of the bone. Thus, HAP is used in composite form (HAP-polymer) to retain useful bioactive properties as well as enhancement in mechanical properties (Mollazadeh, Javadpour, & Khavandi, 2007).

The goal of the study was to produce HAP coating on stainless steel substrates with properties of uniform, homogeneous and porous structure which are some of the general requirements for the bioactive HAP coatings, and to investigate the changes caused by various process parameters on morphology and phase structure of the CaP based coatings. In this context, this study could be essentially divided in two parts namely surface modification of the substrate and structural and morphological investigation of HAP coatings produced by sol-gel technique. Surface modification of 316L SS substrate prior to coating process was aimed to improve the coating's capability of the substrate by alkali treatment, acid treatment and formation of CaP seeds on the surface by electrodeposition technique. In the second part, effect of some parameters such as aging of the sol, its pH and additives in the sol solution on the structure and morphology of the coating was investigated. Coatings were

produced by using different sol solution with aging times up to 48h. In line with the aim of this study, silica and polymer (PVA) additives were also made to the sol solutions used. Additionally, morphological properties of the coatings were examined with respect to the applied heat treatment regime. Finally, corrosion performances of the obtained coatings with porous structure were investigated by anodic polarization and impedance technique and results were compared with the uncoated substrate.

The results demonstrated that production of the HAP coating with porous structure was achieved by using sol solution with pH of 2.25. Besides, formation of the CaP seeds by pulse electrodeposition technique on surface of the substrates favorable improved coating capability of substrate and final morphology of the film. Production of the HAP coatings on 316L SS by sol-gel technique result in improvement of corrosion properties compared to uncoated 316L SS.

CHAPTER TWO

BIOMATERIALS

2.1 Introduction

A biomaterial is any substance, other than a drug, or combination of substances, synthetic or natural in origin, which can be used for any period of time, as a whole or as a part of a system which treats, augments, or replaces any tissue, organ, or function of the body.

Biomaterials are widely used in repair, replacement, or augmentation of diseased or damaged parts of the musculoskeletal system such as bones, joints and teeth. A majority of the applications are summarized in Figure 2.1 (Hench, Interranate, Caspar, & Ellis, 1985). The fundamental requirement of a biomaterial is that the material and the tissue environment of the body should coexist without having any undesirable or inappropriate effect on each other. Biocompatibility, an essential requirement for any biomaterial, implies the ability of the material to perform effectively with an appropriate host response for the desired application. Common medical devices made of biomaterials include hip replacements, prosthetic heart valves and the less common neurological prostheses and implanted drug delivery systems. These devices when placed inside the body are termed implants when they are intended to remain there for a substantial period of time, and as prosthesis when they are permanently fixed in the body for long-term application till the end of lifetime (Recum, 1999).

Orthopedic implant devices are generally mounted on to the skeletal system of the human body for aiding healing, correcting deformities and restoring the lost functions of the original part. These are supporting bone plates, screws, total hip joints, knee joints, elbow joints, shoulder joints and reattachments for tendons or ligaments. The implants are exposed to the biochemical and dynamic environment of

the human body and their design is dictated by anatomy and restricted by physiological conditions.

In the past few decades, increase in the utilization of self-operating machines, participation of many persons in sports, defence activities, increased interest in motorcycles and bicycles, and day-to-day increasing traffic, has resulted in enormous increase in the number of accidents. This has necessarily led people to opt for orthopedic implants for early and speedy recovery and resumption of their routine activities (Kamachi, Sridhar, & Raj, 2003).

Because the ultimate goal of using biomaterials is to restore function of natural living tissues and organs in the body, it is essential to understand relationships among properties, functions, and structures of biological materials. Thus, three aspects of study on the subject of biomaterials can be envisioned: biological materials implant materials, and interaction between the two in the body. This is a very difficult task to master unless one possesses a fundamental knowledge of the whole system under study.

Survivability of an implant requires formation of a stable interface with the living host tissue. The mechanism of tissue attachment is directly related to the type of tissue response at the implant interface. No material implanted in living tissues is completely inert; all materials elicit a response from living tissue. The three types of response allow different means of achieving attachment of prostheses to the musculo-sketal system. These are bioinert, bioactive and bioresorbable.

Bioresorbable refers to a material that, upon placement within the human body, starts to dissolve and is slowly replaced by advancing tissue. Common examples of bioresorbable materials are tricalcium phosphate [$Ca_3(PO_4)_2$] and polylactic-polyglycolic acid copolymers. Calcium oxide, calcium carbonate (coral) and gypsum are other common materials that have been utilized during the last three decades.

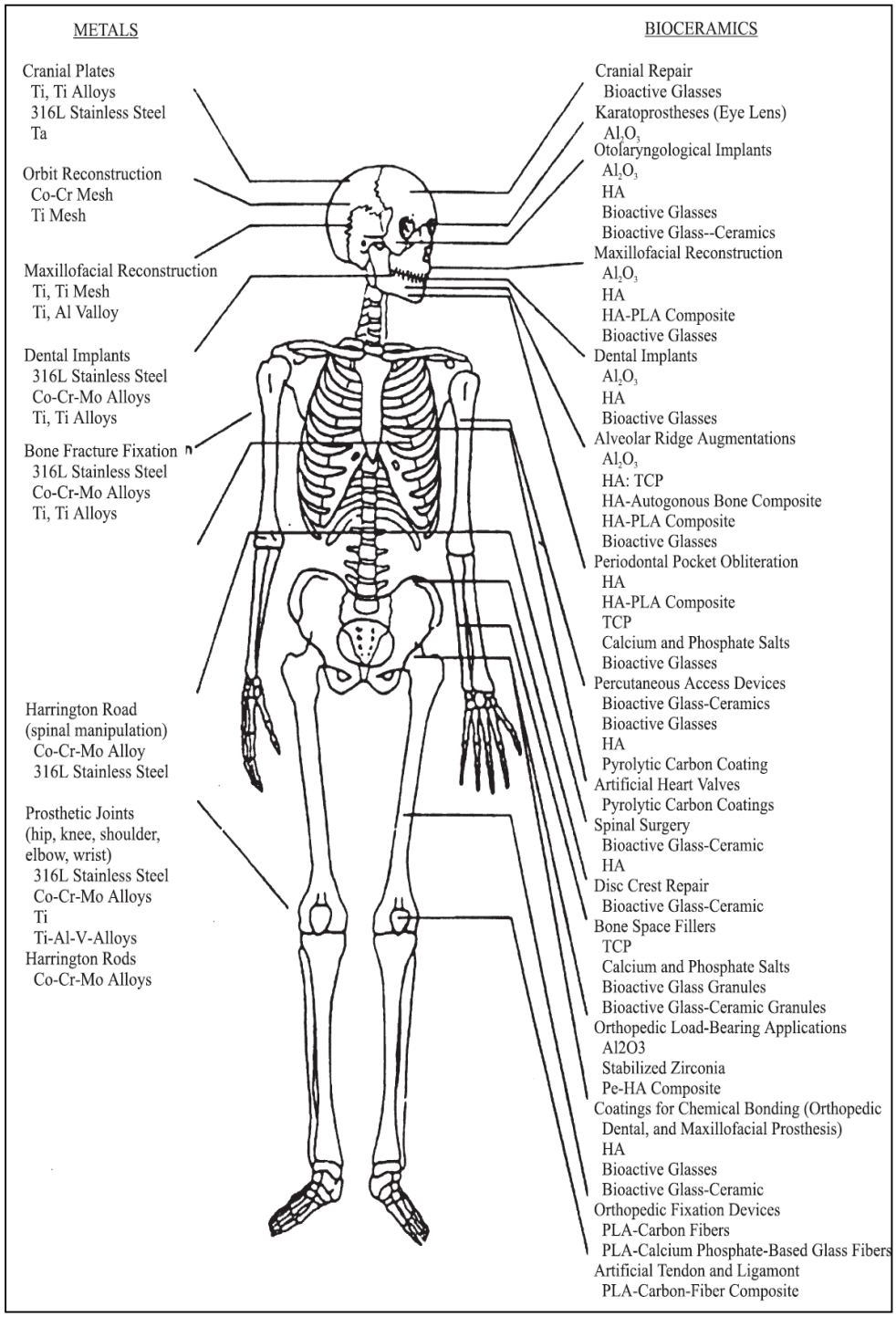

Figure 2.1 Clinical uses of inorganic biomaterials.

Bioactive refers to a material, which, upon being placed within the human body, interacts with the surrounding bone and, in some cases, even soft tissue. An ion exchange reaction between the bioactive implant and surrounding body fluids in some cases results in the formation of a biologically active carbonate apatite (CHA) layer on the implant that is chemically and crystallographically equivalent to the mineral phase of bone. Prime examples of these materials are synthetic hydroxyapatite ($Ca_{10}(PO_4)_6(OH)_2$), glass-ceramic and bioglass.

The term bioinert refers to any material that, once placed within the human body, has minimal interaction with its surrounding tissue. Generally, a fibrous capsule might form around bioinert implants; hence its biofunctionality relies on tissue integration through the implant. Examples of these bioinert materials are stainless steel, titanium, cobalt-chromium molybdenum alloy (Zimmer alloy), alumina, partially stabilized zirconia, new generation zirconia and allumina alloys and ultrahigh molecular weight polyethylene (Nissan, 2005). The list in Table 2.1 illustrates some of the advantages and disadvantages for three main groups of synthetic (man-made) materials used for implantation (Park, 1984).

Table 2.1 General comparison of materials for implants.

Material Class	**Advantages**	**Disadvantages**
Metals	Strong Wear resistant Tough Easy to fabricate	Corrode in a physiological environment High E High density Not usually bioactive Not resorbable
Polymers	Resilient Tough Easy to fabricate Low density	Weak Low E Not usually bioactive Nor resorbable
Ceramics	Biocompatible Wear resistant Lightweight composite	Low tensile strength Difficult to fabricate Low toughness Not resilient

2.2 Metallic Biomaterials

Metals are used as biomaterials due to their excellent electrical and thermal conductivity and mechanical properties. Since some electrons are independent in metals, they can quickly transfer an electric charge and thermal energy. The mobile free electrons act as the binding force to hold the positive metal ions together. This attraction is strong, as evidenced by the closely packed atomic arrangement resulting in high specific gravity and high melting points of most metals. Since the metallic bond is essentially no directional, the position of the metal ions can be altered without destroying the crystal structure resulting in a plastically deformable solid. Some metals are used as passive substitutes for hard tissue replacement such as total hip and knee joints, for fracture healing aids as bone plates and screws, spinal fixation devices, and dental implants because of their excellent mechanical properties and corrosion resistance. Some metallic alloys are used for more active roles in devices such as vascular stents, catheter guide wires, orthodontic arch wires, and cochlea implants.

The first metal alloy developed specifically for human use was the vanadium steel which was used to manufacture bone fracture plates (Sherman plates) and screws. Most metals such as iron (Fe), chromium (Cr), cobalt (Co), nickel (Ni), titanium (Ti), tantalum (Ta), niobium (Nb), molybdenum (Mo), and tungsten (W) that were used to make alloys for manufacturing implants can only be tolerated by the body in minute amounts. Sometimes those metallic elements, in naturally occurring forms, are essential in red blood cell functions (Fe) or synthesis of a vitamin B12 (Co), but cannot be tolerated in large amounts in the body (Black, 1992). The biocompatibility of the metallic implant is of considerable concern because these implants can corrode in an *in vivo* environment (Williams, 1994). The consequences of corrosion are the disintegration of the implant material per se, which will weaken the implant, and the harmful effect of corrosion products on the surrounding tissues and organs.

2.2.1 Stainless Steel

The first stainless steel utilized for implant fabrication was the 18-8 (type 302, AISI classification), which is stronger and more resistant to corrosion than the vanadium steel. Vanadium steel is no longer used in implants since its corrosion resistance is inadequate *in vivo*. Later 18-8Mo stainless steel was introduced which contains a small percentage of molybdenum to improve the corrosion resistance in chloride solution (salt water). This alloy became known as type 316 stainless steel. In the 1950s the carbon content of 316 stainless steel was reduced from 0.08 to a maximum amount of 0.03% (all are weight percent unless specified) for better corrosion resistance to chloride solution and to minimize the sensitization, and hence became known as type 316L stainless steel. The minimum effective concentration of chromium is 11% to impart corrosion resistance in stainless steels. The chromium is a reactive element, but it and its alloys can be passivated by 30% nitric acid to give excellent corrosion resistance.

The austenitic stainless steels, especially types 316 and 316L, are most widely used for implant fabrication. These cannot be hardened by heat treatment but can be hardened by cold-working. This group of stainless steels is nonmagnetic and possesses better corrosion resistance than any others. The inclusion of molybdenum enhances resistance to pitting corrosion in salt water. The American Society for Testing and Materials (ASTM) recommends type 316L rather than 316 for implant fabrication. According to the ASTM F139-86, specifications for 316L stainless steel are given in Table 2.2. The only difference in composition between the 316L and 316 stainless steel is the maximum content of carbon, i.e., 0.03% and 0.08%, respectively, as noted earlier. The nickel stabilizes the austenitic phase [γ, face centered cubic crystal (fcc) structure], at room temperature and enhances corrosion resistance.

Today, stainless steel is one of the most frequently used biomaterials for internal fixation devices because of a favorable combination of mechanical properties, corrosion resistance and cost effectiveness when compared to other metallic implants

(Disegi, & Eschbach, 2000). Even the 316L stainless steels may corrode inside the body under certain circumstances in a highly stressed and oxygen depleted region, such as the contacts under the screws of the bone fracture plate. Thus, these stainless steels are suit for use only in temporary implant devices such as fracture plates, screws, and hip nails. Surface modification methods such as anodization, passivation, and glow-discharge nitrogen implantation are widely used in order to improve corrosion resistance, wear resistance, and fatigue strength of 316L stainless steel (Bordiji, 1996; Wong, & Bronzino, 2007).

Table 2.2 Composition of 316L Stainless Steel

Element	Composition (%)
Carbon	0.03 max
Manganese	2.00 max
Phosphorous	0.03 max
Sulfur	0.03 max
Silicon	0.75 max
Chromium	17.00-20.00
Nickel	12.00-14.00
Molybdenum	2.00-4.00

2.2.2 Cobalt-based Alloys

By the early 1930s, a cobalt-chromium alloy called Vitallium was introduced to dentistry as an alternative to gold alloys. Cobalt-chromium alloy soon found application in orthopaedic surgery for fabrication of hip prostheses and internal fixation plates and has become one of the three major biomedical metallic materials (Merchant, & Wang, 1994).

There are basically two types of cobalt-chromium alloys: (1) the castable CoCrMo alloy and (2) the CoNiCrMo alloy which is usually wrought by (hot) forging. The castable CoCrMo alloy has been used for many decades in dentistry and, relatively recently, in making artificial joints. The wrought CoNiCrMo alloy is relatively new, now used for making the stems of prostheses for heavily loaded joints such as the

knee and hip. The two basic elements of the CoCr alloys form a solid solution of up to 65% Co. The molybdenum is added to produce finer grains which results in higher strengths after casting or forging. The chromium enhances corrosion resistance as well as solid solution strengthening of the alloy.

The CoNiCrMo alloy originally called MP35N (Standard Pressed Steel Co.) contains approximately 35% Co and Ni each. The alloy is highly corrosion resistant to seawater (containing chloride ions) under stress. Cold working can increase the strength of the alloy considerably but there is a considerable difficulty of cold working on this alloy, especially when making large devices such as hip joint stems. Only hot-forging can be used to fabricate a large implant with the alloy. The superior fatigue and ultimate tensile strength of the wrought CoNiCrMo alloy make it suitable for the applications which require long service life without fracture or stress fatigue. Such is the case for the stems of the hip joint prostheses.

2.2.3 Titanium-based Alloys

Attempts to use titanium for implant fabrication dates to the late 1930s. It was found that titanium was tolerated in cat femurs, as was stainless steel and Vitallium (CoCrMo alloy). Titanium's lightness (4.5 g/cm^3 see Table 2.3) and good mechanochemical properties are salient features for implant application (Dowson, 1992).

Titanium and some titanium-based alloys seem to have been well established for heavy load-bearing skeletal implants, such as artificial tooth roots or joint endoprostheses. Stainless steel or cobalt-based alloys for implants exhibit corrosion pitting when subjected to cyclic loading and thus are unsatisfactory corrosion fatigue properties. The corrosion products are correlated to biocompatibility problems. Titanium is known for its high corrosion resistant due to instant formation of an inert oxide surface layer. This is given titanium a reputation of being a biocompatible implant material. However, the low wear resistance and poor tribological properties of titanium and its alloys have resulted in the release of significant amounts of metal

into the adjacent tissues. This can induce immunological responses and influence negatively the long-term biocompatibility of titanium implants (Papakyriacou, Mayer, Pypen, Plenk, & Stanzl-Tschegg, 2000).

Table 2.3 Physical and mechanical properties of implant metals and alloys used in orthopedic surgery applications

Materials			316 SS (wrought)	Co-Cr-Mo alloy (cast)	Titanium (wrought)	Ti-Al-V alloy (wrought)
Physical and Mechanical properties	Density (g/cm^3)		7.90	7.80	4.50	4.40
	Young's modulus (GPa)		200	200	127	111
	Tensile strength (MPa)		465	665	575	900
	0.2% proof stress (MPa)		170	455	465	830
	Fracture strain, %		40	10	15	8
	Fatigue stress (MPa), 10^8 cycles	Air	241	290	250	380
		Saline	103	140	120	140

2.3 Polymeric Biomaterials

Polymers are long-chain molecules that consist of a number of small repeating units. The repeat units or "mers" differ from the small molecules which were used in the original synthesis procedures, the monomers, in the loss of instauration or the elimination of a small molecule such as water or HCl during polymerization. The exact difference between the monomer and the mer unit depends on the mode of polymerization.

The wide variety of polymers includes such natural materials as cellulose, starches, natural rubber and deoxyribonucleic acid (DNA), the genetic material of all living creatures. While these polymers are undoubtedly interesting and have seen widespread use in numerous applications, they are sometimes eclipsed by seeming endless variety of synthetic polymers that are available today.

Synthetic polymeric materials have been widely used in medical disposable supplies, prosthetic materials, dental materials, implants, dressings, extracorporeal

devices, encapsulants, polymeric drug delivery systems, tissue engineered products, and orthodoses like those of metal and ceramics substituents. The main advantages of the polymeric biomaterials compared to metal or ceramic materials are ease of manufacturability to produce various shapes (latex, film, sheet, fibers, etc.), ease of secondary processability, reasonable cost, and availability with desired mechanical and physical properties. The required properties of polymeric biomaterials are similar to other biomaterials, that is, biocompatibility, sterilizability, adequate mechanical and physical properties, and manufacturability as given in Table 2.4 (Wong, & Bronzino, 2007).

Table 2.4 Requirements for biomedical polymers

Property	Description
Biocompatibility	Noncarcinogenesisi, nonpyrogenicity, nontoxicity, and nonallergic response
Sterilizability	Autoclave, dry heating, ethylenoxide, gas, and radiation
Physical property	Strength, elasticity, and durability
Manufacturability	Machining, molding, extruding and fiber forming

The task of the biomedical engineer is to select a biomaterial with properties that most closely match those required for a particular application. Because polymers are long-chain molecules, their properties tend to be more complex than their short-chain counterparts. Thus, in order to choose a polymer type for a particular application, the unusual properties of polymers must be understood. Many types of polymers are used for biomedical purposes. Polymeric biomaterials are classified in two groups as homoplymers and copolymers.

2.3.1 Homopolymers

Homopolymers are composed of single type of monomer. Poly(methyl methacrylate) (PMMA) is a hydrophobic, linear chain polymer that is glassy at room temperature and may be more easily recognized by such trade names as Lucite or Plexiglas (Ratner, 1996). PMMA is used broadly in medical applications

such as a blood pump and reservoir, membranes for blood dialyzer, and in in vitro diagnostics. It is also found in contact lenses and implantable ocular lenses due to excellent optical properties, dentures, and maxillofacial prostheses due to good physical and coloring properties, and bone cement for joint prostheses fixation (ASTM standard F451), (Wong, & Bronzino, 2007).

Polyethylene (PE) is used for its high-density in biomedical applications because low-density material cannot withstand sterilization temperatures. It is used in tubing for drains and catheters, and in very high-molecular-weight form as the acetabular component in artificial hips. The material has good toughness, resistance to fats and oils, and a relatively low cost.

Polypropylene (PP) is closely related to PE and has high rigidity, good chemical resistance, ad good tensile strength. Its stress cracking resistance is superior to that of PE, and it is used for many of the same applications as PE.

Poly(tetrafluorethylene) (PTFE), also known as Teflon, has the same structure as PE, except that the hydrogen in PE is replaced by fluorine, PTFE is a very stable polymer, both thermally and chemically, and as a result it is very difficult to process. It is very hydrophobic and has excellent lubricity. In micro-porous (Gore-Tex) form, it is used in vascular grafts.

Poly(vinyl chloride) (PVC) is used mainly in tubing in biomedical applications. Typical tubing uses include blood transfusion, feeding and dialysis. Pure PVC is a hard, brittle material, but with the addition of plasticizers, it can be made flexible and soft. PVC can pose problems for long-term applications because the plasticizers can be extracted by the body. While these plasticizers have low toxicities, their loss makes the PVC less flexible.

2.3.2 Copolymers

Copolymers are another important class of biomedical materials. Poly(glycolide lactide) (PGL) is a random copolymer used in resorbable surgical sutures. PGL polymerization occurs in a ring-opening reaction of glycolide and a lactate. The presence of ester linkages in the polymer backbone allows gradual resorbable suture material poly(glycolic acid), or catgut, a homopolymer, the PGL copolymer retains more of its strength over the first 14 days after implantation. A copolymer of tetraflourethylene and hexafluoropropylene (FEP) is used in many applications similar to those of PTFE. FEP has a crystalline melting point near 265°C compared with 327°C fro PTFE. This enhances the processability of FEP compared with PTFE while maintaining the excellent chemical inertness and low friction characteristic of PTFE. Polyurethanes are tough elastomers with good fatigue and blood-containing properties. They are used in pace maker lad insulation, vascular grafts, heart assist balloon pumps, and artificial heart bladders (Wong, & Bronzino, 2007).

2.3.3 Biodegradable Polymers

Since a degradable polymeric implant does not have to be removed surgically once it is no longer needed, degradable polymers are of value in short-term applications that require only the temporary presence of a polymeric implant. An additional advantage is that the use of degradable implants can circumvent some of the problems related to the long-term safety of permanently implanted devices. Some typical short-term applications are listed in Table 2.5.

From a practical perspective, it is convenient to distinguish among four main types of degradable implants: the temporary scaffold, the temporary barrier, the drug delivery device, and the multifunctional implant. The use of a temporary scaffold can be envisioned in those circumstances where the natural tissue bed has been weakened by disease, injury, or surgery and requires some artificial support. A healing wound, a broken bone, or a damaged blood vessel is examples of such situations. Sutures,

bone fixation devices (e.g., bone nails, screws, or plates), and vascular grafts would be examples of the corresponding support devices. The major medical application of a temporary barrier is in adhesion prevention. A temporary barrier could take from of a thin polymeric film or a mesh-like device that would be placed between adhesion-prone tissues at the time of surgery. Artificial skin for the treatment of burns and other skin lesions is another widely investigated application for temporary barrier-type devices. Implantable drug delivery devices are by necessity temporary devices, the development of implantable drug delivery systems is probably the most widely investigated application of degradable polymers.

Table 2.5 Some "short-term" medical applications of degradable polymeric biomaterials

Application	Comments
Sutures	The earliest, successful application of synthetic degradable polymers in human medicine
Drug delivery devices	One of the most widely investigated medical applications for degradable polymers
Orthopedic fixation devices	Requires polymers of exceptionally high membranes/films
Adhesion prevention	Requires polymers that can form soft membranes or films
Temporary vascular grafts and stents	Only investigational devices are presently avaliabale. Blood compatibility is a major concern

Over the past few years, there has been a trend toward increasingly sophisticated applications for degradable biomaterials. Usually these applications envision the combination of several functions within the same device (hence the name "multifunctional devices") and require the design of custom made materials with a narrow range of biodegradable bone nails and bone screws made of ultrahigh-strength poly(lactic acid) opens the possibility of combining the mechanical support function with a site-specific drug delivery function: A biodegradable bone nail that holds the fractured bone in place can simultaneously stimulate the growth of new bone tissue at the fracture site by slowly releasing bone

growth factors (e.g., bone morphogenic protein or transforming factor-β) throughout its degradation process.

2.4 Ceramic Biomaterials

Ceramics in the form of pottery have been used by humans for thousands of years. Until recently, their use was somewhat limited because of their inherent brittleness, susceptibility to notches or microcracks, low tensile strength, and low impact strength. However, within the last 100 years, innovative techniques for fabricating ceramics have led to their use as "high tech" materials. In recent years, humans have realized that ceramics and their composites can also be used to augment or replace various parts of the body, particularly bone. Thus, the ceramics used for the latter purposes are classified as bioceramics. Their relative inertness to the body fluids, high compressive strength, and aesthetically pleasing appearance led to the use of ceramics in dentistry as dental crowns. Bioceramics are used as implants to repair parts of the body, usually the hard tissues of the musculo-skeletal system, such as bones, joints, or teeth, although use of carbon coatings for replacement of heart valves also is included. Clinical success requires the simultaneous achievement of a stable interface with connective tissue and a match of the mechanical behavior of the implant with the tissue to be replaced (Hench, 1998).

Survivability of a bioceramic requires formation of a stable interface with living host tissue. Desired properties of implantable bioceramic are listed as follows:

- Should be nontoxic
- Should be noncarcinogenic
- Should be nonallergic
- Should be noninflammatory
- Should be biocompatible
- Should be biofunctional for its lifetime in the host.

Figure 2.2 shows a number of clinical uses of bioceramics (Hench, 1991). The uses go from head to toe and include repairs to bones, joints, and teeth. These repairs become necessary when the existing part becomes diseased, damaged, or just simply wears out. There are many other applications of bioceramics including pyrolytic carbon coatings for heart valves and special radioactive glass formulations for the treatment of certain tumors (Carter, & Norton, 2007). Classification of the bioceramics is given in Table 2.6 (Hench, 1998).

Table 2.6 Types of bioceramic tissue attachments

Types of attachment	**Types of bioceramic**
Dense, nonporous, almost inert ceramics attach by bone growth into surface irregularities by cementing the device into the tissue, or by press-fitting into a defect (morphological fixation)	Al_2O_3 ZrO_2
For porous implants, bone ingrowth occurs, which mechanically attaches the bone to the material (biological fixation)	Porous hydroxyapatite Hydroxyapatite-coated porous metals
Surface-reactive ceramics, glasses, and glass-ceramics attach directly by chemical bonding with the bone (bioactive fixation)	Bioactive glasses Bioactive glass-ceramics Dense hydroxyapatite
Resorbable ceramics and glasses in bulk or powder form designed to be slowly replaced by bone	Calcium sulfate (plaster of Paris) Tricalcium phosphate Calcium phosphate salts Bioactive glasses

2.4.1 Bioinert Ceramics

Relatively bioinert ceramics maintain their physical and mechanical properties while in the host. They resist corrosion and wear and have all the properties listed for bioceramics as described above. Examples of relatively bioinert ceramics are dense and porous aluminum oxides, zirconia ceramics, and single-phase calcium aluminates. Relatively bioinert ceramics are typically used as structural-support implants. Some of these are bone plates, bone screws, and femoral heads. Examples of nonstructural support uses are ventilation tubes, sterilization devices and drug

delivery devices (Carter, & Norton, 2007). Commercial bioinert bioceramics include alumina (Al_2O_3) and zirconia (Zr_2O_3) that are used for both dental and orthopedic applications (Wong, & Bronzino, 2007).

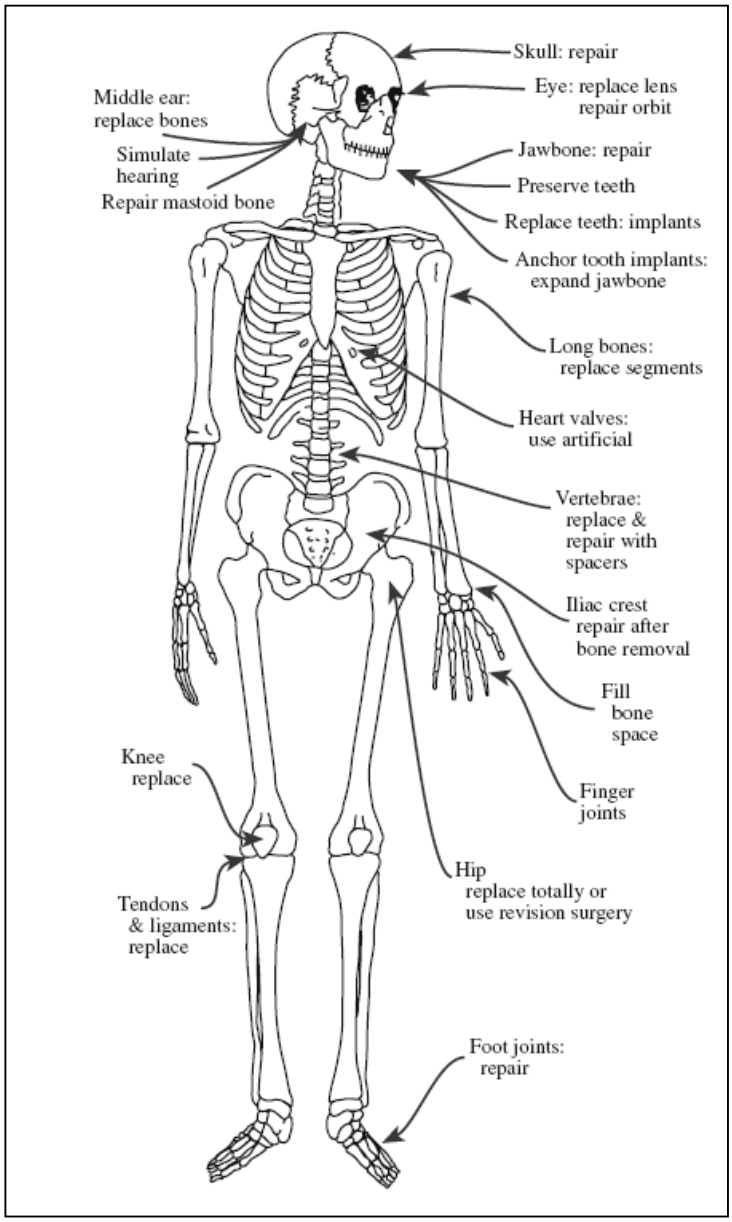

Figure 2.2 Illustration of the head-to-toe clinical uses for bioceramic.

2.4.1.1 Alumina (Al_2O_3)

The main source of high purity alumina (aluminum oxide, Al_2O_3) is bauxite and native corundum. The commonly available alumina (alpha, α) can be prepared by calcining alumina trihydrate. The ASTM specifies that alumina for implant use should contain 99.5% pure alumina and less than 0.1% combined SiO_2 and alkali oxides (mostly Na_2O) (F603-78). High-density high-purity α-alumina was the first bioceramic widely used clinically. The high hardness is accompanied by low friction and wear and inertness to the *in vivo* environment. These properties make alumina an ideal material for use in joint replacements (Park, & Lakes, 2007). It is used in total hip prostheses and dental implants because of its combination of excellent corrosion resistance, good biocompatibility, low friction, high strength (Hench, 1998). Low wear rates have lead to widespread use in Europe of alumina noncemented cups press-fitted into the acetabulum of the hip (Ratner, 1996).

Aluminum oxide hip prostheses with an ultra-high-molecular-weight polyethylene (UHMWPE) socket have been claimed to be a better device than a metal prosthesis with a UHMWPE socket. Alumina on load-bearing, wearing surfaces, such as in hip prostheses, must have a very high degree of sphericity, which is produced by grinding and polishing the two mating surfaces together. For example, the alumina ball and socket in a hip prosthesis are polished together and used as a pair. The long term coefficient of friction of an alumina-alumina joint decrases with time and approaches the value of a normal joint. This leads to wear on alumina-articulating surfaces being nearly 10 times lower than metal-polyethylene surfaces (Ratner, 1996).

2.4.1.2 Zirconia (ZrO_2)

Zirconia (ZrO_2) is also used as the articulating ball in total hip prostheses. The potential advantages of zirconia in load-bearing prostheses are its lower modulus of elasticity and higher strength (Ratner, 1996). High-density zirconia oxide showed excellent compatibility with autogenous rhesus monkey bone and was completely

nonreactive to the body environment for the duration of the 350-day study. Zirconia has shown excellent biocompatibility and good wear and friction when combined with ultra-high-molecular-weight polyethylene (Wong, & Bronzino, 2007).

2.4.2 Bioactive and Bioresorbable Ceramics

The first x-ray diffraction study of bone was initiated by De Jong in 1926, in which apatite (dahllite-carbonated apatite) was identified as the only recognizable mineral phase. He also reported marked broadening of the diffraction lines of bone apatite, which he attributed to small crystal size. It was not until the 1970s that synthetic hydroxyapatite [$Ca_{10}(PO_4)_2(OH)_2$] was accepted as a potential biomaterial that forms a strong chemical bond with bone *in vivo*, while remaining stable, under the harsh conditions encountered in the physiologic environment.

Currently used bioactive bioceramics are either of biologic or synthetic origin. Bioceramics of biologic origin include: natural coral, coral converted to hydroxyapatite, apatite from bovine bone or apatite derived from marine algae. Calcium phosphate (CaP) bioceramics include: calcium deficient apatite (CDA), hydroxyapatite (HAP), beta-tricalcium phosphate (β-TCP) and biphasic calcium phosphate (BCP)-an intimate mixture of HAP and β-TCP. Bioactive bioceramics are available as powders, granules, pellets and blocks (dense or porous), as cements (CPC), as composites (CaP/polymer) and as coatings on orthopedic and dental implants (Pietrzak, 2008).

2.4.2.1 Biologic Origin of Bioceramics

2.4.2.1.1 Natural Coral (Calcium Carbonate) and Coral-derived Hydroxyapatite. Both natural coral and converted coralline hydroxyapatite have been used as bone grafts and orbital implants since the 1980s, as the porous nature of the structure allows in-growth of blood vessels to supply blood for bone, which eventually infiltrates the implant. Coralline apatites can be derived from sea coral. Coral is composed of calcium carbonate in the form of aragonite as a naturally occurring

structure and has optimal strength and structural characteristics. The pore structure of coralline calcium phosphate produced by certain species is similar to human cancellous bone, making it a suitable material for bone graft applications (Figure 2.3).

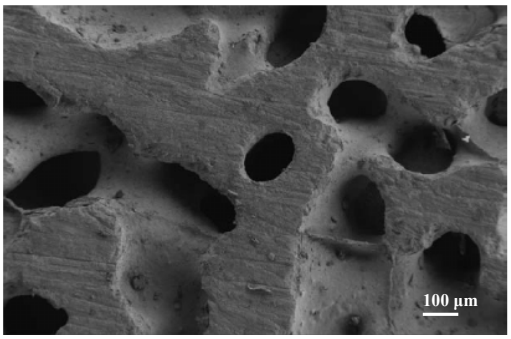

Figure 2.3 SEM of the coralline structure showing macro pores and interpore regions.

Bone pore sizes range from 200 to 400 µm in trabecular bone and 1 to 100 µm in normal cortical bone and the pores are interconnected. Porosity (macroporosity) is introduced in synthetic calcium phosphates (HAP, β-TCP, BCP) by the addition of volatile compounds (for example, naphthalene or hydrogen peroxide). The original macroporosity of the coral is retained after the hydrothermal conversion to coralline HAP. The macroporosity of bovine-bone derived apatite is preserved from the original macroporosity of the bone.

In synthetic and natural bone graft materials the pore size and their interconnectivity are of utmost importance when hard and soft tissue in-growth is required. Kühne et al. (1994) showed that implants with average pore sizes of around 260 µm had the most successful in-growth as compared to no implants (simply leaving the segment empty). It was further reported that the interaction of the primary osteons between the pores via the interconnections allows propagation of osteoblasts.

Roy, & Linnehan (1974) were the first to use the hydrothermal method for hydroxyapatite formation directly from corals. It was reported that complete

replacement of aragonite ($CaCO_3$) by phosphatic material was achieved at 260°C and 103 MPa by using the hydrothermal process. During the hydrothermal treatment, hydroxyapatite replaces the aragonite whilst preserving the porous structure. The following exchange takes place:

$$10CaCO_3 + 6(NH_4)_2HPO_4 + 2H_2O \rightarrow$$
$$Ca_{10}(PO_4)_6(OH)_2 + 6(NH_4)CO_3 + 4H_3CO_3 \quad (1)$$

The resulting material is known as coralline hydroxyapatite. Coral provides an excellent structure for the ingrowth of bone, and the main component, calcium carbonate, is gradually resorbed by the body. Both pure coral (Biocoral) and coral transformed to hydroxyapatite are currently used to repair traumatized bone, replace diseased bone, and correct various bone defects.

2.4.2.1.2 Bovine-derived Apatite. Bovine-derived materials are prepared by removing the organic phase and the bone mineral (carbonate apatite) is either unsintered (BioOss®, EdGeitslich, Switzerland) or sintered (Ostegraft®, Ceramed, Endobon®, Merck, Darmstad, Germany). The unsintered and sintered bone mineral differ in crystallinity reflecting crystal size (sintered>unsintered) and dissolution properties (unsintered>sintered). The sintering process causes the loss of carbonate and an increase in crystal size of the bone apatite. The loss in carbonate and increase in crystal size account for the lower solubility of the sintered bone mineral (e.g., Endobon®, Merck, Germany), compared to the unsintered one (e.g., BioOss®. EdGeitslich, Switzerland) (Pietrzak, 2008).

2.4.2.2 Synthetic Calcium Phosphates

Calcium phosphate has been used to make artificial bone. Recently, this material has been synthesized and used for manufacturing various forms of implant as well as for solid or porous coatings on other implants. Calcium phosphate can be crystallized into the salts mono-, di- tri-, and tetra-calcium phosphate, hydroxyapatite, and β-whitlockite, depending on the Ca/P ratio, presence of water, impurities, and

temperature (Park, & Lakes, 2007). The stability in solution generally increases with increasing Ca/P ratios. Hydoxyapatite is the most important among the calcium compounds since it is found in natural hard tissues as mineral phase. Hydroxyapatite acts as reinforcement in hard tissues and is responsible for the stiffness of bone, dentin, and enamel (Park, & Lakes, 2007). Synthetic bioactive calcium phosphate compounds with various calcium and phosphate ratios are given in Table 2.7 (Putlyaev, & Safronova, 2006; Regi, & Calbet, 2004).

The first successful medical application of calcium phosphate (ambiguously described as 'triple calcium phosphate') was reported by Albee & Morrison (1920). Albee used 'triple calcium phosphate,' presumably a chemical reagent. Nery, Lynch, Hirthe, & Mueller (1975) reported successful treatment of surgically created periodontal defects using a calcium phosphate he described as 'porous tricalcium phosphate, 'TCP'. X-ray diffraction analysis of this material by LeGeros (1988) revealed that Nery's 'TCP' was actually a mixture of 80HAP and 20β-TCP, prompting Nery to rename his material and others like it (i.e., mixtures of HAP and β-TCP) as biphasic calcium phosphate (BCP). Initial basic studies on BCP and focused studies on its potential applications led to the commercialization of BCP (Pietrzak, 2008).

Commercial calcium phosphate products currently available are: calcium deficient apatite (CDA); hydroxyapatite (HAP), $Ca_{10}(PO_4)_6(OH)_2$; β-tricalcium phosphate (β-TCP), $Ca_3(PO_4)_2$, and biphasic calcium phosphate (BCP), an intimate mixture of HAP and β-TCP, with various HAP/β-TCP weight ratios.

2.4.2.2.1 Calcium-deficient Apatite (CDA). Pure HAP has a Ca/P molar ratio of 1.67. Calcium deficient apatite, CDA, has a Ca/P molar ratio lower than 1.67 and may be represented by the formula: $(Ca,Na)_{10}(HPO_4)(PO_4)_5(OH)_2$. CDA is prepared by precipitation at neutral pH or by hydrolysis of calcium phosphate dihydrate (DCPD), $CaHPO_4{\cdot}2H_2O$ or dicalciumphosphate anhydrous (DCPA), $CaHPO_4$. CDA is much more soluble than either coralline HAP or ceramic HAP. Besides its limited

use in dentistry, it is used as one of the components of calcium phosphate cements (Pietrzak, 2008).

Table 2.7 Calcium phosphate compounds and calcium to phosphate ratios

Chemical Name	**Abbreviation**	**Chemical Formula**	**Ca/P ratio**
Amorphous calcium phosphate	ACP	-	-
Monocalcium phosphate (calcium dihydrophosphate)	MCP	$Ca(H_2PO_4)_2$	0.50
Tetracalcium dihydrogen phosphate	TDHP	$Ca_4H_2P_6O_{20}$	0.67
Heptacalcium phosphate	HCP	$Ca_7(P_5O_{16})_2$	0.70
Dicalcium phosphate dihydrate (brushite)	DCPD	$CaHPO_4 .2H_2O$	1.00
Dicalcium phosphate (calcium hydrophosphate, monetite)	DCP	$CaHPO_4$	1.00
Calcium pyrophosphate	CPP	$Ca_2P_2O_7$	1.00
Calcium pyrophosphate dihydrate	CPDD	$Ca_2P_2O_7.2H_2O$	1.00
Octacalcium phosphate	OCP	$Ca_8H_2(PO_4)_6. 5H_2O$	1.33
Pentacalcium hydroxyl apatite (Hydroxyapatite)	HAP	$Ca_{10}(PO_4)_6(OH)_2$	1.67
Tricalcium phosphate (calcium orthophosphate)	α-TCP	$Ca_3(PO_4)_2$	1.50
Tricalcium phosphate (calcium orthophosphate, whitlockite)	β-TCP	$Ca_3(PO_4)_2$	1.50
Tetracalcium phosphate (hilgenstockite)	TTCP	$Ca_4O(PO_4)_2$	2.00

2.4.2.2.2 Tricalcium Phosphate (TCP) Ceramics. A multicrystalline porous form of β-tricalcium phosphate [β-$Ca_3(PO_4)_2$] (β-TCP) has been used successfully to correct periodontal defects and augment bony contours. When β-tricalcium phosphate was injected into bone defects, Albee, & Morrison (1920) proposed the use of calcium phosphate ceramics for biomedical applications after observing accelerated bone growth. Pure β-tricalcium phosphate is more soluble in the physiological environment than other phosphate ceramics (bioresorbable). Consequently, it can be used in situations where accelerated bone growth is desirable. β-tricalcium phosphates have been used successfully, as fillers for bone defects to stimulate the formation of new bone (Nissan, 2005).

β-TCP is prepared by sintering precipitated calcium deficient apatite with a Ca/P molar ratio of about 1.5. It can also be prepared by solid state reaction between appropriate amounts of $CaHPO_4$ and $CaCO_3$ or CaO (Pietrzak, 2008).

This work also showed that after a 12-month period, β-tricalcium phosphate was totally absorbed. These materials are intended to be used in filling voids in bone structure that will dissolve over a period of time while the dissolution takes place, and the bone re-growth or advancement takes place at similar rates. In current commercial products (β-TCP) and HAP are mixed in predetermined proportions to induce a controlled dissolution rate.

It has also been stated that, as the pH decreases, other precursor phases such as dicalcium phosphate dehydrate (DCPD) may form. Therefore, it has been accepted that other calcium phosphate phases could actively participate in the crystallization reaction of biological (biogenic) apatites (Nissan, 2005).

2.4.2.2.3 Calcium Hydroxyapatite (HAP), Ceramic HAP. HAP was the first calcium phosphate product that became commercially available and was used in dentistry and medicine in dense and porous forms. Of all the calcium phosphate-based bioceramics, HAP is the least soluble (Pietrzak, 2008). Hydroxyapatite is the most important among the calcium compounds since it is found in natural hard tissues as mineral phase. Hydroxyapatite acts as reinforcement in hard tissues and is responsible for the stiffness of bone, dentin, and enamel (Park, & Lakes, 2007).

The mineral part of teeth and bones is made of an apatite of calcium and phosphorus similar to HAP ($Ca_{10}(PO_4)_6(OH)_2$) crystals. Natural bone is 70% HAP by weight and 50% HAP by volume. Synthetic, stoichiometric HAP has the formula $Ca_{10}(PO_4)_6(OH)_2$ and belongs to a broad group of calcium-containing minerals based around the phosphate (PO_4^{3-}) group and is characterized by a calcium/phosphorus (Ca/P) molar ratio of 1.67 and the calculated density is 3.219 g/cm^3.

The apatite family of mineral [$A_{10}(BO_4)_6X_2$; A=Ca, B=P and X=OH] crystallizes into hexagonal rhombic prisms and has unit cell dimensions a=9.432 Å and c=6.881 Å. The atomic structure of hydroxyapatite projected down the c-axis onto the basal plane is shown in Figure 2.4. Note that the hydroxyl ions lie on the corners of the projected basal plane and they occur at equidistant intervals [one-half of the cell (3.44 Å)] along the columns perpendicular to the basal plane and parallel to the c-axis. Six of the ten calcium ions in the unit cell are associated with the hydroxyls in these columns, resulting in strong interactions among them (Park, & Lakes, 2007).

One group of three Ca^{2+} ions describing a triangle, surrounding the OH group, is located at z=0.25 and the other set of three is located at z=0.75. The six phosphate $(PO_4)^{3-}$ tetrahedral are in a helical arrangement from levels z=0.25 to z=0.75. The network of $(PO_4)^{3-}$ groups provides the skeletal framework that gives the apatite structure its stability. (It is complicated but certainly crystalline and very natural (Feenstra, & Groot, 1983). Table 2.8 shows the chemical and physical data for HAP.

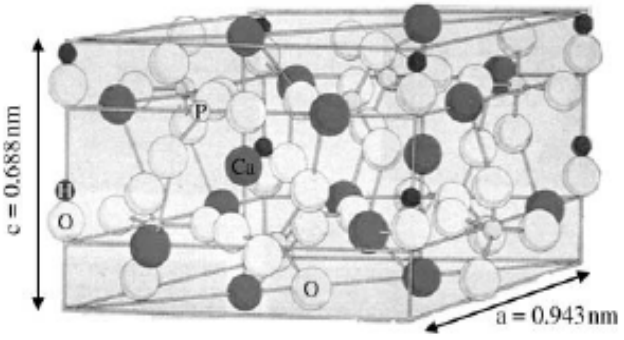

Figure 2.4 The structure of hydroxyapatite.

However, synthetic HAP differs in composition from bone mineral, as, in addition to calcium, phosphorus, oxygen, and hydrogen ions, bone mineral contains a number of ionic substitutions in its lattice and can also be non-stoichiometric with Ca/P≠1.67 (Porter, Patel, & Best, 2007). Substitutions in the HAP structure are possible. Substitutions for Ca, PO_4, and OH groups result in changes in the lattice parameter as well as changes in some of the properties of the crystal, such as solubility. Substituted apatites recommended for bone graft or bone substitute biomaterial or as coating on dental and orthopedic implants include: carbonate apatite

$Ca_{10}(PO_4)_6CO_3$ (CA); carbonate hydroxyapatite $(Ca,Na)_{10}(PO_4,CO_3)_6(OH)_2$ (CHA); Fluorapatite, $Ca_{10}(PO_4)_6(F,OH)_2$ (FA); strontium-substituted apatite, $(Ca,Sr)_{10}(PO_4)_6(OH)_2$. Substitutions in the apatite structure cause changes in its crystallographic, physical and chemical properties (Nissan, 2005). If the OH^- groups in HAP are replaced by F^-, the anions are closer to the neighboring Ca^{2+} ions. This substitution helps to further stabilize the structure and is proposed as one of the reasons that fluoridation helps reduce tooth decay as shown by the study of the incorporation of F into HAP and its effect on solubility (Park, & Lakes, 2007).

Table 2.8 Chemical and physical data for HAP

Property	
Lattice parameter (Å)	a= 9.432 c=6.8810
Bravais lattice	Hexagonal
Coefficient of thermal expansion (10^{-6} x W/m/K)	13.3
Solubility product K_{sp}	2.34×10^{-59}
Density (g/cm^3)	3.156
Thermal conductivity (W/m/K)	0.72

The wide variations in properties of polycrystalline calcium phosphates are due to the variations in the structure and manufacturing processes. Depending on the final firing conditions, the calcium phosphate can be calcium hydroxyapatite or β-whitlockite. In many instances, both types of structures exist in the same final product.

Polycrystalline hydroxyapatite has a high elastic modulus (40 to 117 GPa). Hard tissue such as bone, dentin, and dental enamel are natural composites which contain hydroxyapatite (or a similar mineral), as well as protein, other organic materials, and water. Enamel is the stiffest hard tissue, with an elastic modulus of 74 GPa, and contains the most mineral. Dentin (E = 21 GPa) and compact bone (E = 12 to 18 GPa) contain comparatively less mineral. The Poisson's ratio for the mineral or synthetic hydroxyapatite is about 0.27, which is close to that of bone (≈0.3) (Park, & Lakes, 2007).

Among the most important properties of hydroxyapatite as a biomaterial is its excellent biocompatibility. Hydroxyapatite appears to form a direct chemical bond with hard tissues on implantation of hydroxyapatite particles or porous blocks in bone, new lamellar cancellous bone forms within 4 to 8 weeks (Wong, & Bronzino, 2007).

2.4.2.2.4 Biphasic Calcium Phosphate (BCP). BCP is prepared by sintering precipitated calcium deficient apatite (Ca/P molar ratio between 1.55 and 1.65), resulting in an intimate mixture of HAP and β-TCP. The HAP/βTCP weight ratio of the BCP depends on the calcium deficiency of the precipitated apatite before sintering. Successful application of BCP was attributed to controlled bioactivity manipulated by controlling the HA/βTCP ratio because of the preferential dissolution of the βTCP component of BCP. Biodegradation or dissolution of BCP depends on the processing and sintering methods that affect the crystallinity and porosity. Thus, BCPs of equivalent HAP/βTCP ratio may exhibit different biodegradation properties.

A composite of BCP (80HAP/20β-TCP) with silicone (Flex™ HAP, Xomed, FL) is available as an ear implant, replacing damaged ear ossicles. A composite of BCP (65HAP/35β-TCP) with bovine-derived collagen in a 1:1 ratio (Collagraft®, Zimmer Corporation, Warsaw, IN) is used with autogenous bone marrow aspirate.

2.4.2.2.5 Calcium Phosphate Cements (CPC). The concept of calcium phosphate cements (CPC) was first introduced by LeGeros, et al. in 1982 showing that apatitic calcium phosphate mixed with calcium hydroxide and dilute phosphoric acid can form cement and may have potential for restorative dentistry or as bone cement. Brown and Chow obtained the first patent on CPC in 1986 based on tetracalcium phosphate (TTCP) and dicalcium phosphate anhydrous (DCPA) as the powder component and sodium phosphate solution as the liquid component. Other CPC formulations were developed with varying components of the powder and liquid components. The setting time depends on the composition of the powder and liquid components and on the powder/liquid ratio. The composition of the product after

setting depends on the composition of powder and liquid components (Pietrzak, 2008).

2.4.3 Bioactive Glass Ceramics

Glass ceramics were first utilized in photosensitive glasses, in which small amounts of copper, silver, and gold are precipitated by ultraviolet light irradiation. These metallic precipitates help to nucleate and crystallize the glass into a fine-grained ceramic that possesses excellent mechanical and thermal properties (Wong, & Bronzino, 2007).

Hench pioneered the development of glass ceramics described as 'bioactive' because it allowed the formation of new bone on its surface and provided a uniquely strong interface with the host bone. The bioactivity of the glass depends on its composition (Hench, 1991). The bioactive glass ceramic developed by Hench is available commercially and is prepared by melting together SiO_2 (network former), Na_2O/K_2O and CaO (network modifiers) and P_2O_5 (internal nucleant for surface apatite formation) in specific proportions (45% SiO_2, 24.5% CaO, 24.5% Na_2O and 6% P_2O_5). Other bioactive glass ceramics of different formulations were subsequently developed: CeraboneRA-W containing crystalline hydroxy or fluoride-containing apatite, $Ca_{10}(PO_4)_6(O,F)_2$, and wollastonite, $CaO.SiO_2$, developed by Kokubo in Japan, and Ceravital developed by Broemer and Deutcher in Germany and described by Gross, et al. (1998). Non-silicate glasses of the system $CaO\text{-}P_2O_5$ were originally developed for processing of dental crowns. An experimental calcium phosphate glass (CPG) based on the system $CaO\text{-}CaF_2\text{-}P_2O_5\text{-}MgO\text{-}ZnO$ with Ca/P molar ratio ranging from 0.2 to 1.2 was developed by LeGeros, & Lee (2004). The biodegradation of these CPGs can be controlled by changing the Ca/P ratio of the glass. Recent animal studies showed the potential of this material for bone repair (Pietrzak, 2008).

A negative characteristic of the glass ceramic is its brittleness. In addition, limitations on the compositions used for producing a biocompatibile

(or osteoconductive) glass ceramic hinders the production of a glass ceramic which has substantially higher mechanical strength. Thus, glass ceramics cannot be used for making major load-bearing implants such as joint implants. However, they can be used as fillers for bone cement, dental restorative composites, and coating material (Wong, & Bronzino, 2007).

2.4.4 Bioceramics in Composites

The main reason for forming composites is to improve the mechanical properties, most often toughness, above that of the stand-alone ceramic. For bioceramic composites we often try to increase K_{IC} and decrease E. Preparation of hydroxyapatite/ceramic composites through the addition of various ceramic reinforcements has been attempted, with metal fibers, Si_3N_4 or hydroxyapatite whiskers, Al_2O_3 platelets and ZrO_2 particles. In many cases, the composites could not be successfully prepared due to the problems related to their poor densification. Hydroxyapatite/metal and hydroxyapatite/polymer composites are two typical classes of materials, which have been examined for improving the toughness characteristics of synthetic hydroxyapatite. In both cases, a toughness improvement can be found, due to a crack-face bridging mechanism operated upon plastic stretching of metallic or polymeric ligaments. Zhang, Gubbels, Terpstra, & Metselaar (1997) proposed a toughened composite consisting of hydroxyapatite dispersed with silver particles. This material was obtained by a conventional sintering method. It was reported that the toughness of these composites increased to 2.45 MPa $m^{1/2}$ upon loading the mixture, with (30 vol %) silver. The use of silver is not only for taking advantage of the ductility of silver in terms of fracture toughness, but also because silver is inert and has anti-bacterial properties (Nissan, 2005).

General summary of biomedical materials and their applications are given in Table 2.9 (Kamachi, 2003).

Table 2.9 Types of biomedical materials and applications

Biomaterials	Objectives	Degradation mechanism	Applications
Metals/alloys 316L SS, Co–Cr alloys, Ti and Ti alloys	Load bearing	Corrosion and mechanical	Fracture fixation plates, screws, pins, nails, joint replacements, orthodontic wires, femoral stems, cases for pacemakers, supports for heart valves, dental implants, dental crowns, bridges, fillings, and inner ear bone replacements.
Ceramics Carbon coatings, alumina, oxides, zirconia, glass, glass ceramics, and hydroxy apatite	High hardness, wear resistance, and better bone bonding	Corrosion and mechanical	Carbon in heart valves, dental implants, joint implants, coatings for dental and joint implants, fill bone voids/cavities by HAP, tissue scaffolds, drug delivery systems, and inner ear implants.
Polymer Ultra high molecular weight polyethylene, polyester, polytetraflouroethylene, PMMA, hydrogels, silicone rubber, PGA/ PLA, collagen, cellulose, and chitosan	Articulating surfaces	Wear, swelling, leaching, chemical	Joint replacement, vascular grafts, bone cement, orthodontic devices (e.g. plates, dentures) contact and intraocular lenses, catheters, hand and toe joints, artificial tendon and ligament, reconstructive surgery, sutures, staples, tissue scaffolds, drug delivery systems, and haemostatic bandages, pace maker leads.

2.5 Detrimental Factors Affecting the Performance of Implant Materials

2.5.1 Mechanical Forces Imposed on the Implant

The complicated service conditions and loads encountered on devices implanted in the human body are generally quite high. Implants are subjected to both static and dynamic loads depending on the activity of the patient. An implant introduced into a patient for the repair of a fractured bone must have sufficient strength to sustain and transmit the load actions resulting from joint and muscular forces. Simple calculation of static loading may be made to evaluate typical loading. For example, during body movement, the load on the head of the femur is approximately twice the body weight. The load varies with the position in the walking cycle and reaches a peak of about four times the body weight at the hip and three times the weight at the knee.

The frequency of loading and load cycles encountered over a specific time period are also important. A fast rate of walking corresponds to one complete walking cycle (two steps) per second. Typically an average person may take one to two million steps per year. For an active person, the number of steps taken may be two or three times more than that taken by a normal person (Sivakumar, Suresh, Rajeswari, & Thulasiraman, 1995).

2.5.2 Biological Environment

The human body is a harsh environment for metals and alloys having to be in an oxygenated saline solution with salt content of about 0.9% at pH ~7.4, and temperature of 37±1°C. When an orthopedic implant is surgically installed into the human body, it is constantly bathed in extracellular tissue fluid (Becker, & Shipley, 2002). All the surgically implantable metallic materials, including the most corrosion-resistant materials, undergo chemical or electrochemical dissolution at some finite rate, due to the complex and corrosive environment of the human body. The body fluid constitutes water, complex compounds, dissolved oxygen and large amounts of sodium (Na^+) and chloride (Cl^-) ions and other electrolytes like bicarbonate and small amounts of potassium, calcium, magnesium, phosphate, sulphate and amino acids, proteins, plasma, lymph etc. The ionic species also perform numerous functions that include maintenance of the body pH and participation in the electron transfer reactions. On surgical implantation, the internal body environment is greatly disturbed i.e, the disturbance of blood supply to the bones and variation in the ionic equilibrium.

Normal imbalance occurs in fluid compartment and transport of ions and non-uniform changes normally accompany disease states. From an electrochemical viewpoint, the initiation of corrosion can be due to the various conditions existing along the implant surface. These conditions may be responsible for the formation of electrochemical cells accompanied by active metal dissolution at favored localized spots at the implant-body fluid interface. There are a series of other factors which can result in altering the local environmental conditions and lead to various forms of

corrosion and/or failure of the implant. An orthopedic implant is considered to have failed if it is prematurely removed from the body due to severe paining, inflammation and other reactions with the body like corrosion and wear.

2.5.3 Tissue–implant Corrosion

In addition to the hostile environment and a significant load encountered by the implant, the interaction between the material and the tissues is of prime importance. Such interactions induce corrosion/ionization of the implanted device. Corrosion can have two effects. First the implant may weaken and the premature failure will result. The second effect is the tissue reaction leading to the release of corrosion products from the implant. No metallic material is totally resistant to corrosion or ionization within living tissues. *In vivo* studies have shown that the implantation of the devices of most alloys significantly increases the concentrations of various ions adjacent to the tissues. Moreover, once a foreign material is implanted, there are several ways in which the body may react unfavorably. The presence of the implant may inhibit the defence mechanisms of the body leading to infection, necessitating the removal of the implant (Helmus, & Tweden, 1995). If infection does not occur or is controlled, the tissue response may range from mild edema to chronic inflammation and alteration in bone and tissue structures. This necessitates that the materials used in making implants must be inert or well tolerated by the body environment. The response of the body to an inert implant will be the development of a fibrous collagen sheath of low cellularity, which encapsulates the implant and separates it from the normal tissue. This obviously matures with time, varies in thickness in its organization and establishes a favorable relationship with the adjacent tissue (Figure 2.5). The capsule may contain an area of necrosis adjacent to the implant surrounded by a region of chronic cellular infiltration. In some cases, the capsule has a well-defined boundary but in other cases, it extends irregularly and diffuses into the surrounding muscle. The thickness of the fibrous sheath depends on the corrosion resistance of the material. The materials producing the thinnest sheaths are regarded as the best tolerated by the body.

2.5.4 Other Variables

Even though innovative metallurgical and technological advances have made striking progress in the design and the selection of implants, invariably failures occur due to underlying reasons. In every orthopedic failure, the concerned patient is made to face the trauma of repeated surgeries besides the severe pain experienced during the process of implantation. Moreover, its replacement is expensive and causes hardship to the patient. Hence, it is highly desirable to keep the number of failures to a minimum. The prominent failures of stainless steel orthopedic implant devices are discussed below.

Direct overloading: The intent of using a fixation device is to hold the ends of the broken bone in close proximity so that healing is promoted. The load is supposed to be shared between the bone and the fixation device. Even with a sharing of the load, it is necessary to limit the load placed on the affected bone until it heals. If excess load (due to the inept mobility of the patient) is transmitted to the implant fixed on the fractured bone slit, fracture of the implant is caused. Therefore, deformation and overload fracture results from a single overload or from a few cycles of overload on an orthopedic fixation device such as a bone plate or a hip nail.

Fatigue loading: Fatigue failure is defined as failure due to dynamic as well as cyclic loading of stresses imposed on the implant. For fatigue crack to develop, it is not necessary for the implant to be loaded in the plastic deformation range. Local stresses that occur under the conditions of loading in the elastic deformation range of the implant are sufficient to initiate fatigue cracks on the surface of an implant. The majority of failures occurring in orthopedic implants are fatigue failures (Williams, 1981). Typical fatigue striations are frequently found on the fractured surfaces. Often fatigue crack nucleation sites are noticed to be present at design induced stress concentration or other structural defects. In many cases, cracks are initiated because of the corrosion phenomena and are propagated mainly by a fatigue mechanism (Sivakumar, Kamachi, & Rajeswari, 1994). Fatigue failure may also

occur due to improper installation and the presence of gap between the fractured bone fragments after implantation.

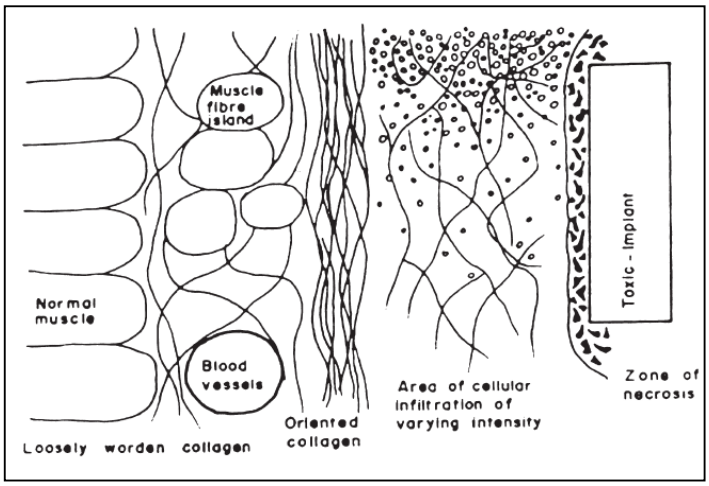

Figure 2.5 Generalised fibrous capsule forming in response to intramuscularly implanted metal.

Wear: Wear is mechanical removal of materials during the process of relative motion between two or more contacting surfaces. The implant device may simply wear out in due course of its use. Wear can mainly affect the performance of joint prostheses. Four types of mechanisms may be implicated in the wear of metal components of joint prostheses. They are: (i) abrasive, (ii) adhesive, (iii) fatigue and (iv) corrosive modes. The adhesive wear is the most prominent on the metal-to-metal combinations. The metal to plastic system will exhibit a lower coefficient of friction but a higher volumetric wear rate. The volumetric wear of stainless steel-polyethylene combination is greater than cobalt-chromium-polyethylene systems. Higher wear rates are generally observed for a few metal-to-plastic combinations in an experimental system. The only combination used extensively in the metal-to-metal system is cobalt-chromium to cobalt-chromium. Neither stainless steel against itself or titanium against itself should provide a low wear rate and a low friction system because of their tendency to gall and seize. The severe wear followed by mechanical damage may lead to the premature removal of the prostheses (Kamachi, Sridhar, & Raj, 2003).

2.6 Bone Structure and Development

Calcium phosphate biomaterials are always discussed in relation with bone repair as calcium phosphate is the main inorganic component of bone. Although the shape of bone varies in different parts of the body, the physicochemical structure of bone for these different shapes is basically similar. Bone is a living material composed of cells and blood supply encased in strong composite structure (Yuan, & Groot, 2005). Calcified bone matrix contains two components: 65 wt% the inorganic matrix and about 25% organic substances. The inorganic substance of bone consists mainly of calcium phosphate, significant amounts of citrate and carbonate ions and traces of fluoride, magnesium and sodium. The calcium phosphate in bone is very similar, but not identical, to mineral hydroxyapatite while the inorganic matter is bone. The mixture of mineral hydroxyapatite and collagen matrix gives bone strength and hardness (Yuan, & Groot, 2005). The organic matrix of bone mainly consists of type I collagen fibrils, which account for over 90% of the whole matrix, with the remaining 10% corresponding to noncollagenous proteins, proteoglycans, and phospholipids.

Whole bone, i.e., bone as an organ, consists not only of calcified bone matrix and bone cells, but also of nonosseous cells, blood vessels, nerve fibres, and bone marrow, whose relative proportions change with the type and age of the bone. Obviously, the physiological properties of bone are closely dependent on the variable presence of these soft structures. However, they can be neglected if bone is considered strictly as a calcified tissue (Bonucci, 2000).

Despite its strength and hardness, bone is dynamic living tissues. On the one hand, bone consists of living cells hath build bone, namely osteocytes and osteoblasts, while on the other hand, bone has living cells of osteoclasts that resorb old bone during bone remodeling. With both osteoblasts and osteclasts, bone constantly being renewed and reconstructed throughout the lifetime of the individual. Bone is one of few human tissues that can regenerate themselves. Remodeling is also a key feature of the shape changes that occur in growing bone and in the healing process of a bone

fracture. For instance, the fracture of bone activates osteogenesis and ultimately the fracture heals without any scar formation.

Bone is a living material composed of cells and a blood supply encased in a strong composite structure. Two of the various types of bone that are of most concern in the use of bioceramics are the dense outer layer of cortical (compact) bone and cancelous (spongy) bone that filled with bone marrow tissue. Cortical bone has an organized structure of densely packed mineralized collagen fibrils and provides the structural component of bone, while cancelous bone has a very loosely organized matrix and provides the metabolic function of bone.

Cancellous bone is less dense than cortical bone. Every bone of the skeleton has a dense outer layer of compact bone covering the spongy bone, which is in the form of a honeycomb of small needle-like or flat pieces called trabeculae. Figure 2.6 is a schematic showing a longitudinal section of a long bone. The open spaces between the trabeculae are filled with red or yellow bone marrow in living bones. Because of its lower density, cancellous bone has a lower E and higher strain-to-failure ratio than cortical bone, as shown in Figure 2.7. Both types of bone have higher E than soft connective tissues, such as tendons and ligaments. The difference in E between the various types of connective tissues ensures a smooth gradient in mechanical stress across a bone, between bones, and between muscles and bones.

The mechanical properties of the implant are clearly very important. Figure 2.7 compares E of various implant materials to that of cortical and cancellous bone. Elasticity modulus of cortical bone is 10-50 times less than that of Al_2O_3. E of cancellous bone is several hundred times less than that of Al_2O_3 (Weiner, & Wagner, 1998).

For replacing natural joints, it is necessary to fix implant components in the bone. The bone/implant interface must be optimized to provide for rigid implants to be fixed in the osseous implant bed reliably over many years. Structural compatibility consist in adaptation of the implant structure to the mechanical behaviour of the

recipient tissue, and surface compatibility consist in adaptation of the chemical, physical, biological and morphological surface properties of the implant to the recipient tissue with the aim of clinical interaction. The task of designers (engineers) and surgeons to provide to good implant fixation over the long term consists in the provision of appropriate primary preconditions to enable reliable long-term connections for implant/bone systems.

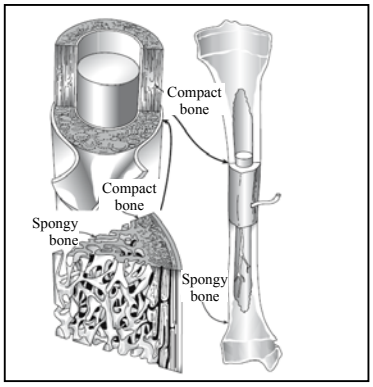

Figure 2.6 Longitudinal section showing the structure of long bone.

It should never be forgotten that the flux of forces in the environment of the implant is different from the one that used to exist before the implantation, and that the implant hence will always represent a disturbing factor in the system, to which the organism will react. Under appropriate biomechanical conditions, bone will be transformed, generated anew and reinforced, whereas it will atrophy under unfavorable conditions. Seen from the point of view of implant design, the problem to be coped with consists in the difference in rigidity of the bone (the elasticity modulus being a few GPa only) and of the implant materials assuming load-carrying functions (the elasticity modulus being approx. 110 GPa for titanium, 220 GPa for cobalt chromium, and 380 GPa for alumina).

The difference in rigidity causes relative movement that causes layers of soft tissue to form between the implant and the implant bed, which in the end causes the implant to loosen. Generally, the transmission of forces to the bone is enabled by pressure (form-fit connection) only since the use of bioinert materials will not enable

the establishment of positive material connections (connective osteogenesis). Such materials do not enable any chemical and biological interaction between the implant and the bone. Bioinert materials will hardly or not at all offer any potential for surface compatibility.

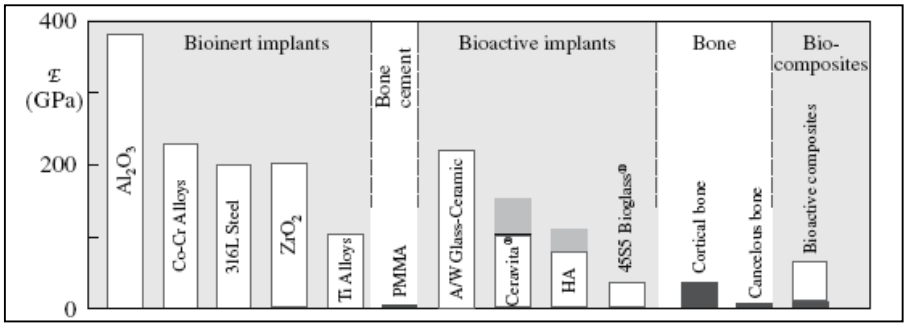

Figure 2.7 Young's modules (E) for various implants compared with bone.

The bone will degenerate if the mechanical stress to which the implant bed is exposed is either too high or too low, or if it is not exposed to any stress at all (stress shielding). Stress shielding weakens bone in the region at which the applied load is lowest or is in compression. (bone must be loaded in tension to remain healthy.) Bone that is unloaded or is loaded in compression will undergo a biological change that leads to resorption (Carter, & Norton, 2007). This was point out to by Wolff as early as in 1982 (Wolff's Law). According to this principle, mechanical stimulation of bone is necessary as a rule, since other wise the bone will regress and atrophy. Hence, the form-fit connection must be optimized in a way to allow for pressure to be applied to the bone in the areas of contact. The substantial prerequisites which must be complied with to enable the establishment of a connection between the bone and the implant are: elimination of micromovement, application of loads which must not be too high on large areas of the implant bed, and the use of structured implant surfaces, and of bioactive surfaces such as hydroxyapatite, if possible.

The implant material does not necessarily play a primary role when it comes to improve implant fixation beyond the level of form-fit or frictional connection. The structure of the implant surface represents a very important parameter. To enable

transformation and generation of new bone tissue in the areas of contact between the implant and the bone, the surface of metal implants must be structured, as was shown by experience. The easiest way of structuring the surface of bioinert implants is to roughen their surface by way of sandblasting. It is also possible to structure implant surfaces by sintering on beads or meshes, which however is somewhat more expensive. Biologically speaking, it is much more efficient to coat implants with bioactive hydroxyapatite, because apart from the implant's rough surface structure, the biological stimuli provided by the HAP coating are very useful (Willmann, 1999).

The concept behind microporous bioceramics [Al_2O_3 (porous crystalline), Hydroxyapatite coated porous metals] is the ingrowth of tissue into pores on the surface or throughout the implant, originated by Hulbert and co-workers many years ago (1972). The increased interfacial area between the implant and the tissues results in an increased resistance to movement of the device in the tissue. The interface is established by the living tissue in the pores. This method of attachment often is termed ‘‘biological fixation.’’ Biological fixation is capable of withstanding more-complex stress states than implants that achieve only ‘‘morphological fixation.’’ However, the limitation associated with porous implants is that, for the tissue to remain viable and healthy, pores must be greater than 100-150 μm in diameter. The large interfacial area required for the porosity is due to the need to provide a blood supply to the ingrown connective tissue. Vascular tissue does not appear in pores that measure smaller than 100 μm. If micromovement occurs at the interface of a porous implant, tissue is damaged, the blood supply may be cut off, the tissue dies, inflammation ensues, and the interfacial stability can be destroyed. When the material is a metal, the large increase in surface area can provide a focus for corrosion of the implant and loss of metal ions into the tissues, which can cause a variety of medical problems. These potential problems can be diminished by using a hydroxyapatite (HAP) bioactive ceramic material as a coating on the porous metal. The HAP coating also speeds up the rate of bone formation in the pores (Hench, 1991).

CHAPTER THREE

PRODUCTION OF CaP COATINGS

3.1 Introduction

While metals or metal alloys meet many of the biomechanical requirements of orthopedic implants, the interfacial bonding between the metallic surface and the surrounding bone is poor to nonexistent. Thus, analysis of metal or metal alloy devices provides convincing evidence that failure originates at the implant-tissue interface. Poor interfacial bonding leads to the formation of a non adherent, fibrous tissue layer. This results in small gaps between the natural bone and implant, leading to movement at the implant-tissue interface. Ultimately, this causes failure of the device and the need for additional surgeries to replace the loose implant. One approach to alleviate this problem has been the use of CaP coatings applied to implant surfaces. Due to its high porosity level, porous HAP has low mechanical strength and cannot be used under load-bearing conditions, unless fixed by external and internal support. For this reason HAP has been applied as thin film coatings on metallic alloy. The CaP mineral hydroxyapatite (HAP; $Ca_{10}(PO_4)_6(OH)_2$), has attracted considerable attention because of its close resemblance to the chemical and mineral components of teeth and bone. As a result of this similarity, HAP has shown good biocompatibility with bone.

Of the coating techniques utilized, thermal spraying (plasma, and, to a lesser extent, flame spraying) tends to be the most commonly used and analyzed. This technique has been faced with the challenge of producing a controllable resorption response in clinical situations due to a number of dissociation products (amorphous calcium phosphates, β-TCP and CaO) which have varying solubilities within the physiological environment. Besides the setbacks, thermally sprayed coatings are continually being improved by using different compositions and post-heat treatments which convert amorphous phases to crystalline calcium phosphates. Other techniques that are capable of producing thin coatings include pulsed-laser deposition and

sputtering, which, like thermal spraying, involves high temperature processing. Other techniques such as biomimetic, electrodeposition, and sol-gel utilize lower temperatures and avoid the challenge associated with the structural instability of HAP at elevated temperatures (Ben-Nissan, 2005; Campbell, 2003).

3.2 Plasma Sprayed Coatings

Plasma spraying has been used since the mid-1950's to form metal alloy, ceramic and cermet coatings on a range of metallic substrates. The variety of applications of plasma sprayed coatings is impressive and their use is evolving rapidly (Herman, Berndt, & Wang, 1993). Plasma spray coating is achieved by introducing HAP particles into a high temperature plasma flame where they are partially or fully melted. The melted particles are accelerated by the plasma flame (ionized gas), acted on by an electric potential, and deposited onto a prepared (roughened) metal substrate surface positioned normal to the particle beam. Figure 3.1 shows the schematic cross-section of a typical plasma spray gun (Sulzer, n.d.). This process utilizes a plasma gun consisting of conical shaped cathode surrounded by a cylindrical or ring shaped water cooled anode. An arc created across the gap between the electrodes ionizes inert gas fed through this space, and the electrons produced are accelerated toward the anode and the positive ions toward the cathode.

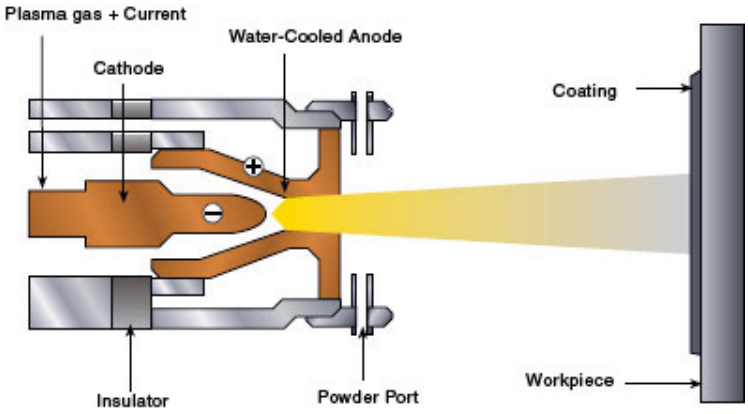

Figure 3.1 A schematic cross-section of a typical plasma spray gun.

Collisions between these moving particles and other neutral atoms or molecules which exist in the gas lead to dissociation of molecules and further ionization, "stretching" and transforming the gas in the arc into characteristic plasma flame with temperature reaching in excess of 12,000°C, through maximum temperature is a function of gun design and operations parameters. Partially or fully melted HAP particles are accelerated to velocities on the order of hundreds of meters per second by viscous drag created by the mass flow rate of the plasma. They are impacted with the substrate surface that has been roughened to enhance the primary mode of mechanical interlock of the coating and substrate. Since the particles solidify, the coating is build up particle by particle, with each particle solidifying before the arrival of the next, resulting in characteristic lamellar structure with inherent porosity as well as unmelted or partially melted inclusions trapped within the layers.

Macroscopic residual stress at the interface due to mismatch of thermal expansion coefficients of coating and substrate can lead to coating delamination while temperature gradients within the coating may create tensile stress leading to cracking of the coating. While plasma spraying is a well understood process, the control of variables is quite complicated. The extremely high temperatures (10,000°C to 12,000°C) used in the plasma spray process can vastly affect the properties of the final coating and result in potentially serious problems such as the coating of complex implant devices containing internal cavities (Campbell, 2003; Gross, & Berndt, 1998).

Furthermore, the reagents used must be strictly controlled in regard to purity, composition and particle size in order to avoid the formation of excessive amounts of non-HAP end products. However, even with the best control, some non-HAP products will still be present in the coating. These non-HAP products with unpredictable properties, voids in the coating, and low crystallinity lead to degradation in situ.

Applying HAP coatings with this technique produces a mixture of various HAP structures (i.e., unmelted, dehydroxylated (OHA), recrystallized (RHA) and impurity

phases including calcium oxide (CaO), tetracalcium phosphate (TTCP), α- and β-tricalcium phosphate (TCPs), as well as amorphous calcium phosphate (ACP). The solubility of all these additional phases and structures formed in spraying is higher than HAP which is in the order of ACP>>TTCP>α-TCP>OHAP>β-TCP>>HAP (Radin, & Ducheyne, 1992). It is believed that an increase in porosity, surface roughness, tensile residual stress and surface area has a promotional effect on the dissolution of the HAP coatings. The situation may compromise the performance of the coating if left unmonitored in a physiological environment. The highly bioresorbable nature of the secondary phases may severely weaken and compromise the functionality of the implant system. The solubility of HAP coatings increases with a decrease in crystallinity (Kweh, Khor, & Cheang, 2002).

However, due to the extremely high temperature of the plasma flame and the rapid cooling rate, the phase and structure of the HAP coatings are greatly changed from those of the feedstock. Variations in feedstock and deposition parameters can lead to different phase composition, crystal structure and microstructures, which result in the alterations of two major coating properties: mechanical properties and dissolution behavior. For example, different phases have demonstrated different solubility and Young's modulus (Mohammadi, Ziaei-Moayyed, & Mesgar, 2008).

Because of its many advantages, such as process feasibility and the retention of the properties of source powder, the plasma-spray technique was frequently used for the deposition of HAP and other calcium phosphates on metals. However, it was found that the bonding between the plasma-sprayed HAP coating and metallic substrate was contributed mainly by a mechanical interlocking mechanism. Such defects as cracking, flaking, and scratching that are often found in plasma-sprayed HAP coatings might eventually lead to delamination of the coating. The delamination of the coating not only enhances the release of metal ions, but it could also lead to loosening of the implant.

To improve bond strength and other properties, such techniques as pulsed laser deposition, ion beam deposition, and magnetron sputtering have been explored to

develop thin (generally less than 10 μm) coatings of HAP and other calcium phosphates (Ding, Ju, & Lin, 1999). Of the alternative deposition techniques available, sputtering has been found to provide thin CaP coatings that have many improved characteristics over those achieved by plasma spraying, due primarily, to its ability to provide a high degree of process control.

3.3 Sputter Coatings

To overcome some disadvantages with the plasma sprayed CaP/HAP coatings magnetron sputtering (ion beam) has been developed. Ion sputtering is a vacuum process in which atoms or molecules are ejected from a target material by high-energy ion bombardment and deposited on a substrate in the vacuum chamber. Many of the initial studies on sputter coating CaP/HAP onto metallic biomaterials employed an ion-beam sputtering technique to produce thin CaP films. In their study, a sintered HAP sputtering target was arranged to obliquely intersect an ion beam of given energy and flux density that was created by independent ion source. The metallic substrates were suitably placed in the vacuum chamber to receive the sputtered target material. Schematic representation of the sputtering chamber is given in Figure 3.2 (Leite, Pereira, Da Silva, & Dias da Silva, 2006). The substrates were first ion beam sputter cleaned before the coating deposition. The introduction of a small partial oxygen pressure to the chamber was employed during the deposition process presumably to counter loss of hydroxyl groups by coating under vacuum. While coating had excellent adhesion strength, as demonstrated by high temperature quench test, crystallinity was variable, with most samples exhibiting amorphous characteristics. Additionally, the deposition process was exceedingly time-consuming, requiring 10 hours to produce a ~1 μm thick film (Ong, Lucas, Lacefield, & Rigney, 1992).

Although radio frequency (RF) magnetron sputtering, which is used extensively in the electronics industry, has been utilized previously for the deposition of bioceramic layers, the technique has yet to find a major clinical application. Notwithstanding this lack of commercial medical application, it is clear that sputtering can offer

significant advantages over plasma spraying and several other coating methodologies. In RF sputtering technique, ionization of the inert, working argon gas is produced in the region adjacent to the target by low-pressure electric discharge (glow discharge).

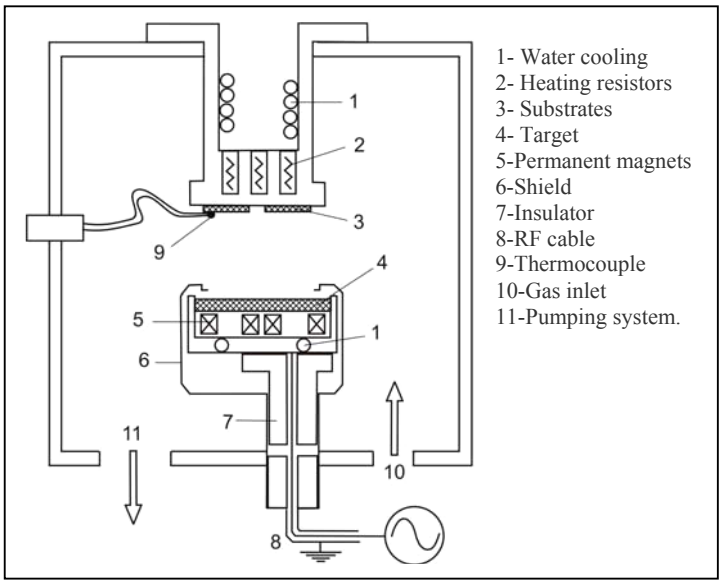

Figure 3.2 Schematic representation of the sputtering chamber geometry and main components.

The target is backed by conducting plate, which is negatively biased so that the target surface is bombarded by positive ions from the plasma. Because of charge accumulation or non-conducting HAP targets, the DC voltage power supply is replaced by a radio frequency power supply which quickly and periodically reverses the polarity of the conducting plate, attracting electrons from the plasma to eliminate the surface charge without affecting the direction of the positive ions. The resulting films obtained by this method had a molecular structure and Ca/P ratio similar to that of the HAP target. It has been suggested previously that target material stoichiometry can have a significant influence on the characteristics of sputter deposited coatings. Hence, the use of compacted HAP powder targets is desirable due to the attendant ability to change readily the stoichiometry and phase of the precursor powder in order to reflect these properties in the subsequent CaP coatings. In this regard, the effective lifespan of HAP powder targets and the effects of their multi-cycle usage on

the composition and structure of the resultant coatings are of considerable importance. The technique has the ability to coat substrates with non-planar geometry. Given this flexibility, coatings with specific predetermined properties can be created to add significant value to surface conditions where the manipulation of biological species is important. It is likely, then, that these advantages will find expression in delivering the conditions required for influencing cell-surface interactions, such as those required in the rapidly emerging field of tissue engineering.

In cell culture experiments, it was demonstrated that magnetron-sputtered CaP coatings can indeed stimulate extracellular matrix and induce apatite formation. In addition, no severe degradation of the amorphous and crystalline coatings was observed (Wolke, Van der Waerden, Schaeken, & Jansen, 2003).

3.4 Electrodeposition

Electrodeposition, also called electroplating or simply plating, is an economical technology to protect and enhance the functionality of parts used in many diverse industries including home appliances, jewelry, automotive, aircraft/aerospace, and electronics -in both decorative and engineering applications. Although electroplating and vacuum deposition processes are generally considered competitive processes, there are increasing applications in which they are (or can be) highly complementary. These involve utilizing the advantages of both deposition technologies are given in Table 3.1: (Schwartz, 1994).

Table 3.1 Comparison of electroplating and vacuum deposition

Vacuum Deposition	**Aqueous Deposition**
Close tolerances	Lower costs
Wide choice of substrates	Thicker coatings
Wide choice of coatings	Coating complex shapes
	Control and modification of deposit properties
	Control of residual stress

Electrochemical methods are increasingly being used for the preparation of thin films and coatings. Recently, electrodeposition of metals attracted renewed attention, due to its adoption by major companies for the processing of advanced microelectronic components. Electrodeposition has been widely investigated to obtain polymer films. The rapidly increasing scientific interest in electrodeposition of ceramic and organoceramic materials has opened new opportunities in the development of advanced thin films for novel applications. Electrodeposition of ceramic materials can be performed by cathodic or anodic methods. However, anodic deposition has limited utility regarding possible materials to be deposited by this method and substrates used for deposition. Cathodic deposition has important advantages for industrial applications. Two processes are commonly used to prepare ceramic coatings by cathodic electrodeposition: the electrophoretic process (EPD), which is based on the use of suspensions of ceramic particles, and the electrolytic process (ELD), which starts from solutions of metal salts (Figure 3.3).

Many processes based on electrophoretic deposition have been described, including deposition of thick films, laminates, and body shaping. Some of these processes are in commercial use. Significant interest has recently focused on cathodic electrodeposition, which offers important advantages for various applications; cathodic electrolytic deposition is a new technique in ceramic processing that has been used to produce a variety of ceramic thin films.

When a metallic salt is dissolved in water it dissociates to form positively charged ions. The solution that contains these charged ions is referred to as an electrolyte or a plating solution. By passing a sufficient amount of electric current through this electrolyte, one can reduce the metal ions to form solid metal. This process is most commonly referred to electroplating or electrochemical deposition (Schlesinger, & Paunovic, 2000). Figure 3.3 shows electrophoretic motion of positively charged ceramic particles and ions (M^+), followed by hydrolysis of the ions to form colloidal nanoparticles and coagulation of the particles to form EPD and ELD deposits.

Electrodeposition offers rigid control of film thickness, uniformity, and deposition rate and is especially attractive owing to its low equipment cost and starting materials. Due to the use of an electric field, electrodeposition is particularly suited for the formation of uniform films on substrates of complicated shape, impregnation of porous substrates, and deposition on selected areas of the substrates.

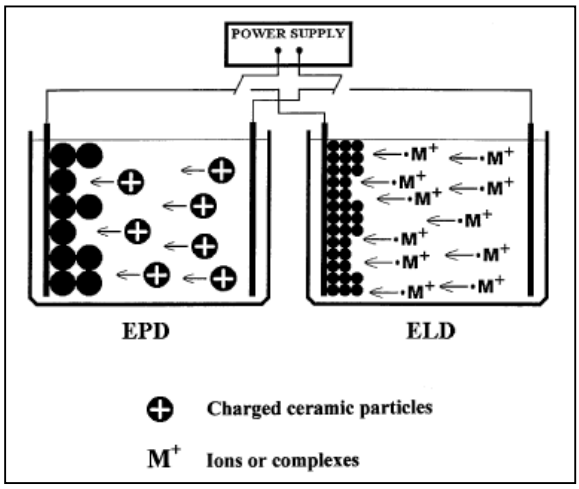

Figure 3.3 Schematic of cathodic electrophoretic deposition (EPD) and electrolytic deposition (ELD).

EPD is an important tool for the preparation of thick ceramic films (Figure 3.4). ELD enables the formation of nanostructured thin ceramic films (Zhitomirsky, 2002). Table 3.2 gives comparison of electrophoretic and electrolytic deposition of ceramic materials in detailed (Zhitomirsky, 2000).

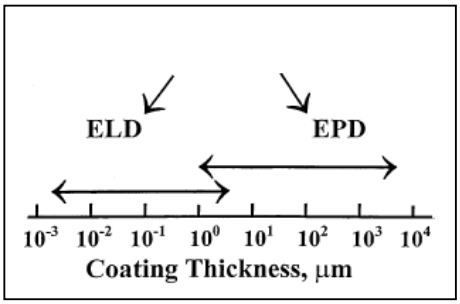

Figure 3.4 Thickness of coatings deposited using ELD and EPD.

3.4.1 Electrophoretic Deposition

Electrophoretic deposition, a process in which ceramic particles, suspended in a liquid medium, migrate in an electric field and deposit on an electrode, has been the subject of considerable interest; review papers are now available (Sarkar, & Nicholson, 1996). Electrophoretic deposition offers important advantages in the deposition of complex compounds and ceramic laminates. The degree of stoichiometry in the electrophoretic deposit is controlled by the degree of stoichiometry in the powder used. According to Sarkar et al. (1996), particle/electrode reactions are not involved in EPD, and ceramic particles do not lose their charge on being deposited. The reversal of the electric field results in stripping-off the deposited layer. Therefore, it is important to use similarly charged particles and similar solvent-binder-dispersant systems for forming laminates of various ceramic materials and gaining better control of layer thickness.

Table 3.2 Comparison of electrophoretic and electrolytic deposition of ceramic materials

	Electrophoretic Deposition	**Electrolytic Deposition**
Medium	Suspension	Solution
Moving Species	Particles	Ions or complexes
Electrode Reactions	None	Electro-generation of OH^- and neutralization of cationic species
Preferred Liquid	Organic solvent	Mixed solvent (water-organic)
Required Conductivity of Liquid	Low	High
Deposition Rate	$1\text{-}10^3$ μm/min	10^{-3}-1 μm/min
Deposit Thickness*	$1\text{-}10^3$ μm	10^{-3}-10 μm
Deposit Uniformity†	Limited by size of particles	On nm scale
Deposit Stoichiometry	Controlled by stoichiometry of powders used for deposition	Can be controlled by use of precursors

*Controlled by variation of deposition time, voltage, or current density.
† Controlled by electric field.

A suspension for EPD is a complex system in which each component has a substantial effect on deposition efficiency. There are two principal types of solvents used: water and organic liquids. Organic liquids are superior to water as a suspension medium since the use of water-based suspensions causes gas formation from the hydrolysis of water. In general, suspensions can be dispersed by electrostatic, steric, or electrosteric stabilization mechanisms. Ceramic particles must be electrically charged to permit forming by electrophoretic deposition. The charge on a colloidal particle could originate from various sources, such as from adsorbed simple inorganic ions or from dispersants. A binder is also added to the liquid to increase the adherence and strength of the deposited material and prevent cracking. The deposition rate depends on applied electric field, suspension concentration, and electrophoretic mobility of articles (Zhitomirsky, & Gal-Or, 1997).

When considering other possible factors that can influence the deposition yield, it is important to note that a certain potential distribution needs to be achieved in the electrophoretic cell in order to supply sufficient voltage at the electrode interface and obtain high deposition rates. Such potential distribution can be realized by adding an appropriate amount of phosphate ester or electrolyte. It was shown that uniformity and adhesion of the deposits can be improved by the use of electrolytes (Ducheyne, Radin, & King, 1993). However, an increase in the electrolyte concentration caused significant aggregation of ceramic particles and their sedimentation. Particle sedimentation resulted in decreased suspension concentration and was accompanied by a decrease in the deposition rate. The deposition process resulted in porous deposits that included a significant amount of agglomerates (Zhitomirsky, 1998).

Constant-current or constant-voltage regimes could be used for EPD. The electric field drives ceramic particles toward the electrode and exerts a pressure on the deposited layer. It is desirable to maintain a high potential difference between the anode and the cathode. The use of high voltages has the advantage of smaller deposition times and higher deposit thickness. It should be noted that in the case of relatively large particles (~1 μm) stirring the suspension is usually performed to

prevent settling. In this respect, higher voltages and smaller deposition times are preferable, because shorter deposition times allow deposition without stirring. It was demonstrated that electrophoretic phenomena has distinctive features for relatively large particles (several micrometers) and for particles on a submicrometer scale. A high electric field and stirring can induce aggregation and sedimentation of submicrometer particles, detracting from the deposition process efficiency. It should be noted that high electric fields bring about porosity in the deposits (Zhitomirsky et al., 1997).

Most of the comprehensive studies of electrophoretically deposited CaP films, particularly early on, were reported by Ducheyne and colleagues (1980, 1993). In electrophoresis, negatively charged colloidal HAP particulates suspended in alcohol or other suitable solution migrate to the substrate to be coated (an anode) by applying an electric field to the suspension. The resulting film is weakly bonded to the substrate; studies have therefore employed a post-deposition heat treatment at temperatures up to 900°C to improve the mechanical properties of this coating.

More recently, Wei, Ruys, Milthorpe, Sorrell, & Evans, (2001) reported a novel approach to deposit dual HAP layers on Ti, Ti6Al4V and 316L stainless steel by using an electrophoretic method. The dual coating route was used to overcome film cracking problems. The dual layers were sintered at 875-1000°C for 1 hour. The coating-sintering-coating process of applying dual coatings from nanoparticle size HAP successfully produced coatings with TCP free surface, good adhesive strength, and minimal loss in the strength of the substrate. When the primarily first layer of coating was applied to metal substrates, it cracked. With the second layer, a high adhesive strength was achieved. The authors hypothesized that cracking of the primary layer was due to the densification of the coating during the sintering process and the thermal expansion coefficient mismatch between the coating and metal substrates. When the second coating layer was coated on top of the primarily layer, it filled in the cracks in the primary layer, thereby creating coating integrity. The primary coating acted as a diffusion barrier, which inhibited the metal ions from further migration into the top coating. As a result, a pure HAP top coating was

achieved. While the formation of a pure HAP layer resulted in this study, this may not be essential and, in fact, may be detrimental for forming modified surfaces that promote more rapid osseointegration *in vivo* (Zhitomirsky et al., 1997).

Compared to plasma-sprayed systems, the advantages of the electrophoresis method included the ability to obtain highly reproducible and uniformly deposited coatings over all the porous-surfaced structure because of precise control of processing parameters (temperature, duration, and atmosphere) and the fact that the deposition is not line-of-sight. Indeed, electrophoretically deposited CaP films do remain promising. However, it is the need for a high temperature heat treatment that has discouraged commercial use of this approach particularly for applications where long-term coating retention is required. Clinical use has not been reported.

3.4.2 Electrolytic Deposition

Electrolytic deposition produces ceramic materials and provides their deposition. In cathodic ELD, metal ions or complexes are hydrolyzed by electrogenerated base (Figure 3.5) to form oxide, hydroxide, or peroxide deposits on cathodic substrates. Hydroxide and peroxide deposits can be converted to corresponding oxides by thermal treatment. Hydrolysis reactions result in the accumulation of colloidal particles near the electrode.

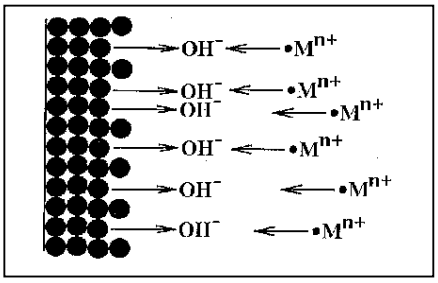

Figure 3.5 The electrolytic deposition of ceramic particles.

In the cathodic electrodeposition method, the following reactions that generate OH^- include the reduction of water, dissolved oxygen, nitrate and perchlorate ions (Zhitomirsky, 2002):

$$2H_2O + 2e^- \rightarrow H_2 + 2OH^- \quad (1)$$

$$NO_3^- + H_2O + 2e^- \rightarrow NO_2^- + 2OH^- \quad (2)$$

$$O_2 + 2H_2O + 4e^- \rightarrow 4OH^- \quad (3)$$

$$NO_3^- + 7H_2O + 8e^- \rightarrow NH_4^+ + 10OH^- \quad (4)$$

$$ClO_4^- + H_2O + 2e^- \rightarrow ClO_3^- + 2OH^- \quad (5)$$

$$ClO_4^- + 4H_2O + 8e^- \rightarrow Cl^- + 8OH^- \quad (6)$$

These reactions consume H_2O to produce OH^- ions, resulting in an appreciable pH increase near the cathode surface (Zhitomirsky, 2000, 2002). Various cationic species could be hydrolyzed by an electrogenerated base to form colloidal particles of oxides, hydroxides or peroxides. It was shown that electrosynthesis is similar to the wet chemical method of powder processing that makes use of electrogenerated base instead of alkali. Hydrolysis reactions result in the accumulation of colloidal particles near the electrode. It was shown that the formation of a deposit is caused by flocculation introduced by the electrolyte. It is important to note that some pH changes take place, even at open circuit, leading to deposit formation (Zhitomirsky, 2000).

Faraday's Laws of electrolysis (1833) are basic to electrodeposition. They relate the current flow, time, and the equivalent weight of the metal with the weight of deposit and may be stated as follows:

1. The amount of chemical change at an electrode is directly proportional to the quantity of electricity passing through the solution.

2. The amounts of different substances liberated at an electrode by a given quantity of electricity are proportional to their chemical equivalent weights.

Faraday's Laws may be expressed quantitatively:

$$W = \frac{I.t.E_q}{F} \tag{7}$$

where: W=weight of deposit in grams, I=current flow in amperes, t=time in seconds, E_q=Equivalent weight of deposited element, F=Faraday constant, =96,500 coulombs (approx.), I.t is the quantity of electricity used (coulombs = ampere-seconds) and E_q, the equivalent weight of the element, is the atomic weight divided by the valence change, i.e., the number of electrons involved (Schwartz, 1994).

Equivalent weight or mass is the grams of substance per equivalent. This can be determined by dividing the atomic mass or molecular mass of the substance by the number of moles of electrons gained or lost under balanced conditions. (E_q = atomic or molecular weight / moles of electrons gained or lost per mole of substance being oxidized or reduced). Thus 1 Faraday of charge is equivalent to one mole of electrons being liberated at the anode. According to the Faraday's Law, the amount of the deposited material can be controlled by varying deposition time or current density.

Aqueous or mixed solvents can be used for electrolytic deposition. It should be noted that the adsorbed water in as-prepared deposits leads to cementation of small particles to form aggregates. However, the deposition process needs a certain amount of water for base generation and prevention of the formation of nonstoichiometric oxides (Zhitomirsky et al., 1995).

3.4.3 Factors Affecting Deposited Coatings

It has been suggested electrodeposited systems protecting materials with coatings are composed of following regions:

1. The substrate interface,
2. The substrate-coating interface
3. The coating, and
4. The coating-environment interface has to be considered (Holleck, 1986).

Many parameters have effect on these regions. First layer is the substrate where potential hydrogen embrittlement effects are of concern. Cathodic concentration polarization may result in the evolution of hydrogen as the competing reaction. The pH of the cathode film increases and hydrates or hydroxides may precipitate and be occluded in the deposit. The co-deposition of hydrogen may result in brittleness of the deposit and, by migration and diffusion into the substrate, result in hydrogen embrittlement (Schwartz, 1994). For the substrate-coating interface, adhesion and interdiffusion are of importance. The third region is the coating itself where composition and microstructure determine properties and factors such as stress, phase transformations and grain growth exert noticeable influences. The final zone is the environment interface where the interaction of the coating in its intended application has to be considered in terms of corrosion and wear (Dini, 1993).

Adhesion refers to the bond (chemical or physical) between two adjacent materials, and is related to the force required to effect their complete separation. Cohesive forces are involved when the separation occurs within one of them rather than between the two. The ASTM defines adhesion as the "condition in which two surfaces are held together by either valence forces or by mechanical anchoring or by both together".

Good adhesion is promoted by:

1. strong bonding across the interfacial region,
2. low stress gradients, either from intrinsic or applied stress,
3. absence of easy fracture modes, and
4. no long term degradation modes.

Adhesion of a coating to its substrate is critical to its function. Mechanical, chemical, and metallurgical factors may contribute to such adhesion. Good adhesion performance of a coating depends on a variety of the attributes of the interface region, including its atomic bonding structure, its elastic modulus and state of stress, its thickness, purity and fracture toughness.

Diffusion is an irreversible and spontaneous reaction in a system to achieve equilibrium through the elimination of concentration gradients of the atomic species comprising the couple. Atoms or molecules within a material move to new sites and the net movement is from the direction of regions of low concentration in order to achieve homogeneity of the solution, which may be a liquid, solid or gas (Sard, Leidheiser, & Ogbum, 1975). The region near the electrode surface where the concentration of the ions differs from that of the bulk of solution is called the diffusion or boundary layer. It is defined somewhat arbitrarily as the region where the concentrations differ by 1% or more. The diffusion layer is much thicker than the electrical double layer (approximately 15,000 to 200,000 times thicker, depending on agitation and temperature. Diffusion can result in degradation of the properties of a deposit, particularly at the basis metal interface (Sard et al., 1975). An effective way to minimize or eliminate potential diffusion problems is the use of barrier coatings. In some instances, diffusion can benefit coating applications. Examples include deposition of alloy coatings and diffusion welding which utilizes diffusion to produce high integrity joints in a range of both similar and dissimilar metals.

The properties of all materials are determined by their structure. Even minor structural differences often have profound effects on the properties of electrodeposited metals (Radin, & Ducheyne, 1992). Four typical structures encountered with electrodeposited metals include; 1) columnar, 2) fibrous, 3) fine-grained, and 4) banded. The crystal structure resulting from an electrodeposition process is strongly dependent on the relative rates of formation of crystal nuclei and the growth of existing crystals. Plating processes have numerous variables that influence structure, e.g., metal ion concentration, addition agents,

current density, temperature, agitation, and polarization. Figure 3.6 does pictorially show how individual plating variables influence grain size of electrodeposits.

Additives are frequently added to plating solutions to alter desirably the character of the deposit. They are usually organic or colloidal in nature although some are soluble inorganic compounds. The potential benefits of additives include: brightening the deposit, reducing grain size, reducing the tendency to tree, increasing the current density range, promoting leveling, changing mechanical and physical properties, reducing stress and reducing pitting tendency (Dini, 1993; Schwartz, 1994).

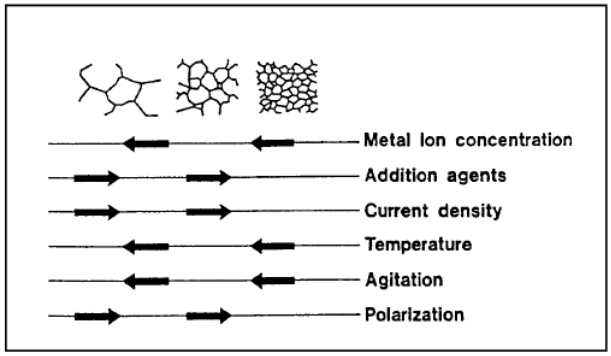

Figure 3.6 Relation of structure of electrodeposits to operating conditions of solutions.

The use of additives in aqueous electroplating solutions is extremely important owing mainly to the interesting and important effects produced on the growth and structure of deposits. It should be noted that the most common binders used in EPD are nonionic-type polymers (polyvinyl alcohol, polyvinyl butyral, ethyl cellulose, and polyacrylamide). The polymeric molecules adsorb onto the surfaces of ceramic particles. Positively charged ceramic particles provide electrophoretic transport of the polymeric molecules to form deposits on cathodic substrates. However, the application of these polymers for electrolytic deposition presents difficulties, as the formation of ceramic particles is achieved near the electrode surface (Figure 3.5). However, it is possible to perform electrochemical intercalation of charged polyelectrolytes into electrolytic deposits (Figure 3.7).

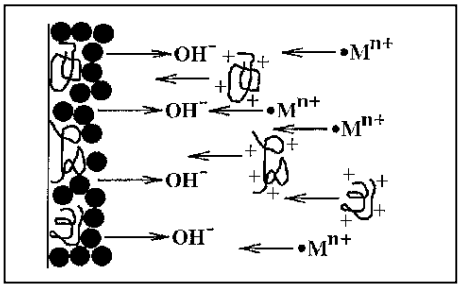

Figure 3.7 Intercalation of cationic polyelectrolytes into electrolytic deposits.

Deposit cracking associated with drying shrinkage is a common problem among wet chemical methods once thick coatings are formed. Oxide films deposited via hydroxide and peroxide precursors exhibited cracking when deposit thickness exceeded ~0.2-0.3 mm. The cracking problem was approached by multiple depositions (Zhitomirsky, 1998).

By using cationic polyelectrolytes, such as poly(dimethyldiallylammonium chloride) (PDDA) or polyethylenimine (PEI) with inherent binding properties, problems related to cracking in electrolytic deposits could be diminished (Zhitomirsky, 2000).

A residual stress may be defined as a stress within a material which is not subjected to load or temperature gradients yet remains in internal equilibrium. The presence of residual stress in almost all electrodeposited coatings is a common feature. Residual stresses in coatings can cause adverse effects on properties. A variety of options are available for reducing deposit stress and these include: choice of substrate, choice of plating solution, use of additives and use of higher plating temperatures. They may be responsible for peeling, tearing, and blistering of the deposits; they may result in warping or cracking of deposits; they may reduce adhesion, particularly when parts are formed after plating and may alter properties of plated sheet. This stress can cause distortion in lattice parameter within the deposited multilayers and the resistance of electrodeposited multilayers to mechanical stress in service is reduced when the deposits are highly stressed. Therefore, it is essential to

investigate the magnitude of internal stress within the electrodeposited multilayer films (Ghosh et al., 2007).

Porosity is one of the main sources of discontinuities in electroplated coatings; the others are cracks from high internal stresses and discontinuities caused by corrosion or subsequent treatments such as wear of deposits after plating. Pores can expose substrates to corrosive agents, reduce mechanical properties, and deleteriously influence density, electrical properties and diffusion characteristics. Any material (coatings, castings, powder metallurgy consolidated alloys, etc.) containing pre-existing porosity or voids is subject to property degradation. The tensile behavior of materials with preexisting porosity is characterized by large decreases in both strength and ductility with increasing porosity level, since ductile fracture in engineering alloys is most often the result of the nucleation and link-up of voids or cavities. Porosity, together with structure and many other properties of an electroplated coating, reflects the effects of 1) nature, composition and history of the substrate surface prior to plating; 2) composition of the plating solution and its manner of use; and 3) post plating treatments such as polishing (abrasive or electrochemical) wear, deformation, heating and corrosion (Dini, 1993; Schwartz, 1994).

3.5 Biomimetic Route

The word biomimetics originates from Greek “Bios” (life, nature) and “Mimesis” (imitation, copy) and can be defined as “the investigation of the structures and functions of biological materials that allows possible future design and synthesis of engineered composites based on the principles obtained from the biological materials” as cited in (Wainwright, 1995). This method involves the immersion of the material into a solution at low temperatures (usually <100°C) to mimic the natural process of apatite formation *in vivo*. Solution is supersaturated with respect to calcium and phosphorus, and known as simulated body fluid (SBF). The composition, ion concentrations, and pH of SBF are close to those found in human blood plasma (Tanahashi, Kokubo, & Nakamura, 1996).

Nevertheless, the deposition of CaP coatings by this technique offers the most promising alternative to plasma spraying and other coating methods. The biomimetic approach has four main advantages:

(a) it is a low temperature process applicable to any heat-sensitive substrate including polymers,
(b) it forms bone-like apatite crystals having high bioactivity and good resorption characteristics,
(c) it is evenly deposited on or even into porous or complex implant geometries,
(d) it can incorporate bone growth stimulating factors (Habibovic, Barrere, Van Blitterswijk, Groot, & Layrolle, 2002).

CaP coatings have been produced in aqueous solutions at physiological temperatures (Abe, Kokubo, & Yamamuro, 1990; Barrere, Layrolle, Van Blitterswijk, & Groot, 1999; Feng, Wang, Cui, & Kim, 1999). Kokubo's group first obtained apatite layers on various substrates using SBF solution. Kokubo, Kim, Miyaji, Takadama, & Miyazaki (1999) developed a technique for coating different organic, inorganic and metallic materials, with bioactive layers, which has been designated as biomimetic coating. The main aim of this biomimetic process is to mimic the biomineralization, leading to the formation of a bone-like carbonated apatite layer on the surface of a substrate. The methodology has been claimed to be very useful for producing highly bioactive and biocompatible composites with different mechanical properties.

CaP coatings, produced by biomimetic routes, offer an opportunity to incorporate protein molecules without compromising its functionality/activity, as they are generated under physiological conditions. Bioactive proteins can be directly integrated in the structure of CaP coatings without any covalent bonding with the inorganic phase and maintain their secondary structure close to their native form (Ben-Nissan, 2005).

Some progress has been made in the biomimetic preparation of CaP coatings on metallic implants (Abe et al., 1990; Feng et al., 1999), especially on titanium and some of its alloys. Most of the reactions in a solution occur at the solution/solid interface. In this sense, the material surface plays an important role, because surface properties are directly related to the in-vitro biological performance such as protein adsorption and cell growth (Castner, & Ratner, 2002). A preliminary mechanical or chemical modification of the material surface before its immersion in the SBF is usually carried out. Various pre-treatments were applied to attach functional groups on substrates and hence to accelerate the coating process, including alkali treatment (Feng et al., 1999), acid treatment (Kokubo et al., 1999), and heat treatment (Kokubo, 1996). Concentrated SBF solution was also used as pre-treatment solutions or as deposition solutions (Wainwright, 1995).

The mechanism of apatite formation on these pretreated materials is assumed to operate in the following way. The Ca^{2+} or Na^{+} ions are released from the surface of the pretreated materials into the SBF via exchange with H_3O^{+} ions. Water molecules react with Ti-O-Ti bonds in these materials to form numerous Ti-OH groups on their surfaces. These Ti-OH groups induce apatite nucleation. The released Ca^{2+} or Na^{+} ions increase the degree of super saturation of the surrounding fluid with respect to the apatite. The increased degree of the supersaturation accelerates apatite nucleation. Once apatite nuclei are formed, they grow spontaneously by consuming the Ca^{2+} and PO_4^{3-} ions from the surrounding fluid. The catalytic effect of the Ti-OH groups (even Si-OH and Ta-OH groups in Bioglass or A-W glass) for apatite nucleation are proven by the observation that even pure gels from the bone-like apatite on their surfaces in SBF (Habibovic et al., 2002). These results suggest that prerequisites for apatite formation on a material are the presence of surface functional groups effective for apatite nucleation, and a local supersaturation of Ca^{2+} and PO_4^{3-}.

Apatite coatings have successfully been formed by the immersion of chemically pretreated substrates such as glasses, metals, and polymers in metastable SBFs. (Wen, Wolke, De Wijn, Cui, & Groot, 1997). Although SBF mimics the inorganic

composition, pH, and temperature of human blood plasma, it is unknown whether these conditions are optimal for a coating process. Inconsistent CaP phases due to multi-submissions in SBF (e.g. Mg^{2+}, Na^{+}, CO_3^{2-}, Cl^{-}, HPO_4^{2-}) and the resulting low coating crystallinity eventually affect coating integrity *in vivo*. All pretreatments of the substrate are complex and time-intensive processes. Indeed, a thin apatite layer has previously been obtained on pretreated substrates by using long immersion time (i.e., 7-14 days) with a daily refreshment of SBFs. (Li, Kangasniemi, Groot, & Kokubo, 1994).

3.6 Sol-gel Route

The sol-gel technique has been widely used in the preparation of transparent oxide glasses by hydrolysis and condensation of metal alkoxides. In a strict sense, "sol-gel processing" is the synthesis of an oxide network via inorganic polymerization starting from molecular precursors in solution. This term frequently is extended to refer to the preparation of inorganic oxides by "wet chemistry". The sol-gel process provides as a new approach to the preparation of glasses and ceramics with many advantages over conventional methods (Rosa-Fox, Pinero, & Esquivias, 2003). Production of CaP coatings by using sol-gel technique received more attention over the past 10 years because of its advantages including: increased homogeneity due to mixing on the molecular scale, reduced synthesis temperatures ability to produce uniform fine-grained structures, use of different chemical routes (alkoxide or aqueous base) and the ease of application to complex shapes (non-line-of-sight process) using a number of coating techniques, e.g. dip or spin coating.

Sol-gel CaP thin films are relatively dense, coherent and adhere strongly to the underlying substrate. The annealing temperature and duration of firing both affect the structure and surface morphology of the resulting CaP thin films with higher temperatures resulting in higher crystallinity. The grain size of the film is also increased with increasing temperature and annealing time (Gross, Chai, Kannangara, & Ben-Nissan, 1998; Liu, Troczynski, Tseng, 2001; Liu, Yang, Troczynski, 2002).

3.6.1 History of Sol-gel Process

Interest in the sol-gel processing of inorganic ceramic and glass materials began as early as the mid-1800s with Ebelman and Graham studies on silica gels. The second publication in 1939 aimed specifically towards SiO_2 layers and, after the Second World War, resulted in the development of rear view mirrors for automobiles, which have been in production since 1953. Anti-reflective coatings followed, which have been in production since 1964, and solar reflecting coatings, deposited on flat-glass, in production since 1969. Several other sol-gel layer products followed. These layers basically consist of SiO_2 and TiO_2, as well as mixtures thereof and a variety of other single oxides.

An extension of the chemical principles involved was shown in 1969-1971 pointing out the importance of reactions of several metal alkoxides in solution under the formation of metal(I)-oxygen-metal(II) bonds. This made possible the production of defined multi-component oxide glasses, glass-ceramics and crystalline layers. This research effort into the involved basic chemistry followed the path used in the study of reactions of metal-organic compounds. It was supplemented with a continuous industrial development for the formation of thin layers, which also resulted in a process for the fabrication of transparent granulates, which can be formed in molding process.

The importance of simple solid-state reactions, e.g. lower temperatures, was already recognized in 1948 for the formation of co-precipated hydroxides and oxalates, sometimes combined as powder of multi component oxides and led to a focused research effort for reactions in solution and those taking place at the solution-substrate interface. This was an absolutely necessary prerequisite. After an incubation period of several years, sol-gel process gained world-wide interest. Fibers and unsupported films were developed (Dislich, 1988).

3.6.2 Unique Advantages and Applications of Sol-Gel Coatings

Sol-gel process is an attractive alternative to other methods for synthesis of ceramics and glasses for many reasons: for example, low temperature synthesis, simple equipments to be used, thin film formability and so on. Particularly, sol-gel process is very useful for thin film deposition because of the capability to coat materials of various shapes and large area, to control the composition easily for obtaining solutions of homogeneity and controlled concentration without using expensive equipment (Nishio, & Tsuchiya, 2004). The most important advantage of sol-gel processing, with respect to most other processes for forming ceramic coatings, is cost. As with more costly techniques such as CVD and plasma coating, a wide variety of films can be made on a plethora of substrates. Non-equilibrium compositions, such as high titania content silica-titania coatings can also be made. Sol-gel processing allows this to be done using simple, non-vacuum methods, which are generally less expensive than methods which require a vacuum. In addition to being generally a less expensive alternative to vacuum processes, sol-gel processes provide the possibility of producing unique structures, hence properties, in materials. Most notable is the ability to dope the solutions, prior to gelation, with almost any other material. Metal, semiconductor, and non-linear active dopants have been added to sol-gel solutions to make two-phase materials with unique properties. It is also possible to include non-hydrolyzable organic moieties, resulting in polymer/ceramic composites, known as ormocers, polycerams, or ormosils. Unlike most ceramic coating techniques, sol-gel coatings are applied as low viscosity solutions, hence they can be used to smooth over rough surfaces. Being applied as low viscosity solutions also allows the solutions to penetrate and partially heal cracks in ceramics. This has been shown to increase the tensile strength of glass when rods or plates are coated with sol-gel solutions (Blum, Platz, & Crawford, 1990).

Since sol-gel coatings are formed first as fragile, porous networks, which strengthen as they densify, forming complicated patterns by embossing (stamping) them with a master die is possible. It is also possible to densify only selected regions in a large coating using confined radiation (such as from a laser).

Finally, the porosity itself can be useful. Porous sol-gel coatings can be infiltrated with fluids much more extensively than the more dense coatings which result from traditional coating processes. Moreover, unlike vapor deposited coatings, the characteristics (geometry, interconnectivity, etc.) of the porosity of sol-gel coatings can be tailored by altering the processing conditions. Yoldas and Partlow (1985), for example, produced sol-gel coatings with graded porosity to make broad band antireflection coatings. However, this is only a simple example of the great potential of tailored porosity in fabricating coatings with new and unique properties.

Sol-gel technology is quite important for processing materials. Since this is one of the technologies for producing materials, application of this technology is valuable only when a better material can be made, a target material can be produced with much lower cost and only this method is available for making the target material. The sol-gel method has proved to be quite versatile as a result of intensive and extensive fundamental researches for the last three decades. The type of materials processed by this method covers metallic, inorganic, organic and hybrid materials. The use of the materials covered by this method ranges from highly advanced materials to materials for general use. The areas of technology covered by this method ranges from photonics to biology. These indicate that the sol-gel method can be applied to processing of an extremely many kinds of materials.

Because the sol-gel processing starts from the solution, the sol-gel processing is quite versatile. Materials of various shapes and microstructures can be prepared. Table 3.3 shows the shapes of materials made by the sol-gel method. With the advantages and characteristics mentioned above, the sol-gel method has been applied to processing of a great many different materials. Antireflection, optical waveguiding, transparent conducting, electro-optical, piezoelectric, anti-corrosion, diffusion and oxidation barrier, abrasion resistant, electrochromic, and superconducting coatings are some examples (Fabes, Zelinski, & Uhlmann, 1993).

The outline of applications of the sol-gel method will be described in the followings by classifying the sol-gel produced materials based on their function (Sakka, 2005).

- Optical and photonic functions
- Electronic functions
- Thermal functions
- Mechanical functions
- Chemical functions
- Biomedical functions

3.6.3 Sol-gel Process Steps

Sol-gel, also known as wet-chemical, processing of ceramics can refer to a multitude of reaction processes which employ a wide variety of chemical precursors to prepare many different products. Most processes can be categorized in one of three general approaches, which are drawn schematically in Figure 3.8 (Brinker, & Scherer, 1990).

Table 3.3 Shapes of the materials produced by sol-gel method

Shape	**Remark**
Bulk bodies	Rod (cylinder), plate, sheet
Fibers	Continuous fibers
Coating films	Thin films, thick films
Unsupported sheets	Sheets
Membranes	Micro filters
Particles	Spherical particles

In the first approach, a colloidal sol is prepared, and powders are precipitated from the sol (usually by changing the pH). The resulting powders are then dried and processed using traditional ceramic processing techniques.

In the second approach, the particles in the colloidal sol are linked (instead of precipitated, as in the first approach) to form a gel, which is subsequently dried, to form a porous ceramic, and fired (if desired) to crystallize and/or densify the material.

In the third approach, a gel is formed by polymerizing individual oligomeric units (instead of colloidal particles). In both the second and third approaches, solutions can be cast, spun, dipped, or sprayed onto substrates prior to gelation, thus providing an extremely convenient method of forming coatings. Although colloidal particles can sometimes be used to form coatings, the vast majority of applications of sol-gel coatings come from applying solutions to substrates prior to gelation.

Thus to begin to understand this process, a sol can be considered dispersions of colloidal particles in a liquid. Colloids are solid particles with diameters of 1-100 nm. On the other hand, gel is in the simplest picture, as a giant molecule, which has been formed as a consequence of the growth by condensation of polymers or aggregation of particles, but no latent heat is evolved. This giant molecule reaches across the vessel that contains it and the coherent solid 3-D network inside the fluid phase is known as a "gel". (Fabes et al., 1993).

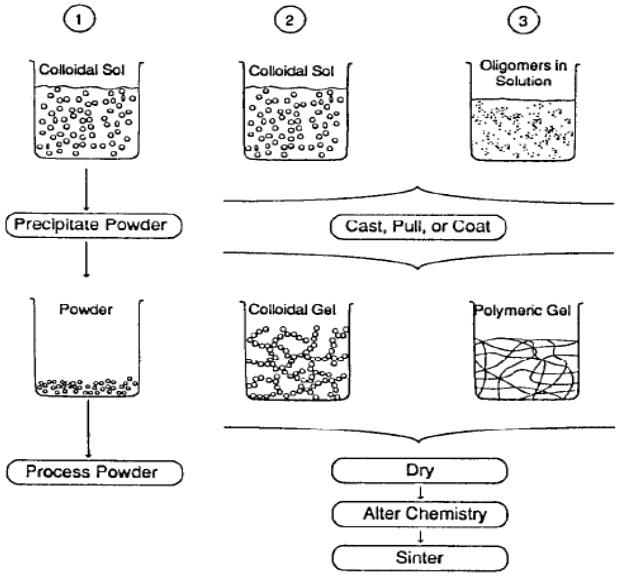

Figure 3.8 Schematic of three general sol-gel routes.

Gels are often classified either as particulate or polymeric. Particulate means that the solid phase forms by aggregation of dense, non-polymeric particles. Particulate gels are obtained by destabilization of an aqueous colloidal solution of oxides, hydroxides or mineral salts, also knows as colloidal gel. While polymeric gel refers to an entangled network of quasilinear chains that obtained by hydrolysis and polycondensation of metal alkoxides. The structure of this continuous solid network depends strongly by the replacement of the corresponding fluid phase. Like this, "alcogel" is termed when the pore liquor is alcohol and "hydrogel" when water is, at this step the structural changes process of the gel immersed in the liquid modify the reaction rates. When the liquid is removed we obtain a "xerogel", if slow evaporation of the pore liquid takes place or an "aerogel" if the pore liquid is removed in its hypercritical conditions of pressure and temperature (Rabinovich, 1988).

The basic idea is to use the techniques of solution chemistry to build ceramic structures from the molecular level. This stands in contrast to traditional solid state ceramic processing techniques, which build structures from the micrometer, or tens of micrometers, scale (Fabes et al., 1993). The processing steps are involved in making sol-gel derived silica monoliths, namely: mixing, gelation, aging, drying, sintering.

3.6.3.1 Mixing

In method 1, a suspension of colloidal powders, or sol, is formed by mechanical mixing of colloidal particles in water at pH that prevents precipitation. In methods 2 and 3 a liquid alkoxides precursor, such as $Si(OR)_4$ where R is CH_3, C_2H_5 or C_3H_7, is hydrolyzed by mixing water (Hijon, Cabanas, Izquierdo-Barba, & Vallet-Regi, 2004). It is commonly asserted that the more attractive feature of sol-gel processing is the possibility of tailoring unique materials, especially, by polymerization of a metalorganic compound to a polymeric gel. The key is to design the proper monomer that will polymerise to form M-O-M structures. Metal alkoxides, $M(OR)_n$, fulfills these requirements, where M is the metal and R an alkyl radical. Popular choices used in the preparation of silica-based gels are

tetramethoxysilane, $Si(OCH_3)_4$, and tetraethoxysilane, $Si(OC_2H_5)_4$, known as TMOS and TEOS, respectively. The liquid alkoxide precursor $Si(OR)_4$ reacts with water and undergo hydrolysis and polycondensation reactions under the following scheme, in presence of a common solvent (normally alcohol)

Hydrolysis $$Si(OR)_4 + 4H_2O \rightarrow Si(OH)_4 + 4ROH \quad (8)$$

Condensation a) $$Si(OH)_4 + Si(OR)_4 \rightarrow 2SiO_2 + 4ROH \quad (9)$$

b) $$Si(OH)_4 + Si(OH)_4 \rightarrow 2SiO_2 + 4H_2O \quad (10)$$

which are produced simultaneously and generally incomplete, but the attainable final oxide is accomplished. The final result of the above reactions is a colloidal dispersion of extremely small particles (1-2 nm) that finally form a 3-D entangled network of the corresponding inorganic oxide. Hydrolysis and condensation can be accelerated or slowed down by employing appropriate acid or base catalyst. Depending on the amount of water present, hydrolysis may go to completion or stop while the metal is only partially hydrolysed. In the case where several different cations are used to form mixed-oxide networks, a complexation step may be required initially. When the alkoxide precursors have different hydrolysis rates (e.g. Al or Ti with regard to Si), a prehydrolysis of the alkoxysilane is preferred (Brinker et al., 1990; Hijon et al., 2004). After a complex sequence of polymerization, sol formation and gelation, a high surface area microporous gel constituted of small particles (≈ 2 nm), with a formula approximated by:

$$(MO)_x(M'O)_x(OH)_y(OR)_z$$

is formed. Radicals -OH and -OR account for reaction by-products that can reasonably easily leave the system yielding a complex three-dimensional oxide polymer -M-O-M'-O-M- which preconfigures the network of corresponding oxide glasses.

Subsequent processes such as aging, drying, stabilization, and densification all depend upon the gel structure. Since it is relative rates of hydrolysis Eq. (8) and

condensation Eq. (9) that determine the structure of the gel, it is essential to understand the kinetics of the hydrolysis and condensation reactions and the ratio of their rate constants (k_H/k_C).

Many factors influence the kinetics of hydrolysis and condensation, and the systems are considerably more complex than represented by the simplified Eqs. (8) and (9) (Orcel, Hench, Artaki, Jones, & Zerda, 1988). Yoldas et al. (1984) concluded that the hydrolysis and condensation reactions are not separated in time but take place simultaneously. The variables of major importance are temperature, nature and concentration of electrolyte (acid, base), nature of the solvent, and type of alkoxide precursor (Hijon et al., 2004).

3.5.3.2 Gelation

With the time the colloidal particles and condensed silica species link together to become a three-dimensional network. In this process the catalyst play an important role due to the ionic charge of the silica particles, with a direct influence on the polycondensation rate. Thus, at low pH for example, the silica particles bear very little ionic charge and thus can collide and aggregate into chains forming a polymeric gel, in other length scale this gel should be similar to a spaghetti dish. This effect is produced around the silica isoelectric point at pH=1.7 where the surface charge is zero. On the opposite side, at high pH, where the rate of dissolution is higher, the particles grow in average size and diminish in number as the smaller ones dissolve (positive curvature) and the silica is deposited upon the larger ones in such a case is formed a colloidal gel, as a visual picture this gel should be similar to a bean pot (Iler, 1979). As a direct consequence of the visual pictures outlined a lower density will be observed in the colloidal gels.

3.6.3.3 Aging

When a gel is maintained in its pore liquid, its structure and properties continue to change with time. This aging process occurs via three steps, polycondensation, syneresis and coarsening.

Polycondensation of unreacted hydroxyl groups increase the connectivity of the gel network, this process runs parallel with some shrinkage. Usually in alkoxide-based gels the chemical hydrolysis reaction is very rapid and is completed in the early stage of sol preparation, especially when the sol is acid catalyzed. For silica gels synthesized in alcoholic solutions, i.e., made by hydrolysis and condensation of alkoxides, nuclear magnetic resonance and Raman spectroscopies show that the number of bridging bonds increases long after gelation. The condensation reaction continues to occur because of the large concentration of silanol (SiOH) groups in a newly formed gel. As the hydroxyls are lost during aging, new bonds are formed, creating more cross-linked structures. Since the chemical reaction is faster at higher temperature, aging can be accelerated by hydrothermal treatment, which increases the rate of the condensation reaction (Hijon et al., 2004; Rosa-Fox et al., 2003).

Shrinkage of the gel and the resulting expulsion of liquid from the pores is called syneresis (Iler, 1979). Syneresis in alcoholic gel systems is generally attributed to formation of new bonds through condensation reactions, which increases the bridging bonds and causes contraction of the gel network. In aqueous gel systems, or colloidal gels, the structure is controlled by the balance between electrostatic repulsion and attractive van der Walls forces. Therefore, the extent of shrinkage is controlled by additions of electrolyte. The rate of contraction of silica gel during syneresis has a minimum at the isoelectric point (IEP). For silica this point is at a pH of 2, at which the silicate species are uncharged. Since the condensation is the slowest at that point, this suggests that the shrinkage is driven by the condensation reaction in Eq. (9).

Coarsening or ripening refers to a process of dissolution and reprecipitation driven by differences in solubility between surfaces with different radii of curvature (Iler, 1979). This process not produce shrinkage of the network but influence the strengthening of the gel and depends by factors that affect the solubility, such as temperature, pH, concentration and type of solvents (Brinker & Scherer 1985).

3.6.3.4 Drying

During drying the liquid is removed from the interconnected pore network. One of the main problems in the preparation of bulk materials is avoiding cracking of the gel during drying, due to the stress caused by the capillary forces associated the gas-liquid interfaces. Fractures are initiated if these stress differences are greater than the tensile strength of the material. The direct solution is to let the liquid evaporate at a very low rate. This strategy, although effective, is not practicable because of the long drying times required. These stress will cause the gels to crack catastrophically unless the drying process is controlled by decreasing the liquid surface energy by addition of surfactants or elimination of very small pores, by hypercritical evaporation, which avoids the solid-liquid interface, or by obtaining monodisperse pore sizes by controlling the rates of hydrolysis and condensation (Hijon et al., 2004).

Condensation reactions between unreacted hydroxy groups also continue to take place, resulting in further shrinkage. If the system is open, the solvent will evaporate. For coatings, the ratio of surface area to volume is so large that evaporation takes place extremely rapidly-sometimes instantaneously. At some point during evaporation, the outside surface of the gel dries out, and a meniscus forms within. The meniscus produces a capillary tension, P, given by

$$P = 2\Delta\gamma/r \tag{11}$$

where Δ_γ is the difference between the solid/vapor and solid/liquid surface energies and r is the radius of the pore.

A detailed model of the shrinkage caused by the capillary stresses during drying has been developed by Scherer (1987) who assumed that contraction is driven by the large differences in surface energies in the porous material, while the rate of contraction is limited by the viscosity of the solid phase and by the rate of transport of the liquid through the pores. Using this model, the capillary stress is more complicated than represented by Eq. (11). However Eq. (11) describes the maximum stress which develops in a drying material, and as such, is a guide to the stresses which must be tolerated by the drying gel. Once dried, coatings are seldom used in the porous state. Often they are fired (i) to burn out the residual carbon; (ii) to alter the chemistry of the coating (for example, to form Si_2N_2O coatings by reacting SiO_2, with NH_3); (iii) to densify the coating; (iv) to crystallize the coating; or to enact any combination of these.

The conversion from the dried gel to the final, desired state is often tricky, since competition between the various processes may require sequential completion of one process before another. On the other end of the process, if a dense, crystalline coating is desired, it is important to densify the coating before crystallization takes place, since the kinetics of densification of crystalline materials are typically orders of magnitude slower than those of the corresponding amorphous materials (Fabes et al., 1993).

3.6.3.5 Sintering

This is the process of the network densification, which is driven by interfacial energy. Solid network moves by viscous flow or diffusion to eliminate porosity. In gels with high pore surface areas the driving force is great enough to produce sintering at exceptionally low temperatures, where the transport process are relatively slow. Indeed, the kinetics of densification in gels is not simple because of the concurrent processes of dehydroxylation and structural relation. As an example, constant heating rate was used by Prassass, Phalippou, & Zarzycki, (1986) to study the sintering process in aerogels (70-90% porosity, 0.1-0.5 g/cm^3 density) and they conclude that several mechanisms evolved in such sintering process. Below 700°C

sintering is conducted by a diffusional process due to chemical reactions, while above 750°C begins the viscous flow mechanism and the activation energy of this process is related to the hydroxyl content.

3.6.4 Coatings via Sol-gel Processing

3.6.4.1. Coating Chemistry

Metal alkoxides (such as tetraethoxysilane, trimethylborate, and titanium ethoxide) and metal salts (such as barium carbonate, magnesium nitrate, and copper chloride) are the most commonly used starting materials for sol-gel processing of oxides. In large volume applications, considerations of cost usually make salts more attractive than alkoxides. Removal of the counter ions can sometimes be troublesome, however, so in applications sensitive to contamination, the alkoxides are often more attractive than the salts. All metals form alkoxides and they have the following general formula:

$$M(OR)_x$$

where M is the metal, R is an alkyl group, an x is the valance state of the metal. The physical properties of metal alkoxides can be varied by changing the alkyl group and for most metals soluble, and in some cases even liquid, products can be obtained.

There is also a limited class of compounds known as double alkoxides. These contain two different metals in the same compound and have the general formula:

$$M_x'M_y'' (OR)$$

where M' and M" are metals, R is an alkyl group and x and y are integers. When alkoxides are used as the starting materials, the formation of ceramic coatings is based on hydrolysis and condensation, as shown in Eqs. (12-14). In the first reaction Eq.(l2), an alkoxide and water are placed in a mutual solvent and a suitable catalyst

is added. Hydrolysis of the metal alkoxide bond (M-OR) results in the formation of a metal hydroxyl bond (M-OH), as shown in this reaction:

$$M(OR)_x + H_2O \leftrightarrow (RO)_{x-1}M\text{-}OH + ROH \quad (12)$$

$$(RO)_{x-1}M - OH + (RO)_x M \leftrightarrow (RO)_{x-1}M - O - M(RO)_{x-1} + ROH \quad (13)$$

$$(RO)_{x-1}M - OH + HO - M(OR)_{x-1} \leftrightarrow (RO)_{x-1}M - O - M(RO)_{x-1} + HOH \quad (14)$$

In the next step, condensation between the hydroxyl and an alkoxide ligand, or between two hydroxyl ligands, result is the formation of a metal-oxygen-metal bridge, which constitutes the backbone of any oxide ceramic structure. Continued condensation leads to an increase in the density of metal-oxygen-metal crosslinks until eventually gelation or precipitation occurs. In solution, the rates, extents, and even the mechanisms of the reactions are shown in Eqs. (12-14) are profoundly affected by the electronegativity of the metal, size of the alkyl ligand on the metal, solution pH, type and concentration of solvent, concentration of water, temperature, and pressure. Each, in turn, can affect the course of structure (hence property) development in the gels and ceramic materials made therefrom. The formation of multicomponent solutions adds further complexity. The goal often is to achieve homogeneous mixing of the components on the atomic scale; but different alkoxides do not, in general, have the same reactivities, hence mixing of different alkoxides with water usually results in preferred hydrolysis and condensation of one species over the others; the result is chemically inhomogeneous gels. Several techniques have been used successfully to increase the homogeneity of multicomponent gels (Yamane, Inoue, & Nakazawa, 1982). These include:

- matching the reaction rates of the alkoxides by increasing the size of the alkyl group on the faster reacting species and decreasing the size of the alkyl group on the slower reacting species;
- partially hydrolyzing the slower reacting species prior to mixing with the faster reacting alkoxide;

- adding water very slowly, so that the rate-limiting step is water addition and not alkoxide reactivity; and
- formation of so-called double alkoxides.

Historically, metal alkoxides have been employed in sol-gel process, which readily undergo catalyzed hydrolysis and condensation to form nanoscale oxide or hydroxide particles. Still in general, metal alkoxides are often used as raw materials in sol-gel process, but many of the alkoxides are very difficult to be obtained and dealt with because of the high sensitivity to the atmospheric moisture. In addition, when multi-component ceramics are to be prepared, the rate of alkoxide hydrolysis should be controlled, which is not very easy (Kodaira et al., 2003).

For some metals it is inconvenient to use alkoxides because of preparation problems or unavailability and alternative starting materials must be found. This is particularly the case with Group I and Group II elements whose alkoxides are solid, non-volatile and in many cases of low solubility; consequently, they are sometimes difficult to obtain pure. Metal salts are very useful, cheaper, very easy to handle than metal alkoxides, and hence are good alternatives if they are readily converted to oxides by thermal decomposition and can be solved in many kinds of organic solvents in which metal complexes are formed. In other words, the sol-gel process with metal salts can be realized by chelating the metal ions by organic ligands. The metal salts include chlorides, acetates, nitrates, sulfides and so on. Chlorides, nitrates and sulfides have high solubility in water or organic solvents. In some cases acetates have lower solubility in water or organic solvents than other metal salts. Nitrates are really the only suitable inorganic salts because others, such as chlorides or sulfates, are more thermally stable and the anion may be difficult to remove (Thomas, 1988). However, acetate ions can stabilize the metal ions in solutions through coordination by groups. If metal salts are just dissolved in water or organic solvents without chemical reaction like a chelating, they are re-crystallized on solvent evaporation. It is important how to stabilize the metal ions in solutions without coordination by anions like or many researchers have carried out the studies on formation of metal complexes with organic ligands. Furthermore, the metal complexes with organic

ligands have been used for preparation of ceramics and metal oxide thin films by sol-gel process, using metal salts like nitrates, chlorides, and acetates as the starting materials (Gash, Tillotson, Satcher, Hrubesh, & Simpson, 2001; Kodaira et al., 2003; Nishio & Tsuchiya, 2004; Ramanan, 2001). The normal method of sol-gel preparation using salts is first to form a solution of all components which are to be added as alkoxides, and then add one or more salts as solutions in alcohol or, if this is not possible, in the water that is to be used for further hydrolysis. All components are then uniformly dispersed and subsequent gelation should then freeze all elements in a gel network (Thomas, 1988). Sol-gel approaches can also be used to synthesize nonoxide materials. Sulfides, for example, can be made by reacting organometallic precursors with H_2S instead of H_2O to generate a sulfide based network.

3.6.4.2. Special Solution Chemistry

To be used for coating, solutions of partially polymerized alkoxides are usually applied to substrates after hydrolysis. In some cases, unhydrolyzed alkoxides can be applied to the substrates, and water from the atmosphere is used for hydrolysis. When prehydrolyzed solutions are used, it is important to recognize that the solutions are live, in that hydrolysis and condensation reactions continue to take place while the solutions age; solution viscosity, hydroxyl content, molecular weight, oligomer morphology, and other properties are evolving continuously. Thus there often (but not always) exists a particular window of aging times for which coatability is optimal. On the long time end, this window is usually bounded by the gelation time, at which the viscosity increases dramatically. On the short time end, the boundary is less well defined. In general, lightly crosslinked, linear polymer species are preferred for producing quality coatings, so some degree of hydrolysis and condensation are prerequisites to producing quality coatings (Butts, LaCourse, & Kim, 1988). Unfortunately, quantitative studies of the effects of olligomer morphology on coatability are scant. Depending on the application, coating solutions need to be stable (i.e. need to have a coatability window) between a few minutes, for exploratory use, up to a few weeks or months, for most commercial uses. Replacing

some of the alkoxy groups with non-hydrolizable ligands can also increase solution stability.

3.6.4.3 Application of Coating Techniques

One a suitably stable solution has been synthesized; sol-gel coatings can be applied by several techniques such as dip, spin, spray, or roller coating. In dip coating, the substrate is immersed into the coating solution, and a film is made either by removing the substrate from the solution or by draining the solution.In spin coating, an excess of coating material is placed on a stationary or slowly spinning substrate. The substrate is then rapidly accelerated to a few thousand RPM, producing a large centrifugal force which throws off all but a thin layer of material. In spray coating, the solution is forced through a nozzle by high pressure, forming an aerosol, which is accelerated toward the substrate with an inert carrier gas. The drops of solution then coalesce on the substrate to form the coating.

Finally, in roller coating, the coating solution is forced onto the substrate with a roller, which may or may not contact the substrate surface and which sometimes contains grooves to carry a reservoir of coating material (Fabes et al., 1985).

CHAPTER FOUR

CORROSION

4.1 Introduction

Corrosion, according to the ASM Materials Engineering Dictionary, is "the chemical or electrochemical reaction between a material, usually a metal, and its environment that produces a deterioration of the material and its properties." Because corrosion is related to the material and its environment, it occurs under an immense variety of conditions. The environment includes not only the gas atmospheres or liquid media in their actual composition surrounding the piece, but also temperature and its changes and specific conditions of flow. This means that corrosion is a materials behavior in a specific environment (Jehn, & Zielonka, 1994).

Corrosion is an inevitable, deteriorating reaction when metallic materials come in contact with an environment such as liquid, gaseous or combination thereof. The physiological solution (body fluid) is considered extremely corrosive to metallic materials and corrosion is one of the major processes that cause problems when metals and alloys are used as implants in the body (Kruger, 1979). Components of physiological environment have a significant role in corrosion of metallic materials. Therefore, the functionality of biomaterial devices in the body greatly depends on the chemistry of the biofluid surrounding the implant. Biofluids (physiological solution), inside tissue cells (intracellular fluid) or outside tissue cells (extracellular fluid) carry several organic and inorganic materials to the need of body. Extracellular fluids are of two types, blood and interstitial fluid. Other extracellular body fluids that occur in smaller amounts are urine, digestive juices, and cerebrospinal fluid. Chemically, blood (plasma) and interstitial fluid (including lymph) are similar while intracellular fluid is chemically different from the extracellular fluids. Body fluids are reported to be a complex and composed of salts, trace metals, amino acids, sugars, proteins, cells, etc. (Slack, 1997). These components of the body fluid produce anions such as chloride (Cl^-), phosphate

(PO_4^{-}), and bicarbonate (HCO_3^{-}) and cations such as potassium (K^{+}), sodium (Na^{+}), calcium (Ca^{+}), and magnesium (Mg^{+}). Body fluid is a buffer solution. The pH of the normal blood and interstitial fluid usually remains between 7.35-7.45, however, it may decrease to 5.2 during implantation in hard tissues, and should return to its normal pH within two weeks of time while the temperature remains about 37°C (Hanawa, 1999). The high Cl^{-} concentration among various anions is considered to accelerate corrosion of implants that can lead metal ion release and disturbances in trace metal ions. The latter can change the biochemical reactions and associated physiological pathologies. For instances, change in Fe contents can either lead to anemia (when it is in low dosage) or may damage the liver by high Fe dosages. In order to develop artificial body fluids, usually, those mineral components of the natural products are included that have shown effects on the processes (Singh, & Dahotre, 2007). The corrosion of metallic implants due to the body environment can affect the human life in different ways:

(i) it may release undesirable metal ions/corrosion products which are non-biocompatible,
(ii) it may reduce the life of implant device and therefore, may impose another costly and painful surgery, and ,
(iii) ultimately reduce the human life.

For instance, the corrosion of a stainless steel implant releases iron, chromium, and nickel ions; titanium and titanium alloy implants release titanium, vanadium, and aluminum ions; and Co-Cr implants are known to release chromium and cobalt ions (Bundy, 1994; Hallab, Jacobs, & Black, 2000; Singh, & Dahotre, 2007). The release of metal ions depends also on the success of the implant procedure and functioning. For example, patients with well-functioning Ti-alloy total joint replacement components had as much as a threefold increase in the concentration of Ti in their serum. In patients with a failed total joint Ti alloy components, there was as much as a 50-fold increase in serum Ti levels compared with controls without implants (Leopold et al., 2000). Dissolved metal ions can accumulate in tissues as well as near the implant or may be transported to other parts of the body. For

example, after 10-13 years of residence of 20 stainless steel Charnley hip arthroplasties in the human body, a significantly higher concentration of metallic species in body fluid was observed as compared to that without implant.

4.2 Electrochemical Nature of Corrosion

Corrosion of metals and alloys in aqueous solution or in any other ionically conducting medium takes place by an electrochemical mechanism. The electrochemical corrosion reaction requires four elements (ACME) (Fig. 4.1): anode (A), cathode (C), metallic conductor (M) and electrolytic conductor (E).

At the anode metallic ions leave the metal surface and go into solution. In this process it leaves electrons behind on the metal surface. Therefore the metal is oxidized (loss of electrons) at the anode (A). This process is corrosion. The anodic (corrosion) reaction can be written as Eq. (4.1):

$$M \rightarrow M^{n+} + ne^{-} \tag{4.1}$$

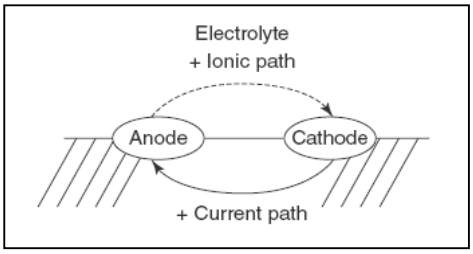

Figure 4.1 Four elements of corrosion process.

The metallic ions, or other reactive species or ions are carried from the anode to the cathode by the ionically-conducting electrolyte (E). Electrolytes are mostly liquids, but they may also be solids. If the electrolyte has more ions then it has higher conductivity and hence it is a beter electrolyte. There are two types of ions: anions and cations. Anions are negatively charged and they move towards the anode. Cations are positively charged and they move towards the cathode. The electrolyte may contain several species that could undergo reduction. The most

commonly occurring reduction reactions at the cathode are: hydrogen ion reduction (Eq.(4.2)) or oxygen reduction (Eq.(4.3)):

$$2H^+ + 2e^- \rightarrow H_2 \quad (4.2)$$

$$O_2 + 2H_2O + 4e^- \rightarrow 4OH^- \quad (4.3)$$

The electrons left by the metal ions at the anode site are carried to the cathodic site by the metallic conductor (M). In order for electrochemical corrosion to take place all four processes should occur simultaneously. Absence of any one of the four elements prevents corrosion from taking place. In the presence of all four elements a balance is established, so that the rate of anodic reaction (oxidation) is equal to that of cathodic reaction (reduction). Electrochemical polarization measurements are used to determine the rate of anodic or cathodic reactions individually or collectively (Papavinasam, 2008).

4.3 Implant Corrosion

Metallic biomaterials corrode in variety of ways including general and localized corrosion types. Extensive research (Fontana, & Greene, 1987; Grosgogeat, Reclaru, Lissac, & Dalard, 1999; Sherwin, Taylor, & Waterhouse, 1971) has been carried out on to understand the dominant forms of corrosion that biomaterials commonly experience and their implications to biological and mechanical functions of the human body. The types of corrosion that are pertinent to the currently used alloys are galvanic, pitting, crevice, intergranular, stress-corrosion cracking, corrosion fatigue and fretting corrosion.

4.3.1 Galvanic Corrosion

Galvanic or two metals corrosion takes place when two different metals are in physical contact in an ionic conducting fluid medium such as serum or interstitial fluid. The differential composition or process variables of a plate and the adjoining screws is responsible for the set-up of a galvanic couple, which results in galvanic

corrosion. Galvanic corrosion depend on a large number of complicating factors including the relative areas of electronic and ionic contact, as well as the actual metal pair involved. However, it is safe to assume that some galvanic corrosion will occur in any dissimilar metal pair in acidic pH. In many practical applications, the contact of dissimilar materials is unavoidable. In surgical implants, galvanic corrosion can occur if bone plate and bone screws are made of dissimilar metals or alloys. Corrosion is likely to occur between the plate and bottom side of the screw holes (Kamachi, Sridhar, & Raj, 2003).

4.3.2 Pitting Corrosion

Pitting is a severe form of localized corrosion attack that results in extensive damage and release of significant amounts of metal ions. Pitting refers to the formation of small cavities/holes at the surface of a material, which is protected otherwise by the presence of an adherent, tenacious and self-healing thin passive film. The formation of such pits is attributed to the interaction of certain aggressive ions with the film at locations where it is defective or weak in nature. The pits may be visible to the naked eye in some cases but in general they are invisible, and dangerous to the extent they can allow the formation of stress corrosion cracking (SCC) or fatigue cracks, which can catastrophically fail the components in service. The importance of pitting significantly depends on the nature of the surface layer or the film that has formed on the surface due to the interaction of the material with the environment.

Thus a state of “passivity” is forced on the material, which safeguards the material from general corrosion by slowing down the dissolution process at the surface (Kamachi et al., 2003). Pitting occurs when the anodic site becomes fixed on a small part of the surface due to a break in the passive layer, irregularities in the surface caused due to variations in the metal itself, incomplete coatings, scaling deposits that build up at selected areas, etc. The cathodic area can be anywhere outside the pit. This results in a high corrosion current density at the base of the pits. Movement of metal ions or HCl ions from the bottom of the pit is restricted by the

film covering the top of the pit (Fontana et al., 1987). The depletion of oxygen creates a difference in electrochemical potential between the pit and the surrounding metal. The formation and breakdown of passivity and the mechanism of pitting attack are shown in Figure 4.2. Once the pit is initiated, the metal ions form precipitates at the top of the pit and often form a film covering the pit. The film restricts entry of the solution and oxygen into the pit, and repassivates, which could renew the protection.

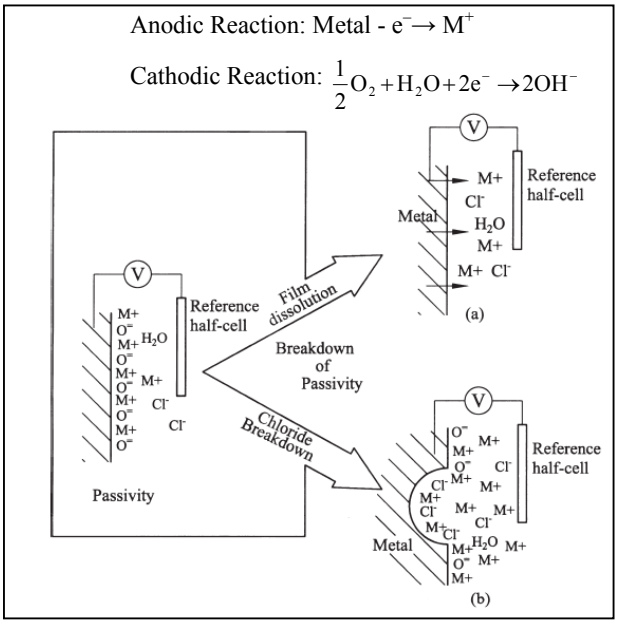

Figure 4.2 Two principles of breakdown passivity: (a) Metal undergoes general corrosion with film dissolution; (b) metal undergoes pitting corrosion.

The importance of assessing pitting corrosion resistance by determining pit propagation rate (PPR) curves is discussed by Kamachi, Dayal, Gnanamoorthy, & Rodriguez, (1996), which also reviews the conventional tests for pitting. These tests involve anodically polarizing the specimen to a breakdown potential E_b, at which pitting ensues. After the pitting potential if the scan is reversed in the opposite direction, a protection potential E_p, is reached where the reversed curve meets the passive range, and below which pits repassivate. In implants, pitting occurs most often on the underside of screw heads. This form of attack occurs more frequently in media containing chloride ions. It is well established that the resistance

to pitting in saline environment can be increased by molybdenum addition and keeping the inclusion contents to a minimum level (Kamachi et al., 2003).

4.3.3 Intergranular Corrosion

Intergranular corrosion is defined as the selective dissolution of grain boundaries, or closely adjacent regions, without appreciable attack of the grains themselves. This dissolution is caused by potential differences between the grain-boundary region and any precipitates, intermetallic phases, or impurities that form at the grain boundaries. The actual mechanism differs with each alloy system. Although a wide variety of alloy systems are susceptible to intergranular corrosion under very specific conditions, the majority of case histories reported in the literature have involved austenitic stainless steels and aluminum alloys and, to a lesser degree, some ferritic stainless steels and nickel-base alloys. Precipitates that form as a result of the exposure of metals at elevated temperatures (for example, during production, fabrication, and welding) often nucleate and grow preferentially at grain boundaries. If these precipitates are rich in alloying elements that are essential for corrosion resistance, the regions adjacent to the grain boundary are depleted of these elements. The metal is thus sensitized and is susceptible to intergranular attack in a corrosive environment. For example, in austenitic stainless steels such as AISI type 304, the cause of intergranular attack is the precipitation of chromium-rich carbides ($(Cr,Fe)_{23}C_6$) at grain boundaries. These chromium-rich precipitates are surrounded by metal that is depleted in chromium; therefore, they are more rapidly attacked at these zones than on undepleted metal surfaces. Impurities that segregate at grain boundaries may promote galvanic action in a corrosive environment by serving as anodic or cathodic sites. Therefore, this would affect the rate of the dissolution of the alloy matrix in the vicinity of the grain boundary. Susceptibility to intergranular corrosion in austenitic stainless steels can be avoided by controlling their carbon contents or by adding elements (titanium and niobium) whose carbides are more stable than those of chromium. For most austenitic stainless steels, restricting their carbon contents to 0.03% or less will prevent sensitization during welding and most heat treatment (Davis, 2001).

4.3.4 Stress-Corrosion Cracking

Stress-corrosion cracking (SCC) is a cracking phenomenon that occurs in susceptible alloys and is caused by the conjoint action of a surface tensile stress and the presence of a specific corrosive environment. For SCC to occur on an engineering structure, three conditions must be met simultaneously, namely, a specific crack-promoting environment must be present, the metallurgy of the material must be susceptible to SCC, and the tensile stresses must be above some threshold value. Stresses required to cause SCC are small, usually below the macroscopic yield stress. The stresses can be externally applied, but residual stresses often cause SCC failures. This cracking phenomenon is of particular importance to users of potentially susceptible structural alloys because SCC occurs under service conditions that can result, often with no warning, in catastrophic failure. There are two distinctive modes of crack propagation according to the path followed by the cracks depending on the metal-environment combination. Cracks are intergranular when they propagate along grain boundaries and are transgranular if they run across the grains, in some cases following preferential crystallographic planes (cleavage planes) (Davis, 2001).

4.3.5 Crevice Corrosion

Crevice corrosion is a form of corrosion, related to structural details. It occurs when a metal surface is partially shielded from the environment. It is usually encountered beneath the screw head that holds the plate or in similar locations such as the intersection of the components of two pieces, hip nail etc. The basic requirement for the occurrence of this process is the presence of a crevice, a narrow, deep crack: either an interface between parts of a device, such as between plate and screw head, or defects such as fatigue crack. Type 316L stainless steel is highly susceptible to crevice corrosion attack as compared to the other commonly used metallic implant material (Bates, 1973). The occurrence of corrosion on the bone plate and screws made of stainless steels especially in the area of contact between screw heads and the counter sinks hole is a common feature. The presence of crevice

corrosion in countersink portion of the bone plate can also induce crack propagation; though such type of crevice induced failures have been seldom identified. Crevice corrosion problem can often be eliminated by appropriate design of device and proper choice of the material (Kamachi et al., 2003).

4.3.6 Corrosion Fatigue

Corrosion fatigue is a fracture failure of metal that occurs because of the combined interaction of electrochemical reactions and cyclic loading. Corrosion fatigue resistance is an important factor of consideration for load-bearing surgical implant metals or for metals used in cyclic motion applications. Normally, a failure may not occur, but cracks can initiate from hidden imperfections, surface damage, minute flaws, chemical attack and other causes. The corrosive environment may result in local corrosive attack that accentuates the effect of the various imperfections. The corrosive attack will be influenced by solution type, solution pH, oxygen content and temperature. The body fluid environment may well decrease the fatigue strength of the implant. Fatigue striations are observed on the fractured surface of the device with colored “beach marks” are indicative of corrosion fatigue. The presence of corrosion pit or pits could induce the fatigue to develop. Failures of mechanical origin in orthopedic implants are most commonly due to fatigue or environmentally assisted fatigue. In some instances, however, the mechanism responsible for crack initiation and crack propagation may be different (Hu, Zhano, & Li, 1993). For example, it has been suggested that cracks could be initiated by fretting and propagated by stress-corrosion cracking (SCC). It is also possible that cracks could initiate because of corrosion phenomena and propagated mainly by a fatigue mechanism (Kamachi et al., 2003).

4.3.7 Fretting Corrosion

Fretting corrosion occurs when two opposing surfaces such as bone plates and the screwheads of the prosthetic devices rub each other continuously in an oscillating fashion in the body environment. It is the result of small relative movements

between the contacting surfaces in a corrosive medium. Even in the absence of corrosive medium, fretting can occur. Clinical significance of fretting attack lies in its intensity that may give rise to a large amount of corrosion products in adjacent tissues or it may be a major factor in crack initiation and fracture failure of an implant (Syrett, & Wing, 1978). Fretting corrosion at countersinks in plates and at hip nails may initiate corrosion fatigue, which occurs through screw hole. Quantification of weight loss of the implant due to fretting corrosion has been studied and was found to be directly proportional to the load transmitted across the surfaces, the number of cycle fretted and the amplitude of stresses. The weight loss has been reported to be inversely proportional to the hardness of the material and the frequency of stroke (Kamachi et al., 2003).

4.4 Electrochemical Methods of Corrosion Testing

The basis of all electrochemical techniques lies in the principle of mixed-potential theory, which was clearly established in a classic paper published in 1938. It was demonstrated that uniform corrosion occurs when anodic and cathodic reactions take place in constant change of location and time of the individual processes. In this concept, it is not necessary to postulate the presence of local anodes and cathodes for corrosion to occur. Nevertheless, in later years it has often been stated that corrosion occurs when local anodes and cathodes have been established, despite the obvious fact that, in this case, uniform corrosion is not possible.

The corrosion potential, E_{corr}, or open-circuit potential (OCP), is a mixed potential; that is, it is the unique potential at which the rates of the anodic and cathodic reaction are exactly equal. The rate of the anodic or the cathodic reaction at E_{corr} equals the corrosion rate. Because the rates of these two reactions are independent of each other, it is possible to inhibit corrosion by reducing the rate of only one of the two reactions by using, for example, anodic or cathodic corrosion inhibitors. Cathodic protection in which the material to be protected is polarized cathodically in order to reduce the rate of the anodic metal dissolution reaction is another example.

The concept of mixed-potential theory and its application in corrosion science and technology has been discussed in many textbooks. The use of mixed-potential theory for the monitoring of corrosion rates was also demonstrated by showing that the slope of a potential versus current density plot at E_{corr} can be used to determine the corrosion rate. Today, this technique is referred to as the polarization resistance technique or, less precisely, as the linear polarization technique. From this research, it also becomes clear that corrosion current densities, I_{corr}, can be obtained from the analysis of anodic and cathodic polarization curves, which is often referred to as Tafel extrapolation. This concept has been developed further. In addition, mechanistic information can be obtained by analysis of the Tafel slopes that have characteristic values, depending on the nature of the rate-determining step in the corrosion mechanism.

Electrochemical techniques available for laboratory studies of corrosion phenomena are summarized in Table 4.1. These techniques range from those in which no external signal is applied, such as E_{corr} and electrochemical noise analysis (ENA), to those in which only a small potential or current perturbation is applied, such as polarization resistance, R_p, and electrochemical impedance spectroscopy (EIS); to those in which the applied potential or current is varied over a wide range, such as anodic and cathodic polarization curves and pitting scans (Mansfeld, 2003).

Besides this classification of electrochemical test methods can be grouped as electrochemical tests are typically grouped as direct current (DC) or alternating current (AC) methods based on the type of perturbation signal that is applied in making the measurements. A number of investigators have used dc and ac electrochemical methods to study the performance and the quality of protective coatings, including passive films on metallic substrates, and to evaluate the effectiveness of various surface pretreatments. (Davis, 2001).

Table 4.1 Electrochemical techniques for corrosion studies

Category	Test method
No applied signal	Open circuit or corrosion potential
	Dissimilar metal corrosion (galvanic corrosion)
	Electrochemical noise analysis
Small-signal polarization	Polarization resistance (linear polarization)
	Electrochemical impedance spectroscopy
Large-signal polarization	Potentiostatic and galvanostatic polarization
	Potentiodynamic and galvanodynamic polarization
Scanning electrode techniques	Potential scans
	Current scans
	Electrochemical impedance spectroscopy scans
Miscellaneous tests	Hydrogen permeation
	Anodized aluminum corrosion test
	Electrolytic corrosion test
	Paint adhesion on a scribed surface
	Impedance test for anodized aluminum
	Critical pitting temperature

4.4.1 Electrochemical Methods for Orthopedic Materials

The mechanism of corrosion taking place in aqueous phase is electrochemical. Therefore a broad range of electrochemical techniques have been developed. The main advantages of electrochemical techniques include sensitivity to low corrosion rates, short experimental duration, and well established theoretical understanding. During electrochemical experiments specimens are polarized to accelerate the corrosion measurement process and the measurements are made within minutes or hours. Electrochemical measurements are used both in the laboratory and in the field. Commonly used electrochemical polarization techniques include polarization resistance methods, Tafel extrapolation methods, cyclic potentiodynamic methods, potentiostatic methods, galvanostatic methods, and galvanic current methods. The electrochemical polarization methods are used to monitor quantitatively general corrosion and galvanic corrosion. They can also be used qualitatively to monitor localized corrosion (pitting and crevice).

There are several methods by which the I-E relationship is established. These involve application of an electrochemical excitation to an electrode and measure the response of the electrode to that excitation. When the excitation is given, because the electrode moves away from the corrosion potential, the electrode is said to be polarized and hence these methods are called polarization methods of determining corrosion rates. If the potential of an electrode is controlled and the response of current is monitored then the method is called potentiostatic. If the potential of the electrode is varied at a constant rate and the response of the current is continuously monitored then the method is called potentiodynamic. On the other hand, if the current of an electrode is controlled and the response of the potential is monitored then the method is called galvanostatic. If the current of the electrode is varied at a constant rate and the response of the potential is continuously recorded then the method is called galvanodynamic.

Most electrochemical measurements are conducted by controlling the potential (potentiostatic or potentiodynamic) rather than by controlling the current (galvanostatic or galvanodynamic), because of the theoretical relationship between potential and energy. The most common electrochemical methods for determining general corrosion rates are polarization resistance (R_p) and Tafel extrapolation. In some studies very high values of potentials are applied and also the direction of the potential is reversed to study localized corrosion (cyclic potentiodynamic polarization). Characteristics of different electrochemical polarization techniques are presented in Table 4.2.

Table 4.2 Characteristics of different electrochemical polarization techniques

Polarization method	Typical measurement	Information obtained	Type of corrosion studied	Relevant standards
Polarization resistance	Application of ± 30 mV (typically ± 10 mV) around corrosion potential.	Corrosion current (I_{corr})	General corrosion	ASTM G3, ASTM G5, ASTM G59, ASTM G102
Tafel extrapolation	Application of an overpotential of +500 mV both in anodic and cathodic directions, from corrosion potential	Corrosion current (I_{corr}), and Tafel slopes (anodic and cathodic)	General corrosion	ASTM G5 ASTM G102
Cyclic potentiodynamic polarization	Application of overpotential from corrosion potential towards noble direction to a potential at which current is 5 mA, where the potential is reversed and scanned until hysteresis loop is completed or until corrosion potential is reached	Critical pitting potential, passive current, transpassive region	Pitting corrosion	ASTM G5, ASTM G61 ASTM G102
Cyclic galvanostatic polarization	Application of current steps (typically in 20μA/cm^2 Increments between 0 to 120μA) both in anodic and cathodic directions	Protection potential (E_{prot}) and breakpoint potential (E_b)	Pitting corrosion	ASTM G100
Potentiostatic polarization	Application of one potential step (typically to 700 mV vs SCE)	Change of current with a variable e.g., temperature (determination of critical pitting temperature)	Pitting corrosion	ASTM G150
	Application of potential step to a more positive potential (above E_b), and stepping it down to a less positive potential (below E_b)	Protection potential and breakpoint potential	Pitting corrosion	ASTM F746
Galvanic corrosion rate	Immersion of two dissimilar metals in an electrolyte and electrically connecting them using zeroresistance ammeter	Galvanic current	Galvanic corrosion	ASTM G71 and ASTM G82

4.4.2 Linear Polarization Resistance Method

About 50 years ago, Stern and Geary (1957) found that the slope of current-potential plot around the corrosion potential is essentially linear. The polarization resistance (R_p) of a material is defined as the slope of the potential-current density ($\Delta E/\Delta I$) curve at the free corrosion potential (Eq. (4.4)), which can be itself related to the corrosion current with the help of Eq. (4.5).

$$R_p = \left(\frac{\Delta E}{\Delta I}\right)_{Ecorr} \tag{4.4}$$

R_p is related to corrosion current (I_{corr}) as in Eq. (4.5):

$$R_p = \frac{B}{I_{corr}} \tag{4.5}$$

The constant B is defined in Eq. (4.6):

$$B = \frac{\beta_a \, \beta_c}{2.303 \, (\beta_a + \beta_c)} \tag{4.6}$$

where β_a and β_c are anodic and cathodic Tafel constants. By combining Equations (4.4)-(4.6), we obtain Eq. (4.7):

$$I_{corr} = \frac{1}{R_p}\left(\frac{\beta_a \, \beta_c}{2.303\,(\beta_a + \beta_c)}\right) \tag{4.7}$$

If β_a and β_c values are known, then the corrosion rate can be calculated from R_p. Because only a very small perturbation potential (less than ±30 mV, typically ±10 mV) is applied, this technique does not interfere with corrosion reactions. A typical polarization resistance plot is presented in Figure 4.3 (Stern et al., 1957).

From the slope, R_p (in ohms/cm^2 if the current density is plotted or in ohms if the current is plotted) is calculated. It should be noted that the I-E curve around corrosion potential may not be linear. Also, the curve in the anodic and cathodic regions may or may not be symmetrical. The symmetrical I-E curve is obtained only when both β_a and β_c are equal.

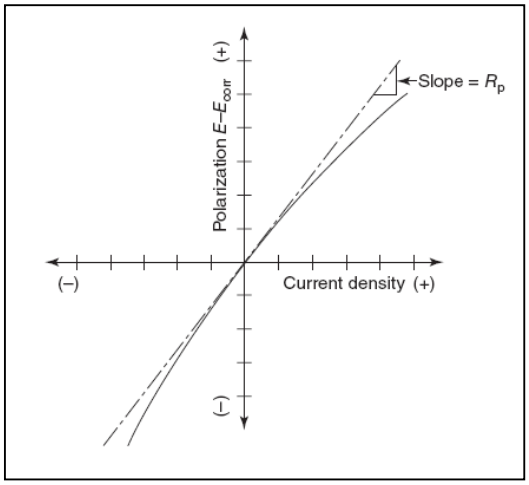

Figure 4.3 Hypothetical linear polarization resistance plot.

The advantages of the polarization resistance method include:

- The corrosion current is determined rapidly, typically within a few minutes and hence this technique can be used as an online monitoring technique.
- Only very small amounts of potential are applied (less than ±30 mV, typically less than ±10 mV), hence the corrosion rate is not affected due to measurements.
- This technique can be used to measure low corrosion rates (less than 2.5μm/yr).
- Measurements can be taken repeatedly.

On the other hand, there is error-producing complications related to the polarization resistance method and possible remedies are reported in the literature. The most common errors involve (1) invalidation of the results through oxidation of

some other electroactive species besides the corroding metal in question, (2) a change in the open-circuit or corrosion potential during the time taken to perform the measurement, (3) use of ΔE that is too large, invalidating the assumption of a linear relationship between I and E required by Eq. (4.4) and Eq. (4.5) (i.e., $\Delta E/\beta < 0.1$), (4) too fast a voltage scan rate or insufficient potential hold time, (5) ohmic solution resistance, and (6) current and potential distributions (Kelly, Scully, Shoesmith, & Buchheit, 2002).

4.4.3 Tafel Extrapolation Method

About 100 years ago, Tafel found that a linear relationship between E and logI exists if an electrode is polarized to sufficiently large potentials, both in anodic and cathodic directions. The regions in which such relationships exist are known as Tafel regions. Mathematically this relationship is given as Eq. (4.8):

$$I = I_{corr}\left[\exp\left\{\frac{2.303(E - E_{corr})}{\beta_a}\right\} - \exp\left\{\frac{2.303(E - E_{corr})}{\beta_c}\right\}\right] \tag{4.8}$$

Where I is the current, I_{corr} is the current at corrosion potential E_{corr}, E is the applied potential, E_{corr} is the corrosion potential, β_a and β_c are Tafel constants which are anodic and cathodic slopes of E-log i plots in the Tafel regions. Corroding metals that show Tafel behaviour when polarized will exhibit a plot similar to the one shown in Figure 4.4 (Papavinasam, 2008). The difference between E and E_{corr} is called overpotential, η. At sufficiently larger values of η (typically between 100 and 500 mV), in the anodic direction, i.e., η_a, Eq. (4.8) becomes Eq. (4.9):

$$\eta_a = \beta_a \log\frac{I}{I_{corr}} \tag{4.9}$$

Similarly at sufficiently large η_c (in the cathodic direction), Eq. (4.8) becomes Eq. (4.10):

$$\eta_c = -\beta_c \log \frac{I}{I_{corr}} \tag{4.10}$$

In cases where Tafel regions are observed, I_{corr} can be determined by the extrapolation of either anodic or cathodic or both Tafel regions to E_{corr}, as illustrated in Figure 4.4.

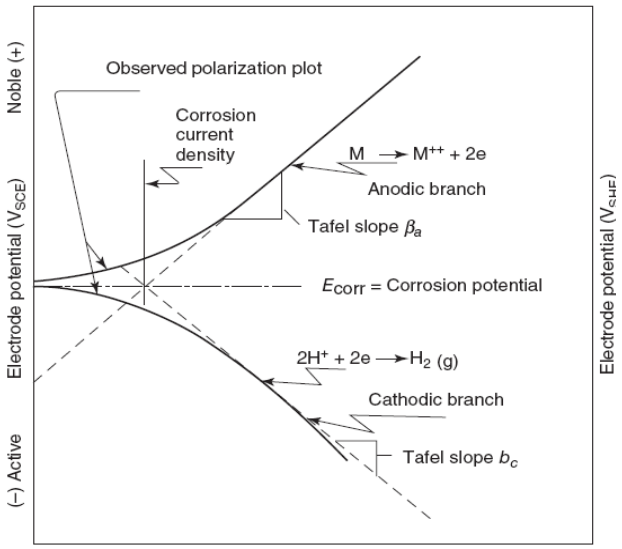

Figure 4.4 Hypothetical cathodic and anodic tafel polarization diagram.

Tafel extrapolation measurements can be performed either by the potentiodynamic method or by the step-wise potentiostatic polarization method. As in R_p measurements, in both methods corrosion potential is first measured, typically for one hour (during which time corrosion potentials of most electrodes are stabilized) or until it stabilizes. After that, the potential step -at increments of ±25 or ±50 or ±100 mV, every 5 minutes, recording the current at the end of each 5-minute period - is applied (potential-step method) or the potential is scanned at a constant rate (typically 0.6 V/h) (potentiodynamic method). In both methods, the experiment is started at the corrosion potential and the cathodic polarization is first conducted by applying an overpotential of approximately 500 mV or until gas (e.g., hydrogen) evaluation occurs at the electrode, at a constant rate of 0.6 V/h. After that the corrosion potential is measured again (typically for an hour), and then

anodic polarization is conducted by applying an overpotential so that the potential at the end of the anodic polarization is ±1.6 V vs SCE. Tafel plots are generated by plotting both anodic and cathodic data in a semi-log paper as E-logI. From the plot, three values are determined: the anodic Tafel slope, the cathodic Tafel slope and I_{corr} (from back-extrapolation of both anodic and cathode curves to E_{corr}) (Papavinasam, 2008).

4.4.4 Cyclic Potentiodynamic Polarization

The cyclic potentiodynamic polarization method is used qualitatively to understand the pitting corrosion tendency of metals and alloys. In this method the potential is scanned in the noble direction, monitoring the current continuously until it reaches 5 mA, at which point, the scan direction is reversed (i.e., scanned in the active direction), until the hysteresis loop closes or until the corrosion potential is reached. The results are plotted as E-logI, as in the Tafel extrapolation method. Some other parameters that can be determined from the potentiodynamic polarization curves (Figure 4.5) are the primary passivation potential (E_{pp}, potential positive to which passive surface layers are formed), the critical current density (I_{cc}, minimum current required before surface layers are formed), the breakdown potential (E_b, potential positive to which passive surface layer is destroyed and transpassive region starts), the protection potential (E_{prot}, potential at which passive layers are stable and protective), passive current (I_p, current of the electrode in E_{prot}) and the area of the hysteresis loop. Many of these parameters determined are based on empirical observations.

4.4.5 Electrochemical Impedance Spectroscopy

The use of Electrochemical Impedance Spectroscopy (EIS) to study the corrosion has been broadened significantly since it was introduced by Epelboin and coworkers**.** It has been proven to be a powerful and accurate method for detecting coating delamination, corroded area under coatings. EIS uses small periodic signals to perturb an electrode surface and measure an electrochemical response that can be

analyzed to gain information on corrosion mechanism and kinetics (Kelly et al., 2002).

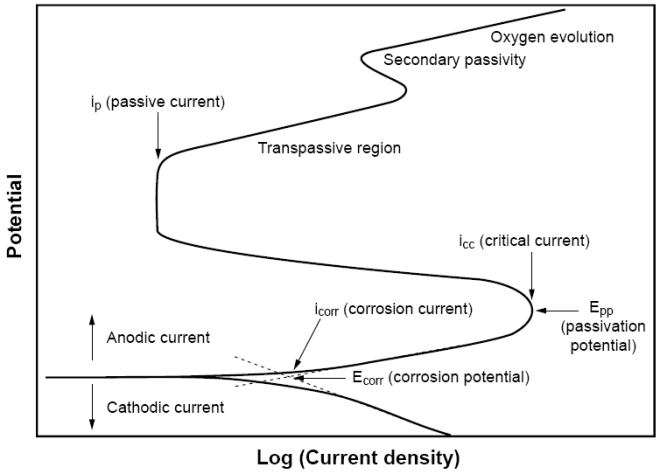

Figure 4.5 Hypothetical cathodic and anodic polarization plots for determining localized corrosion parameters.

The response can be analyzed by transfer functions due to an applied small-amplitude potential excitation at varying signals or sweep rates. In turn, the potential excitation yield current response and vice verse (Perez, 2004). EIS data are recorded as a function of frequency of an applied alternating current (AC) signal at a fixed working point (E, I) of a polarization curve. In corrosion studies, this working point is often E_{corr} ($E = E_{corr}$, $I = 0$) (Mansfeld, 2003).

In these experiments, a three-electrode cell is used in the conventional manner, and the potential program imposed on the working electrode is a dc mean value, E_{DC}, which is scanned slowly with time, plus a sinusoidal component, E_{AC}, of perhaps 5mV peak-to-peak amplitude. The measured responses are the magnitude of the AC component of the current at the frequency of E_{AC} and its phase angle with respect to E_{AC}. (Bard, & Faulkner, 2001).

EIS has been explored as an alternative proof test for evaluation of conversion coatings. In these tests, conversion coated surfaces are exposed to an aggressive electrolyte for some period of time during which coating damage will accumulate.

An impedance spectrum is collected and evaluated using a suitable equivalent circuit model and complex nonlinear least-squares fitting (Kelly et al., 2002). Information obtained with EIS differs from that determined with other techniques previously described, because the corrosion system is analyzed at a fixed potential (or current) (Mansfeld, 2003). Besides this, EIS has advantages for evaluations of conversion coatings. First, it is a small-signal technique, and the electrode is never polarized very far away from its corrosion potential as the measurement is made. Second, application of small signal making it is a nondestructive technique. Third, EIS can be very quantitative as it yields both kinetic and mechanistic information about the corrosion process taking place on the sample.

Ohm's law can be viwed in two different current imposition cases as per ASTM G-106 standart testing method. Hence,

$$E = I\,R \qquad \text{For DC, } f = 0 \text{ Hz}$$

$$E = I\,|Z(\omega)| \qquad \text{For AC, } f \neq 0 \text{ Hz}$$

Here, $|Z(\omega)|$ is the magnitude of the impedance containing elements of an equivalent circuit, such as capacitors and inductors. Capacitors oppose or impede the current flow. In modeling an electrochemical system as an electrochemical circuit, a potential waveform is applied across the circuit and a current response to the frequency signal generates impedance data. Thus, the impedance data is related to a phase shift angle and a variation in potential and current amplitudes (Perez, 2004).

The potential excitation and its current response are schematically shown in Figure 4.6. as sinusoidal excitations. The EIS method is conducted according to the ASTM G-106 standard practice, in which a range of small amplitude sinusoidal potential perturbation is applied to the electrode/solution interface at discrete frequencies. Typically a small amplitude sinusoidal potential, usually a voltage between 5 and 50 mV, perturbation is applied to the working electrode over a range of frequencies from 0.001 to 100,000 Hz (Kelly et al., 2002).

These frequencies cause an out of phase current response with respect to the applied sinusoidal potential waveform (Perez, 2004). At each one of these discrete frequencies, the resulting current waveform will exhibit a sinusoidal response that is out of phase with the applied potential signal by an amount depending upon the circuit parameters of the corroding interface and has current amplitude that is inversely proportional to the impedance of interface (Kelly et al., 2002).

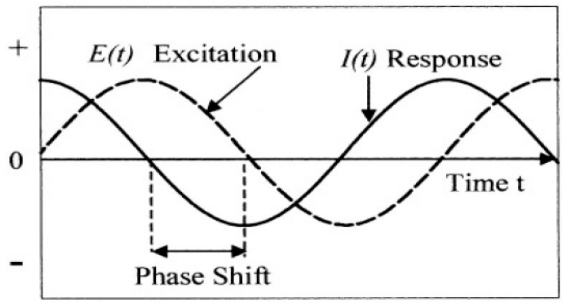

Figure 4.6 Schematic sinusoidal potential excitation.

If a sinusoidal potential excitation is applied to the electrode/solution interface, the potential, current and impedance can be predicted as per Barn and Faulkner mathematical models (1980). Thus,

$$Z(\omega) = \frac{E(t)}{I(t)} = \frac{E_o \sin(\omega t)}{I_o \sin(\omega t + \theta)} \tag{4.11}$$

Where E_o, I_o = constants, E(t) = the time-varying voltage across the circuit, I(t) = the time-varying current density through the circuit, θ = phase shift angle between E(t) and I(t), Z(ω) = the impedance (ohm-cm^2), ω = 2πf, and t = time (s) (Kelly et al., 2002; Perez, 2004).

This electrochemical impedance, *Z*(ω), is the frequency-dependent proportionality factor that acts as a transfer function by establishing a relationship between the excitation voltage signal and the current response of the electrochemical system *Z*(ω) is complex-valued vector quantity with real and imaginary components whose values are frequently dependent:

$$Z(\omega)= Z'(\omega) + j\, Z''(\omega) \tag{4.12}$$

where $Z'(\omega)$ = the real component of impedance, $Z'(\omega) = |Z(\omega)|\cos(\theta)$, $Z''(\omega)$ = the imaginary component of impedance where $Z''(\omega) = |Z(\omega)|\sin(\theta)$, j^2 = the square of the imaginary number, or -1, The magnitude of impedance is

$$|Z(\omega)| = ((Z'(\omega)^2 - Z''(\omega)^2)^{1/2} \tag{4.13}$$

and the phase shift angle is defined as

$$\theta = \tan^{-1} Z''(\omega)/Z'(\omega) \tag{4.14}$$

An example of an impedance $Z(\omega)$ vector with real and imaginary (capacitive) components is shown in the complex plane plot in Figure 4.7. The impedance vector indicated changes as a function of ω and is illustrated at a single frequency here. Experimental impedance spectra can be displayed by using Bode and Nyquist plots. Nyquistic plot is derived by using linear coordinates in complex plane plots in which the negative value of the imaginary impedance (-Z″) is plotted versus the real part (Z′). Notice that in this plot the Y-axis is negative and that each point on the Nyquist Plot is the impedance at one frequency.

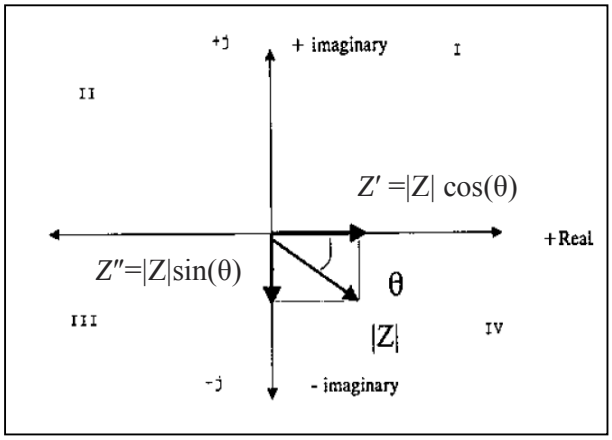

Figure 4.7 Cartesian coordinate system with imaginary j notation depicting an impedance vector |Z| and its real and imaginary components Z' and Z'' as well as phase angle θ.

At each frequency, the magnitude of the complex impedance is equal to the length of the vector drawn to the point from the plot origin. The phase angle is defined as the angle the impedance magnitude vector makes with the real axis (Kelly et al., 2002). Figure 4.8 has been annotated to show that low frequency data are on the right side of the plot and higher frequencies are on the left (Gamry, 2008). The preferred another format for display of EIS data is the Bode plot in which log |Z| and the phase angle (θ) are plotted versus the logarithm of the frequency (f) of the applied signal, with |Z| being the modulus of the impedance (Mansfeld, 2003). Nyquist, or complex plane plots, may be used to indicate the presence of diffusion process occurring in the coating system (Metroke, Gandhi, Apblett, 2004).

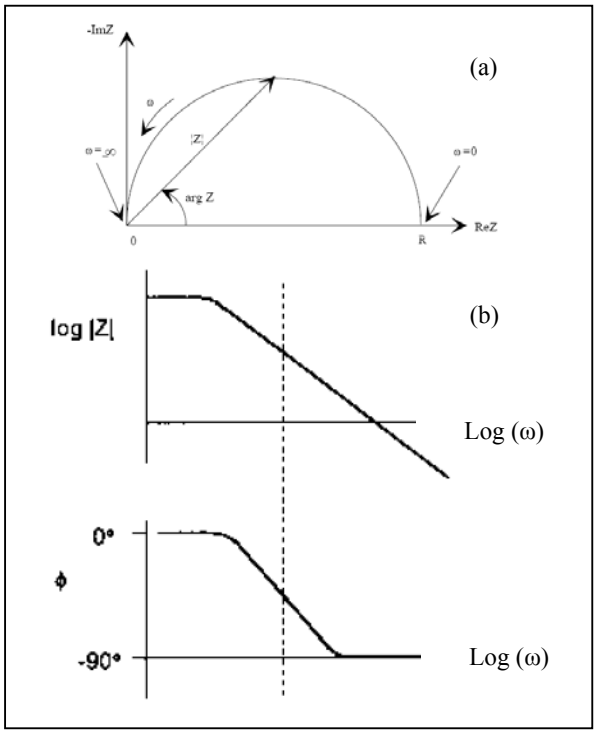

Figure 4.8 Common graphical representations of EIS data in corrosion studies. (a) Complex plane plot, (b) Bode magnitude and Bode phase angle plots.

4.4.5.1 Equivalent Circuit of a Cell

The electrochemical impedance is fundamental characteristic of the electrochemical system it describes. Corrosion and degradation of both bare and coated metals can be investigated. This technique is especially suited for coated metals because the coating acts as a capacitor and is amenable to AC but not to DC techniques. Knowledge of the frequency dependence of impedance for a corroding system enables a determination of an appropriate equivalent electrical circuit describing that system.

Such a circuit is typically constructed from resistor and capacitors. Table 4.3 shows the transfer functions for resistors, capacitors, and inductors (Kelly et al., 2002). The typical models for a coated metal are shown in Figure 4.9. An equivalent circuit model usually consists of R_Ω, R_p and C_c that characterize the solution resistance, coating resistance (or pore resistance), and coating capacitance, respectively.

Table 4.3 Linear circuit elements commonly used in electrochemical impedance

Circuit component	Impedance
Resistor (R)	$Z(\omega)=R$
Capacitor (C)	$Z(\omega)= 1/j\omega C$
Inductor (L)	$Z(\omega)= j\omega L$

The Z1 component in the general model in many systems consists of a capacitance that characterizes the double layer behavior and a resistance that reflects the charge transfer resistance (or polarization resistance). In the case that diffusion through the coating is of concern, the Z1 component can be characterized with the charge transfer resistance and Warburg impedance. Notice that and are connected in series.

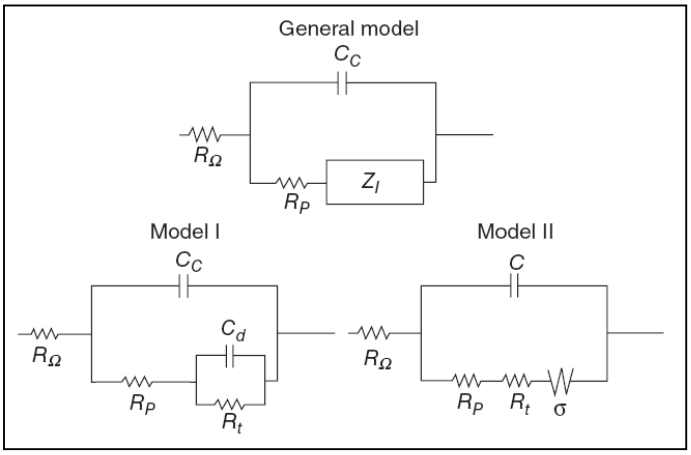

Figure 4.9 Typical equivalent circuit models for coating.

Much information can be obtained by carefully fitting the EIS data to a meaningful equivalent circuit model, such as coating capacitance, pore resistance (coating resistance), double layer capacitance and charge transfer resistance (polarization resistance). These parameters can be related to the coating performance, such as delamination area and corroded area under coating, for many coating systems. Coating capacitance depends on the thickness of the coating (d) and the total sample area (A) that was tested:

$$C_c = \frac{\varepsilon\varepsilon_o A}{d} \tag{4.15}$$

where ε and ε_o are the coating dielectric constant and the free space dielectric constant, respectively. Thus, by monitoring the change in the coating capacitance, it is possible to monitor possible water uptake in a coating system. This is an essential step to evaluate the coating performance because water uptake would subsequently cause the loss of adhesion at the coating-metal interface.

Coating resistance is usually influenced by the presence of defects and conductivity through the pores. Frequently, coating resistance was observed to decrease as the exposure time increased (Mansfeld, 1995). The coating resistance was related to the delamination area:

$$R_p = \frac{R_p^o}{A_d} \tag{4.16}$$

where $R_p^o = \rho.d\,(\text{ohm-cm}^2)$ and A_d is the delamination area. The coating resistivity (ρ) and the coating thickness (d) were assumed to be constant during the exposure. Thus caution should be taken when water uptake in the coating resulted in the change in the coating thickness.

After the electrolyte is absorbed by the coating and the metal/coating interface penetrated, a double layer forms and corrosion is initiated. As a result, the double layer capacitance is increased from zero and can be related to the disbonded area (A_d):

$$C_d = C_d^o A_d \tag{4.17}$$

where C_d^o is the area specific capacitance that can be determined from bare metal with known area in a simulated under film solution. Using Eq. (4.17), the disbonded area could be determined from double layer capacitance. The double layer capacitance has been used by people to calculate the corroded area or delaminated area under coatings (Bonora, Deflorian, & Fedrizzi, 1996; Deflorian, Fedrizzi, & Bonora, 1993).

Charge transfer resistance R_t (polarization resistance) describes the electrochemical processes taking place at the metal/coating interface. Similar to the polarization resistance determined via DC electrochemical techniques, such as the linear polarization resistance (LPR) method, a corrosion rate could be obtained but this rate corresponds with the undercoating corrosion (Amirudin, & Thierry, 1995).

4.4.5.2 Randles Cell

The Randles cell is a simple, yet useful combination of a capacitor and two resistors (Figure 4.10). This electrical circuit can be used to represent a coating or a corroding metal, although the values and meanings of the components are different. When this equivalent circuit model is applied to a coating immersed in an electrolyte, R1 represents the resistance of the electrolyte solution between the reference electrode tip and the surface of the coating.

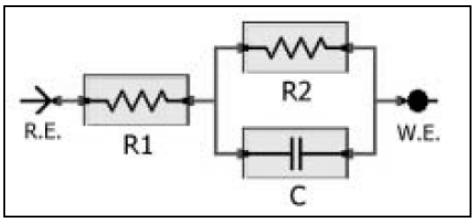

Figure 4.10 The randless cell equivalent circuit.

The capacitor, C, represents the coating and can be characterized by the thickness and dielectric constant of the coating material. It is associated the resistor, R2, with the resistance of the coating. It is also a property of the material of the coating and varies with the thickness and composition of the coating. The same equivalent circuit can also be applied to a bare, corroding metal in an electrolyte solution. Once again, R1 is associated with the electrolyte resistance (R_{sol}). However, in this system, the capacitor, C, is associated with the double layer capacitance (C_{dl}) of the metal/electrolyte interface. In this application, the resistor R2 is the Polarization Resistance, R_p (Loveday, Peterson, & Rodgers, 2004).

Following expression describes for impedance of the actively corroding metal system:

$$Z(\omega) = R_{sol} + \frac{R_p}{(1+\omega^2 R_p C_{dl}^2)} - \frac{j\omega C_{dl} R_p^2}{(1+\omega^2 R_p C_{dl}^2)} \tag{4.18}$$

It can be seen that at very low frequencies,

$$Z_{\omega \to 0}(\omega) = R_{sol} + R_p \tag{4.19}$$

While at very high frequencies,

$$Z_{\omega \to \infty}(\omega) = R_{sol} \tag{4.20}$$

Combining eqs. (4.19) and (4.20) yield the polarization resistance as

$$R_p = Z_{\omega \to 0}(\omega) - R_{sol} = Z_{\omega \to 0}(\omega) - Z_{\omega \to \infty}(\omega) \tag{4.21}$$

which is the sought output in electrochemical impedance measurements.

The nondestructive nature of EIS has made it one of the most frequently used electrochemical techniques for corrosion performance evaluation of coating systems. As discussed, the parameters determined from impedance data can generally be related to the coating performance, characterized by water uptake, delaminated or disbonded area, and corroded area under coating. However, caution needs to be taken when using EIS simply because much information could be obtained from a single measurement (Papavinasam, 2008).

CHAPTER FIVE

EXPERIMENTAL STUDY

5.1 Materials

316L stainless steel (SS) was selected as the substrate material (Sandvick) with surface area of 2 cm^2. Substrates were abraded in series with 220, 400, 600, 1000 and 1200 SiC paper and polished with the 5 μm diamond paste in order to obtain scratch-free mirror-finish surface. The polished specimens were washed with acetone in an ultrasonic cleaner for 10 min.

5.1.1 Surface Modification of the 316L SS Substrates

In order to obtain coating with homogeneous structure surface modification was performed to the substrates prior to coating process. Applied surface modification techniques are named as formation of CaP seeds by cathodic polarization, alkali or acid treatment. Modification processes are given in detail as follows.

5.1.1.1 Cathodic Polarization Process for Surface Modification

316L SS substrate surface was modified electrochemically in order to provide the surface with uniform primer CaP layer promoting subsequent growth of coating. Therefore, substrate surface was seeded with crystalline CaP compounds by cathodic polarization. Polarization was carried out by using Gamry's potentiostat P4/750 under galvanostatic and pulse current mode. Test solution was prepared by dissolving 42 mM $Ca(NO_3)_2.4H_2O$ and 25 mM $NH_4H_2PO_4$ in distilled water at 50°C to give a Ca/P ratio of 1.67.

Conditions set for galvanostatic and pulse-current mode used to nucleate crystalline CaP compounds on the surface are given in Table 5.1 and Table 5.2, GM and PM at these tables indicate galvanostatically and pulse modified surfaces,

respectively. Forms of the currents for galvanostatic and pulse electrodeposition are given in Figure 5.1 and Figure 5.2.

Table 5.1 Galvanostatic process parameters used to deposit CaP based compound for surface modification

Process	GM1	GM2	GM3
Current (mA)	-10	-10	-20
Time (s)	10	30	30

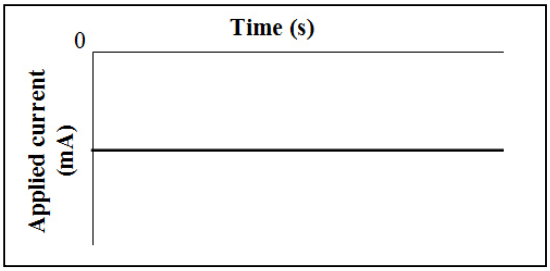

Figure 5.1 Current versus time relation of galvanostatic electrodeposition technique.

Pulse deposition refers to deposition where the potential or current density is altered rapidly between two different values. This is accomplished with series of pulses of equal amplitude, duration and polarity. Duty cycle is defined as the ratio of the t_1 time to the total time (t_1+ t_2) (Eq. 5.1) (Ghaemi, & Binder, 2002; Murali, 2007). In the study, puls deposition was performed at 50% duty cycle and 10 hertz frequency.

$$\text{duty cycle} = \frac{t_1}{t_1 + t_2} \text{x} 100\% \qquad (5.1)$$

Table 5.2 Pulse process parameters used to deposit CaP based compound for surface modification

Process	PM1	PM2	PM3
Current (mA)	-5/-15	-5/-15	-5/-15
Time (s)	5	10	30

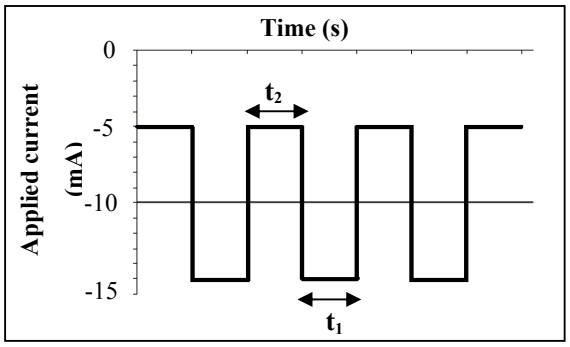

Figure 5.2 Current versus time relation of puls electrodeposition technique.

5.1.1.2 Surface Modification by Alkali Treatment

The aim of alkali treatment is to form a bond layer rich in functional ions, namely OH^-, to promote crystal nuclei and enhance crystal growth between the metallic substrate and HAP layer. Alkali treatment was performed by soaking 316L SS substrates in 10M NaOH aqueous solution at 60°C for 24 h. After the alkali treatment, the substrates were gently washed with distilled water and dried at 40°C for 24h in an air atmosphere. The alkali treated substrates were then heated to 500-700°C at a rate of 5°C/min in tube furnace, kept at a set temperature for 1 h, and cooled to room temperature in the furnace. Abbreviated names of the alkali treated samples via alkali treatment were summarized in Table 5.3 (AT1, AT2, AT3 and AT4).

Table 5.3 Surface modified stainless steel substrates with 10M NaOH alkali treatment

Batch temperature/ Duration time	Drying Process	Heat treatment	Process No
10 M NaOH 60°C, 24h	40°C, 24 h	no heat treatment	AT1
		0→500°C at a rate of 5°C/min and kept 500°C 1h	AT2
		0→600°C at a rate of 5°C/min and kept 600°C 1h	AT3
		0→700°C at a rate of 5°C/min and kept 700°C 1h	AT4

5.1.1.3 Surface Modification by Acid Treatment

Different kinds of surface treatments for stainless steels have been developed to increase the corrosion resistance. The primary aim of the surface treatments is to enhance the protective passive film changing composition, structure and thickness and reducing weak points such as non metallic inclusions. Nitric acid based solutions have been widely used as the passivating solutions (Thamaraiselvi, & Rajeswari, 2005).

In the study, the entire sample surface was subjected to surface treatments by complete immersion in volume concentrations of 40% of nitric acid (HNO_3) for 1h. According to the Kannan, Balamurugan, & Rajeswari, (2005) studies, this concentration shows optimum corrosion resistance. It is particular to note that all immersions were carried out at room temperature with no effort taken to prevent the atmospheric activities. Following acid treatment, the samples were washed with running distilled water and dried at 50°C for 30 min. Acid treated substrate was marked as ACT.

5.2 Solution Preparation and Coating Production

5.2.1 Solution Preparation

The sol-gel method offers a molecular-level mixing of the calcium and phosphorus precursors, which is capable of improving chemical homogeneity of the resulting HAP (hydroxyapatite) to a significant extent. Calcium (Ca) and phosphorous (P) based precursors are used for sol-gel HAP synthesis in recent years. For phosphorous precursors, triethylphosphate and triethylphosphite are major precursors among them. But, the activity of the triethylphosphate to hydrolyze is relatively poor and a higher solution temperature together with a prolonged time period (of several days) is needed to form the HAP phase. Because of this reason, triethylphosphite ($C_6H_{15}O_3P$) is chosen as a phosphorous precursor that offers a much higher activity for hydrolysis.

On the other hand, calcium nitrate or different calcium alkoxides were used as calcium precursors. The major limitation for calcium alkoxide applications was found to be the very low solubility of them in the organic solvents and their low reactivity which caused deviations from the stoichiometry of the final materials. Thus, calcium nitrate ($Ca(NO_3)_2.4H_2O$) was used as a calcium precursor (Beganskiene, Bogdanoviciene, & Kareiva, 2006).

Beside this, another important factor for sol preparation is the mixing rate of the calcium and the phosphorous precursors. Fast mixing calcium nitrate in triehyl phosphite has to be done drop by drop, otherwise chemical inhomogenity takes place due to the precipitation. Slow titration and diluted solutions must be used to improve chemical homogeneity and stoichiometry of the resulting HAP. Careful control of the solution condition is critical in the wet precipitation (Balamurugan, Kannan, & Rajeswari, 2004; Liu, Troczynski, & Tseng, 2001).

In the study, in order to synthesize HAP by using wet chemical technique called sol-gel, phosphorous and calcium precursors are used with specific amounts to obtain the stoichiometric Ca/P ratio (1.67) of HAP. Distilled water and ethanol (C_2H_5OH) were used as solvents of the triethylphosphate and calcium nitrate, respectively. Triethylphosphite (Fluka) sol was diluted in distilled water then hydrolyzed for 24 hours in a sealed container under vigorous stirring with magnetic stirrer. Initially the mixture was opaque, because of the immiscibility between the phosphate and water, light being scattered emulsion phase. But after approximately 30 min of mixing, the emulsion phase transformed into a clear solution. Stoichiometric amount (to maintain molar ratio of Ca/P=1.67) of 4M calcium nitrate (Merck) dissolved in ethanol, was subsequently added dropwise into hydrolyzed phosphorous sol. Vigorous stirring continued for additional 20 minutes after titration. As a result of this process, a clear solution was obtained and aged at ambient temperature for periods of 0h, 12h, 24h, 36h and 48h. Then surface treated samples were dip coated in aged solution. Coatings were firstly dried at 80°C for 1 hour and subsequently heated at 500°C for 1 hour. Coatings synthesized by using sol solutions of varying aging times are called as A0, A12, A24, A36 and A48 with respect to the increasing

aging times from the no aging to 48h aging. Coatings thus are obtained given in Table 5.4 according to the substrate condition and sol solution aging parameters. Coating process was also carried out on unmodified stainless steels substrate by using gel solutions with various aging conditions. Production flow chart of the coating synthesis method is given step by step in Figure 5.3.

Additionally, stainless steel substrates modified with alkali treatment (AT1, AT2, AT3 and AT4) and acid treatment (ACT) were coated by using 24h aged sol solution, in accordance with the results of the optimum aging time determination studies. XRD results and surface morphologies were used to optimize the coating characteristic in term of porosity and cracks in the film and crystallinities of the HAP coatings. These coatings are named as A24-AT1, A24-AT2, A24-AT3 and A24-AT4. Similarly, acid treated sample was named as A24-ACT.

Table 5.4 Preparation of the coatings with respect to the aging time of the sol and substrates surface condition

Solution Aging Time (Process Name)	**Types of surface modification**	**Process No**
0h (A0)	Seeded substrate with GM1	A0-GM1
	Seeded substrate with GM2	A0-GM2
	Seeded substrate with GM3	A0-GM3
12h (A12)	Seeded substrate with GM1	A12-GM1
	Seeded substrate with GM2	A12-GM2
	Seeded substrate with GM3	A12-GM3
24h (A24)	Seeded substrate with GM1	A24-GM1
	Seeded substrate with GM2	A24-GM2
	Seeded substrate with GM3	A24-GM3
36h (A36)	Seeded substrate with GM1	A36-GM1
	Seeded substrate with GM2	A36-GM2
	Seeded substrate with GM3	A36-GM3
48h (A48)	Seeded substrate with GM1	A48-GM1
	Seeded substrate with GM2	A48-GM2
	Seeded substrate with GM3	A48-GM3

Morphology and the composition of the thin films can be relatively easy to be controlled by sol-gel processing parameters such as starting pH of the sol, annealing for crystallization temperature and addition of auxiliary chemical reagents (Stan, & Ferreira, 2006; You, Oh, & Kim, 2001).

pH adjustment of the sol solution was carried out in order to improve the gelation of the sol solution. The preparation procedure of sol solution was identical to that of described above. Ammonia solution (28% NH_3, Merck) as a basic catalyst was added to the transparent sol solution a mounting to 3% and 7% volume fraction ratio. Sol solutions were aged for 24h at ambient temperature following stirring process for 30 min with magnetic stirrer. Coating produced with sol solution that contains 3% and 7% volume fraction ammonia is named as PH1 and PH2, respectively. Then, substrate surface-modified by via pulse electrodeposition technique (PM1, PM2 and PM3) was coated with ammonia-catalyzed sol solution marked as PH1 and PH2. Abbreviated coating names are given in Table 5.5.

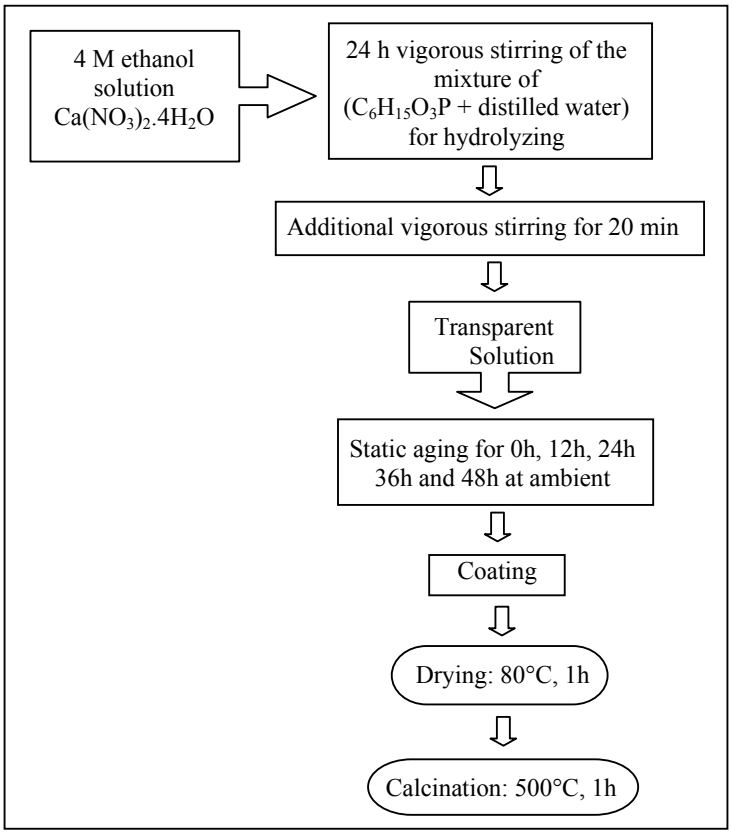

Figure 5.3 Production flow charts of the coatings synthesis method.

Table 5.5 Production of coatings with respect to the sol solution with varying pH value and substrates surface condition

pH of the Sol solution before /after 24h aging process	Types of solutions	Types of surface modification	Process No
2.25/1.60 (Addition of 3% vol ammonia)	PH1	Seeded substrate with PM1	PH1-PM1
		Seeded substrate with PM2	PH1-PM2
		Seeded substrate with PM3	PH1-PM3
8.60/4.30 (Addition of 7% vol ammonia)	PH2	Seeded substrate with PM1	PH2-PM1
		Seeded substrate with PM2	PH2-PM2
		Seeded substrate with PM3	PH2-PM3

5.2.2 Modification of the Sol Solution with Additives

The approach of growing cells in three-dimensional scaffolds for tissue engineering has paved the way for the development of different polymeric scaffolds for usage in bone, cartilage, and corneal disorder. Among synthetic polymers, poly(glycolic acid) (PGA), poly(lactic acid) (PLA) and poly(lactic acid-co-glycolic acid) (PLGA) are extensively researched with and without hydroxyapatite (HAP) particulates for bone and cartilage related applications. All the above synthetic hydrogels, although biodegradable, lack the required mechanical stability. Under physiological conditions the uncontrolled dissolution kinetics of these hydrogels lead to the formation of undesirable glycolic acid/lactic acid that lowers the pH at implantation site. The last one decade has also witnessed the development of high-density polyethylene-HAP composites but even this does not meet all required specifications (Sinha et al., 2007). Recently, PVA gels and films have attracted great attention for various applications because of their easy preparation, excellent chemical resistance and physical properties, biocompatibility, and low price. Furthermore, the high water content and elastic properties make PVA gels advantageous for many biological applications, including wound dressings, bioreactors, controlled release matrices, and bioadhesives. Hydroxyapatite and their composites have attracted much attention as materials suitable for repairing and substituting for hard tissues, and their clinical applications are gradually expanding

because of their excellent biocompatibility and overall safety and the fact that they have a chemical structure similar to that of the mineral found in hard tissues of the body. An ideal prosthetic material must fulfill such basic requirements as biocompatibility with bone tissue, sufficient initial strength, strength retention over an adequate period of time, and nontoxicity of degradation byproducts. PVA has been used extensively in the treatment of defects in load-bearing joints such as cartilage because of the similarity of its tensile strength to that of human articular cartilage and its good lubrication (Chung et al., 2007).

It is known that the bone regeneration rate depends on the several factors such as porosity, composition, solubility and presence of certain elements that released during the resorption of the ceramic material; facilitate the bone regeneration carried out by the osteoblats. Thus, for instance small amounts of strontium, zinc or silicates stimulate the action of these osteoblats and, in consequence, the new bone formation. Carbonate and strontium favor the dissolution, and therefore the resorption of the implant. Silicates increase the mechanical strength, a very important factor in particular for porous ceramics, and also accelerate the bioactivity of apatite. Therefore, the current trend is to obtain calcium phosphate bioceramic partially substituted by these elements (Vallet-Regia, Ramila, Padilla, & Munoz, 2003; Vallet-Regia, & Gonzalez-Calbet, 2004).

In this study, polyvinyl alcohol (PVA) and silica based precursor were used as additives to investigate their effect on coating morphology.

In order to produce silicon substituted hydroxyapatite (Si-HAP) coatings Tetraethyl orthosilina ($Si(OCH_2CH_3)_4$) (Fluka) used as a silicon based precursors. Silicon incorporation into the apatite structure constitutes method to improve calcium phosphate coating applications. Figure 5.4 shows flow chart of the receipt indicating steps to prepare Si-HAP coating. The coatings were firstly dried at 80°C for 1 hour and subsequently heated at 500°C for 1 hour. Abbreviated names of the coatings are indicated in Table 5.6. The amounts of reagents were calculated considering a

constant Ca/(P+Si) molar ratio, equal to HAP stoichiometry (1.67), assuming that silicate ions would substitute the phosphate groups (Table 5.6).

PVA was chosen as polymer additives owing to its film forming, emulsifying, and adhesive properties. The first step was the preparation of Ca and P based solution by a sol-gel routine described previously. In addition, solution of PVA with 10% w/v ratio was separately prepared by mixing PVA with distilled water at 90°C for 6h and homogeneous solution of polymer was obtained.

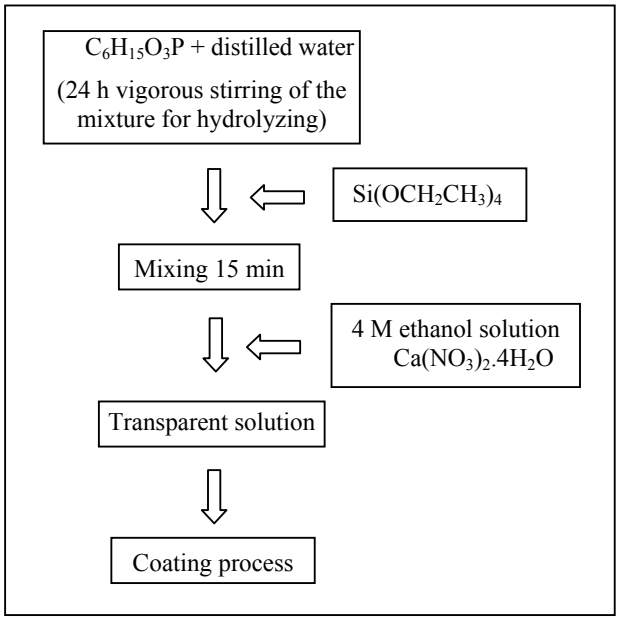

Figure 5.4 Production flow chart of the Si substituted HAP coatings.

Table 5.6 Quantities of Ca, P and Si precursors and expected molar ratios

Ca source (M)	P source (M)	Ca/P molar ratio	Si source (M)	Ca/ (P+Si) molar ratio	Names of coating
10×10^{-2}	5.50×10^{-2}	1.82	0.50×10^{-2}	1.67	Si-1
10×10^{-2}	5×10^{-2}	2.00	1.00×10^{-2}	1.67	Si-2

Afterwards, the viscous PVA solution was stored at room temperature for 30 min due to degassing of the air trapped in solution during the stirring process. Subsequently, a stock PVA solution was added to the CaP based solution aged at room temperature. In order to study the effect of the amount, different percentages of

PVA namely 20% and 40% volume fraction were used in the study. The solution mixture was then sealed and vigorous stirring was continued for 4h at 25°C. Next, the stirring was stopped to facilitate the removal of gas bubbles. 316L stainless steel substrates coated with CaP sol + PVA solution dried at 150°C for 1h, then, calcination process was carried out at 500°C for 3h. Addition of PVA to the sol solution is called as PVA. Names of obtained coatings thus are abbreviated as PVA1 and PVA2 for 20% and 40% vol PVA solution additive, respectively.

5.2.3 Heat Treatment Regime Effect

Sol-gel derived HAP coating can be synthesized at a relatively low firing temperature, which is below the decomposition temperature of HAP and the transformation temperature of 316L stainless steel substrate. However, some common flaws such as cracking, peeling, and pores are originate during drying or firing of HAP coated specimens, in the sol-gel-derived HAP coating technique. And the optimum heat-treatment condition of the sol-gel-derived HAP coatings has not been well established yet. Research has shown that the crystallinity, homogeneity, and surface morphology of the coated HAP layer depend on various heating conditions. In this work, morphological characteristics of the sol-gel derived HAP layer coated on stainless steel substrates were investigated in terms of the heating conditions with respect to heating rate. Sol-gel coating process performed to substrates with unmodified surface property by using PH1 sol solution. Apart from the heat treatment described above, the samples were dried at 80°C for 1 h, following two different heat treatment regimes which are shown in Figure 5.5. Coating obtained by slow heating regime of 2°C/min is named HT1, while high heating regime of 10°C/min is called HT2.

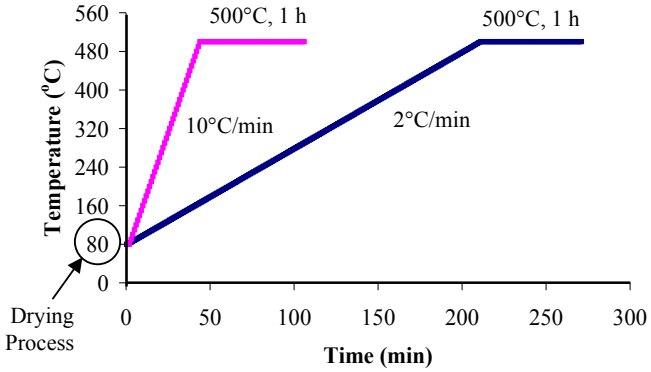

Figure 5.5 Heat treatment schedules of the coatings.

5.3 Solution Characterization

5.3.1 pH Measurement

pH measurement refers to determination of the activity of hydrogen ions in an aqueous solution. Many important properties of a solution can be determined from an accurate measurement of pH, including the acidity of a solution and the extent of a reaction in the solution. Many chemical processes and properties, such as the speed of a reaction and the solubility of a compound, can also depend greatly on the pH of a solution. In the study, pH values of the sol solutions were determined with Mettler Toledo Inlab 412 pH meter.

5.3.2 Turbidity Measurement

Turbidity (or the relative cloudiness of a liquid) measurement gives the optical characteristics of suspended particles in a liquid. Light is passed through the sample and is scattered in all directions. The light that is scattered at a 90° angle to the incident light is then detected by a photo diode and is converted into a signal linearized by the analyzer and displayed as an NTU (Nephelometric Turbidity Units) value. The more suspended particles there are in a liquid, the more light will be scattered, resulting in a higher NTU value. In the experiment, turbidity measurements were performed by using TB1 Turbidimeter (VELP, Scientifica Srl,

Italy). The sample was placed in the vessel with a dimension of Ø25 mm and height of 50 mm. Formazine is recognized throughout the world as a primary standard. Formazin solution was used to calibrate the turbidity.

5.4 Characterization Techniques

5.4.1 X-Ray Diffraction (XRD)

X-ray diffraction is one of the primary techniques to analyze all kinds of materials such as fluids, powders and crystals. XRD can provide information about crystalline structure and structural phases. It is extensively used to investigate the structural properties of powder solids and thin coatings on substrates. Synthesized coatings were analyzed using X-Ray Diffraction (XRD) with a grazing angle attachment and an incident angle of 1° (Rigaku, D/Max-2200/PC). X-Ray radiation of CuK_{α} was set at 40 kV and 36 mA with a scanning speed of 2° 2θ/min, from 3° to 90°.

5.4.2 Scanning Electron Microscopy (SEM) and Energy Dispersive Spectrum Analyse (EDS)

Scanning electron microscopy (SEM) is one of the most common analytical methods to examine surface morphology of the solid-state specimen. In SEM, a tiny high-energy electron beam is scanned across the sample surface. Series of radiations can be produced due to the interaction between the electron beam and the sample. Normally, two types of radiation are utilized for image formation: primary backscattered electrons and secondary electrons. Backscattered electrons reveal the compositional and topographical information of the specimen. The secondary electron images produce a depth of field which shows the surface topography. The signal modulation of the two types of radiation is viewed as images in the CRT and provides the morphology, surface topology and composition of the specimen surface.

The energy dispersive spectroscopy (EDS) is often attached to the SEM. The X-rays generated from the interaction between the electron beam and the specimen is used to identify and measure quantitatively the elemental composition of the specimen. Therefore, SEM/EDS can detect the elemental composition and obtain the morphology of the specimen simultaneously. In this study, the surface and elemental composition of the films was examined by using JEOL JSM-6060 instrument.

5.4.3 Fourier Transform Infrared Spectroscopy (FTIR)

Fourier Transform Infrared (FTIR or IR) spectroscopy is generally a non-destructive technique, which is used to measure the absorption of various infrared light wavelengths of organic or inorganic materials of interest. The infrared absorption bands identify the specific molecular components or structures, and provide chemical bonding information of the materials because of the vibrational motions of the chemical bond showing frequencies in the infrared regime.

Infrared spectra record the infrared intensity (transmission percentage or absorption) versus wavelength (wavenumber) of light. The IR spectrum can be generally divided into three frequency (or wavenumber/wavelength) regions: the far IR (10~400 cm^{-1}), the middle IR (400~4,000 cm^{-1}) and the near IR (4,000~14,000 cm^{-1}), with the middle IR region being employed in most IR spectroscopic investigations. The basic infrared experiment is to measure the changes of infrared light intensity after interacting with the sample (Almeida, & Marques, 2004). Intensity can be expressed as percent transmittance (%T) or absorbance (A) (Marcott, 1998). If I_0 is the energy, or radiant power, reaching the infrared detector with no sample in the beam, and I is the energy detected with a sample present, transmittance is,

$$T = \frac{I}{I_0} \tag{5.1}$$

And percent transmittance:

$$\%T = \frac{I}{I_0} x 100 \tag{5.2}$$

Absorbance is:

$$A = \log\left(\frac{1}{T}\right) = \log\left(\frac{I_0}{I}\right) \tag{5.3}$$

FTIR spectra are utilized to identify types of chemical bonds (functional groups). The infrared absorption band position, peak number and intensity stand for the characteristics of molecular structures or functional groups like molecular fingerprints, which are utilized to identify the unknown materials by comparison with a library of known compounds (Kesenci, Fambri, Migliaresi, & Piskin, 2000).

FTIR spectra were obtained using a Perkin Elmer Spectrum BX FTIR spectrometer with thin film attachment and spectra were obtained at 4 cm^{-1} resolution averaging 25 scans.

5.4.4 Thermal Analysis Techniques

Thermal Analysis (TA) is defined as a group of techniques in which a physical property of the substance and its reaction products are measured as a function of temperature whilst the substance is subjected to a controlled temperature program (Hill, 1991).

Thermogravimetry is a technique in which the mass of the sample is monitored against time or temperature while the temperature of the sample is programmed. A plot of mass loss or percent loss versus temperature or time can be obtained. The reaction is shown as one or more steps, each of which represents a mass change. DTA is a technique in which the difference in energy between the sample and the reference material is measured against time or temperature. The DTA curve is generally a plot of the difference in energy as the ordinate against temperature T, as

the abscissa. By convention, in DTA endothermic peaks are drawn downwards and exothermic upwards.

Temperature change in the samples brings about the chemical (phase transition, reduction and oxidation, decomposition) and physical (boiling, melting, and sublimation) changes of a sample and these can be endothermic or exothermic. DTA can be used to study any process in which heat is absorbed or evolved. The number, shape and position of the various endothermic and exothermic peaks in DTA curve can be used for qualitative identification of the substance. Simultaneous techniques refer to the application of two or more techniques to a sample at the same time. In the present study, TG-DTA simultaneous techniques are used. It is an advantage to use simultaneous techniques because it saves time and sample and it gives an opportunity to set an experiment at the same conditions.

In this work, TG/DTA analysis was conducted using a Shimadzu DTG-60H/TA-60WS simultaneous thermal analyzer. Heating regime was selected as 10°C/min to 500°C then held for 15 min at that temperature and subjected to heating at a lower rate (3.3°C/min) to 1000°C.

5.4.5 Electrochemical Method

Electrochemical methods are commonly used to evaluate the barrier, corrosion resistance, and the degradation properties of protective organic coatings, including paints and conversion coatings on metal substrates. Potentiodynamic polarization curve analysis has been found useful for analyzing the properties of sol-gel derived coatings on metal substrates. The limitations of DC measurements are obvious: if the ohmic resistance across the electrode and solution is large, the current density becomes very small for any given potential. Thus, the use of the DC techniques in situations involving a large electrodic resistance requires very careful evaluation. This is the case in instances where a coating has been applied to a metal or the metal is passive, as in stainless steels, aluminium or titanium alloys. EIS analysis has recently been used to analyze the corrosion protective properties of sol-gel derived

coatings on metal substrates. The use of EIS by electrochemists to study the corrosion protective properties of organic coatings over metals has been dominated by an emphasis on the methodologies and instrumentation of EIS. The primary consideration is the corrosion occurring on the metal itself, and on the metal/coating interface and what happened when this occurred (Shi, Jiang, & Bauer, 2002).

Electrochemical tests were performed to observe corrosion behavior of coating and 316L steel substrate system in physiological saline solution (0.9% NaCl) in vitro by using Gamry potentiostat model P4/750 which has three electrode test cell. Graphite was used as the counter electrode while saturated calomel electrode (SCE) was used as a reference electrode. During the corrosion tests temperature was maintained at 37±1°C by means of a thermostat water bath which kept it circulating through a double-walled test cell to simulate the human body temperature. Triplicate tests for each group of specimens were performed.

The electrochemical measurements were carried out on the coated and uncoated samples. The open circuit potential (OCP) was recorded for 30 minutes prior to anodic polarization. The gradual variation in the potential is called a scan and the rate at which the potential is changed is called scan rate. Potentiodynamic anodic polarization technique is used to determine the active/passive characteristics of a given metal-solution system

During the potentiodynamic polarization study, the potential of the test sample was increased from 0.2 V below OCP towards the noble direction at a scan rate of 0.5 mV/s until current density reached 1 mA/cm^2. Once the data plot was obtained, the applied potential vs. current (log of current) curve can be used to observe passivation phenomena, pitting tendencies or assess the corrosion rate. Different techniques like Tafel plot, polarization resistance, potentiodynamic anodic polarization, are employed to measure the corrosion response of a material-solution system. Polarization resistance was measured by sweeping the test sample at rate of 0.5 mV/s ± 0.020 V around an OCP. Triplicate tests for each group of specimens were performed.

Common characteristics of bioactive materials are the formation of a CaP rich layer at the interface between the implant and bone. It has been established that bioactivity occurs only within certain compositional limits. Another factor that affects the bioactivity is the surface area, as it directly determines the dissolution rates of any solid materials. The porous structure of HAP provides a template for fibrovascular ingrowth, which, when followed by osteoblast differentiation, results in the deposition of new lamellar bone. In the development of bone substitutes high porosity level is required for the following reasons: (a) porous materials have large surface area, resulting in a high tendency to bioresorb, which induces bioactivity; (b) interconnected pores can provide a framework for bone growth into the matrix of the implant, and thus anchor the prosthesis with the surrounding bone, preventing loosening of implants, and (c) interconnected porosity acts like an organization of vascular canals, which can insure the blood and nutrition supply for the bone (Tato, & Landolt, 1998).

HAP coated implant also have corrosion resistance in rigorous body environment besides the bioactivity property. Therefore, porosity measurement in the coating is essential to determine the corrosion resistance of coating owing to the generation of corrosion resulting from the contact between the substrate and the corrosive environment. In spite of intensive studies on porosity measurements using the electrochemical methods, the reliable and systematic methods of porosity measurements still remain obscure. The most often used method for calculating the porosity is the equation introduced by Tato et al. (1998). This equation corresponds to the ratio of the polarization resistances of the uncoated and coated substrate. The porosity calculated by Tato's equation indicated the relative comparison given in deposition conditions. After that, the measurement of porosity for coatings on metallic substrates has been a subject of some contention for many years. More recently, Liu, Bi, Leyland, & Matthews (2003) proposed an empirical equation to estimate the porosity (F) of the coating. This equation is a complemented equation of porosity measurement suggested by Matthews and co-workers (1991). The determination of the total coating porosity (F) is possible according to Eq. (5.4):

$$F = \frac{R_{pm(substrate)}}{R_{p(coating-substrate)}} x 10^{-\left|\Delta E_{cor} / \beta_a\right|} \quad (5.4)$$

where F is the total coating porosity, R_{pm} the polarization resistance of the substrate, R_p the polarization resistance of the coated steel system. ΔE_{corr} is the difference of the corrosion potential between the coating and the substrate, and β_a the anodic Tafel slope of the substrate (Ahn, Lee, Kim, & Kim, 2004).

Very often the period of time during which a coating completely protected a metal was given minimal consideration, for the interest was in what happened to a metal surface as it corroded, and how the coating changed the mechanisms of corrosion. Attention was not directly paid to the coating and the measurement of the properties of the system before failure by corrosion began at the metal/coating interface. Much attention was paid to the metal substrate and its composition. Equivalent circuits with many elements were used to provide physical models for failed systems, but not much modeling of the changes occurring in coatings systems leading to failure was performed. Impedance data on coatings have been in use extensively in a semi-quantitative way to measure and predict the corrosion protective lifetimes of organic coatings on metals (Bierwagen, Tallman, Li, He, & Jeffcoate, 2003; Scully, 1989).

Furthermore, corrosion performance of the coating was investigated via electrochemical impedance spectroscopy tests (EIS). EIS tests were carried out at open circuit potential using a frequency scan from 10 kHz to 1 mHz with constant perturbing AC signal amplitude of ±5 mV. The impedance parameters, polarization resistance R_p and capacitances C were calculated from Nyquist and Bode plots using Gamry, Echem analysis software program.

CHAPTER SIX

RESULTS AND DISCUSSION

6.1 Substrate Preparation

There are many experimental variables for the sol-gel coating process. Investigation of the solution preparation by using different precursors and application of heat treatment are well-known parameters. Additionally, substrate preparation should be considered as an important factor like other common parameters due to its effect on coating quality. In this study, HAP coating was performed on 316L stainless steel substrate of unmodified and modified surfaces. Stainless steel substrate that was abraded with SiC paper and then polished with the 5 μm diamond paste was called unmodified stainless steel. By using unmodified substrate, coating with an insufficient coverage of the substrate hence non uniform structure was obtained. Coating inability of the bare substrate led to surface modification conducted by seeding process, alkali or acid treatment. Modification processes are given in detail as follows.

6.1.1 Substrate Surface Modification and Characterization

6.1.1.1 Formation of the Seeded Surface by Electrodeposition Technique

316L stainless steel substrate surface was modified electrochemically in order to partially or totally cover the surface with uniform primer CaP layer for subsequent growth of the coating to be promoted. In this route, substrate surface was seeded with the crystalline CaP compounds via galvanostatic and puls electrodeposition technique. It was, therefore, essential to prepare the metal surface with a thin and uniform primer calcium phosphate layer for subsequent growth of the final coating. In galvanostatic and puls electrodeposition method conditions were set for a predetermined current density in a set period of time in order to form CaP seeds. Galvanostatically electrochemical deposition was carried out at a cathodic current

value of -10 and -20 mA. The pulse electrochemical deposition applied current was varied in a range between -5 mA and -15 mA with an average of -10 mA.

Habibovic, Barre`re, Blitterswijk, Groot, & Layrolle (2002) indicated that the nucleation and growth kinetics of these crystals depend on the temperature, pH, composition, and saturation of the solution. In this study, test solution was prepared by dissolving 42 mM $Ca(NO_3)_2.4H_2O$ and 25 mM $NH_4H_2PO_4$ in distilled water at 50^oC to give a Ca/P ratio of 1.67 for both technique.

XRD patterns of the substrate with seeded surface by galvanostatic and pulse electrodeposition technique is given in Figure 6.1 and Figure 6.2, respectively. Both of the surfaces were composed of the $CaHPO_4.2H_2O$ phase (dicalcium phosphate dehydrate: brushite - JCPDS 09-0077). A brushite coating is an important synthetic intermediate phase to prepare highly pure hydroxyapatite by electrodeposition technique and initially formed brushite coatings can be transformed into the HAP through chemical methods (Kumar, Dasarathy, & Riley 1999; Lu, Zhao, & Leng, 2005; Redepenning, Schlessinger, Burnham, Lippiello, & Miyano, 1998).

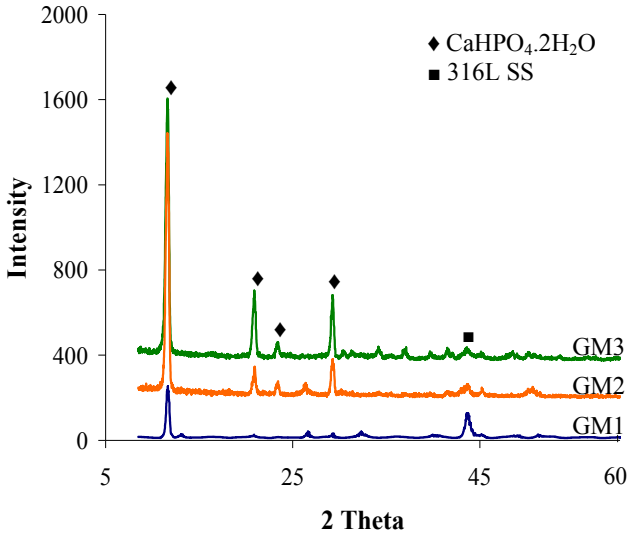

Figure 6.1 XRD patterns of the substrates seeded by galvanostatic-current method.

As seen from the XRD patterns, an increase in time and current of the electrodeposition were resulted in a gradual improvement in the crystallinity of the formed layer, especially for GM2 and GM3. Similar improvement is also exist for the pulse deposited technique as seen in Figure 6.2. SEM micrographs of the CaP seeds are shown in Figure 6.3 and 6.4 for galvanostatic and puls technique, respectively.

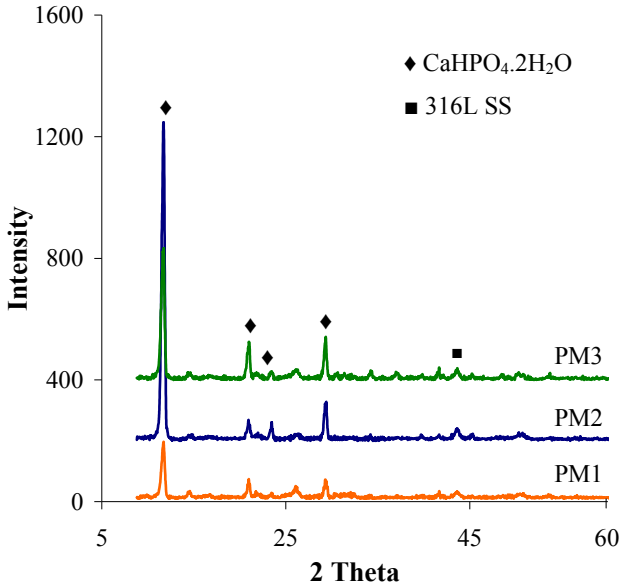

Figure 6.2 XRD paterns of the substrates seeded by pulse current method.

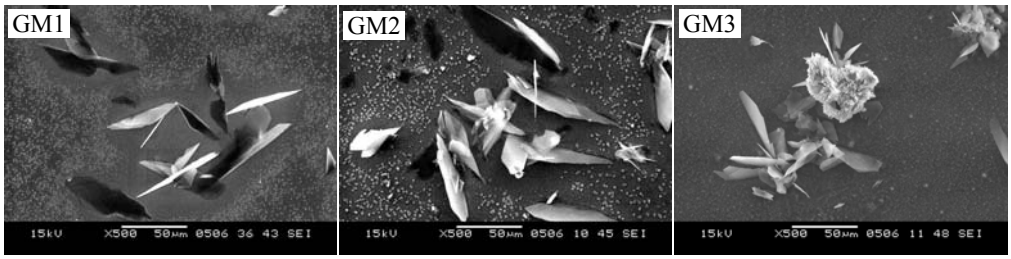

Figure 6.3 SEM micrographs of the substrates seeded by galvanostatic technique.

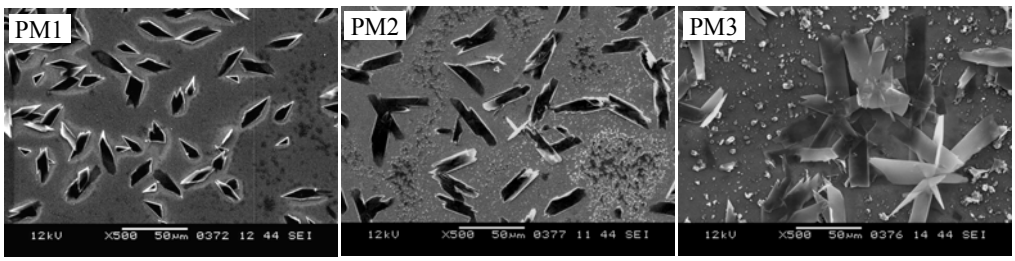

Figure 6.4 SEM micrographs of the substrates seeded by pulse technique.

Dimension of the crystals and density of the homogeneously distributed nucleuses on the surface were found to increase with increasing current and time, for both techniques.

CaP seed deposited on the surface consist of two layers: sponge-like structure accompanied with the plate-like crystal structure as seen in Figure 6.5. Consequentially the rate of surface coverage by plate-like structure deposited on top of the sponge-like film increased with increasing time. EDS analyses was performed in order to see if there was any structural change between two types of the film. Sponge-like structure had a Ca/P ratio of 1.16 and the plate-like crystal structure had 1.12, both of closely correspond to brushite.

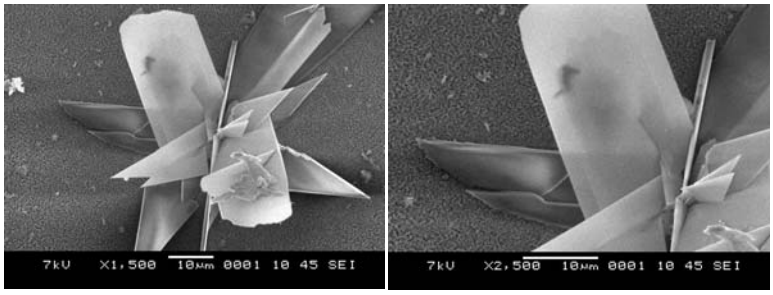

Figure 6.5 SEM micrographs of the CaP seeds produced by PM3 condition with high magnification.

According to the EDS analysis, Ca/P ratios of the seeded surface obtained by galvanostatic deposition route 0.74, 0.80 and 0.89 for sample of GM1, GM2 and GM3, respectively. On the other hand, these ratios for seeded surface using pulse deposition were 0.90, 0.98 and 1.18 for sample of PM1, PM2 and PM3, respectively. EDS analysis results of sample GM3 and PM3 are given in Figure 6.6.

6.1.1.2 Alkali Treatment of the Substrate

Several authors have studied the effect of alkali treatment on titanium and its alloys. *In vivo* studies with alkali treated titanium have shown that it can bond directly to bone after alkali treatment. Nevertheless, there were a few studies about the investigation of the effect of alkali treatment on 316L stainless steel substrates.

As known, 316L stainless steel is a metal with a metallic bond and HAP is a ceramic with a covalent bond. It is not possible to form a stable interface between the two materials without inter-compound bridging up. The peeling of bioactive ceramics from the metallic substrate always happened after heat treatment because of the great difference of metals and ceramics in thermal coefficient. The internal stress was generated along the interface between substrates and ceramics that also exaggerated the peeling (Lin, Hsu, Lin, & Sun, 2002; Thamaraiselvi & Rajeswari, 2005). The aim of alkali treatment in the work was formation of a bonding layer with a good bonding strength to the metallic substrate, which is essential for stable HAP coating.

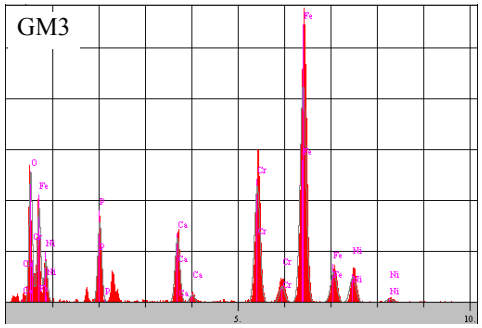

Element	Concentration (wt%)
Ca	4.33
P	4.87
O	32.13
Fe	38.96
Cr	12.83
Ni	6.88
Ca / P	0.89

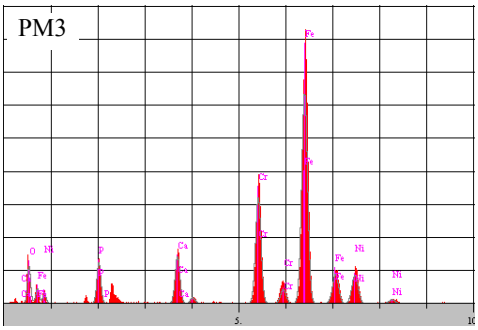

Element	Concentration (wt%)
Ca	4.36
P	3.67
O	13.67
Fe	51.91
Cr	15.50
Ni	10.89
Ca / P	1.18

Figure 6.6 EDS analysis of seeded surface sample of GM3 and PM3.

Alkali treatment was performed by soaking 316L SS substrates in 10M NaOH aqueous solution at 60°C for 24h. After the alkali treatment, the substrates were gently washed with distilled water and dried at 40°C for 24 h in an air atmosphere. The alkali treated substrates were then heated to 500-700°C at a rate of 5°C/min in tube furnace, kept at a given temperature for 1h, and cooled to room temperature in the furnace. Abbreviations of alkali treated samples are summarized in Table 6.1 (AT1, AT2, AT3 and AT4).

Figure 6.7 presents the XRD patterns of the surface of 316L stainless steel substrates treated with 10M NaOH at 60°C for 24h and heated to various temperatures as named AT1, AT2, AT3, and AT4 details of which are given in Table 6.1.

Table 6.1 Modification conditions of the substrates obtained by alkali treatment

Batch temperature/ Duration time	Drying Process	Heat treatment	Process No
10 M NaOH 60°C, 24h	40°C, 24 h	no heat treatment	AT1
		0→500°C at a rate of 5°C/min and kept 500°C 1h	AT2
		0→600°C at a rate of 5°C/min and kept 600°C 1h	AT3
		0→700°C at a rate of 5°C/min and kept 700°C 1h	AT4

Hydrated sodium chromium oxide phase traced at the lower angle of the XRD pattern when the 316L stainless steel was treated by AT1. This phase turned into sodium chromium oxide (Na_4CrO_4) when the temperature was raised up to 500°C. When sample was subjected to AT3 additionally iron chromium oxide phase was occured. After the AT4 sodium chromium oxide would be phased out.

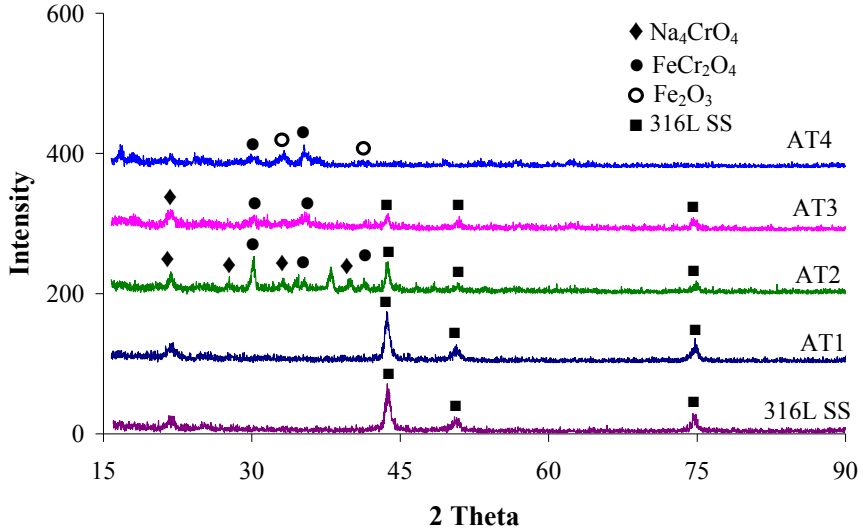

Figure 6.7 XRD pattern of the alkali treated substrate sample of AT1, AT2, AT3 and AT4.

Instead, the iron oxide and iron chromium oxide were appeared. This assignment is in reasonable agreement with the study of Lin et al. (2002). Phase of the Na_4CrO_4 was formed on the surface of the substrate which would act as bond layer after being treated with NaOH and immediately afterwards heated to 500°C. This finding was conflicted with the result of the Lin et al. in terms of the intercompound phase formation temperature value of 600°C. According to Lin et al., following reaction was assumed:

$$8Na(OH) + Cr_2O_3 \rightarrow 2Na_4CrO_4 + 3H_2O + H_2 \quad (6.1)$$

As can be seen in Figure 6.7, formation of the iron chromium oxide and iron oxide is attributed to the activity of the iron with increasing temperature. And additional these phase lead to loosening of the structure that deteriorate bond layer and causes peeling of deposited coating layer later formed on this.

SEM images and EDS analysis of stainless steel substrate obtained by AT1, AT2 conditions are given in Figure 6.8 and 6.9, respectively. Besides, SEM images of AT3 and AT4 conditions are displayed in Figure 6.10. After AT1 treatment surface showed a thin-coated layer with flower like network structure. When EDS line analysis of this sample was examined, it was clearly seen that peaks of the elements of Na, Cr and O were indicative of the layer of hydrate sodium chromium oxide. SEM micrograph of the surface AT2 showed thin film with prism sodium chromium oxide covered. At the surface obtained by AT2 condition showed a thin film with prism of sodium chromium oxide was covered on the surface. As shown in Figure 6.10, an increase of the dimension of the flower like structure was observed with elevated temperature.

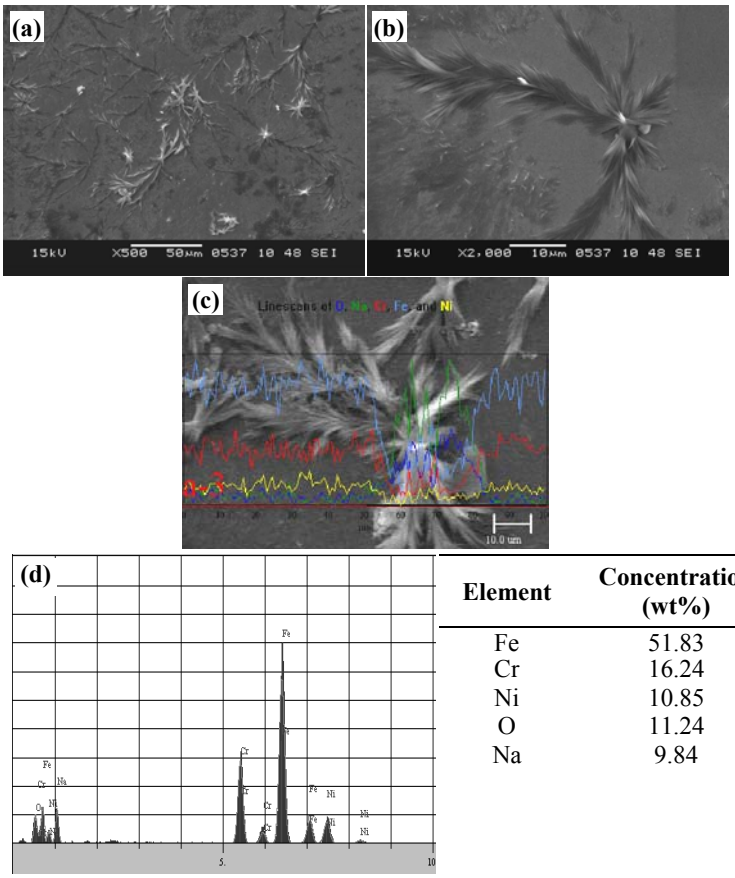

Element	Concentration (wt%)
Fe	51.83
Cr	16.24
Ni	10.85
O	11.24
Na	9.84

Figure 6.8 (a), (b) SEM micrograph of the substrate surface produced by condition AT1 and (c) EDS line analysis image (d) EDS analysis result.

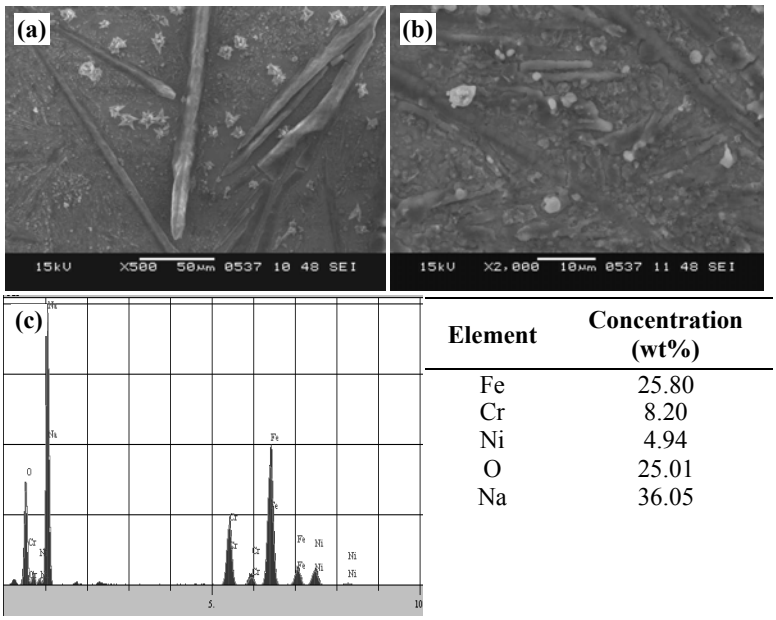

Element	Concentration (wt%)
Fe	25.80
Cr	8.20
Ni	4.94
O	25.01
Na	36.05

Figure 6.9 (a), (b) SEM micrograph of the substrate surface produced by condition AT2 and (c) EDS analysis result.

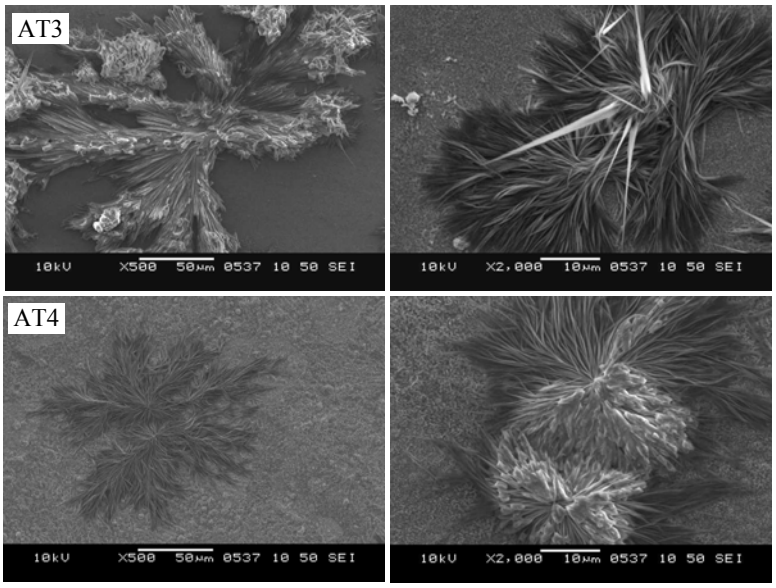

Figure 6.10 SEM micrographs of the alkali treated substrate samples of AT3 and AT4.

6.1.1.3 Acid Treatment of the Substrate

It is anticipated that a thin oxide film is immediately formed on 316L stainless steel surface, when it is exposed to an oxygen containing environment. The thickness of this passive oxide film is about a few nanometers and acts as a protective barrier in the corrosive media. However, the film is not sufficient during long-term implantation procedures as they are susceptible to corrosion related problems and lack of biocompatibility to ensure new bone formation at the implant site. A metallic surface, which is quite passive due to protective oxide layer, may still allow a significant release of ions or atoms into the surrounding tissue under certain conditions. Hence, the development of ceramic coatings on a passivated surface tends to ensure bioactivity and resists the metal leach from the surface. Hydroxyapatite (HAP) coatings on the surface of metallic implants can integrate the advantage of both materials, the bioactivity of ceramics and excellent mechanical properties of metals. Many studies have explored the possibility of HNO_3 passivation on stainless steels but least have explored the possibility of coatings on passivated metallic implants (Kannan, Balamurugan, & Rajeswari, 2005). Treatment procedure

was given in Chapter V. XRD characterization demonstrated that there was no alteration on the substrate caused by acid treatment (Figure 6.11).

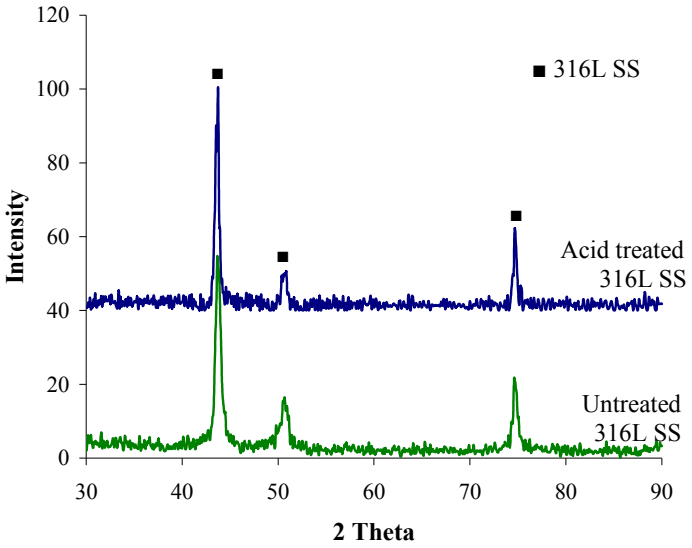

Figure 6.11 XRD patterns of the samples of untreated 316L stainless steel substrate and acid treated substrate.

Similarly, SEM observations revealed that there was no remarkable difference between surfaces of the acid treated substrates and untreated sample (Figure 6.12). Further, EDS analysis was performed in order to see if there was any surface changes occurred due to HNO_3 passivation. During immersion, chromium, one of the major alloying elements in type 316L stainless steel forms a passive oxide layer on the stainless steel surface. Table 6.2 shows elemental analysis of untreated and HNO_3 treated 316L SS. As seen from the table an increment in amounts of chromium, molybdenum and oxygen was occurred as a result of acid treatment.

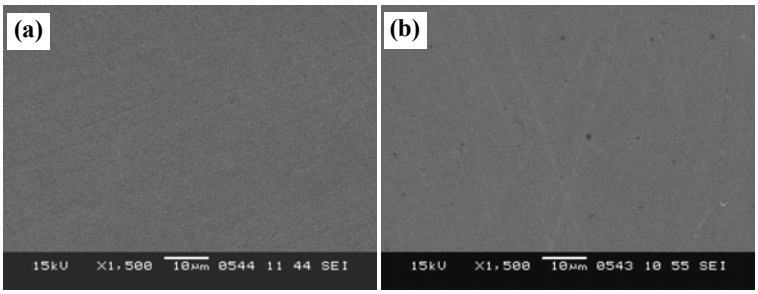

Figure 6.12 SEM micrograph of the sample of (a) untreated 316L stainless steel substrate and (b) acid treated substrate.

Table 6.2 Elementel analysis of untreated and HNO_3 treated 316L SS as obtained by EDS analysis

Element (%)	Fe	Cr	Ni	Mo	O
Untreated 316L SS	63.90	18.16	13.33	3.25	1.37
Acid treated 316L SS	60.97	18.70	12.88	4.69	2.76

6.2 Production of HAP Coatings

Controlling of the surface morphologies and structural compositions of the ceramic based coatings processed on implant materials by sol-gel technique shows great importance. Therefore, different process parameters such as aging time, pH of sol solution, heat treatment, and chemical additives have identifying functions on the properties of the formed film. From this point of view, effects of these process parameters on the properties of the coating were investigated and performed works were summarized as follows.

6.2.1 Effect of Aging Time

6.2.1.1 Characterization of Sol Solution

Triethyl phosphate can be hydrolyzed in the presence of water to form diethyl phosphrous ester (Masuda, Matubara, & Sakka, 1990).

$$P(OC_2H_5)_3 + H_2O \rightarrow HPO(OC_2H_5)_2 + C_2H_5OH \quad (6.2)$$

According to the Masuda et al. (1990) progress of the reaction (6.2) takes place exceedingly slowly, e.g. 10h or more to complete. Nevertheless, a convenient and direct qualitative observation of the hydrolysis is the loss of phosphate odor, together with the disappearance of emulsion phase that appeared immediately after initial mixing with water, to transform a clear solution (Liu, Troczynskia, & Tseng, 2002). However, continues decrease of solution pH with time was determined for up to 24h (Figure 6.13), suggesting a continued hydrolysis, by release of proton according to the reaction (6.3). This was strongly argued that an extended hydrolysis of the

diethyl phosphorous ester may proceed more –OR groups which are replaced by –OH groups as follows:

$$HPO(OC_2H_5)_2 + H_2O \rightarrow HPO(OC_2H_5)_{2-x}(OH)_x + xC_2H_5OH \quad (6.3)$$

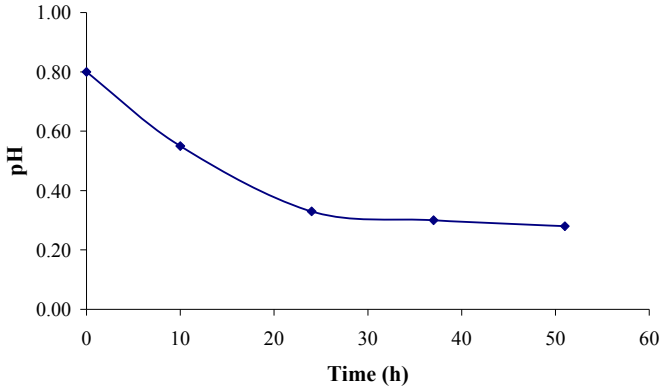

Figure 6.13 pH of the solution versus time graph.

It was reported that the hydrolyzed phosphite interacts with Ca^{2+} ions in aqueous solution through a polymerization reaction to form a Ca-P intermediate, releasing protons during the reaction (Liu, Troczynski, & Hakimi, 2002):

$$HPO(OC_2H_5)_{2-x}(OH)_x + Ca^{2+} \rightarrow [(OC_2H_5)_{2-x}O(H)P\text{-}O]_2Ca + H^+ \quad (6.4)$$

The liberation of proton in reaction (6.4) was verified by the change of the solution pH as shown in Figure 6.13. The solution pH decreases from 0.8 to 0.3 as a function of aging time for over a period of 50h. This also indicates a slow reaction between hydrolyzed phosphite and calcium ions. But the rate of pH decrease is negligibly small after 24 h.

Similarly, P NMR study showed that the hydrolysis taking place during the sol aging of the triethylphosphite yielded diethyl phosphite, which reacts with the calcium precursors, whereby the coordination number of phosphorus changes from III to V. The liberation of protons during the reaction is said to justify the pH decrease observed (Ben-Nissan, Green, Kannangara, Chai, & Milev, 2001; Gross, Chai, Kannagara, & Ben-Nissan, 1998).

Liu et al. (2002) suggest that reaction (6.4) may still be an oversimplified form since some unknown reactions may also be concurrently taking place, which makes a detailed investigation on the chemical mechanism more difficult. Besides, they show that dried gels obtained from the shorter-term aging time process i.e. 4h consist in mixture of impurity phases of $Ca_2P_2O_7$, $Ca_3(PO_4)_2$, $CaCO_3$ and $Ca(NO_3)_2$. These crystalline phases imply the complexity of the "real" reaction pathways which are certainly more complex than that suggested by reaction (6.4). Therefore, it would be pertinent to re-phase reaction (6.4) to a more practical expression:

$$HPO(OC_2H_5)_{2-x}(OH)_x + Ca^{2+} + NO_3^- \rightarrow \text{Ca-P intermediate} + H^+ \qquad (6.5)$$

The "Ca-P intermediate" is likely to be X-ray amorphous rather than crystalline phase. Since Liu et al. (2002) demonstrated that "Ca-P intermediate" transforms to crystalline apatite at elevated temperature. Apatite can evolve from either the transformation of the amorphous Ca-P intermediate or the reaction among $Ca_2P_2O_7$, $Ca_3(PO_4)_2$, $CaCO_3$ and $Ca(NO_3)_2$, combination of both when the calcinations temperature reached about 500°C.

$$\frac{1}{2}Ca_2P_2O_7 + Ca(PO_4)_2 + Ca(NO_3)_2 + CaCO_3 + \frac{1}{2}H_2O \rightarrow$$
$$Ca_5(PO_4)_3(OH) + CaO + 2NO_2 + 2CO_2 \qquad (6.6)$$

Another approach about the poor crystallinity of the apatite phase has an affinity with the some organic ligands (e.g. alkyl groups) may still chemically bond to the phosphorous, e.g. $(OC_2H_5)_{2-x}O(H)P\text{-}O\text{-}Ca$, rather than being liberated as a by-products, such as C_2H_5OH, which is much easier to burnout. These residues may retard crystallization as evidenced by a poor crystallinity of the apatitic phase observed at 300 and 400°C, which is presented in Figure 6.14. XRD patterns of the HAP coatings produced on unmodified 316L substrates by using sols with 24h aging time were obtained subsequent to the heat treatment carried out at 300, 400 and 500°C, for 1h in air and are shown in Fig. 6.14. The major phase was $Ca_5(PO_4)_6(OH)_2$ (HAP) with accompanying phase of $Ca_2P_2O_7$. Patterns of HAP and calcium pyrophosphate correlate well with ICCS standard hydroxyapatite patterns

(PDF number 09-432) and calcium pyrophosphate patterns (PDF number 9-346), respectively.

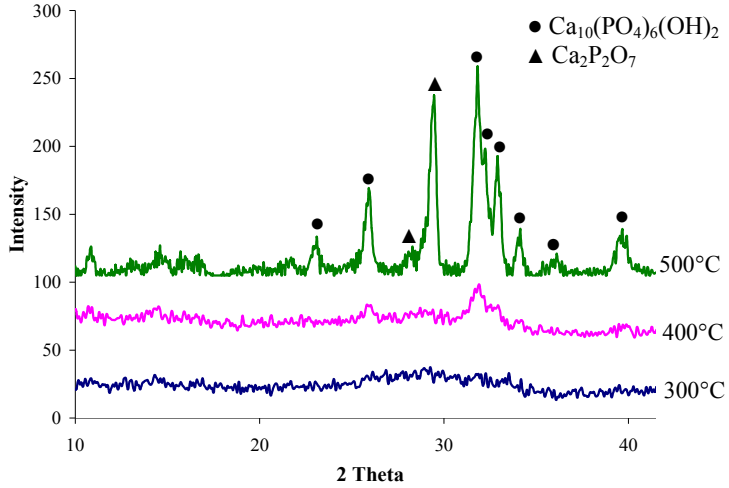

Figure 6.14 XRD patterns of the coatings on unmodified substrates derived from the sol solution with 24h aging.

Furthermore, study of the Liu et al. (2002) was clarified formation of calcium pyrophosphate and apatite phases in the coating synthesized at 500°C. They suggested that the reaction pathways did not follow reaction (6.6). Because of the presence of the $Ca_2P_2O_7$ phases with the appreciable amount of apatite phase whilst the carbonate peak disappeared. This suggested that the apatite is derived mostly from the transformation of the amorphous Ca-P intermediate, together with a smaller fraction being a product of reaction between $Ca_2P_2O_7$ and $CaCO_3$:

$$\frac{3}{2}Ca_2P_2O_7 + 2CaCO_3 + \frac{1}{2}H_2O \rightarrow Ca_5(PO_4)_3(OH) + 2CO_2 \qquad (6.7)$$

The existence of $Ca_2P_2O_7$ phase indicates to be residual reactant according to the reaction (6.7), once the $CaCO_3$ is completely consumed and reacted to form apatite. $Ca_2P_2O_7$ phase is not a detrimental component of bioceramic, because it contributes to dissolution rate faster than apatite in physiological environment, as interpreted by Daculsi (1998). This would be an advantage from the bioresorption point of view. From the stand point of clinical usage, implant materials accomplish their function best when they are replaced by the host tissues upon a resorption-apposition

mechanism. Furthermore, bioresorption process accelerates growing mechanism of defective hard tissues and this mechanism implies the important role of resorption in biological response. For this reason, none or less resorbable nature of synthetic HAP can be modified by incorporation of more bioresorbable second phase such as $Ca_2P_2O_7$ (Daculsi, 1998; Liu et al., 2002). Additionally, a lot of attention has been paid to pyrophosphate (pyro) ceramics in recent years. As an intermediate product in the biological mineralization process, pyro has been demonstrated to have great potential as an *in vivo* biodegradable bone substitute (Kasuga, Nogami, & Niiomi, 2001). Anderson, Cape, Crilly, Hodsman, & Wokfe, (1984) indicated that synthetic pyro can inhibit osteoclastic bone resorption, and therefore is used for the treatment of bone diseases including tumor-induced hypercalcemia and osteoporosis. On the other hand, Ge & Deitz, (1955) reported that occurrence of the impurity phase of $Ca_2P_2O_7$ having a lower Ca/P ratio than the stoichiometric hydroxyapatite is attributed to the acidic conditions of the used sol solutions.

An XRD pattern of the coatings obtained on unmodified 316L stainless steel substrates by using different aged sol solution is illustrated in Figure 6.15. Sharp reflection peaks together with a weak background appearing at 2θ of 43.3° and 50.6° correspond austenite phase (PDF no 33-397) that represents 316L SS substrate. There is a gradual improvement in crystallinity in terms of peak sharpness of HAP phase and accompanying phase ($Ca_2P_2O_7$) with increase in aging time until the 24h. Over the 24h aging time, XRD pattern of the coatings that obtained from sol solution aged time of 36h and 48h indicate a notable decline of intensity of the hydroxyapatite phase. On the other hand, intensities of $Ca_2P_2O_7$ and austenite phases for the aging time of 36h were both slightly increased when compared with HAP peaks. Besides, intensities of all phases diminished for the coating derived from the sol with aging time of 48h.

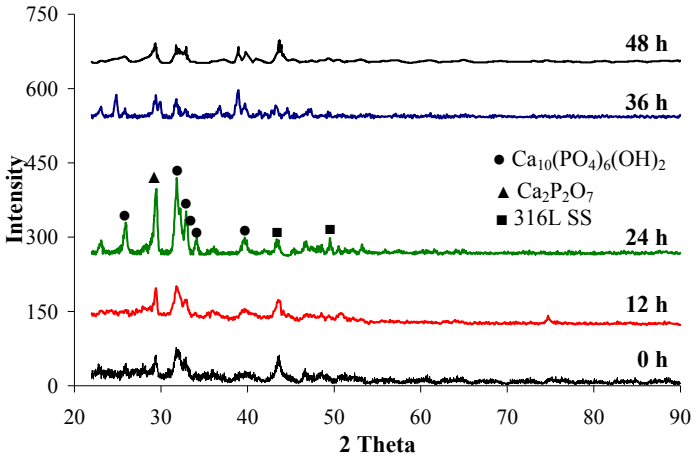

Figure 6.15 XRD patterns of the coatings on unmodified substrates derived from the sol solution with different aging times.

To assess the solution condition during the aging time period, turbidity measurements of the solutions was measured at different time intervals. Turbidity value was decreased from 3.5 to 2.8 NTU (nephelometric turbidity units) with the increasing time of the aging. This low alteration at the turbidity value showed that the sol solution remains transparent and distinguishable from each other, regardless of the aging period indicating the stability of the sols without any gelation. Besides, this measurement showed that there was no precipitate and decrease in turbidity occurred in the solution over a period of two days.

The full FTIR spectra all of the coatings produced by using five different aged times plotted in Figure 6.16. Bands were observed at 550-650, 960, 1000-1100 cm^{-1} which corresponds to the vibration modes of the PO_4^{3-} groups. PO_4^{3-} bands including the ν_1 stretching mode at 960 cm^{-1}, ν_2 bending mode between 400-500 cm^{-1}, ν_4 bending mode between 550-650 cm^{-1} and ν_3 stretching mode between 1000-1100 cm^{-1} are assigned according to the literature (Koutsopoulos, 2002; Ou-Yang, Paschalis, Boskey, Mendelsohn, 2000).

The characteristic of PO_4^{3-} groups is not apparently seen for coating (A0) obtained via 0h aged solution. On the other hand, spectra's of the other coatings appear roughly similar except for the slight differences in amplitude of PO_4^{3-} bands,

apart from coating (A24) produced by using 24h aged solution. Characteristic band for O-H stretching peak at 3570 cm^{-1} was only obvious in the spectra of coating produced by using A24 solution. On the other hand, broad band from 2500 to 3700 and at 1630 cm^{-1} associated with the adsorption of water (Stoch et al., 2000) in these coatings named as A12, A36 and A48. Since XRD results of the coatings confirmed this argument there was no indication of water incorporated into crystal lattice. All of the coatings have absorbance band with varying intensity and broadening located at a range of 710-705 cm^{-1} be ascribed to calcium pyrophosphate $(P_2O_7)^{4-}$ in agreement with the reported in the literature (Gimenez, Mazali, & Alves, 2001; Penel et al., 1999).

Furthermore, a small shoulder at 1070-1076 cm^{-1} and the broad band at about 1420-1500 cm^{-1} were resulted form the carbonate CO_3^{2-} groups incorporated in the apatite structure. These carbonated groups also induced to the band at 874 cm^{-1} (Koutsopoulos, 2002; Müller, Conforto, Caillard, & Müler, 2007; Peltola, Patsi, Rahiala, Kangasniemi, & Yli-Urpo,1998). Essentially, properties of the low cost and simplicity becomes the sol-gel techniques preference but during the synthesis should be elaborately performed because of the formation of non stoichiometric products. Existence of the carbonate in the coatings is arisen from the absorbance of carbon dioxide from the air during synthesis of the samples as reported by others in the literature (Gibson, Best, & Bonfield, 1999; Kim, Riu, Lee, & Kim, 2002; Pleshko, Boskey, & Mendelsohn, 1991).

In the mid-1960s, based on X-ray diffraction analysis LeGeros, Trautz, Klein, & Legeros (1969) recognized that biological apatite contain substantial amounts of CO_3^{2-}. For almost 40 years, it has been claimed by many different researchers that CO_3^{2-} occupies two different sites within the lattice of bone apatite. Synthesis experiments have produced two different types of carbonated apatites, one in which the carbonate ion substitute PO_4^{3-} ion is called “B-type substitution”, and another in which the carbonate ion substitute OH^- ion is called “A-type substitution”.

Previous Raman studies on carbonated apatites have reported variable numbers of bands in the ν_3 PO_4^{3-} domain. The ν_1 phosphate band at 960 cm^{-1} shifts slightly due to carbonate substitution in both A and B sites. The spectrum of type A carbonated apatite exhibits two ν_1 PO_4^{3-} bands at 947 and 957 cm^{-1}. No significant change was observed in the ν_2 and ν_4 phosphate mode regions in any carbonated samples. The ν_3 PO_4^{3-} region seems to be more affected by carbonation: two main bands were observed as in the HAP spectrum, but with a lower wave numbers (Penel, Leroy, Rey, Bres, 1998). The presence of B-type carbonate in apatite has long been associated with a Raman band at 1070-1073 cm^{-1}. Nishino, Yamashita, Aoba, Okazaki, & Moriwaki (1981) said that the CO_3^{2-} ν_1 peak included the PO_4^{3-} ν_3 peak, and Penel et al. (1998) consistently assigned it as an overlapped band. When our results are compared with the literature, coating produced in this study corresponds to B-type carbonate-hydroxyapatite, similar to biological apatites (LeGeros, 1981).

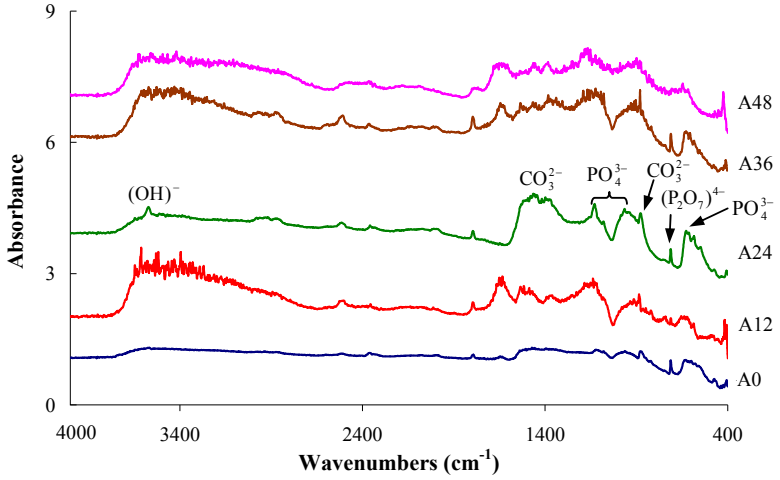

Figure 6.16 FTIR spectra of the coatings on unmodified substrates derived form the different aged times sol solutions.

Dental enamel with carbonate content amounting to 2-4 wt% is the most mineralized tissue of the human body (97 wt%). Mature bone mineral and dentine generally contain carbonate 5-8 wt% of the mineral (LeGeros, 1990; Rey, Collins, Goehl, Dickson, & Glimcher, 1989). Because of this reason, synthesizing of carbonate substituted apatites is not a disadvantage for human body. Thus, the

synthesized HAP with partial substitution of carbonate for phosphate groups was reported to be closer to the mineral constituent of bones (Pleshko et al., 1991).

Figure 6.17 shows the FTIR spectra of the coatings annealed at different temperatures. For annealing at 300°C, the characteristic band for PO_4^{3-} groups is not clearly discernable at 600-550 cm^{-1} that is in agreement with Russel, Luptak, Suchicital, Alford, & Pizzicoui, (1996). This was attributed to the absorption modes associated with PO_4^{3-} groups. With increasing temperature to 400°C, the spectra clearly illustrate characteristic ν_4 PO_4^{3-} bands at 563 cm^{-1} and 600 cm^{-1}, ν_1 PO_4^{3-} band at 942 cm^{-1}, and a strong ν_3 PO_4^{3-} absorption band in the range 1100-1000 cm^{-1}, which are typical of apatite structure. These adsorption spectra become stronger in intensity and better in resolution as the annealing temperature increases to 500°C. Furthermore, hydroxyl groups stretch mode band was observed at 3570 cm^{-1} which was attributed to characteristic HAP structure (Stoch et al., 2000).

Additionally, an adsorption bands at 870, 1460 and 1500 cm^{-1} are attributed to CO_3^{2-} group appeared for all annealing temperature. When XRD results of the coatings were examined this structure is no visible.

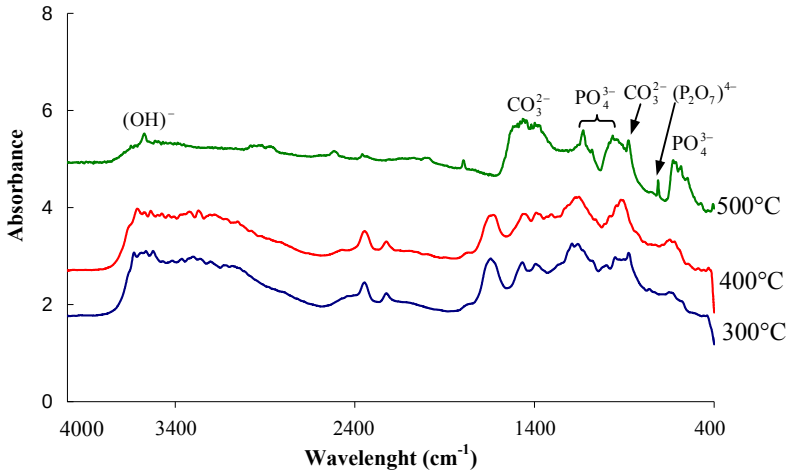

Figure 6.17 FTIR spectra of the coating on unmodified substrate annealed at different temperatures.

This CO_3^{2-} band is getting stronger in intensity for higher temperatures, suggesting carbonate concentration in the film. The resolution of the absorbtion bands within the coatings were improved considerably with the increasing temperature.

Thermal behavior of CaP based gels prepared by sol-gel technique using sols aged for 0h, 24h and 48h were depicted in Figure 6.18 (a) and (b). Thermogravimetric analysis of the samples showed that the total weight loss of samples were 58%, 32% and 20% for aging times 0h, 24h and 48 h, respectively (Figure 6.18(a)). As can be clearly seen that three weight loss stages exist for all samples, especially they are distinguishable for sample of A24. The first stage (30-100°C) indicates the evaporation of ethanol and absorbed water. The second stage (100-300°C) reveals removal of residuals, such as structural water and the third stage (230-500°C) occurs because of the nitrate decomposition. Occurrence of the greater weight loss with the decreasing aging time could be attributed to the greater amount of the residuals as reported in elsewhere (Liu, Troczynski, & Tseng, 2001). Above the temperature of ~500°C no further weight loss was seen indicating the completely removal of the residues. In the DTA curves of all samples with different aging times, big endothermic peak appearing at about 30-200°C range is related to evaporation of volatile components such as alcohols (C_2H_5O) and adsorbed water. Hydrolyzed phosphate was not completed as given in reaction (6.4) for sol solution of A0. Because of this reason, intense endothermic peak observed at 160°C which might be due hydrolyzed phosphate decomposition compared to the sol solution of A24 and A48. A weak exothermic peak at ~500°C for all samples is ascribed to the formation of crystalline apatite (Figure 6.18(b)).

Figure 6.19-6.23 presents SEM micrographs of the coatings obtained by using sols with different aging time. Some surface cracks are visible for the coating that obtained A24 sol solution (Figure 6.21). Surface cracks for this kind of coatings have a detrimental effect since integrity of surface can not be sustained for long period. Formation of the cracks is attributed to the excessive drying and sintering stress (Liu, Yang, & Tronczynski, 2002).

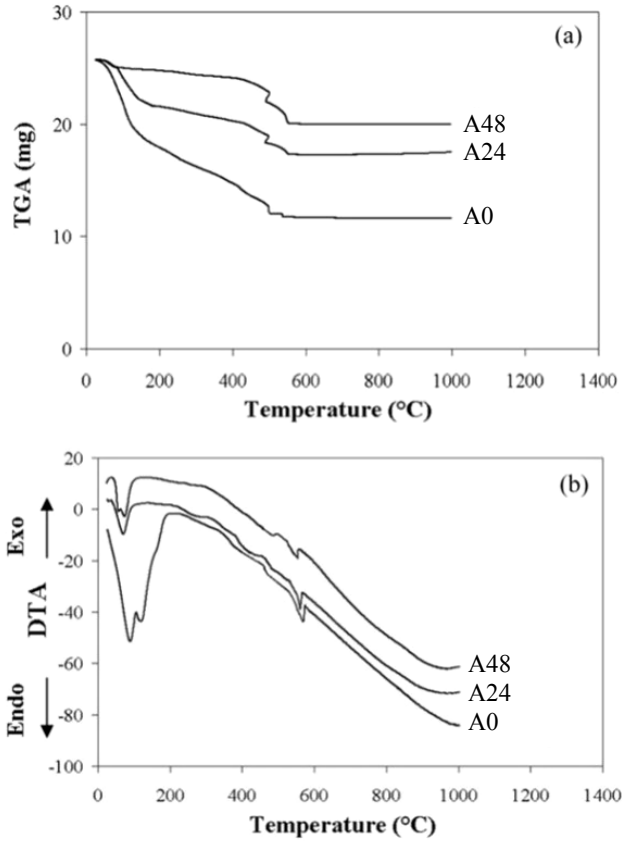

Figure 6.18 (a) TGA and (b) DTA curves of the samples prepared with 0h, 24 h and 48h aged sols.

SEM micrographs of the coatings by using A0 and A48 sol solutions show the surface of coating which was dense in appearance with considerable microcracks (Figure 6.19, Figure 6.23). Moreover, SEM observations of the coating A48 revealed the presence of nearly spherical agglomerates. On the other hand, the coating prepared by using A12 sol solution consists in adherent granules, leaving internal voids that produce somewhat porous structure. Besides this, cracks were present in structure. The pores developed in the coating are believed to be a result of gas evolution during thermal pyrolysis of residues as argued in elsewhere (Cheng, Gaorong, Wenjian, & Haibo, 2003).

Similar morphology with less porous structure can be seen for coating produced via A36 sol solution (Figure 6.22). Porosity is always required for biocompatible implants because living cells need a proper scaffold to proliferate and nutrition can

be supplied as cells migrate into to the porous space. However, existence of these cracks cause loss of structural integrity of the coating in application. Thus, desired coating should be porous and crack free structure. Among the coating produced by using sol solution of different aging time only the coating obtained by A24 seem to comply with the desired properties.

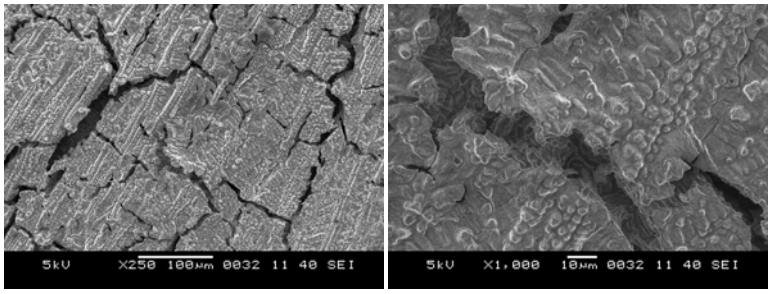

Figure 6.19 SEM images of the coating on unmodified substrate derived from A0 sol solution.

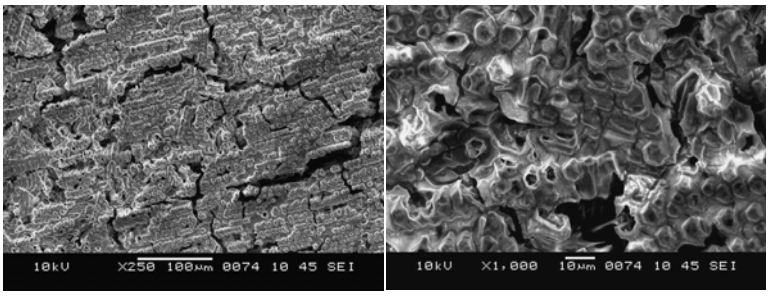

Figure 6.20 SEM images of the coating on unmodified substrate derived from A12 sol solution.

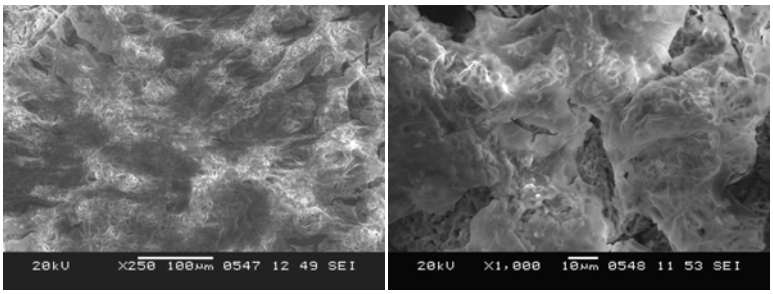

Figure 6.21 SEM images of the coating on unmodified substrate derived from A24 sol solution.

The EDS spectrum of the coating with A24 solution on untreated substrate surface is illustrated in Figure 6.24, where indicates the elemental composition of the coated

substrate is indicated. Intense peaks for calcium and phosphorous were obtained. Small peaks corresponding to Fe, Cr and Ni present in the alloy were also detected. The intense peaks for Ca and P suggest the presence of HAP coating. Deviation of the Ca/P ratio from the stoichiometric HAP value is ascribed to the existence of the $Ca_2P_2O_7$ phase.

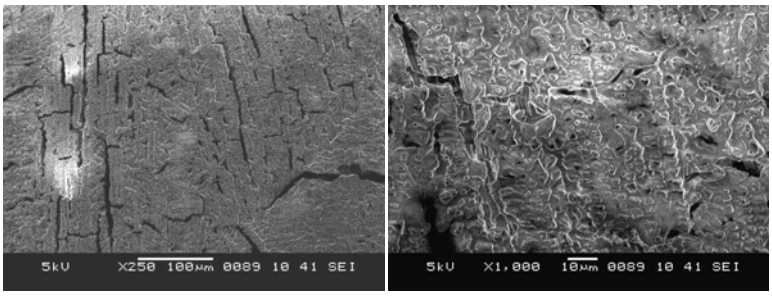

Figure 6.22 SEM images of the coating on unmodified substrate derived from A36 sol solution.

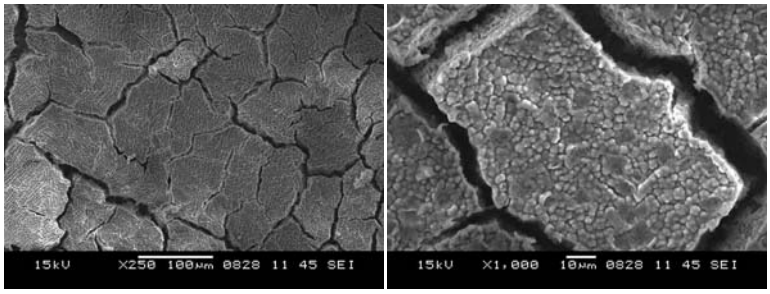

Figure 6.23 SEM images of the coating on unmodified substrate derived from A48 sol solution.

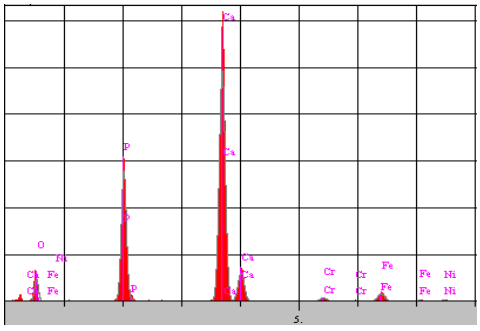

Element	Concentration (wt%)
Ca	33.22
P	16.05
O	45.49
Fe	3.40
Cr	1.14
Ni	0.70
Ca / P	2.06

Figure 6.24 EDS of the coating on unmodified stainless steel substrate synthesis with the A24 sol solutions.

Figure 6.25 depicts the variation of the Ca/P ratio of the coatings versus aging time of the sol solution. It can be seen that Ca/P ratio of coatings with different aging time are close to each other and fluctuate between 1.75 and 2.01.

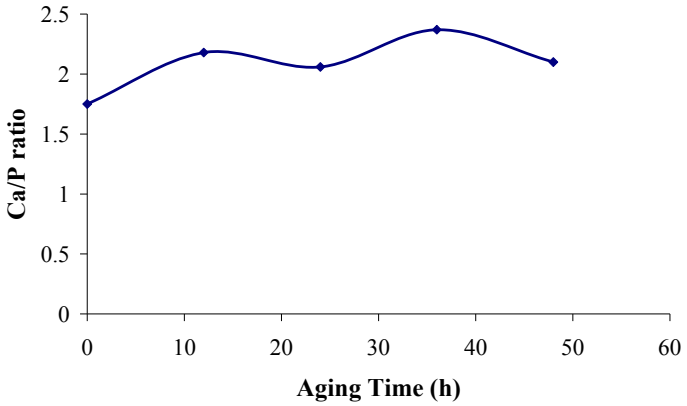

Figure 6.25 Change in Ca/P ratio as a function of aging time for coatings produced on unmodified substrates.

6.2.1.2 Effect of Substrate Surface Modification on the Coating Morphology

In order to investigate surface modification of substrate on coating morphology coatings were synthesized on substrates modified by galvanostatic cathodic polarization technique, alkali and acid treatment.

6.2.1.2.1 Coating Production on the Substrate Modified by Galvanostatic Cathodic Polarization. In this section, coatings were produced on substrate surface with CaP seed that was deposited by galvanostatic cathodic polarization. Substrates galvanostatically modified are named as GM1, GM2 and GM3 with respect to the current applied, as described in Chapter V.

Then, coatings were produced on these modified substrates by using sol solutions aged for 0h, 12h, 24h, 36h and 48h. Process names derived from sol solutions with varying aging time are given as A0, A12, A24, A36 and A48 for 0h, 12h, 24h, 36h and 48h aging, respectively. Substrate modification code is attached to the process names. For example, sample named as A0-GM1, represents coating on

galvanostatically modified stainless steel (GM1) synthesized by using sol solution with 0h aging (A0).

XRD patterns of the coatings on modified substrate by using A0 and A24 solutions are given in Figure 6.26 and 6.27, respectively. All of the coatings were shown to have been composed of the hydroxyapatite and calcium pyrophosphate.

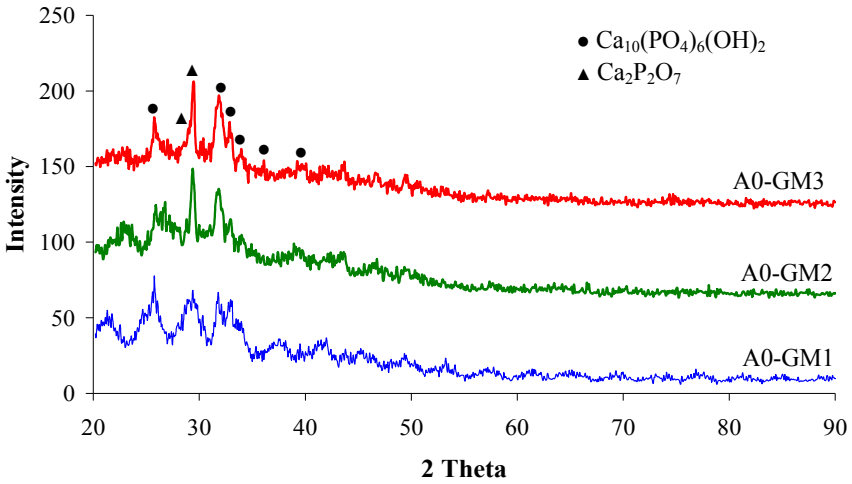

Figure 6.26 XRD patterns of the coatings on modified substrate using A0 sol solution by galvanostatic deposition.

All of the patterns appear similar except for the slight differences in peak intensities. XRD patterns given in Figure 6.26 and 6.27 look similar to those given in Figure 6.15 for coatings produced on unmodified surface using sol solution of different aging time. Besides, for all of the coating in both spectra peak intensities (corresponding to $Ca_{10}(PO_4)_6(OH)_2$ and $Ca_2P_2O_7$) were found to increase with the increasing amount of cathodic current used to deposit the CaP seeds under process as conditions of GM1, GM2 and GM3.

SEM micrographs of the coatings are given in Figure 6.28-6.32. SEM observations show that surface cracks are still existent especially for coatings of sol solutions aged for 0h, 12h and 48h. Surface modification induced by galvanostatic polarization seemed not to have provided a significant improvement for the coatings of A0, A12 and A48. However, a progress in terms of cracks in the coating was made

when coatings were produced by using A12 and A24 sol solutions, especially for coating A24.

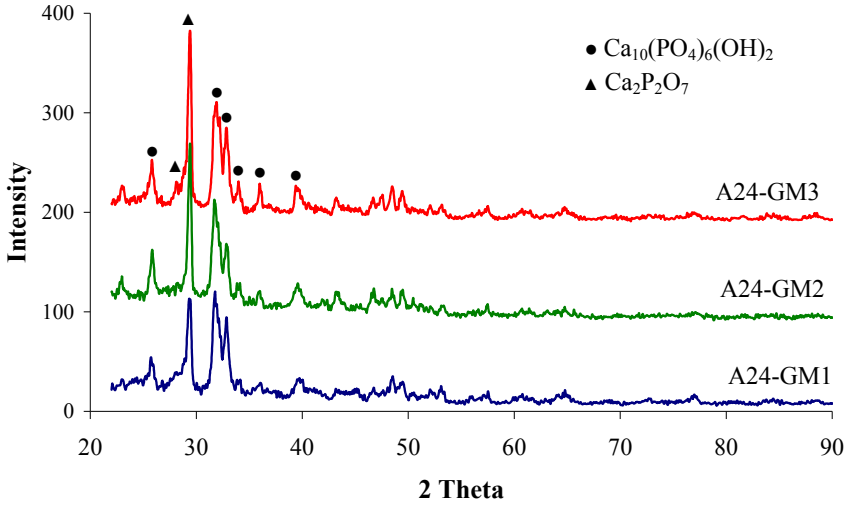

Figure 6.27 XRD patterns of the coatings on modified substrate using A24 sol solution by galvanostatic deposition.

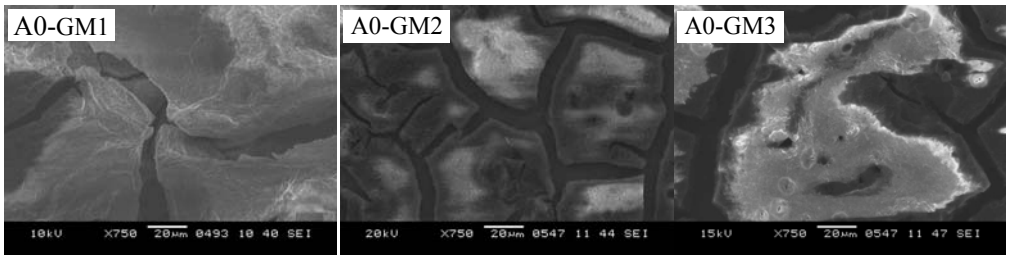

Figure 6.28 SEM images of the coatings on modified substrate by galvanostatic deposition by using A0 sol solution.

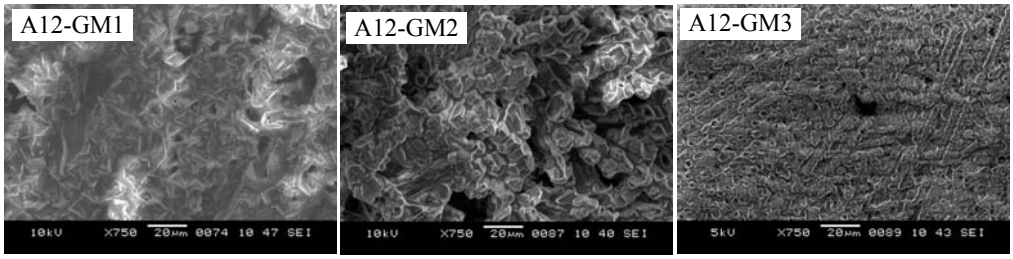

Figure 6.29 SEM images of the coatings on modified substrate by galvanostatic deposition by using A12 sol solution.

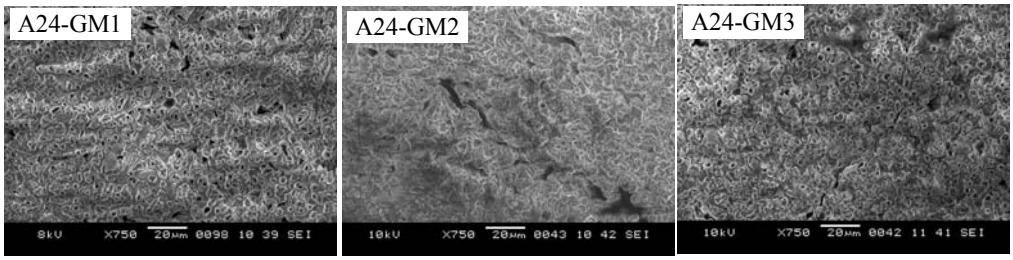

Figure 6.30 SEM images of the coatings on modified substrate by galvanostatic deposition by using A24 sol solution.

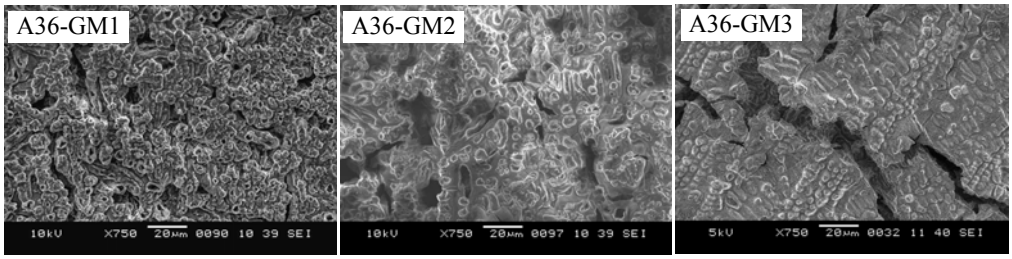

Figure 6.31 SEM images of the coatings on modified substrate by galvanostatic deposition by using A36 sol solution.

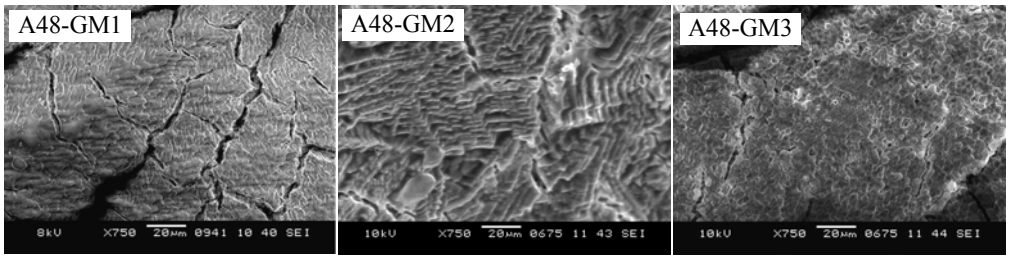

Figure 6.32 SEM images of the coatings on modified substrate by galvanostatic deposition by using A48 sol solution.

In order to determine Ca/P ratio of the coating EDS analysis was performed. Ca/P ratio was 2.19, 2.33 and 2.56 for coatings of A0-GM1, A0-GM2 and A0-GM3, respectively. Besides, for coating produced by using A12 on modified substrate with condition GM1, GM2 and GM3 Ca/P ratio was found as 3.33, 2.47 and 3.61, respectively. Ca/P ratio of coatings prepared by A24 solution was 1.84, 1.68 and 1.75 with similar sort order. These coatings' EDS analyses results are given in Figure 6.33. Ca/P ratio was determined as 3.25, 3.83 and 2.80 for coating of A36-GM1, A36-GM2, and A36-GM3, respectively. Finally, for coatings synthesized by using A48 have Ca/P ratio of 1.97, 1.69, 1.44 with increasing modified condition

named as GM1, GM2 and GM3, respectively. It is seen from the EDS results that no correlation can be identified between the aging time and modification conditions.

6.2.1.2.2 Coating Production on the Substrate Modified by Alkali Treatment. XRD patterns of coatings produced on alkali treated samples by using A24 sol solution are illustrated in Figure 6.34. There was not distinguishable difference of the XRD trace of the coatings. All of the coatings composed of hydroxyapatite and $Ca_2P_2O_7$ phases.

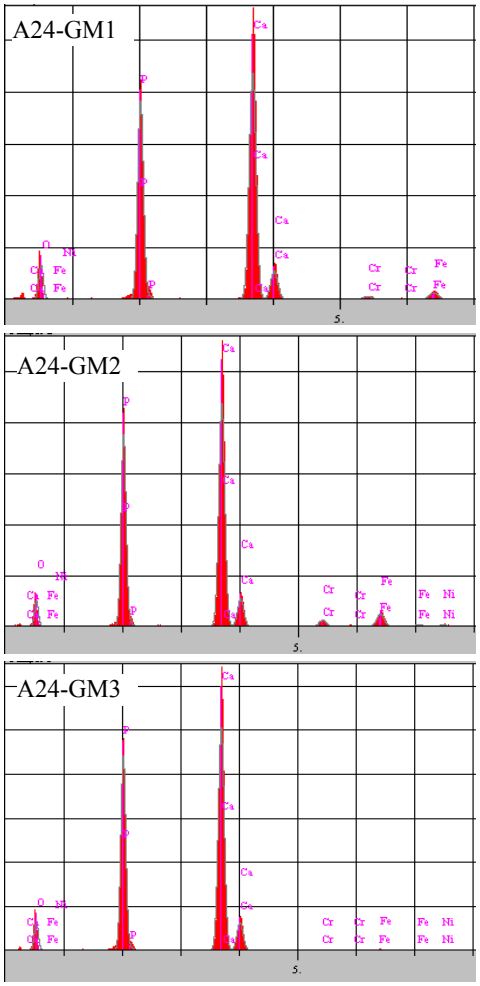

Element	Concentration (wt%)
Ca	35.29
P	19.18
O	41.61
Fe	2.12
Cr	0.95
Ni	0.85
Ca / P	1.84

Element	Concentration (wt%)
Ca	35.03
P	20.85
O	41.15
Fe	1.24
Cr	0.92
Ni	0.81
Ca / P	1.68

Element	Concentration (wt%)
Ca	33.95
P	19.40
O	45.08
Fe	0.70
Cr	0.41
Ni	0.46
Ca / P	1.75

Figure 6.33 EDS analysis of the coatings produced on alkali treated substrate by using A24 sol solution.

SEM micrographs of the coatings produced under the process conditions of A24-AT1, A24-AT2, A24-AT3 and A24-AT4 are shown in Figure 6.35. Coating

named as A24-AT2 shows better property with respect to porous network and homogeneous structure.

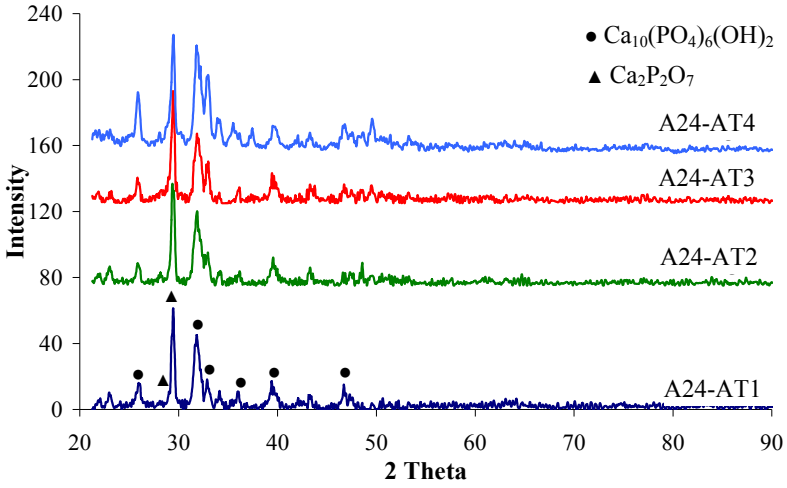

Figure 6.34 XRD patterns of the coatings on alkali treated substrate by using A24 sol solution.

After the coating process, peeling took place for the coatings of A24-AT3 and A24-AT4, which was attributed to the instable layer that composed of iron oxide and iron chromium oxide phases formed by alkali treatment at 600 and 700°C. For coating of A24-AT2 peeling was not occurred, this was considered due to a stable layer of sodium chromium oxide (see Figure 6.7) which would act as a bond layer to bridge up metallic substrate and later deposited apatite formed at 500°C. According to the EDS analysis result and spectra of the coating named as A24-AT1 is showed in Figure 6.36. Ca/P ratio values of the coatings of A24-AT2, A24-AT3 and A24-AT1 were estimated to be 2.38, 2.52 and 2.26, respectively.

6.2.1.2.3 Coating Production on the Substrate Modified by Acid Treatment. Coating produced on acid treated substrate was loosely adhered to the surface and easily peeled of; therefore it was investigated in form of powder. Thus, it was concluded that acid treatment of the substrate has not result in any improvement in coating quality in terms of it's the adhesion to the surface. XRD characterization showed that hydroxyapatite and calcium pyrophosphate phases were present in the

powder peeled of the surface (Figure 6.37). SEM micrograph and EDS analyze results are given in Figure 6.38.

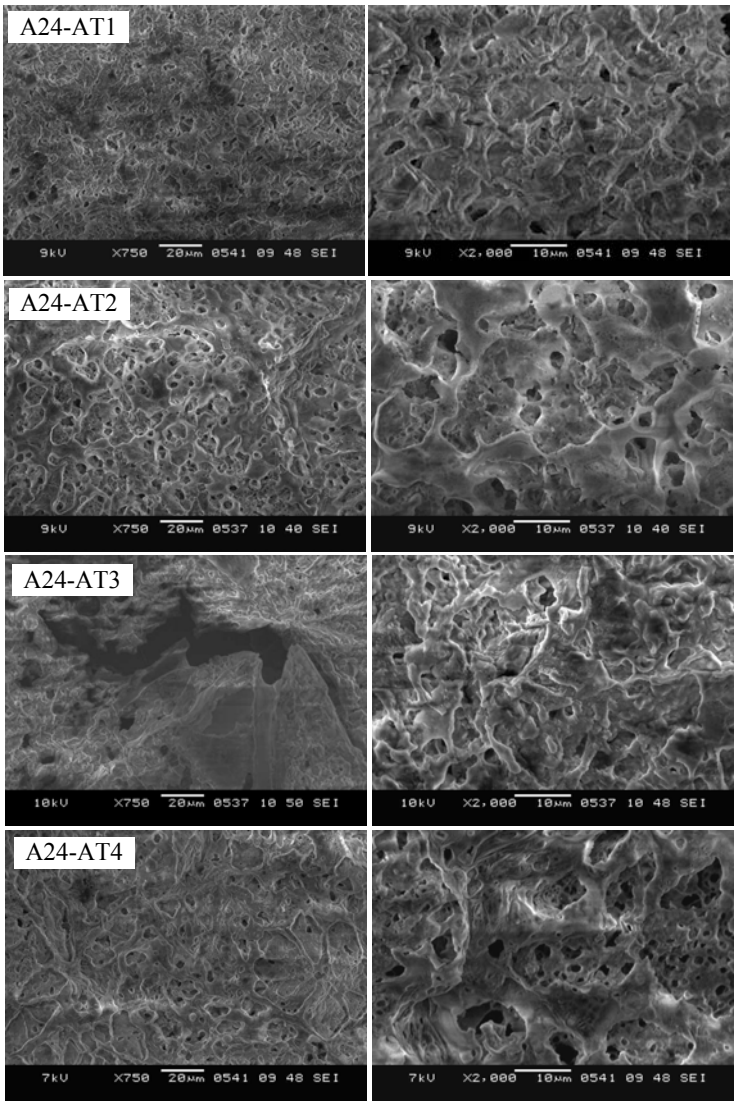

Figure 6.35 XRD patterns of the coatings on alkali treated substrate using A24 sol solution.

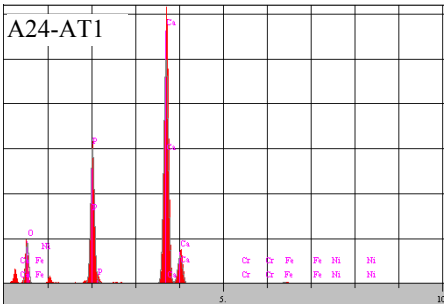

Element	Concentration (wt%)
Ca	31.83
P	13.55
O	53.95
Fe	0.37
Cr	0.14
Ni	0.16
Ca/P	2.35

Figure 6.36 EDS analysis of the coatings named as A24-AT1.

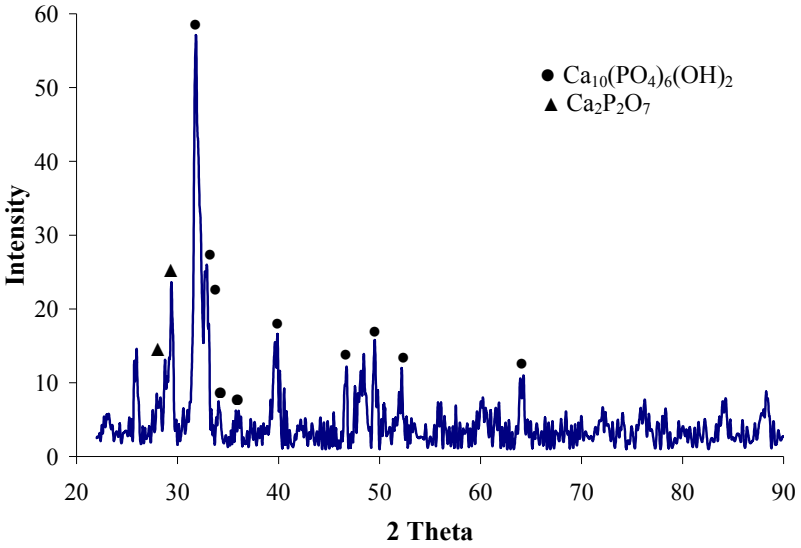

Figure 6.37 XRD pattern of the coating on modified substrate by acid treated using 24h aged sol solution.

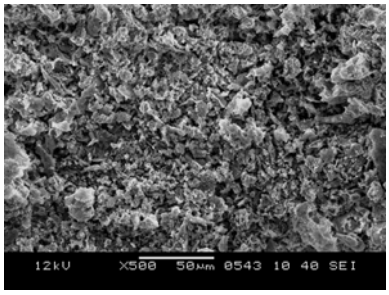

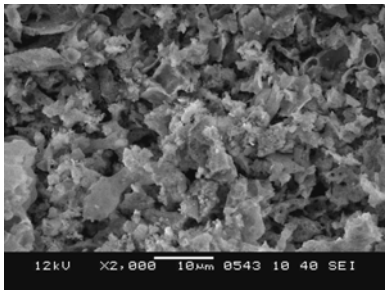

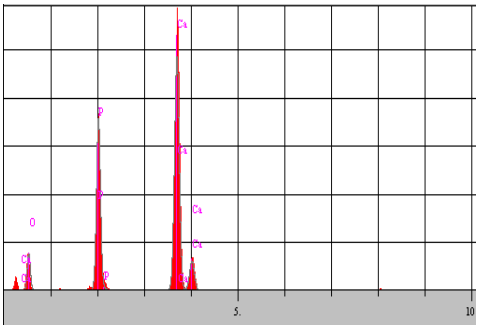

Element	Concentration (wt%)
Ca	32.63
P	16.73
O	50.64
Ca / P	1.95

Figure 6.38 SEM micrograph of the powder obtained form the sample named as A24-ACT and EDS analysis.

6.2.2 pH Effect of the Sol Solution

Sol-gel synthesis of HAP ceramics offers a molecular-level mixing of calcium and phosphorous precursors. A slow reaction between calcium and phosphorous precursors in the sol phase is necessary to lead gelation. For this reason, 24h or longer preparation time, named as aging period, prior to heat-treating in the sol-gel route is commonly reported in literature in order to obtain desirable product. During aging, the precursors react to form [-Ca-O-P-] multiple chains, i.e., polymerization and gelation occur, and the gelation increases with increasing time of aging. However, in some situations, precisely controlled conditions, such as prolonged aging periods (3-7 days) and aging at elevated temperatures (40-70°C) are needed to lead a gelation of the solution in order to obtain crystallization of the coatings in the course of heat treatment. Because of the instability of the solution without a complete gelation, the coating is frequently observed to form by-products such as calcium oxides (CaO), calcium carbonate ($CaCO_3$), and tricalcium phosphate (TCP) in an ambient atmosphere. Therefore the gelation conditions of sol are important and yet to be improved in order to obtain final coating properties satisfying homogeneity, structure uniformity and mechanical integrity. Kim, & Knowles (2005) were signified that sol stability should be progressed by means of accelerating the [-Ca-O-P-] chain formation, i.e. enhancing polymerization and gelation process. For this purpose acid or base catalyst is frequently added in order to alter pH of the sol solution to retard or increase the gelation and condensation process (Beganskiene, Dudko, Sirutkaitis, & Giraitis, 2003).

To assess the effect of basic catalyst in sol-gel solution on the uniformity and the final properties of the sol-gel derived HAP coating ammonia solution (28% NH_3, Merck) was used.

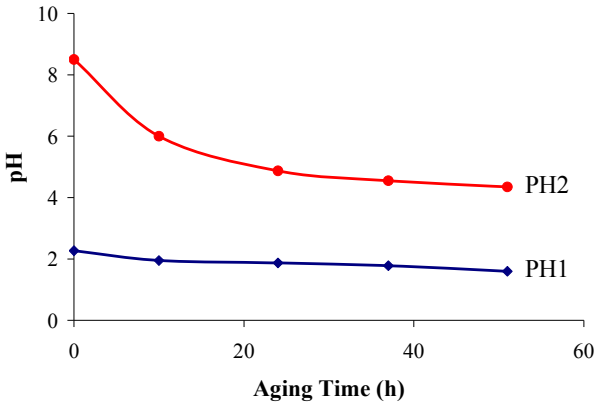

Figure 6.39 pH changes in the solution with various concentration of ammonia solution with respect to aging time.

6.2.2.1 Characterization of the Sol Solution

According to the Liu et al., (2002) when a calcium solution is added to the phosphorus solution, hydrolyzed phosphorous interacts with Ca^{2+} ions in aqueous solution through a polymerization reaction to form Ca-P intermediate, releasing protons during the reaction as given reaction (6.5).

Kim et al. (2002) reported that the aging process continued, the (Ca-P intermediate) constituted multiple chains and large amount of H^+ is produced, i.e., polymerization or gelation occurs. During the reaction the liberation of protons justifies the pH decreasing. At this point, the effect of basic ammonia additive provides a large number of OH^- ions to the solution. The OH^- ions surely acted as capturing the released H^+ ions; thereby the solution became less acidic and more importantly accelerating the reaction in forward direction. Following the addition of basic catalyst ammonia, the abrupt decrease in pH value of the sol was reported, which was reasoned to prove an increase in gelation reactions. Until the pH was stabilized, the OH^- ion continued to neutralize the H^+ ion once it was produced by the gelation reaction (Asomoza et al., 1998; Kim et al., 2005; Livage, Barboux, Vandenborre, Schmutz, & Taulelle, 1992).

Alteration of the pH value of the sol solution with ammonia addition versus aging time is given in Figure 6.39. The pH value of the sol solutions was measured during 50 hours and any significant change in pH value of the sol solution was observed after the aging time of 24h and nearly stabilized at certain values for all systems.

Because of this reason, coatings were synthesized after the aging time of 24h. pH value of the solution with 7% volume fraction of ammonia depicts sudden decreases relatively at short periods, and the pH decreased temperately with the increasing aging time. There was no significant change in pH value of the sol solution after the aging time of 24h and nearly stabilized at certain values for both systems. These pH values were 4.3 and 1.6 for volume fraction of ammonia solution of 7% and 3%, respectively. In order to obtain transparent sol solution, 7% ammonia addition was assigned as an upper limit of the addition because higher amount of ammonia addition causes precipitations in the solution.

Turbidity value was increased from 2.88 to 3.65 NTU (nephelometric turbidity units) with the increasing ammonia addition. This is attributed that addition of ammonia to the sol showed not detrimental effect in terms of the solution turbidity.

Figure 6.40 demonstrates XRD patterns of the coatings derived from the sol solution named as PH1 and PH2. Coatings of PH1 and PH2 that produced on unmodified stainless steel substrate have similar diffraction patterns, irrespective of the pH of the solution. Both of the coatings obtained with ammonia solution composed of pure HAP phase.

DTA-TGA analysis of the samples obtained from PH1 and PH2 sol solutions are given in Figure 6.41. Temperature regions and corresponding weight losses for the curves are summarized in Table 6.3. The first endothermic peak at low temperature is related to the removal of alcohols and absorbed water. The second exothermic peak is associated with the combustion of the organics. Besides, the crystallization temperature of the sample is defined as an exothermic peak. This peak can be clearly seen for sample produced by PH2 sol solution.

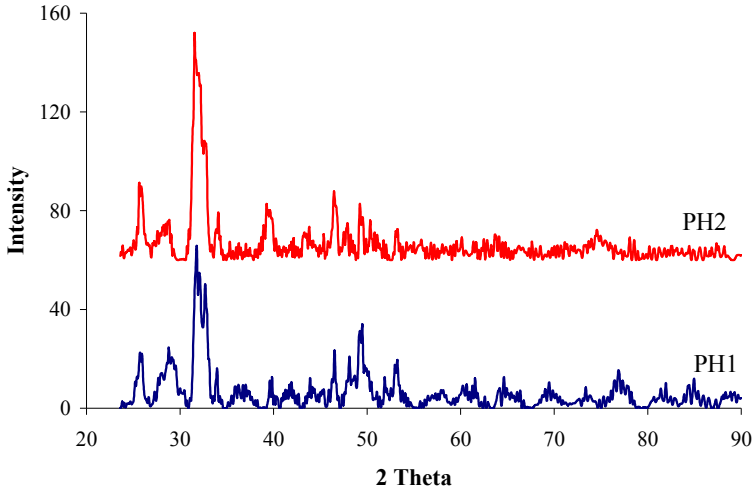

Figure 6.40 XRD patterns of the coatings on unmodified substrates by using various concentration of ammonia solution.

Table 6.3 DTA/TGA results of the samples obtained from PH1 and PH2 sol solutions.

Sample	Temperature Range (°C)	Effects		Weight Loss(%)
		Endo	Exo	
PH1	25-97	✓	-	8.94
	110-300	-	-	
	310-480	-	-	20.98
	480-510	✓	-	16.45
PH2	28-148	✓	-	15.43
	245-312	-	✓	14.06
	420-493	-	✓	14.85

Morphologies of coatings by using solutions of PH1 and PH2 are given in Figure 6.42. As indicated in figure morphology of the coating PH1 has a porous and crack free structure which is essential for implant longevity. Porosity is always required for biocompatible implants because living cells need a proper scaffold to proliferate and nutrition can be supplied as cells migrate into to the porous space. It is believed that pores are developed in the coating as a result of gas evolution during thermal pyrolysis of residues (Cheng et al., 2003). SEM observation revealed that production of coating with PH2 sol solution induced a coating coalescence process which caused the obliteration of pores and gave a more smooth appearance to the coating. Elementel analysis signified that the coatings prepared by using of PH1 and

PH2 sol solutions have Ca/P ratio values of 2.20 and 2.27, respectively.

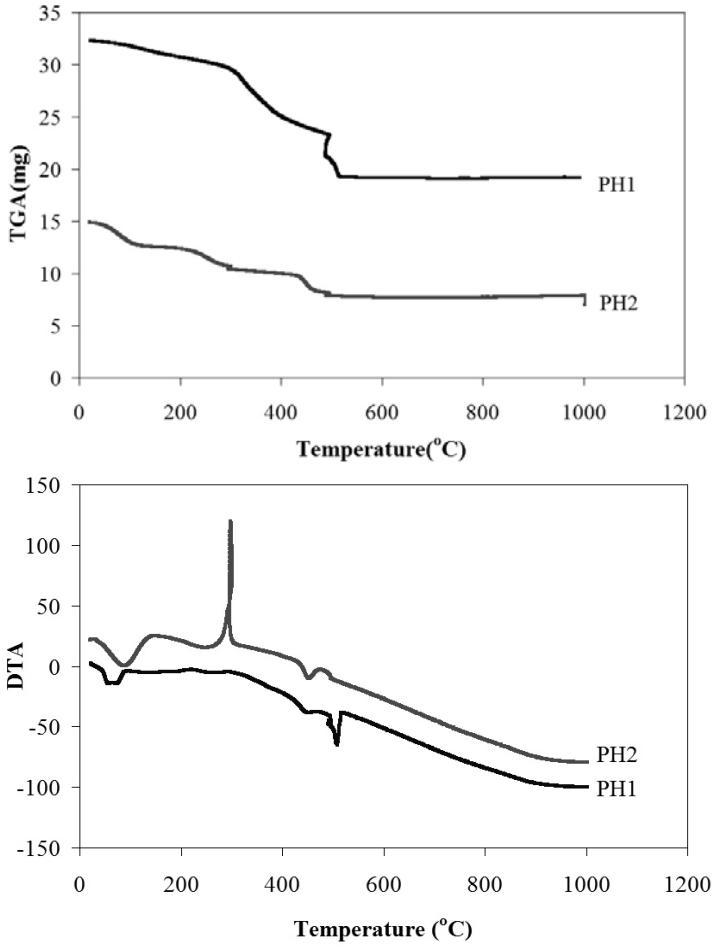

Figure 6.41 DTA-TGA analyses of PH1 and PH2 sol solutions.

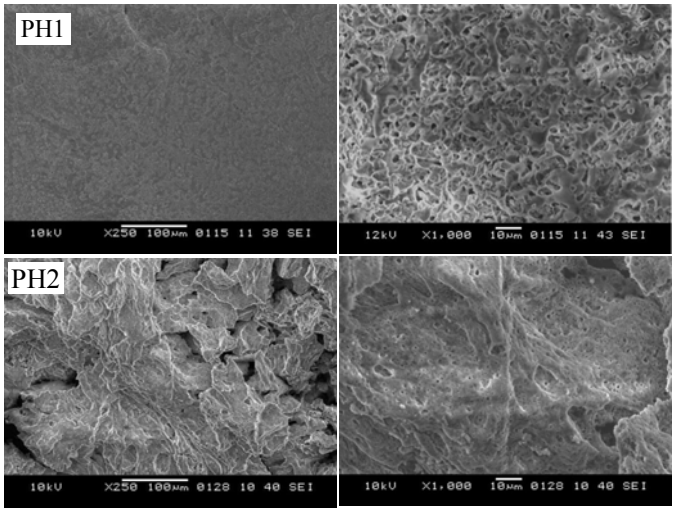

Figure 6.42 SEM micrographs of coatings on unmodified substrates by using PH1 and PH2 sol solution.

The FTIR spectrum of the coating produced by using PH1 and PH2 solution containing 3% and 7% vol ammonia respectively is shown in Figure 6.43. Both of the spectra similar each other aside from the diffuse peak observed around 3400 cm^{-1} for PH2 which indicated are adsorption of water in the coating. Therefore, in the spectra of this coating characteristic band for O-H stretching peak at 3570 cm^{-1} was not so obvious as observed in the coating of PH1. On the other hand, vibrations located in the range from 1100 to 960 cm^{-1}, and 606, 550 and 468 cm^{-1} are associated with the PO_4^{3-} group.

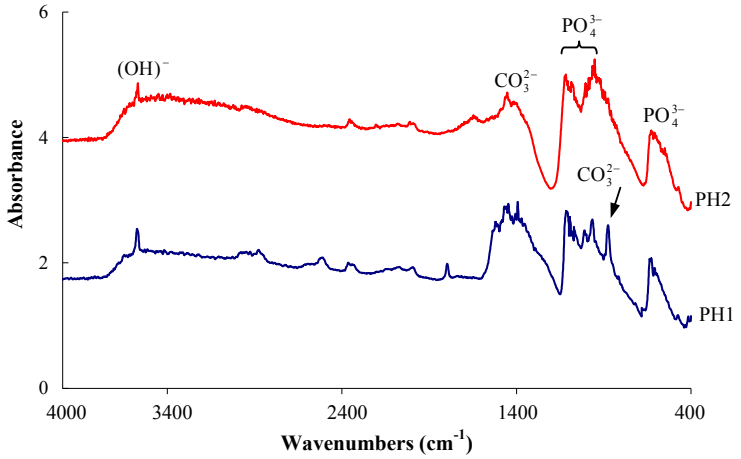

Figure 6.43 FTIR spectrum of the coatings on unmodified substrates derived form the PH1 and PH2 sol solutions.

The bands detected at 1500, 1460, 1410, 1068 and 872 cm^{-1} are assigned to the CO_3^{2-} group of B-type carbonated apatite. As can be seen in figure, there is no peak related with the calcium pyrophosphate. Thus, a result of the FTIR spectra of coatings corroborates the XRD results, showing only the HAP phase.

In order to investigate the effect of CaP seeds on the film forming capability of the surface modified substrate were coated by sol solution using PH1 (3% vol) and PH2 (7% vol) ammonia added sol solutions. Coatings were produced on modified substrate as marked of PM1, PM2 and PM3 according to the pulse current mode. XRD patterns of the coatings obtained from PH1 sol solution on these modified substrates are illustrated in Figure 6.44. All of the coatings constituted from the

hydroxyapatite and calcium pyrophosphate. It can be seen that the intensity of the patterns increases with the increasing of amount CaP seeds on the surface that was controlled by means of deposition parameters such as current and deposition time. Formation of the calcium pyrophosphate is a remarkable result of this coating process. This structural change in coating was thought to have been induced by presence of brushite on the pulse modified surface that somewhat promoted of the secondary phase $Ca_2P_2O_7$, since coatings on unmodified substrate synthesized by using this sol solution was composed of only hydroxyapatite phase. Same results were also found for coatings synthesized by using PH2 on pulse modified surfaces group that consist of PH2-PM1, PH2-PM2 and PH2-PM3. Therefore demonstration of these coatings XRD pattern was found unnecessary.

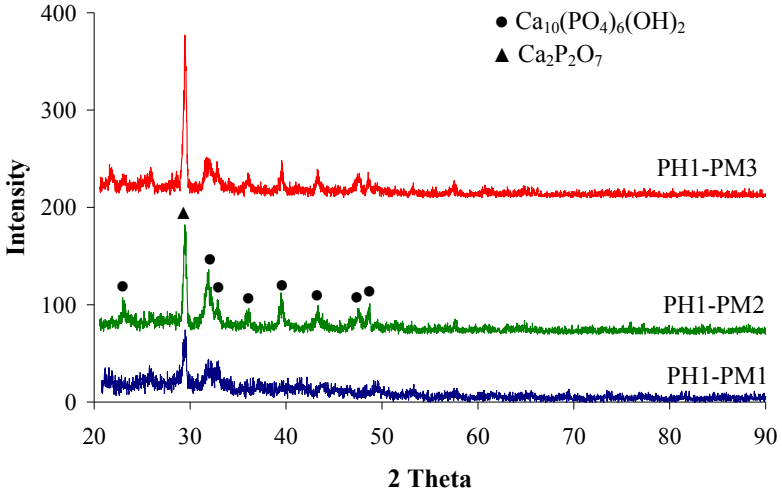

Figure 6.44 XRD patterns of the coatings on cathodic pulse-current modified substrates via puls deposition technique by using PH1 sol solution.

SEM micrographs of the coatings of PH1-PM1, PH1-PM2 and PH1-PM3 are given in Figure 6.45. Coating named as PH1-PM3 appeared to be relatively dense and porous structure when compared with the other coatings. These pores seem connected to each other form a continuous network. When SEM micrographs of the coatings of PH2-PM1, PH2-PM2 and PH2-PM3 are examined, coating of PH2-PM1 has better morphology with porous and homogenous structure among them. Coating named as PH2-PM3 has somewhat smooth structure when compared to coating of PH2-PM1, but with somewhat more irregular form of pores (Figure 6.46).

EDS analysis results of the coatings of PH1-PM3 and PH2-PM3 are depicted in Figure 6.47. According to the EDS results of coatings amount of elements of Fe, Cr and Ni are quite low indicating a highly dense structure of the coatings. Table 6.4 shows the Ca/P ratio values of aforementioned coatings.

Table 6.4 Ca/P ratio of the coatings synthesized on pulse modified substrate by using PH1 and PH2 sol solutions.

Coating	**PH1**			**PH2**		
	PM1	PM2	PM3	PM1	PM2	PM3
Ca/P ratio	2.42	2.64	2.96	2.78	3.2	2.89

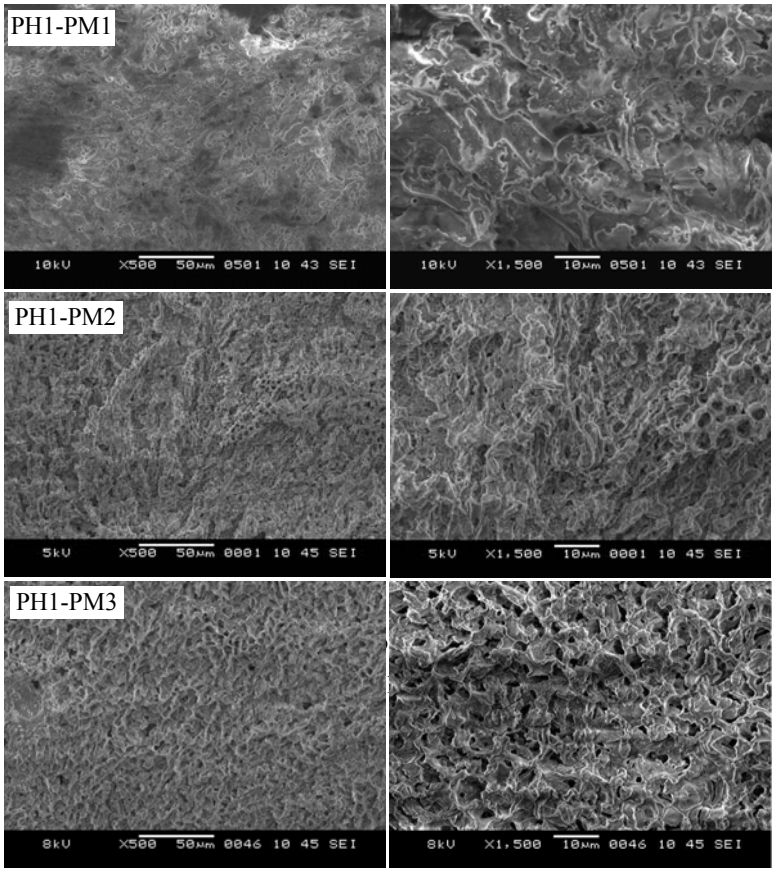

Figure 6.45 SEM images of the coatings on modified substrates via puls deposition technique by using PH1 sol solution.

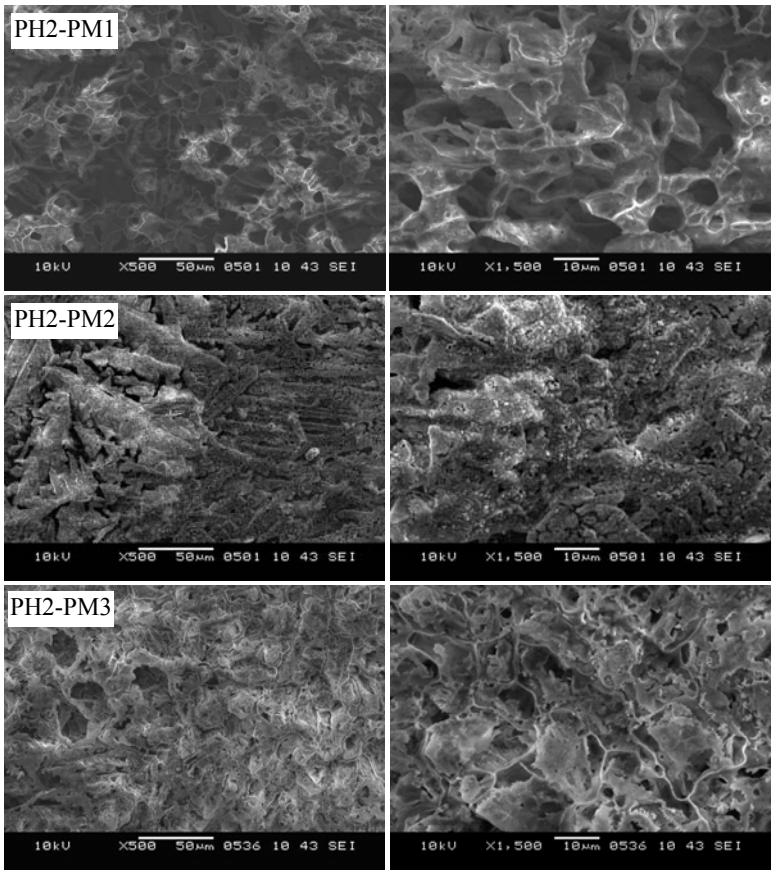

Figure 6.46 SEM images of the coatings on modified substrates via puls deposition technique by using PH2 sol solution.

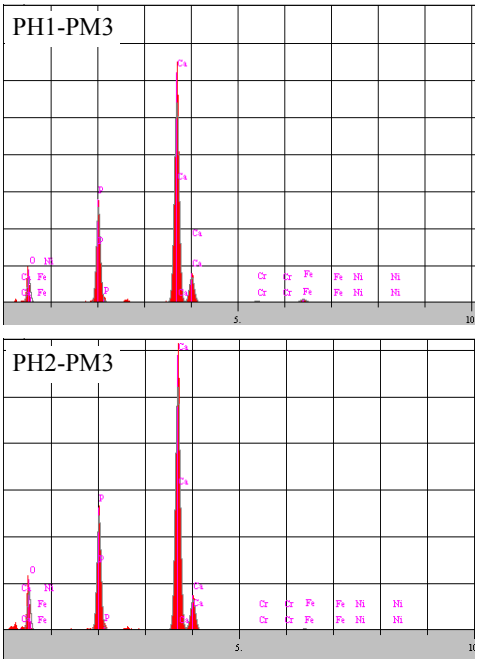

Element	Concentration (wt%)
Ca	36.83
P	12.45
O	48.37
Fe	1.58
Cr	0.48
Ni	0.29
Ca / P	2.96

Element	Concentration (wt%)
Ca	34.08
P	11.44
O	53.77
Fe	0.42
Cr	0.12
Ni	0.17
Ca / P	2.98

Figure 6.47 EDS analysis of the coatings named as PH1-PM3 and PH2-PM3.

6.2.3 Effect of the Additives into the Sol Solution

6.2.3.1 Silica Addition to the Sol Solution

Recently, silicon substituted HAP (SiHAP) has been explored as an alternative to pure HAP in coating applications. This interest arose from previous studies that indicated that small amounts of Si in bulk HAP ceramics accelerated the bone remodeling process and the quality of bone formed (Thian, Huang, Best, Barber, & Bonfield, 2006).

In this section of the study, two different levels of silica based precursors ($Si(OCH_2CH_3)_4$) were added to the sol solution to investigate this addition on morphology and structure of the coating. Coatings were named according to the quantity of the silica based precursor as Si-1 and Si-2 preparation details of which are given in Chapter V.

Introduction of silica based precursor did not cause a significant alteration for the pH value of solution. The pH of the prepared CaP+Si sol at the beginning was measured 0.7 then decreased to the value of 0.3 in the course of 24h aging process. On the other hand, the effect of silica addition on turbidity was insignificant. Turbidity value of the CaP+Si sol was increased from 4.78 to 5.42, depending on the increase in the amount of silica based precursor.

XRD pattern of the coating named as Si-1 and Si-2 is depicted in Figure 6.48. The XRD characterization demonstrated that patterns for both coatings showed similar profiles. And both of the coatings were composed of HAP and $Ca_2P_2O_7$ phases, no additional phases were detected indicating incorporation of silicon (or silicate) into the apatite structure. This argument is in agreement with the results obtained by other researchers who showed silicate ions are substituting phosphate groups (Arcos, Rodriguez-Carvajal, & Vallet-Regi, 2004; Gibson et al. 1999; Van Dijk, Schaeken, Wolke, & Jansen, 1996). Gibson et al. (1999) indicated that incorporation of the silicate into apatite lattice where it occupied a “phosphorous” site is correct, only if

there is a reduction in the number of OH groups in the unit cell. In order to compensate the extra negative charge of the SiO_4^{4-} groups, some of the OH^- ions would be lost to retain the charge balance; hence, initially the composition of the coatings could be described as $Ca_{10}(PO_4)_{6-x}(SiO_4)_x(OH)_{2-x}$.

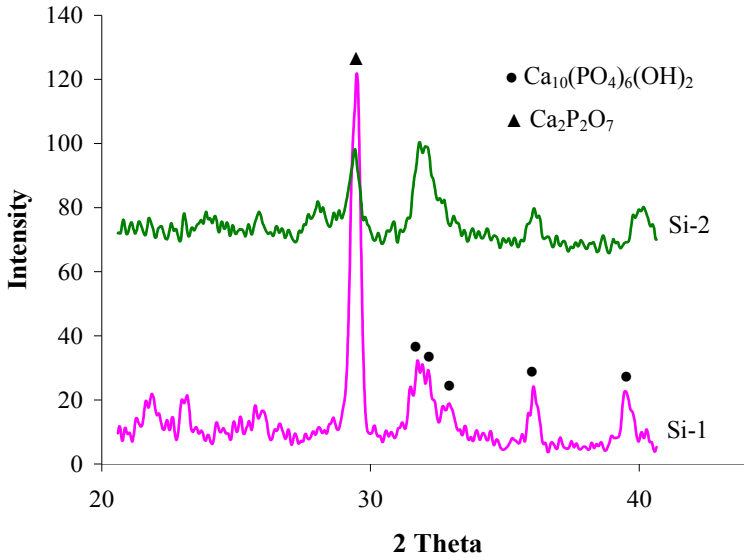

Figure 6.48 XRD patterns of coatings produced by using sol solution with silica based precursor.

Besides, it can be clearly seen that broadening of the hydroxyapatite maxima peak occur with the introduction of the silicon precursor into the CaP based sol. This broadening induced by silicon precursor incorporation is consistent with the findings of Hijon, Cabanas, Pena, & Vallet-Regi, (2006).

Figure 6.49 presents the FTIR spectra of the coatings produced by produced Si-1 and Si-2 sol solutions. The intense bands in the ranges 570-600 and 960-1100 cm^{-1} attributed to the major absorption modes of the phosphate groups, the O-P-O bending mode and P-O stretching mode, respectively. The carbonate groups in the apatite structure can be detected in both of the coatings by the appearance of bands at 873, 1430, 1460 and 1500 cm^{-1}. The broad band from 2500 to 3700 cm^{-1} is due to the moisture in the samples, while a weak hydroxyl band appear at 3570 cm^{-1}. Absorbance band at 725 cm^{-1} is associated with the calcium pyrophosphate (Gimenez et al., 2001; Müller et al., 2007). The modification of PO_4^{3-} bands in the presence of

silicon could be associated with the incorporation of silicate ions into some phosphate sites of lattice, which provoke changes in the bonding and asymmetry of the phosphate groups. In addition, the contribution of the intense Si-O-Si asymmetric stretching mode around 1080 cm^{-1} could also justify the broadening of these bands. This finding is in agreement with the literature (Hijon et al., 2006). Besides, additional peaks at 840 and 950 cm^{-1} arise from the silicate. This result is in concurrence with the study of Gibson et al. (1999) on silicon-substituted hydroxyapatite. They also indicated that one more additional peak at 890 cm^{-1}, but this peak is blocked in our finding because of the sharp carbonate peak at 870 cm^{-1}. As a result FTIR results corroborate the XRD results.

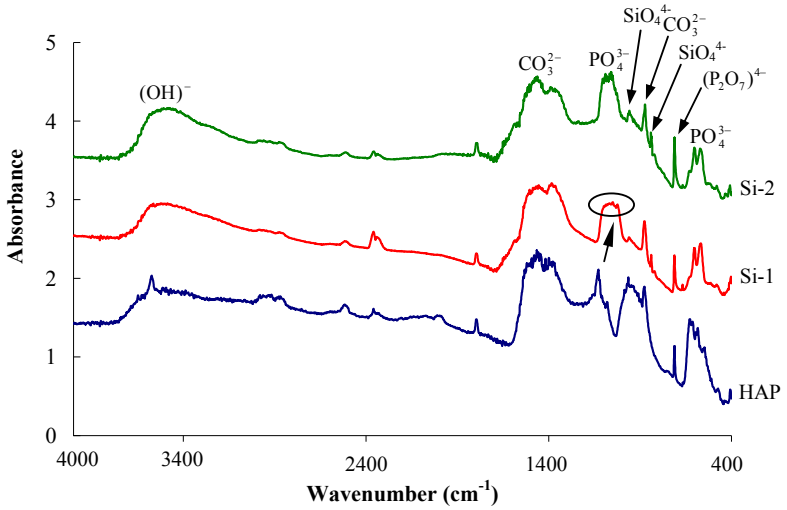

Figure 6.49 FTIR analysis of coatings produced by using different silica containing solution.

SEM observations showed that the surface of the coatings was homogeneous and dense in appearance and that no cracks were found, as shown in Figure 6.50. Increasing silica content converted the morphology to more dense porous structure EDS analysis of the coatings are given in Figure 6.51. It is seen from results that Ca/(P+Si) ratios of the coatings were fairly deviated from the stoichiometric Ca/P ratio of the HAP. It can be thought that incorporation of some silicate ions into some phosphate ions give rise to increment of Ca/P ratio. Besides, EDS analyze shows that silica content was found as 2.25 and 2.6 for coatings produced by Si-1 and Si-2 sol solutions, respectively.

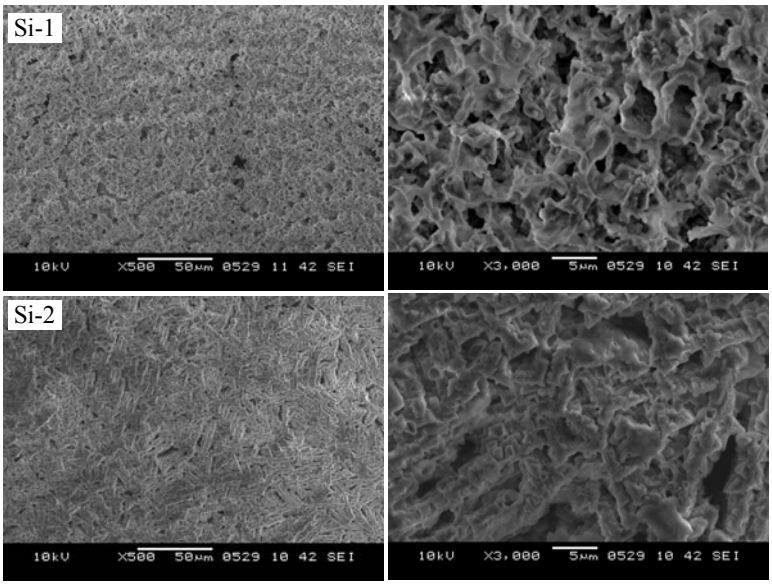

Figure 6.50 SEM micrographs of coatings prepared by using silica based precursor additive.

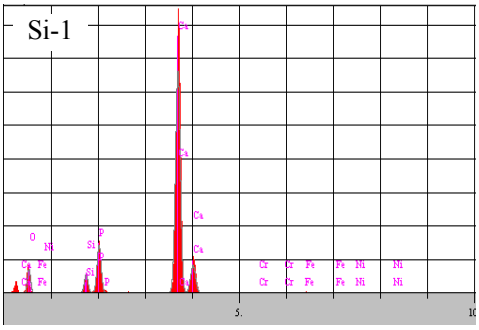

Element	Concentration (wt%)
Ca	40.66
P	6.48
O	49.97
Si	2.25
Fe	0.32
Cr	0.15
Ni	0.17
Ca /P+Si	4.65

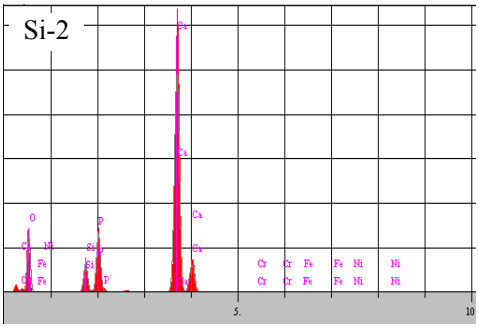

Element	Concentration (wt%)
Ca	27.62
P	5.84
O	63.57
Si	2.65
Fe	0.16
Cr	0.08
Ni	0.08
Ca / P+Si	3.25

Figure 6.51 EDS analysis of the coatings by using silica based precursor additive.

6.2.3.2 Polyvinyl alcohol (PVA) Addition to Sol Solution

Preparation of the coatings called as PVA1, PVA2 was performed using sol solution by means of different PVA content in the sol solution. Preparation details were given in chapter V. Introduction of the polyvinyl alcohol into the aged sol solution was not caused a significant change in pH of the mixed solution. After the addition of PVA, pH value of the mixing was measured as 0.3 and 0.5 with increasing amount of the addition for PVA1 (20% vol) and PVA2 (40% vol) respectively. Similarly, turbidity measurements indicated that addition of PVA did not show a negative effect on the turbidity of the mixture. Turbidity of the mixing was measured as 3.8 and 3.60 for PVA2 and PVA1 sol solutions, respectively.

After the coating process, coating named as PVA2 has flake-like appearance and loosely bond to the substrate. Therefore, this coating was investigated in form of powder scraped from the surface for its surface morphology and phase analysis. XRD patterns of the coating PVA1 and PVA2 were given in Figure 6.52. XRD revealed the formation of hydroxyapatite and $Ca_2P_2O_7$ phases. Both of the coatings exhibited almost similar diffraction pattern with characteristic peak of HAP. There was no additional phase caused by PVA addition to the sol solution.

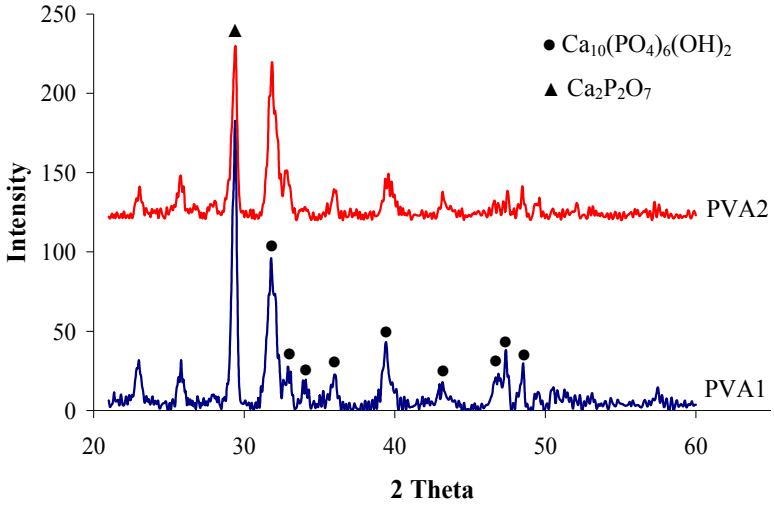

Figure 6.52 XRD patterns of the coatings produced by using sol solution with polyvinyl alcohol (PVA) additive.

Based on the available theory, polymers containing polar functional groups such as COOH, PO_4H_2 and OH -PVA contains OH polar functional groups- have been found to be useful as they provide a site for the selective adhesion of Ca ions because of the greater affinity to positive Ca ions. As the calcium ions accumulate on the surface, the surface gains an overall positive charge. Then, these positively charged surface sites will combine the negatively charged phosphate ions. Thus, nucleation of hydroxyapatite crystals in the solution was occurred (Mollazadeh, Javadpour, & Khavandi, 2007; Ramakrisha, Mayer, Wintermantel, & Leong, 2001).

FTIR spectra of the coatings prepared by using PVA added solutions are illustrated in Figure 6. 53. When spectra of the coatings derived from PVA added sol solutions are compared with the spectrum of HAP coating an increase in the (C-O) band at 1127 cm^{-1} was observed as PVA content was increased. PVA bands are identified by peaks at 3000-3500 cm^{-1} (H-bonded OH), 2940 cm^{-1} (C-H stretching) and 1085-1127 cm^{-1} (C-O stretching). Moreover, all spectra show a broad band 2700-3500 cm^{-1} corresponding to the hydrogen bonding.

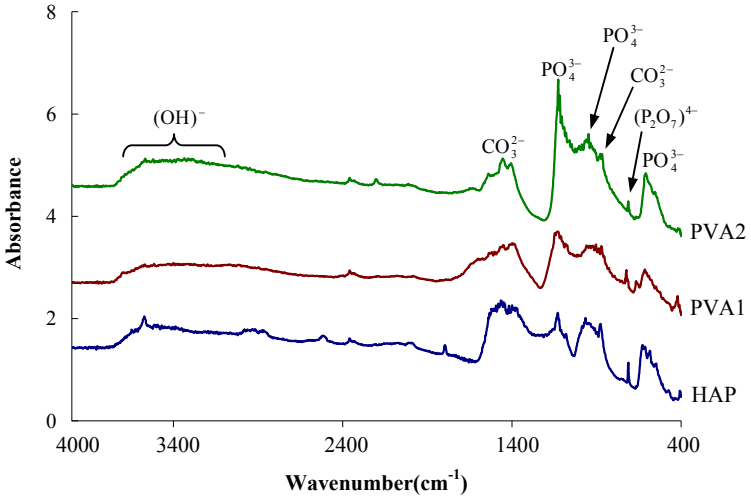

Figure 6.53 FTIR analyses of coatings produced by using different PVA containing solution.

The surface morphologies of the coatings PVA1 and PVA2 with various PVA contents are shown in Figure 6.54. The surface structure of the coating called as PVA1 was rough and porous, and has more cracks. Structure of the pores was

distinctly different from the coatings produced by PH1 sol solution, which seem to be connected with each other forming a continuous sponge-like network. On the other hand, Ca/P ratios of the coatings were close to each other with values of 2.70 and 2.94 for coating PVA1 and PVA2, respectively.

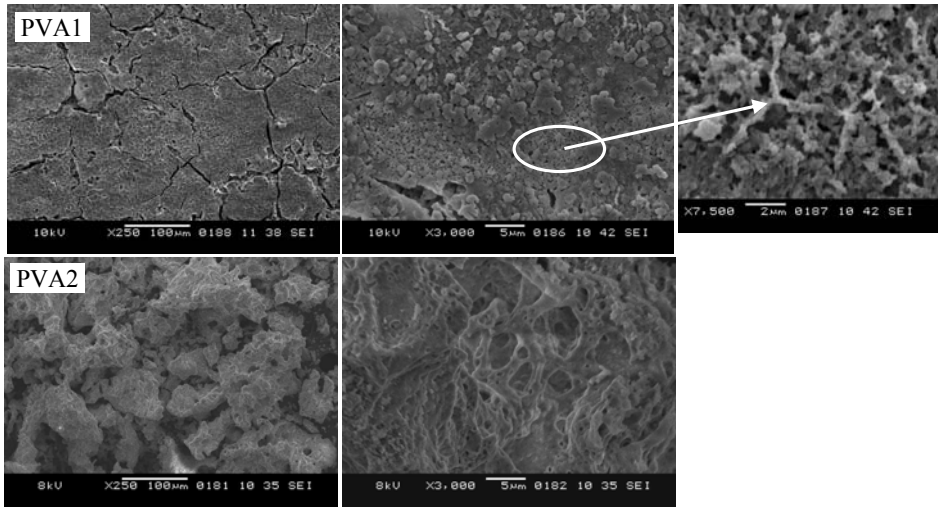

Figure 6.54 SEM micrographs of coatings produced by using sol solution with polyvinyl alcohol (PVA).

6.2.4 Effect of the Heat Treatment Regime on the Morphology of the Coating

Coatings were produced on unmodified substrate by using PH1 sol solution at the different heat treatment regime (HT1: 2°C/min and HT2: 10°C/min) in order to examine effect of the heat treatment regime on morphology of the coatings. XRD characterization demonstrated that both of the coatings were composed of hydroxyapatite and $Ca_2P_2O_7$ (Figure 6.55).

Koo, Kim, Yoon, No, & Bae, (1997) indicated that abrupt and fast heat treatment may induce the cracks or pores in the layers due to the thermal stress during the heat treatment or the evaporation of volatile organic materials. SEM observations revealed that morphology of the coatings becomes relatively smooth and characteristic porous structure was disappeared with decreasing rate of heating (Figure 6.56). It can be seen that voids with cellular structure are formed in regions

where organic materials leave the structure. Ca/P ratio value of the coatings is determined as 2.00 and 1.99 for sample of HT1 and HT2, respectively.

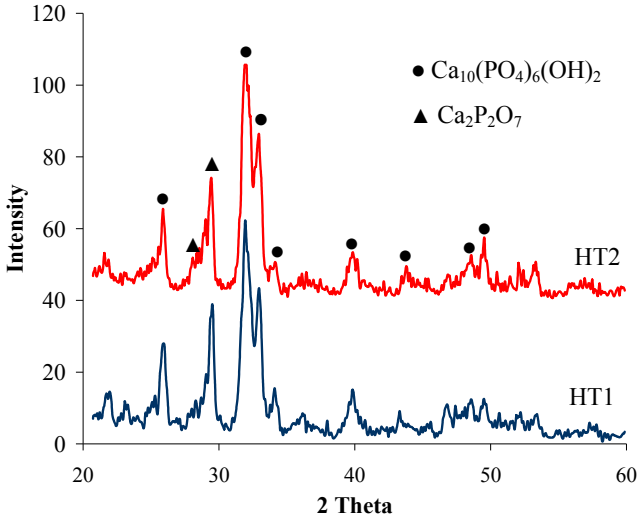

Figure 6.55 XRD patterns of coatings produced under different heat treatment regime.

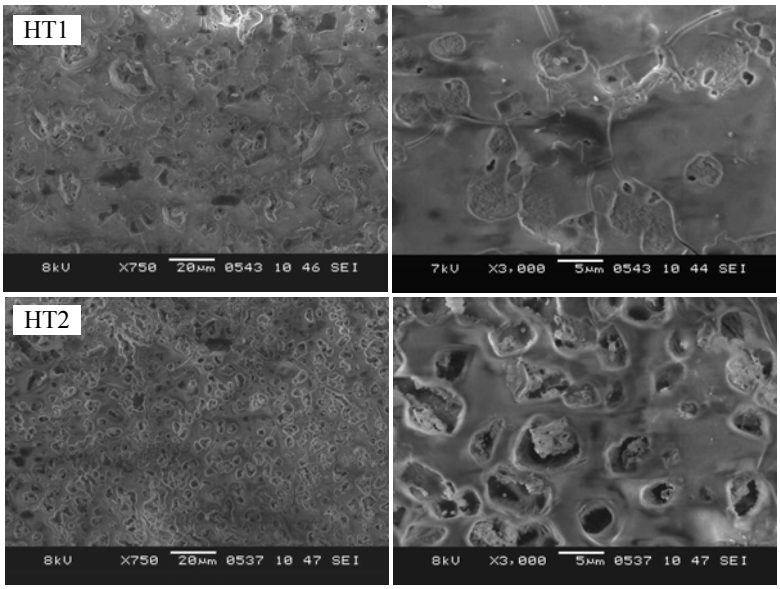

Figure 6.56 SEM micrographs of the coatings produced under the different heat treatment regime conditions by using PH1 sol solution on unmodified substrates.

6.3 Corrosion Properties

Corrosion properties of the coatings were investigated by using DC and AC corrosion techniques.

6.3.1 DC Polarization Technique

This method technique involves various polarization measurements such as potentiodynamic polarization for the determination the breakdown or critical pitting potential (E_b), the corrosion or open circuit potential (E_{corr}), corrosion current (I_{cor}) and the polarization resistance based on Tafel analysis which are all contained within the Gamry corrosion measurement software package. Corrosion testing was performed on the produced coatings named as PH1-GM3 and PH1-PM3 which were coated on seeded surface by galvanostatic (GM3) and pulse (PM3) electrodeposition technique using PH1 sol solution. Furthermore, a corrosion property of uncoated bare stainless steel substrate was examined in order to compare the corrosion performance of HAP coatings. Corrosion tests were conducted in physiological saline solution of 0.9% NaCl which was not deaerated.

Figure 6.57 shows the open circuit potential versus time curves for the uncoated and HAP coated 316L SS. The OCP of uncoated sample shifted towards active direction and reached a potential of -0.230 V vs. SCE in 30 min. This could be due to the dissolution taking place at the alloy surface indicating the disintegration of the passive film on the surface. The OCP-time curves of the HAP coated samples shifted towards noble direction.

The noble behavior of the HAP coated 316L SS could be due to the insulating nature of the surface lending itself expectedly to an improved corrosion resistance. The coatings on PH1-GM3 performed better. It is seen from Figure 6.57 that an initial OCP of -0.135 V (vs SCE), reached steady state within 20 min and attained a potential of -0.098 V (vs SCE). after 30 min. Electrochemical parameters of the

plain 316L SS and sol-gel coated 316L SS with surface modification through direct and pulsed current technique are shown in Table 6.5.

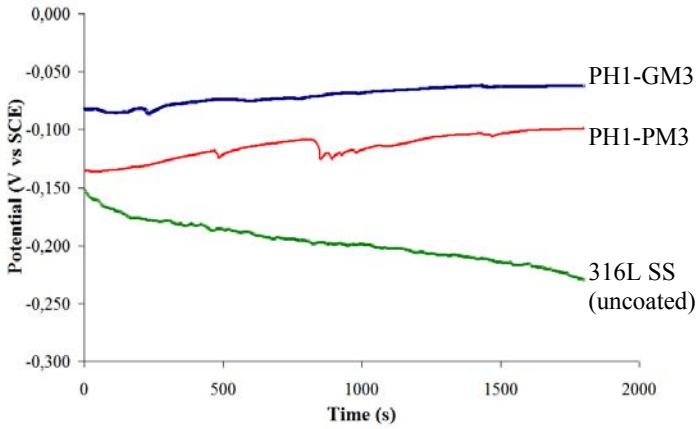

Figure 6.57 OCP versus time measurements of 316L SS with and without HAP coating in physiological saline solution.

Table 6.5 Electrochemical parameters of 316L SS with and without coatings in physiological saline solution (0.9% NaCl).

Sample	β_a (mV/decade)	β_c (mV/decade)	E_{corr} (mV)	E_b (mV)	I_{corr} (mA/cm^2)	R_p (MΩ cm^2)	Porosity (%)
316L SS	299.8	130.7	-230	245	2.63×10^{-4}	0.15	-
PH1-GM3	277.9	123.2	-62.6	280	2.34×10^{-5}	1.58	2.63
PH1-PM3	317.8	67.2	-98.8	253	4.85×10^{-5}	0.50	11.07

The uncoated 316L SS possesses higher corrosion current density thus lower corrosion resistance compared with coatings of PH1-GM3 and PH1-PM3 in physiological saline solution. Coating named as PH1-GM3 provided the lowest i_{corr} while the coating on PH1-PM3 showed a slightly higher i_{corr} than that of PH1-GM3. According to the corrosion current density of the coated steels, it was found that coating named as PH1-PM3 has stronger tendency towards corrosion in physiological saline solution. This is probably caused by higher porosity in the coating. It is clear that coating with a lower porosity exhibited an efficient barrier property against corrosion, whereby providing a decrease in diffusion rate of ions through the film to the substrate. The effect of the porosity can be seen clearly in polarization curve given in Figure 6.58. Polarization curve of the coating on PH1-PM3 shows more scatter and higher passive current density than coating of

PH1-GM3. This case could be explained with the existence of the pores providing open channels to the substrate for the corrosive species to diffuse through the coating to the substrate. The increment of the ion concentration in the pores may accelerate the rate of dissolution prompted by increase in the effective surface area of the coating. Fluctuation in the current density may be attributed to the sequential effect of pore-clogging by corrosion products and further dissolution aggravated by the increase in potential. Moreover, coating on PH1-GM3 have higher resistance to pitting corrosion as was indicated by a higher breakdown potential (E_b) than coating on PH1-PM3.

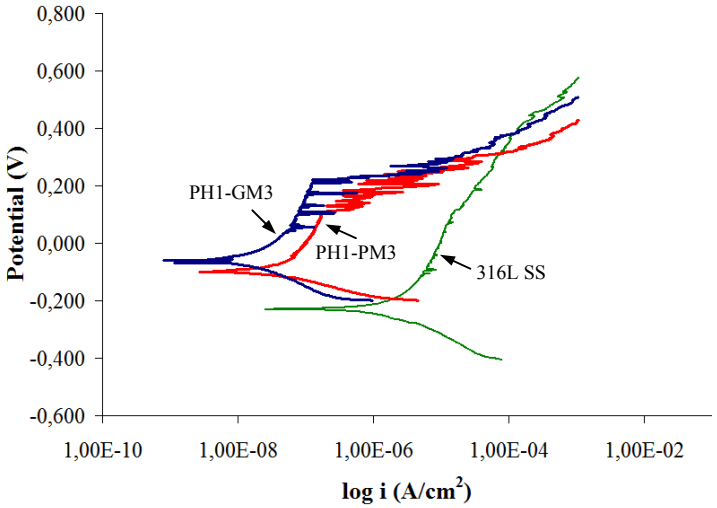

Figure 6.58 Polarization curves of coated and uncoated 316L SS in physiological saline solution.

Before and after corrosion testing, morphology of the coatings are illustrated in Figure 6.59-6.60(a) and (b). As explained coating of PH1-PM3 has completely porous structure but additionally, pores of this structure constitute a continuous network that separated with thick walls. Arrows indicated regions where dissolution process took place after the corrosion test.

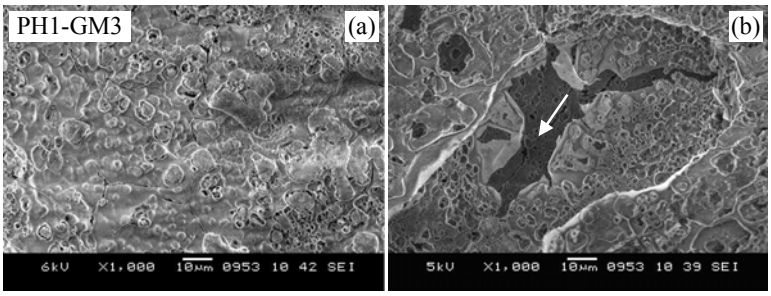

Figure 6.59 SEM micrographs of the coatings of PH1-GM3. (a) before corrosion test, (b) after corrosion test.

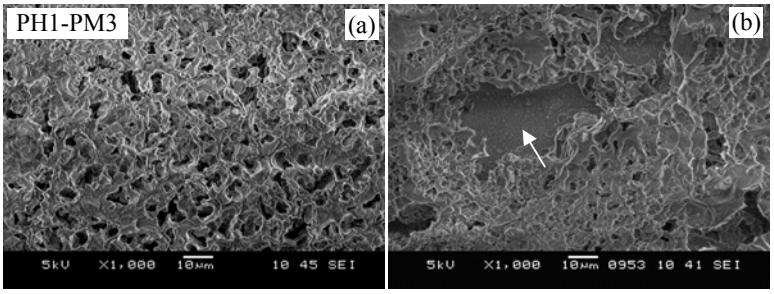

Figure 6.60 SEM micrographs of the coatings of PH1-PM3, (a) before corrosion test, (b) after corrosion test.

SEM micrograph and EDS spectrum for the coating of PH1-GM3 is given Figure 6.61. High peak intensity of the Ca, P and O elements prove the existence of the coating in the area indicated with the arrow dissolved region. Figure 6.62 depicts SEM micrograph and EDS spectrum of two different region of the coating named as PH1-PM3. When spectrums are compared, increment of the peak intensities of Fe, Cr and Ni elements that represent stainless steel substrate identifies intense dissolution in this region. On the other hand, peaks of Ca, P and O elements that refer HAP coating represent the existence of the coating.

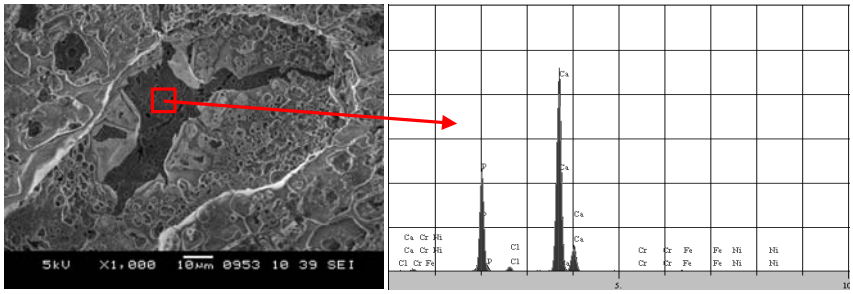

Figure 6.61 SEM micrographs and EDS analyze spectra of the coatings of PH1-GM3.

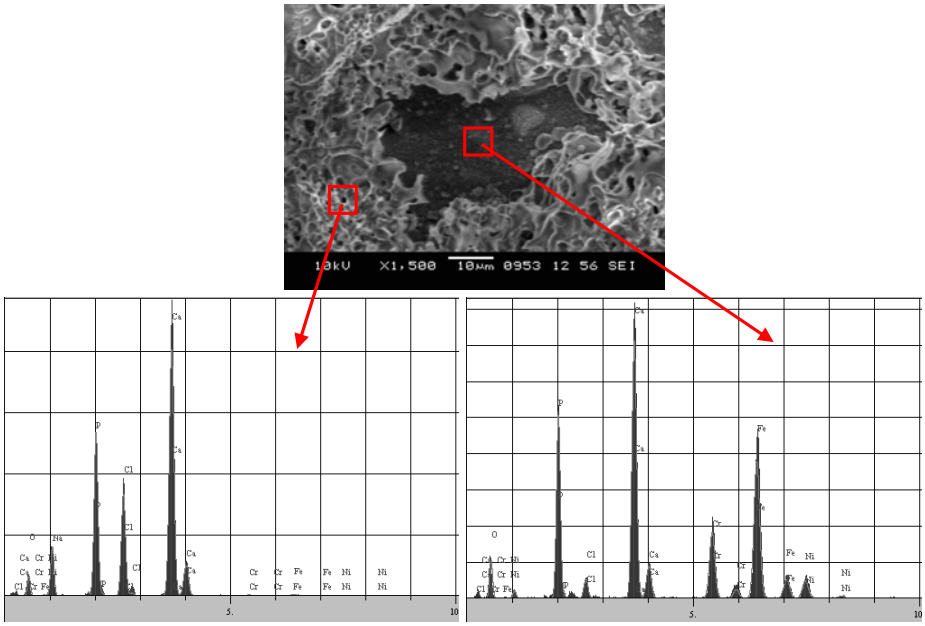

Figure 6.62 SEM micrographs and EDS analyze spectra of the coatings of PH1-PM3.

6.3.2 AC Impedance Technique

Results of EIS analysis are commonly presented as Bode and Nyquist plots. The Bode plot comprises two curves: the impedance curve (|Z| vs. frequency) and the phase angle curve (Z(ω) phase vs. frequency) measured over a range of frequencies in logarithmic scale. The expression for Z(ω) is composed of a real and an imaginary part. To get Nyquist plot, real part (Z') is plotted on the X axis and the imaginary part (Z") on the Y axis of a chart. Nyquist, or complex plane plots, may be used to indicate the presence of diffusion process occurring in the coating system (Hukovic, Tkalcec, Kwokal, & Piliac 2003).

In order to perform a quantitative analysis of EIS data obtained from plots aforementioned, it is necessary to use an appropriate equivalent electrical circuit (EEC) that describes accurately the physical properties of the system under investigation. EEC given in Figure 6.63 designed for both uncoated and coated samples in order to explain electrochemical processes in the physiological saline solution.

Elements of EEC model for all EIS tests are composed of solution resistance (R_{sol}), pore resistance (R_{po}), coating resistance (R_c), double layer capacitance which is a constant phase element (CPE_{dl}), and coating capacitance which is also a constant phase element (CPE_c) components.

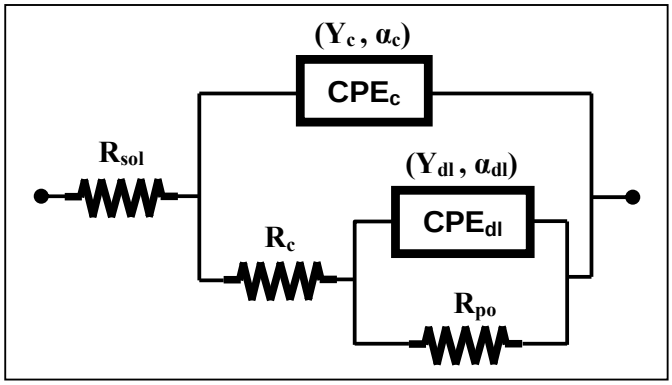

Figure 6.63 Equivalent electrical circuit (EEC) model of the corrosion system for the uncoated 316L SS and HAP coated specimens.

R_{sol} is the resistance of the electrolyte between the working electrode and reference electrode. R_{po} shows total resistance against corrosion process occurred within the pores for the coating and oxide layer on the uncoated 316L sample. Pore resistance involves the sum of R_{ct} (charge transfer resistance), R_d (diffuse layer resistance) and $R_{species}$ (resistance of corrosion species). $R_{species}$ is formed because of the corrosion process that could occur within the pores and the corrosion species (dissolved oxygen, chloride ions) must diffuse along these pores to interact with metal surface (Tüken, Yazıcı, & Erbil, 2006). Consequently, pore resistance involves the sum of R_{ct}, R_d and $R_{species}$.

The interface between the solution and the metal is modelled as a constant phase element (CPE_{dl}) which represents double layer capacitance in parallel with pore resistance. CPE_{dl} is the electrical impedance element that maintains a constant impedance angle as a function of frequency. Namely, the ratio of the real to the imaginary impedance is constant with frequency. Constant phase elements (CPEs) account for deviation from ideal dielectric behaviour related to surface

inhomogenity. Since CPEs which define inhomogeneity of the surface and charge distribution are useful for describing the impedance formed at the interface between a metal electrode and an electrolyte the capacitance is replaced with a CPE for a better fit quality (Ahn, Choi, Kim, & Han, 2002). This was also normalized since it is electrode area dependent. This impedance is commonly expressed as $Z_c(\varpi) = Y^{-1}(j\varpi)^{-\alpha}$, where Y is constant with dimension of F, ω is angular frequency, and α is a real, positive number between 0.5 and 1. Constant phase element CPE_c represent passive oxide film formed on the surface of the uncoated 316L SS during corrosion process. On the other hand, for the HAP coated samples CPE_c simulate capacitance the combination of the HAP coating and oxide layer which was formed during the heat treatment. R_c is the coating resistance and behaves as a protective barrier between corrosion media and HAP coated substrate. For uncoated 316L sample R_c represents the oxide resistance.

Parameters obtained from curve fitting using EEC are given in Table 6.6. Last lines of the tables give χ^2 parameters which are the sensitivity of each component. The sensitivity is checked by the percent error. The percent error of a component is the percentage change of the impedance with a small change in the component value. The smaller the value of χ^2, the better is the fitness of the curve. Very low χ^2 values point to a very good correlation between the experimental and simulated values, accomplished through the use of CPEs in the fitting procedure.

Phenomenon originating on the surface of the coated and uncoated specimens along with the immersion time can be explained using Bode plots given in Figure 6.64-6.66 and EEC parameters from the Table 6.6. The Bode plot shows a straight line of 45° with high impedance at low frequency and a phase angle of –90° throughout the entire frequency range, characteristic of a pure capacitor. This behavior leads to a diffusion controlled process. Upon initial exposure to an electrolyte, a high performance coating with excellent barrier properties must act as an almost-perfect capacitor.

At this stage, R_{po} was extremely high for uncoated 316L SS because of the initiation of new passive oxide film. This is not true for the coated samples of PH1-GM3, and PH1-PM3 at the beginning of the immersion since open pores provided free path ways for the solution. As the electrolyte penetrates the coating in the course of time, an ever-increasing area of the metal substrate is contacted and corrosion is initiated (Loveday, Peterson, & Rodgers, 2004). The HAP coatings present an open structure with interconnected pores that permits the access of the electrolyte into the coating. At the end of the 20 days immersion time, R_{po} of the coated specimens were commenced to increase slightly because of plugging initiation of the pores while 316L SS showed lower values due to activations of Cl^- ions on the oxide film. The impedance from the Bode plot decreases when the coating absorbs solution, but maintains a linear relationship with frequency. The slope does not change and the phase angle remains at –90°. The shape of the Nyquist plot did not change in the low frequency region and remained uninteresting until it began to see resistive elements develop in the coating. The pore resistance and double layer capacitance are area dependent. As the exposed area increases, the observed R_{po} decreases and the observed CPE_{dl} increases for 316L SS. The magnitude of the total impedance at low frequency in the Bode plot continues to drop. The effects of pore resistance and the double layer capacitance are now impacting the Bode plot. Plugging of the pores by the corrosion products from the surface of the metal caused the pore resistance to increase thus leading to general corrosion resistance to increase for PH1-GM3, and PH1-PM3. In addition, since 316L SS in 0.9% NaCl solution is typically in the passive region of the measuring potentials, a very thin and stable oxide film formed at the pores eliminates localized corrosion. This inert film protects the coated 316L SS from degradation at the pores and generating a capacitive response (Liu, Bi, Leyland, & Matthews, 2003). With the development of the lower pore resistance, which is due to the deteriorate effects of the Cl^- ions all over the open oxide film, the Nyquist plot exhibited the characteristic semi-circle of a Randles-like cell for uncoated 316L SS.

Table 6.6 Impedance parameters derived from the EEC to simulate the corrosion behavior

			Exposure Time						
Params.		**Units**	**90 min**	**1 day**	**7 days**	**14 days**	**21 days**	**28 days**	**49 days**
316L SS	$\mathbf{R_{sol}}$	Ωcm^2	44.69	25.95	24.83	16.19	28.44	22.79	30.04
	$\mathbf{R_{po}}$	$M\Omega cm^2$	1.715	0.949	0.276	0.580	0.803	0.100	0.460
	$\mathbf{R_c}$	$k\Omega cm^2$	356	812	155	267	94	94	109
	$\mathbf{Y_c}$	μFcm^{-2}	43.69	41.22	62.72	52.73	54.41	62.05	56.35
	$\boldsymbol{\alpha_c}$	-	0.91	0.91	0.92	0.93	0.93	0.92	0.92
	$\mathbf{Y_{dl}}$	μFcm^{-2}	8.53	1.27	26.91	15.53	5.13	22.99	14.11
	$\boldsymbol{\alpha_{dl}}$	-	1.00	0.85	0.73	1.00	0.56	0.69	0.80
	$\boldsymbol{\chi^2}$	‰	1.89	2.69	2.70	8.17	1.47	1.37	5.82
PH1-PM3	$\mathbf{R_{sol}}$	Ωcm^2	14.22	15.05	14.52	18.37	16.78	16.39	17.34
	$\mathbf{R_{po}}$	$M\Omega cm^2$	0.958	1.151	1.240	1.403	1.383	1.408	1.397
	$\mathbf{R_c}$	$k\Omega cm^2$	44.520	7.162	84.210	0.012	0.013	0.017	0.026
	$\mathbf{Y_c}$	μFcm^{-2}	57.00	59.60	57.90	23.50	23.90	24.60	22.60
	$\boldsymbol{\alpha_c}$	-	0.87	0.90	0.92	1.00	1.00	1.00	1.00
	$\mathbf{Y_{dl}}$	μFcm^{-2}	7.37	7.58	6.55	39.70	38.60	36.00	30.40
	$\boldsymbol{\alpha_{dl}}$	-	0.63	0.72	0.70	0.84	0.83	0.82	0.77
	$\boldsymbol{\chi^2}$	‰	3.12	2.79	3.15	2.07	2.35	2.57	2.71
PH1-GM3	$\mathbf{R_{sol}}$	Ωcm^2	15.73	17.52	18.10	16.74	17.23	16.25	17.09
	$\mathbf{R_{po}}$	$M\Omega cm^2$	1.323	1.347	1.331	1.352	1.574	2.025	1.968
	$\mathbf{R_c}$	$k\Omega cm^2$	897	453	747	456	400	204	189
	$\mathbf{Y_c}$	μFcm^{-2}	50.20	43.20	40.20	44.80	44.93	41.00	41.50
	$\boldsymbol{\alpha_c}$	-	0.92	0.92	0.92	0.92	0.92	0.92	0.92
	$\mathbf{Y_{dl}}$	μFcm^{-2}	8.93	1.29	6.75	5.75	4.99	3.80	4.35
	$\boldsymbol{\alpha_{dl}}$	-	1.00	0.96	0.97	0.78	0.81	0.81	0.81
	$\boldsymbol{\chi^2}$	‰	3.39	2.05	1.78	2.29	2.12	2.48	2.14

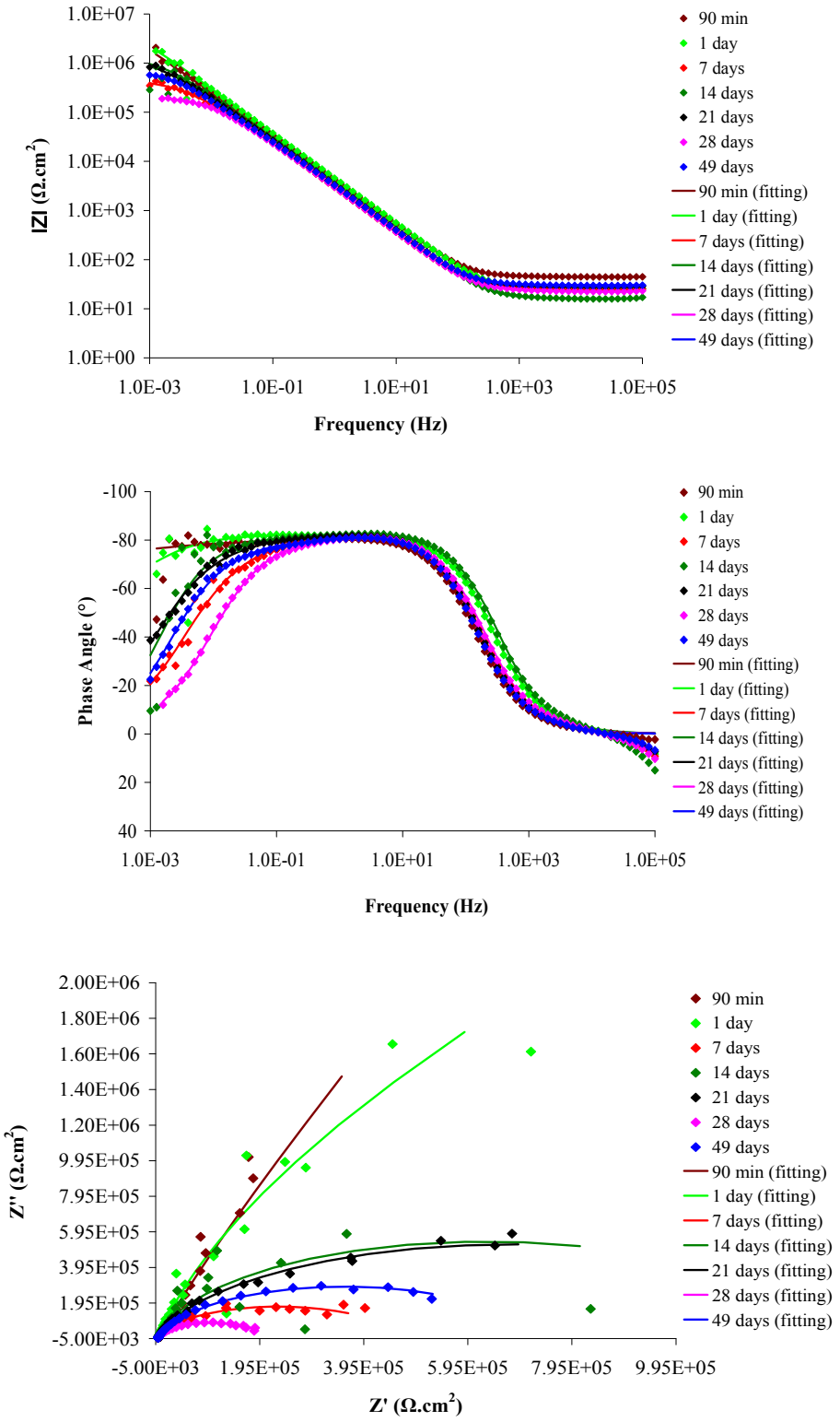

Figure 6.64 Bode and Nyquist plots of the uncoated 316L SS.

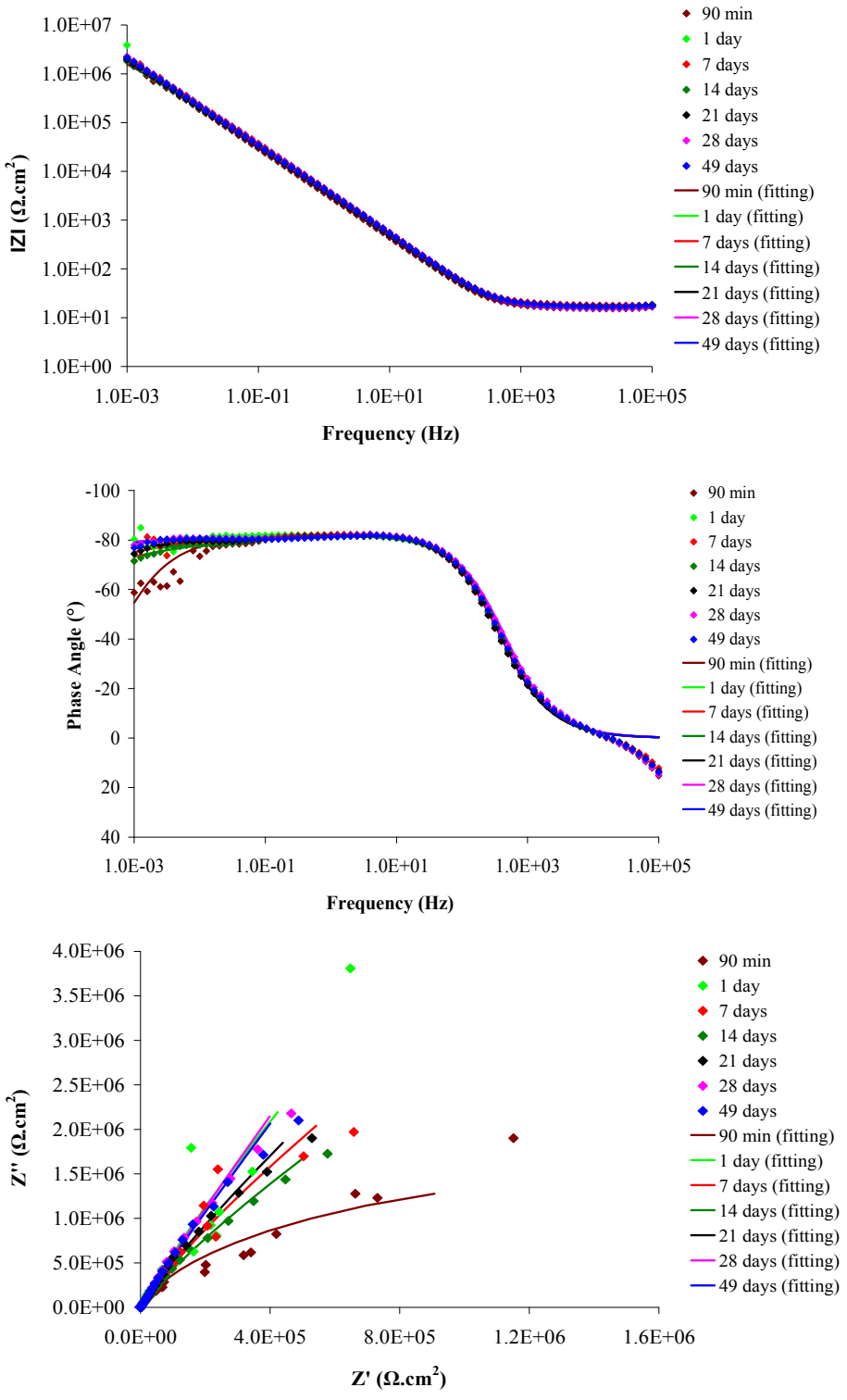

Figure 6.65 Bode and Nyquist plots of the HAP coated sample, PH1-GM3.

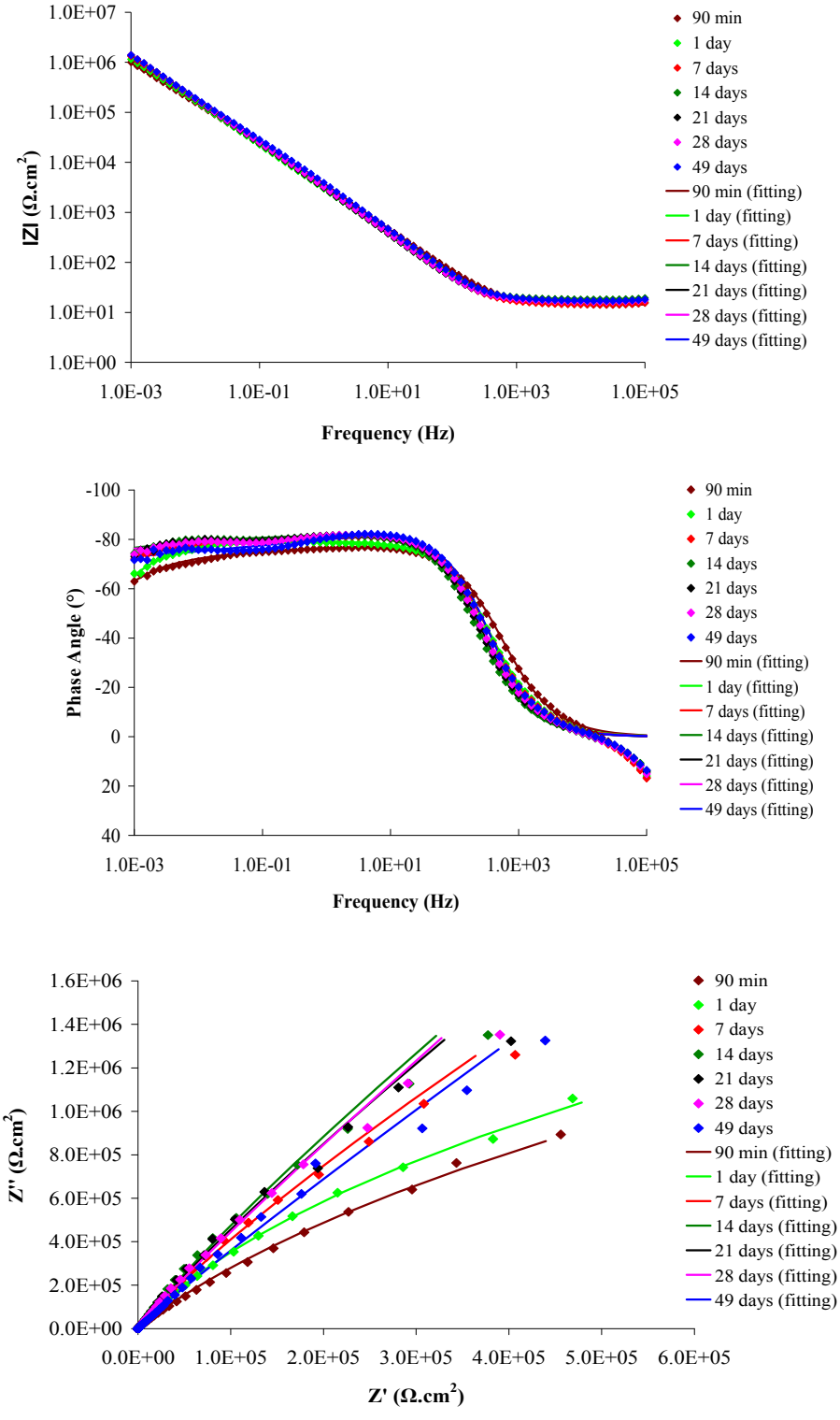

Figure 6.66 Bode and Nyquist plots of the HAP coated sample, PH1-PM3.

Figure 6.67 shows total impedance variations of the specimens for 49 days period. It can be clearly observed that PH1-GM3 has the greatest impedance against general corrosion while 316L SS shows lowest value amongst them. This can be attributed to the behaviour of the HAP coating as a barrier film.

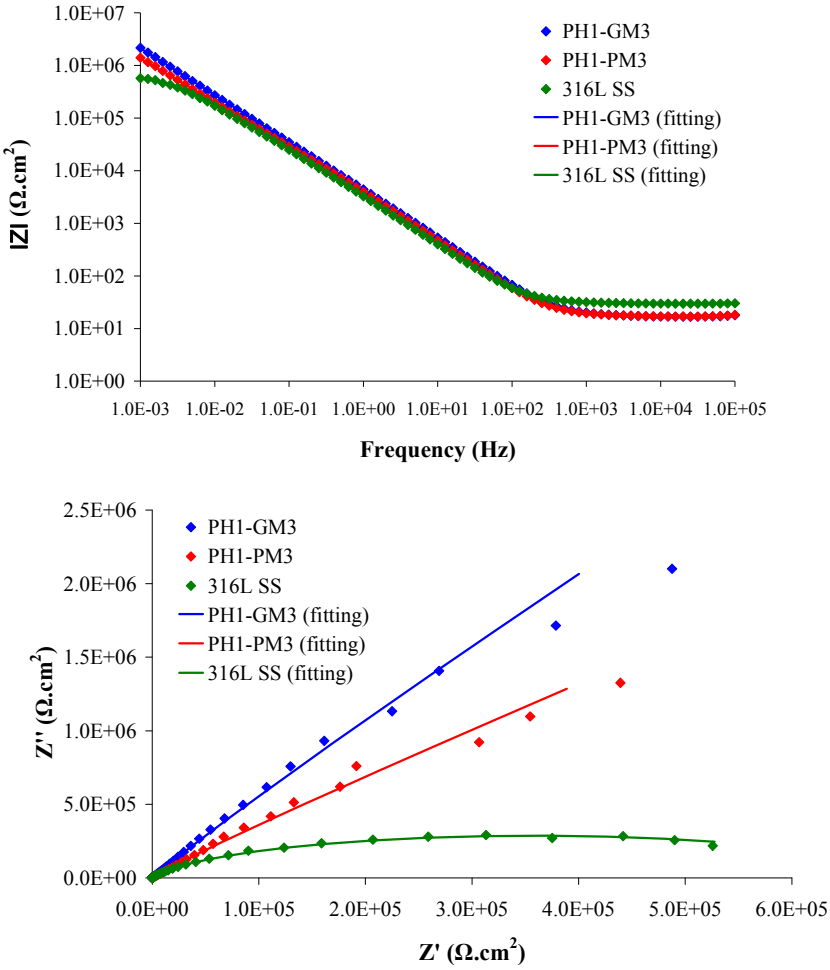

Figure 6.67 Bode and Nyquist plots of HAP coated and uncoated samples obtained at the end of the 49 days.

Figure 6.68 gives variation of pore resistance of the coatings PH1-GM3, PH1-PM3 and uncoated 316L SS for 49 days period. It is clear that after 20 days PH1-GM3 shows a great increase in R_{po}, which may be concluded because of the low porous structure of this coating. It is assigned that all pores plugged completely by the corrosion products, blocking penetration of the electrolyte toward to the

substrate. This is also expected for the coating PH1-PM3, but plugging of the all pores requires more time due to much porous structure of this coatings.

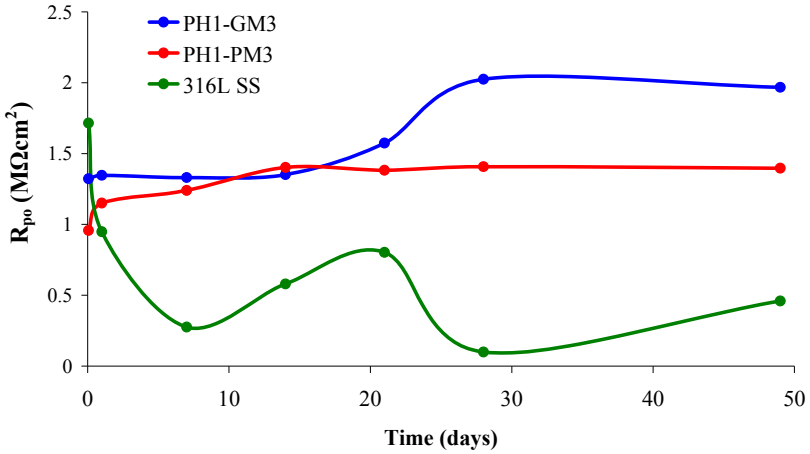

Figure 6.68 Pore resistance variations of PH1-GM3, PH1-PM3, and uncoated 316L SS in time.

At the first measurement, both of the HAP coated specimens show relatively lower pore resistance than uncoated 316L SS. Great decrease in R_{po} for uncoated 316L SS can be explained by the activity of Cl^- ions on the passive oxide layer. Pore resistance of the PH1-PM3 specimens does not change so much. The high values of pore resistance 1.97 MΩcm^2 and 1.40 MΩcm^2 of the PH1-GM3 and PH1-PM3 for 49 days immersion period point to their insulating protection properties compared to 0.46 MΩcm^2 value of uncoated steel, and high corrosion stability of the HAP coated 316L SS in physiological solution.

CHAPTER SEVEN

CONCLUSIONS

In this work, productions of hydroxyapatite coatings on 316L stainless steel substrate were performed by sol-gel technique. Aiming to improve coating properties, some pre-modifications with different techniques were applied to the surface of the 316L SS substrate prior to coating. Additionally, effect of the sol-gel process parameters such as aging time, pH effect, and introducing some chemical additives into the sol solution was investigated on morphological and structural properties of the synthesized coatings.

Findings achieved from the experimental works can be summarized as follows.

1. Production of an intermediate phase of brushite crystals on the surface of 316L SS, named as a process of CaP seeding, by means of galvanostatic and pulse electrodeposition improved film forming ability of the surface. Dimension and density of the CaP crystals seeded on the surface were found to increase with increasing current and time of polarization for both of the methods.

2. It was found that application of alkali treatment to the substrate and subsequent heat treatment of alkali treated substrate at 500°C resulted in formation of sodium chromium oxide which acted as a bond layer to bridge up metallic substrate and synthesized HAP coating. Heat treatment of the alkali treated substrates at 600 and 700°C caused the formation of iron oxide and iron chromium oxide which were caused the scale off the produced coating.

3. Execution of the acid treatment on 316L stainless steel did not show any positive effect on improving coatability property of the substrate.

4. Among the aging time from 0 to 48h, 24h aging of sol solution produced coatings with improved morphology in terms of integrity and porous structure. However, it contained cracks which can be associated with increasing crystallinity.

5. All coatings were ascertained to constitute of hydroxyapatite (HAP) and calcium pyrophosphate ($Ca_2P_2O_7$) phases. Coating quality and crystallinity of the formed structure were found to change with the aging time. Existence of the carbonate in the coatings was thought to have arisen from carbon dioxide from the air during synthesis of the coatings.

6. Coatings with the porous, crack free and dense structure were successfully synthesized by the solution aged for 24h on the substrate pre-modified with the galvanostatic method.

7. In consequence of increasing the sol solution pH range from 0.7 to 2.25 (PH1) and 8.60 (PH2) coatings that were produced are composed of pure HAP phase. Coating produced with PH1 sol solution fulfilled the requirement of porous and crack free properties of HAP coating in morphological point of view.

8. Coating produced on the surface modified by cathodic pulse-current method using solution PH1 was found to be composed of HAP and $Ca_2P_2O_7$ phases. This structural change in coating was thought to have been induced by presence of brushite on the pulse modified surface that somewhat promoted the secondary phase of $Ca_2P_2O_7$. Thus coatings synthesized on the unmodified substrate by using this sol solution were composed of only hydroxyapatite phase. Same results were also found for coatings synthesized on pulse modified surfaces by using solution PH2.

9. HAP coating was successfully synthesized as porous and crack free structure by addition of silica to the solution. However, the surface structure of the produced coating was porous, but has more cracks by addition of PVA to the sol solution.

10. Heating regime as one of the production parameters of sol-gel technique was also investigated. Reduced rate of the heating regime resulted in decreasing porosity of the coating morphology and made the structure smoother.

11. Porous structure of the coatings that was investigated by SEM analyses was also confirmed by electrochemical technique. Pore percentages of the coatings were found as 2.63 and 11.07 for the coatings of PH1-GM3 and PH1-PM3, respectively. Results showed that the presence of the pores increased the surface area of the coating exposed to the electrolytic attack which was verified by decrease in breakdown potential from 280 mV to 253 mV with increasing porosity. Besides, fluctuation especially observed in the polarization was attributed to the sequential effect of pore-plugging by corrosion products and reactivation process taking place at same or different places. Corrosion study of the coatings by the anodic polarization and Tafel methods showed that PH1-PM3 coating exhibiting more porous morphology displayed lower protection compared to PH1-GM3 with lower porosity. However, both of the coatings revealed more protective properties than uncoated 316L stainless steel in the physiological saline solution when breakdown potentials are take into consideration.

12. Corrosion behavior of the coatings observed by EIS study was, compatible with results of anodic polarization. The high values of pore resistance 1.97 $M\Omega cm^2$ and 1.40 $M\Omega cm^2$ found for the PH1-GM3 and PH1-PM3 coatings for 49 days immersion period indicated their insulating protection properties when compared to 0.46 $M\Omega cm^2$ value of the uncoated substrate. This was attributed to high corrosion stability of the HAP coated 316L SS in the physiological solution.

REFERENCES

Abe, Y., Kokubo, T., & Yamamuro, T. (1990). Apatite coating on ceramics, metals and polymers utilizing a biological process. *Journal of Materials Science: Materials in Medicine, 1*, 233-238.

Ahn, S. H., Choi, Y. S., Kim, J.G., & Han, J. G. (2002). A study on corrosion resistance characteristics of PVD Cr-N coated steels by electrochemical method. *Surface and Coatings, 150*, 319-326.

Ahn, S. H., Lee, J. H., Kim, H. G., & Kim, J. G. (2004). A study on the quantitative determination of through-coating porosity in PVD grown coatings. *Applied Surface Science, 233,* 105-114.

Albee, F. H., & Morrison, H. F. (1920). Studies in bone growth: Triple calcium phosphate as astimulus to osteogenesis. *Annals of Surgery, 71*, 32-36.

Almeida, R. M., & Marques, A. C. (2004). Characterization of sol-gel materials by infrared spectroscopy. In R. M. Almeida, (Ed.). *Handbook of Sol-gel science and technology: processing characterization and applications, Volume II: characterization and properties of sol-gel materials and products.* (65-90). USA: Kluwer academic Publishers, Springer.

Amirudin, A., & Thierry, D. (1995). Application of electrochemical impedance spectroscopy to study the degradation of polymer-coated metals**.** *Progress in Organic Coatings*, *26*, 1-28.

Anderson, C., Cape, R. D. T., Crilly, R. G., Hodsman, A.B., & Wokfe, B. M. J. (1984). Preliminary observations of a form of coherence therapy for osteoporosis. *Calcified Tissue International*, *36*, 341-343.

Arcos, D., Rodriguez-Carvajal, J., & Vallet-Regi, M. (2004). The effect of the silicon incorporation on the hydroxylapatite structure. A neutron diffraction study. *Solid State Science*, *6*, 987-94.

Asomoza, M., Dominguez, M. P., Solis, S., Lara, V. H., Bosch, P., & Lopez, T. (1998). Hydrolysis catalyst effect on sol–gel silica structure, *Materials Letters*, *36*, 249-53.

Balamurugan, A., Balossier, G., Kannan, S., & Rajeswari, S. (2006). Elaboration of sol-gel derived apatite films on surgical grade stainless steel for biomedical applications. *Materials Letters, 60*, 2288-2293.

Balamurugan, A., Kannan, S., & Rajeswari, S. (2004). Electrochemical evaluation of sol-gel hydroxyapatite coatings on type 316L stainless steel - in vitro study. *Canadian Metallurgical Quarterly, 43* (3), 293-296.

Bard, A. J., & Faulkner, L. R. (Eds.). (2001). Electrochemical Methods fundamentals and applications (2nd ed.). USA: John Wiley & Sons.

Bard, A.J., & Faulkner, L.R. (Eds.). (1980). *Electrochemical methods*. USA: John Wiley & Sons.

Barrere, F., Layrolle, P., Van Blitterswijk, C. A., & Groot, K. (1999). Physical and chemical characteristic of plasma sprayed and biomimetic apatite coating. *Bioceramics*, *12*, 125-128.

Bates, J. B. (1973). Cathodic protection to prevent crevice corrosion of stainless steel in halide media. *Corrosion, 29*, 28-32.

Beganskiene, A., Bogdanoviciene, I., & Kareiva, A. (2006). Calcium acetylacetonate - a novel calcium precursor for sol-gel preparation of $Ca_{10}(PO_4)_6(OH)_2$. *Chemija, 17,* 16-20.

Beganskiene, A., Dudko, O., Sirutkaitis, R., & Giraitis, R. (2003). Water based sol-gel synthesis of hydroxyapatite. *Materials Science*, *9* (4), 383-86.

Ben-Nissan, B. (2005). Biomimetics And Bioceramics. In Reis, R. L., & Weiner, S. (Eds.), *NATO Science series 171: Learning from nature how to design new implantable biomaterials: From biomineralization fundamentals to biomimetic materials and processing* (89-166). New York: Kluwer Academic Publishers.

Ben-Nissan, B., Green, D., Kannangara, G., Chai, C., & Milev, A. (2001). P NMR studies of eiethyl phosphite derived nanocrystalline hydroxyapatite. *Journal of Sol-Gel Science and Technology*, *21*, 27-37.

Bierwagen, G., Tallman, D., Li, J., He, L., & Jeffcoate, C. (2003). EIS studies of coated metals in accelerated exposure, *Progress in Organic Coatings, 46,* 148-157.

Black, J. (1992). *Biological Performance of materials: Fundamentals of Biocompatibility* (2nd ed.). New York: Marcel Decker Inc.

Blum, Y. D., Platz, R. M., & Crawford, E. J. (1990). Glass strengthening by polymer-derived ceramic coatings. *Journal of American Ceramic Society, 73,* 170-172.

Bonora, P. L., Deflorian, F., & Fedrizzi, L. (1996). Electrochemical impedance spectroscopy as a tool for investigating underpaint corrosion. *Electrochimica Acta, 41*, 1073-1082.

Bonucci, E. (2000). Basic Composition and Structure of Bone. In Yuehuei, H. A., & Robert, A. D. (Eds.), *Mechanical testing of bone and the bone–implant interface* (3-17). New York: CRC Press.

Bordiji, K., Jouzeau, J., Mainard, D., Payan, E., Delagoutte, J., & Netter, P. (1996). Evaluation of the effect of three surface treatments on the biocompatibility of 316L stainless steel using human differentiated cells. *Biomaterials, 17*, 491-500.

Brinker J. & Scherer G. (1985). Sol → gel → glass: I. Gelation and gel structure, *Journal of Non-Crystalline Solids*, *70*, 301-322.

Brinker, J. & Scherer, G. (1990). *Sol-gel science: the physics and chemistry of sol-gel processing*. San Diego, CA: Academic Press.

Brown, W. E., & Chow, L. C. (1986). A new calcium phosphate water-setting cement In P.W. Brown, (Ed.), *Cements Research Progress (*352–379). Westerville, OH: American Ceramic Society.

Bundy, K. J. (1994). Corrosion and other electrochemical aspects of biomaterials. *Critical Reviews in Biomedical Engineering, 22,* 139-251.

Butts, D. I., LaCourse, W.C., & Kim, S. (1988). Influence of sol and substrate chemistry on the formation of sol-gel derived coatings, *Journal of Non-Crystalline Solids*, *100,*514-518.

Cameron, S., Chai, Gross, K. A., & Ben-Nissan, B. (1998). Critical ageing of hydroxyapatite sol-gel solutions. *Biomaterials, 19*, 2291-2296.

Campbell, A. A. (2003). Bioceramics for implant coatings. *Materials Today, 6* (11), 26-30.

Carter, C. B., & Norton, M. G. (2007). *Ceramic materials science and engineering*. New York: Springer.

Castner, D. G., & Ratner, B. D. (2002). Biomedical surface science: foundations to frontiers. *Surface Science*, *500*, 28-60.

Chang, J., Chen, C., Huang, K., & Wang, G. (2006). Eight-year results of hydroxyapatite-coated hip arthroplasty. *The journal of Arthroplasty, 21* (4), 541-546.

Cheng, K., Gaorong, H., Wenjian, W., & Haibo, Q. (2003). Sol-gel derived fluoridated hydroxyapatite films. *Materials Research Bulletin*, *38*, 89-97.

Chung, Y. S., Kang, S., Kwon, O. W., Shin, D. S., Lee, S. G., Shin, E. J., Min, B. G., Bae, H. J., Han, S. S., Jeon, H. Y., Noh, S. K., & Lyoo, W. S. (2007). Preparation of hydroxyapatite/poly(vinyl alcohol) composite fibers by wet spinning and their characterization. *Journal of Applied Polymer Science, 106,* 3423-3429.

Daculsi, G. (1998). Biphasic calcium phosphate concept applied to artificial bone, implant coating and injectable bone substitute. *Biomaterials*, *19*, 1473-1478.

Davis, J. R. (2001). *Surface engineering of stainless steel.* In Cotell, C. M., Sprague, J. A., & Smidt, F. A., (Eds.). *ASM Handbook vol 5: Surface engineering* (10th ed.) (1980-2032). USA: ASM International.

Deflorian, F., Fedrizzi, L., & Bonora, P. L. (1993). Impedance study of the corrosion protection properties of fluoropolymer coatings. *Progress in Organic Coatings, 23* (1), 73-88.

Ding, S. J., Ju, C. P., & Lin, J. H. C. (1999). Characterization of hydroxyapatite and titanium coatings sputtered on Ti-6Al-4V substrate. *Journal of Biomedical Materials Research, 44*, *3*, 266-279.

Dini, J. W. (1993). Electrodeposition: *The materials science of coatings and substrates* (2nd ed.). USA: Noyes Publications.

Disegi, J. A. & Eschbach, L. (2000). Stainless steel in bone surgery. *Injury, 31,* 2-6.

Dislich, H. (1988). Thin films from the sol-gel process. In L. C. Klein, (Ed.). *Sol-gel technology for thin films, fibres, preforms, electronics and specialty shapes*. (50-79). USA: Noyes Publishers.

Dowson, D. (1992). Friction and wear of medical implants and prosthetic devices. In Blau, P., J. (Ed.). *ASM handbook v18: Friction, lubrication, and wear technology* (1342-1360). Ohio: ASM International.

Ducheyne, P., Hench, L. L, Kogan, A., Martens, M., Bursens, A., & Mulier, J. C. (1980). Effect of hydroxyapatite impregnation on sketal bonding of porous coated implants. *Journal of Biomedical Materials Research*, *14*, 225-237.

Ducheyne, P., Radin, S., & King, L. (1993). The effect of calcium phosphate ceramic composition and structure on in vitro behaviour. I. Dissolution. *Journal of Biomedical Materials Research*, *27*, 25-34.

Fabes, B. D., Zelinski, B. J. J. & Uhlmann, D. R. (1993). Sol-Gel Derived Ceramic Coating. In J. B. Wachtman, & R. A. Haber. (Eds.). *Ceramic films and coatings*. (224-283). USA: Noyes Publications.

Feenstra L., & Groot K. (Eds.). (1983). *Bioceramics of calcium phosphate: Medical use of calcium phosphate ceramics*. Florida: CRC Press.

Feng, Q. L., Wang, H., Cui, F. Z., & Kim, T.N. (1999). Controlled crystal growth of calcium phosphate on titanium surface by NaOH-treatment. *Journal of Crystal Growth, 200*, 550-557.

Fontana, M. G., & Greene, N. D. (Eds.). (1987). *Corrosion Engineering*. England: McGraw Hill International.

Furlong, R. J., & Osborn, J. F. (1991). Fixation of hip prostheses by hydroxyapatite ceramic coatings. *Jornal of Bone and Joint Surgery, 73*, 741-745.

Electrochemical Instrumentation and Potentiostats, November 11 2008, Gamry Instruments, Basics of EIS (n.d.). Retrieved July 20, 2008, from http://www.gamry.com/App_Notes/EIS_Primer/EIS_Primer_2007.pdf.

Gash, A. E., Tillotson, T. M., Satcher, J. H., Hrubesh, L. W., Simpson, R. L. (2001). New sol-gel synthetic route to transition and main-group metal oxide aerogels using inorganic salt precursors. *Journal of Non-Crystalline Solids*, *285*, 22-28.

Gee, A., & Deitz, V. R. (1955). Pyrophosphate formation upon ignition of precipitated basic calcium phosphates. *Journal of American Ceramic Society*, *77*, 2961-2965.

Geesink, R. G. T. (1990). Hydroxyapatite-coated to total hip prostheses. *Clinical Orthopedics and Related Research, 261*, 39-58.

Geesink, R. G. T. (2002). Osteoconductive coating for total joint arthroplasty. *Clinical Orthopedics and Related Research, 395,* 53-65.

Geesink, R. G. T., & Hoefnagels, H. M. (1995). Six-year results of hydroxyapatite-coated total hip replacement. *Journal of Bone and Joint Surgery,77,* 534-547.

Ghaemi, M., & Binder, L. (2002). Effects of direct and pulse current on electrodeposition of manganese dioxide, *Journal of Power Sources, 11,* 248-254.

Ghosh, S. K., Limaye, P. K., Swain, B. P., Soni, N. L., Agrawal, R. G., Dusane, R.O. (2007). Tribological behaviour and residual stress of electrodeposited Ni/Cu multilayer films on stainless steel substrate. *Surface and Coatings Technology*, *201*, 4609–4618.

Gibson, I. R., Best, S. M., & Bonfield, W. (1999). Chemical characterization of silicon-substituted hydroxyapatite. *Journal of Biomedical Materials Research*, *44*, 422-428.

Gimenez, I. F., Mazali, I. O., & Alves, O. L. (2001). Application of raman spectroscopy to the study of the phase composition of phosphate based glass-ceramics. *Journal of Physics and Chemistry of Solids*, *62*, 1251-1255.

Goyenvalle, E., Aguado, E., Nguyen, J., Passuti, N., Guehennec, L., & Layrolle, P. (2006) Osteointegration of femoral stem prostheses with a bilayered calcium phosphate coating. *Biomaterials, 27*, 1119-1128.

Grosgogeat, B., Reclaru, L., Lissac, M., & Dalard, F. (1999). Measurement and evaluation of galvanic corrosion between titanium/Ti6Al4V implants and dental alloys by electrochemical techniques and auger spectrometry, *Biomaterials, 20*, 933-941.

Gross, K. A., Chai, C. S., Kannangara, G. K., & Ben-Nissan, B. (1998). Thin hydroxyapatite coatings via sol-gel synthesis. *Journal of Materials Science: Materials in Medicine, 9*, 839 - 843.

Gross, K., & Berndt, C. C. (1998). Thermal processing of hydroxyapatite for coating production. *Journal of Biomedical Materials Research*, *39*, 580-587.

Habibovic, P., Barre`re, F., Blitterswijk, C. A., Groot, K., & Layrolle, P. (2002). Biomimetic Hydroxyapatite Coating on Metal Implants. *Journal of American Ceramic Society*, *85* (3), 517-22.

Hallab, N. J., Jacobs, J. J., & Black, J. (2000). Hypersensitivity to metallic biomaterials: a review of leukocyte migration inhibition assays. *Biomaterials, 21*,1301-1314.

Hanawa, T. (1999). In vivo metallic biomaterials and surface modification. *Materials Science and Engineering, 267*, 260-266.

Helmus, M. N., & Tweden, K. (1995). Materials selection. In Wise, D. L., Trantolo, D. J., Altobelli, D. E., Yaszemski, M. J., Gresser. J. D., & Schwartz, E. R. (Eds.), *Encyclopedic handbook of biomaterials and bioengineering, Part A: Materials* (27-45). NewYork: Marcel Dekker.

Hench L. L. (1991). Bioceramics: From concept to clinic. *Journal of American Ceramic Society, 74,* (7), 1487-1510.

Hench, L. L., (1998). Bioceramics. *Journal of American Ceramic Society, 81* (7), 1705-1728.

Hench, L. L., Interranate, L. V., Caspar, L. A., & Ellis, A. B. (Eds.). (1985). *Inorganic biomaterials. In advances in chemistry series 245: Materials chemistry: An emerging discipline.* Washington DC: American Chemical Society.

Herman, H., Berndt, C. C., & Wang, H. (1993). Plasma sprayed ceramic coatings. In J. B. Wachtman, & R. A. Haber. (Eds.). *Ceramic films and coatings*. (131-189). USA: Noyes Publications.

Hijon, N., Cabanas, M. V., Izquierdo-Barba, I., & Vallet-Regi, M. (2004). Bioactive carbonate-hydroxyapatite coatings deposited onto Ti6Al4V substrate. *Chemistry Materials*, *16,* 1451-1455.

Hijon, N., Cabanas, M. V., Pena, J., & Vallet-Regi, M. (2006). Dip coated silicon-substituted hydroxyapatite films. *Acta-Biomaterialia*, *2*, 567-574.

Hill, J. O. (1991). For better thermal analysis and calorimetry (3rd ed.). Canada: International Confederation for Thermal Analysis.

Holleck, H. (1986). Material selection for hard coatings. *The Journal of Vacuum Science and Technology, A4* (6), 2661-2669.

Hu, J., Zhano, Z. J., & Li, L. X. (1993). Corrosion fatigue resistance of surgical implant stainless steels and titanium alloys. *Corrosion Science, 35*, 587-97.

Hukovic, M., M., Tkalcec, E., Kwokal, A., & Piliac. J. (2003). An in vitro study of Ti and Ti-alloys coated with sol-gel derived hydroxyapatite coatings. *Surface and Coatings Technology, 165,* 40-50.

Hulbert, S. F., & Klawitter, J. J. (1972). Application of porous ceramics for attachment of load bearing internal orthopedic applications. *Journal of Biomeical Materials Research*, *2*, 161-229.

Iler, R. K. (1979). *The Chemistry of silica: solubility, polymerization, colloid and surface properties and biochemistry of silica the chemistry of silica* (43-95). New York: Wiley-Interscience.

Jarcho, M. (1981). Calcium phosphate ceramics as hard tissue prosthetics. *Clinical Orthopedics and Related Research, 157*, 259-278.

Jehn, H. A., & Zielonka, A. (2001). Corrosion testing of coatings. In C. M. Cotell, J. A. Sprague, & F. A. Smidt, (Eds.). *ASM Handbook vol 5: Surface Enginnering* (10th ed.) (1740-1753). USA: ASM International.

Kamachi M., U., Sridhar, T. M., & Raj, B. (2003). Corrosion of bio implants. *Sadhana, 28*, 601-637.

Kamachi Mudali, U., Dayal, R. K., Gnanamoorthy, J. B., & Rodriguez, P. (1996) Pitting corrosion studies on nitrogen-bearing types 304, 316 and 317 stainless steels. *Materials Transactions, Japan Institute of Metals, 37*, 1568-1573.

Kannan S., Balamurugan, A., & Rajeswari, S. (2005). Electrochemical characterization of hydroxyapatite coatings on HNO_3 passivated 316L SS for implant applications. *Electrochimica Acta, 50* (10), 2065-2072.

Kannan, S., Balamurugan, A., & Rajeswari, S. (2002). Development of calcium phosphate coatings on type 316L SS and their in vitro response. *Trends in Biomaterials & Artificial Organs, 16*, 8-11.

Kasuga, T., Nogami, M., & Niiomi, M. (2001). Preparation of bioactive calcium pyrophosphate glass-ceramics. *Journal of Materials Science Letters*, *20*, 1249-1251.

Kelly, R. G., Scully, J. R., Shoesmith, D. W., & Buchheit, R.G. (Eds.). (2002). *Electrochemical Techniques in Corrosion Science and Engineering*. USA: Marcel Dekker**,** Inc**.**

Kesenci, K., Fambri, L., Migliaresi, C., & Piskin, E. (2000). Preparation and properties of Poly(L-Lactide)/Hydroxyapatite Composites. *Journal of Biomaterials Science, Polymer Edition, 11* (6), 617-632.

Kim, H., Kim, H., & Knowles, J. C. (2005). Improvement of hydroxyapatite sol-gel coating on titanium with ammonium hydroxide addition. *Journal of American Ceramic Society*, *88* (1), 154-159.

Kim, S. R., Riu, D. H., Lee, Y. J., & Kim, Y. H. (2002). Synthesis and characterization of silicon substituted hydroxyapatite. *Key Engineering Materials*, *218* (220), 85-88.

Klein, C., Pratka, P., Vander L. B., Wolke, J. G., & DeGroot, K. (1991). Plasma sprayed coatings of tetracalciumphosphate, hydroxylapatite and alpha tricalciumphosphate on titanium alloy: an interface study. *Journal of Biomedical Materials Research, 25* (1), 53-65.

Kodaira, T., Nishio, K., Yamaguchi, I., Suzuki, S., Tsukada, K., & Tsuchiya, T. (2003). Synthesis and properties of highly conductive thin films as buffer layer from sol–gel process. *Journal of Sol–Gel Science Techonology*, *26*, 1049-1053.

Kokubo, T. (1996). Formation of biologically active bone-like apatite on metals and polymers by a biomimetic process. *Thermochimica Acta*, *280/281*, 479-490.

Kokubo, T., Kim, H. M., Miyaji, F., Takadama, H., & Miyazaki, T. (1999). Ceramic-metal and ceramic polymer composites prepared by a biomimetic process. *Composites Part A-Applied Science and Manufacturing, 30*, 405-409.

Koo, J., Kim, S. U., Yoon, D. S., No K., & Bae, B.S. (1997). Effect of heat treatment on formation of sol-gel (Pb,La)TiO_3 films for optical application. *Journal of Materials Research*, *12* (3), 812-818.

Koutsopoulos, S. (2002). Synthesis and characterization of hydroxyapatite crystals: A review study on the analytical methods. *Journal of Biomedical Materials Research*, *62*, 600-612.

Kruger, J. (1979). Fundamental aspects of corrosion of metallic implants. In B. C. Syrett, & A. Acharya (Ed.). *Corrosion and degradation of implant materials, ASTM STP 684* (107-128). ASM International.

Kuhne, J.H., Bartl, R., Frisch, B., Hammer, C., Jannson, V., & Zimmer, M. (1994). Bone formation in coralline hydroxyapatite: Effects of pore size studied in rabbits. *Acta Orthopedica Scandinava, 65* (3), 246-252.

Kumar, M., Dasarathy, H., & Riley C. (1999). Electrodeposition of brushite coatings and their transformation to hydroxyapatite in aqueous solutions. *Journal of Biomedical Materials Research*, *45* (4), 302-310.

Kweh, S. W. K., Khor, K. A., & Cheang, P. (2002). An in vitro investigation of plasma sprayed hydroxyapatite (HA) coatings produced with flame-spheroidized feedstock. *Biomaterials*, *23*, 775–785.

Leea, I. U., Kim, H., & Kim, S. (2000). Studies on calcium phosphate coatings. *Surface and Coatings Technology, 131*, 181-186.

LeGeros R.Z., & Lee, Y.K. (2004). Synthesis of amorphous calcium phosphates for hard tissue repair using conventional melting technique. *Journal of Materials Science, 39*, 5577-5579.

LeGeros, R. Z. (1981). Apatites in biological systems. *Progress in Crystal Growth and Characterization of Materials*, *4*, 1-45.

LeGeros, R. Z. (1990). Chemical and crystallographic events in the caries process. *Journal of Dental Research*, *69* (spec. issue), 567-574.

LeGeros, R. Z., Trautz, O. R., Klein, E., Legeros, J. P. (1969). Two types of carbonate substitution in the apatite structure. *Experientia*, *25*, 5-7.

LeGeros, R.Z. (1988). Calcium phosphate materials. *Advances in Dental Research, 3*, 164-180.

Leite, D. G., Pereira, A. J., Da Silva, L. F., & Dias da Silva, J. H. (2006). Nanocrystalline GaN and GaN:H films grown by RF-magnetron sputtering. *Brazilian Journal of Physics, 36,* 978-981.

Leopold, S. S., Berger, R. A., Patterson, L., Skipor, A. K., Urban, R. M., & Jacobs, J. J. (2000). Serum titanium level for diagnosis of a failed, metal-backed, patellar component, *Journal of Arthroplasty, 15*, 938-943.

Li, P., Kangasniemi, I., Groot, K., & Kokubo, T. (1994). Bonelike hydroxyapatite induction by a gel-derived titania on a titanium substrate. *Journal of American Ceramic Society, 77*, 1307-1312.

Lin, F. H., Hsu, Y. S., Lin S. H., & Sun, J. S. (2002). The effect of Ca/P concentration and temperature of SBF on the growth of HAP coating on 316L SS. *Biomaterials, 23*, 4029-4038.

Liu, C., Bi, Q., Leyland, A., & Mathews, A. (2003). An electrochemical impedance spectroscopy study of corrosion behavior of PVD coated steels in 0.5 N NaCl aqueous solution. *Corrosion Science, 45,* 1243-1256.

Liu, C., Bi, Q., Leyland, A., & Matthews, A. (2003). An electrochemical impedance spectroscopy study of the corrosion behaviour of PVD coated steels in 0.5 N NaCl aqueous solution: Part II. EIS interpretation of corrosion behaviour. *Corrosion Science, 45,* 1257-1273.

Liu, D. M., Troczynski, T., Tseng, W. J. (2001). Water-based sol-gel synthesis of hydroxyapatite: process development. *Biomaterials, 22*, 1721-1730.

Liu, D. M., Yang, Q., Troczynski, T. (2002). Sol-gel hydroxyapatite coatings on stainless steel substrates. *Biomaterials, 23*, 691–698.

Liu, D., Troczynski, T., & Hakimi, D. J. (2002). Effect of hydrolysis on the phase evolution of water-based sol-gel hydroxyapatite and its application to bioactive coatings. *Journal of Materials Science: Materials in Medicine*, *13*, 657-665.

Liu, D., Troczynskia, T., & Tseng, W. J. (2002). Aging effect on the phase evolution of water-based sol-gel hydroxyapatite. *Biomaterials*, *23*, 1227-1236.

Livage, J., Barboux, P., Vandenborre, M. T., Schmutz, C., & Taulelle F. (1992). Sol-gel synthesis of phosphates. *Journal of Non-Crystaline Solids*, *147*, 18-23.

Loveday, D., Peterson, P., & Rodgers, B. (2004). Evaluation of organic coatings with electrochemical impedance spectroscopy Part I: Evaluation of organic coatings with electrochemical impedance spectroscopy. *JCT Coatings Tech,* 46-52. Retrieved August 2004, from http://www.gamry.com/HomePage/JCT%20Article%201.pdf.

Lu, X., Zhao, Z., & Leng, Y. (2005). Calcium phosphate crystal growth under controlled atmosphere in electrochemical deposition. *Journal of Crystal Growth*, *284*, 506-516.

Lventouri, T., Bunaciu, C. E., & Perdikatsis, V. (2003). Neutron powder diffraction studies of silicon-substituted Hydroxyapatite. *Biomaterials, 24*, 4205-4211.

MaNally, S. A., Shepperd, H., Mann, C. V., & Walczak, J. P. (2000). The results at nine to twelve years of the use of a Hydroxyapatite coated femoral stem. *Journal of Bone and Joint Surgery, 82,* 378-382.

Mansfeld, F. (1995). Use of electrochemical impedance spectroscopy for the study of corrosion protection by polymer coatings. *Journal of Applied Electrochemistry*, *25,* 187-202.

Mansfeld, F. (2003). Electrochemical methods of corrosion testing. In S. D. Cramer, & B. S. Covino, (Eds.). *ASM handbook vol 13A: Corrosion: Fundamentals, testing, and protection* (9th ed.) (446-462). USA: ASM International.

Marcott, C. (1998). Infrared Spectroscopy. In R. E. Whan, (Ed.). *ASM Metals Hanbooks: vol 10, materials characterization* (5th ed.) (239-241). USA: ASM International.

Masuda, Y., Matubara, K., & Sakka, S. (1990). Synthesis of hydroxyapatite from metal alkoxides through sol–gel technique. *Journal of the Ceramic Society of Japan*, *98*, 1266-1277.

Matthews A., Broszeit, E., Aromaa, J., Ronkainen, H., Hannula, S. P., Leyland, A., & Matthes, B. (1991). Corrosion performance of some titanium-based hard coatings. *Surface and Coatings Technology, 49*, 489-495.

Merchant, R. E. & Wang, I. (1994). Physical and chemical aspects of biomaterials used in humans. In Greco, R. S. (Ed.). *Implantation biology: The Host Response and Biomedical Devices* (13-38). London: CRC Press.

Metroke, T.L., Gandhi, J.S., Apblett, A. (2004). Corrosion resistance properties of Ormosil coatings on 2024-T3 aluminum alloy. *Progress in Organic Coatings, 50*, 231–246.

Mohammadi, Z., Ziaei-Moayyed, A. A., & Mesgar, S. M. A. (2008). In vitro dissolution of plasma-sprayed hydroxyapatite coatings with different characteristics: experimental study and modeling. *Biomedical Materials, 3*, 1-7.

Mollazadeh, S., Javadpour, J., & Khavandi, A. (2007). In situ synthesis and characterization of nano-size hydroxyapatite in poly(vinyl alcohol) matrix. *Ceramics International, 33* (8), 1579-1583.

Mont, M. A., & Hungerford, D. S. (1997). Proximally coated ingrowth prostheses: a review. *Clinical orthopaedics and Related Research*, *344*, 139-149.

Müller, L., Conforto, E., Caillard, D., & Müler, F. A. (2007). Biomimetic apatite coatings-carbonate substitution and preferred growth orientation. *Biomolecular Engineering*, *24*, 462-466.

Murali, K. R. (2007). Properties of GaAs films deposited by pulse periodic technique. *Journal of Materials Science, 42,* 1321-1324.

Nery, E. B., Lynch K. L., Hirthe W. M., & Mueller K.H. (1975). Bioceramics implants in surgically produced infrabony defecs. *Journal of Periodontol, 46*, 328-339.

Nishino, M., Yamashita, S., Aoba, T., Okazaki, M., & Moriwaki, Y. (1981). The laser-raman spectroscopic studies on human-enamel and precipitated carbonate-containing apatites. *Journal of Dental Research*, *60*, 751-755.

Nishio, K., & Tsuchiya, T. (2004). Sol-gel processing of thin films with metal salts. In Kozuka, H. (Ed.). *Handbook of sol-gel science and technology: processing characterization and application, Volume I. Sol-gel processing* (59-85). USA: Kluwer Academic Publishers, Springer.

Nissan B. B. (2005). Biomimetics and bioceramics. In Reis, R. L., & Weiner, S. (Eds.), *NATO Science series 171: Learning from nature how to design new implantable biomaterials: From biomineralization fundamentals to biomimetic materials and processing* (89-103). New York: Kluwer Academic Publishers.

Okazaki, Y., Rao, S., Ito, Y., & Tateishi, T. (1998). Corrosion resistance, mechanical properties, corrosion fatigue strength and cytocompatibility of new Ti alloys without Al and V. *Biomaterials, 19*, 1197-1215.

Ong, J. L., Lucas, L. C., Lacefield, W. R., & Rigney, E. D. (1992). Structure, solubility and bond strength of thin calcium phosphate coatings produced by ion beam sputter deposition. *Biomaterials*, *13* (4), 249-254.

Orcel, G., Hench, L. L., Artaki, I., Jones, J., & Zerda, T. (1988). Effect of formamide additive on the chemistry of silica sol-gels II. Gel structure. *Journal of Non-Crystalline Solids*, *105*, 223-231.

Ou-Yang, H., Paschalis, E. P., Boskey, A. L., Mendelsohn, R. (2000). Two-dimensional vibrational correlation spectroscopy of in vitro hydroxyapatite maturation. *Biopolymers (Biospectroscopy)*, *57*, 129-139.

Papakyriacou, M., Mayer, H., Pypen, C., Plenk H., & Stanzl-Tschegg, S. (2000). Effects of surface treatments on high cycle corrosion fatigue of metallic implant materials. *International Journal of Fatigue, 22,* 873-886

Papavinasam, S. (2008). Electrochemical polarization techniques for corrosion monitoring. In L. Yang, (Ed.). *Techniques for corrosion monitoring* (49-83). England and USA: Woodhead Publishing Limited and CRC Press LLC.

Park, J. B. (1984). *Biomaterials science and engineering*. New York: Plenum Press.

Park, J.B., & Lakes, R.S. (2007). *Biomaterials: An introduction* (3rd ed.). New York: Springer.

Peltola T., Patsi, M., Rahiala, H., Kangasniemi, I., & Yli-Urpo, A. (1998). Calcium phosphate induction by sol-gel-derived titania coatings on titanium substrates in vitro. *Journal of Biomedical Materials Research*, *41* (3), 504-510.

Penel, G., Leroy, G., Rey, C., Bres, E. (1998). MicroRaman spectral study of the PO_4 and CO_3 vibrational modes in synthetic and biological apatites. *Calcified Tissue International*, *63*, 475-481.

Penel, G., Leroy, N., Van Landuyt, P., Flautre, B., Hardouin, P., Lemaitre, J., et al. (1999). Raman microspectrometry studies of brushite cement: in vivo svolution in a sheep model. *Bone*, *25*, 81-84.

Perez, N. (Ed.). (2004). *Electrochemistry and corrosion science*. Boston: Kluwer Academic Publishers.

Pholer, O. E. M. (2002). Failure of orthopaedic metallic implants. In Becker, W. T., & Shipley, R. J. (Eds.). *ASM handbook v11: Failure analysis and prevention* (2740-2790). Ohio: ASM International.

Pietrzak, W. S. (Ed.). (2008). *Musculoskeletal tissue regeneration biological materials and methods*. Totowa/USA: Humana Press.

Piveteau, L., Gasser, B., & Schlapbach, L. (2000). Evaluating mechanical adhesion of sol-gel titanium dioxide coatings containing calcium phosphate for metal implant application. *Biomaterials, 21*, 2193-2201.

Pleshko, N., Boskey, A., & Mendelsohn, R. (1991). Novel infrared spectroscopic for the determination of crystallinity of hydroxyapatite minerals. *Biophysical Journal*, *60*, 786-793.

Porter, A. E., Patel, N., & Best, S. (2007). Hydroxyapatite. In Bowlin, G. L., & Wnek, G. (Eds.). *Encyclopedia of biomaterials and biomedical engineering* (2nd ed.) (1-13). Florida: Taylor & Francis.

Prassass, M, Phalippou, J., & Zarzycki J. (1986). Sintering of monolithic silica aerogels. In L. L. Hench, & D. R. Ulrich, (Eds.). *Science of ceramic chemical processing* (156-168). New York: Wiley.

Putlyaev, V. I., & Safronova, T. V. (2006). A new generation of calcium phosphate biomaterials: The role of phase and chemical compositions. *Glass and Ceramics: Biomaterials, 63* (3), 30-33,

Rabinovich, E. M. (1988). Particulate silica gels and glasses from the sol-gel process. In L. C. Klein,(Ed.). *Sol-gel technology for thin films, fibers, preforms, electronics and special Shapes* (260-294). USA: Noyes Publications.

Radin, S. R., & Ducheyne, P. (1992). Plasma spraying induced changes of calcium phosphate ceramic characteristics and the effect on in vitro stability. *Journal of Materials Science: Materials in Medicine, 3,* 33-42.

Ramakrisha, S., Mayer, J., Wintermantel, E., & Leong, K. W. (2001). Biomedical applications of polymer-composite materials: a review. *Composites Science and Technology*, *61*, 1189-1224.

Ramanan, S.R. (2001). Dip coated ITO thin-films through sol-gel process using metal salts. *Thin Solid Films*, *389*, 207–212.

Ratner, B. D. (1996). *Biomaterilas science: An introduction to materials in medicine*. San Diego: Academic Press.

Recum, A. F. (1999). *Handbook of biomaterials evaluation: Scientific, technical and clinical testing of implant materials* (2nd ed.). Philadelphia: Taylor & Francis.

Redepenning, J., Schlessinger, T., Burnham, S., Lippiello, L., & Miyano, J. (1998). Characterization of electrolytically prepared brushite and hydroxyapatite coatings on orthopedic alloys. *Journal of Biomedical Materials Research*, *30*, 287-294.

Regi, M. V., & Calbet, J .M. G. (2004). Calcium phosphates as substitution of bone tissues. *Progress in Solid State Chemistry, 32*, 1-31.

Rey, C., Collins, B., Goehl, T., Dickson, R. I., & Glimcher, M. J. (1989). The carbonate environment in bone mineral: A resolution enhanced fourier transform infrared spectroscopy study. *Calcified Tissue International*, *45*, 157-164.

Rigidgels, V., & Scherer, G. W. (1987). Drying gels. *Journal of Non-Crystalline Solids, 92,* 122-144.

Rosa-Fox, N., Pinero, M., & Esquivias, L. (2003). Organic-inorganic hybrid materials from sonogels. In H. S. Nalwa, (Ed.), Handbook of organic-inorganic hybrid materials and nanocomposites (1-92). USA: American Scientific Publishers.

Roy, D.M., & Linnehan, S.K. (1974). Hydroxyapatite formed from coral skeletal carbonate by hydrothermal exchange. *Nature, 247*, 220-222.

Russel, S. W., Luptak, K. A., Suchicital, C. T. A., Alford, T. L. & Pizzicoui, V. B. (1996). Chemical and structural evolution of sol-gel derived hydroxyapatite thin films under rapid thermal processing. *Journal of American Ceramic Society*, *79* (4), 837-842.

Sakka, S. (2005). The outline of applications of the sol-gel method. Sakka, S. (Ed.) *Handbook of sol-gel science and technology: processing characterization and applications, Volume III: Applications of sol-gel technology.* (3-26). USA: Kluwer academic Publishers, Springer.

Sard, R., Leidheiser, H., Jr., & Ogbum, F. (1975). *Properties of Electrodeposits: Their Measurement and Significance*. USA: The Electrochemical Society Incorporation.

Sarkar, P., & Nicholson, S. (1996). Electrophoretic deposition (EPD): mechanisms, kinetics, and applications to ceramics. *Journal of American Ceramic Society, 79*, 1987-2002.

Schlesinger, M., & Paunovic, M. (Eds.). (2000). *Modern electroplating* (4th ed.). New York: Wiley.

Schwartz, M. (1994). Deposition from aqueous solutions: An overview. In R. F. Bunshah, (Ed.), Handbook of deposition technologies for films and coatings: science, technology and applications (2nd ed.) (506-617). USA: Noyes Publications.

Scully, J. R. (1989). Electrochemical impedance of organic-coated steel: correlation of impedance parameters with long-term coating deterioration. *Journal of Electrochemical Society, 136* (4), 979-990.

Sherwin, M. P., Taylor, D. E., & Waterhouse, R. B. (1971). An electrochemical investigation of fretting corrosion in stainless steel, *Corrosion Science, 19*, 419-429.

Shi, D., Jiang, G., & Bauer, J. (2002). The effect of structural characteristics on the in vitro bioactivity of hydroxyapatite. *Journal of Biomedical Materials Research, 63,* 71-78.

Singh, R., & Dahotre, N. B. (2007). Corrosion degradation and prevention by surface modification of biometallic materials. *Journal Materials Sceince: Materials in Medicine,* 18, 725-751.

Sinha, A., Das, G., Sharma, B. K., Roy, R. P., Pramanick, A. K., & Nayar, S. (2007). Poly(vinyl alcohol)–hydroxyapatite biomimetic scaffold for tissue regeneration. *Materials Science and Engineering C, 27,* 70-74.

Sivakumar, M., Kamachi, M. U., & Rajeswari, S. (1994). Investigation of failures in stainless steel orthopaedic implant devices: Fatigue failure due to improper fixation of a compression bone plate. *Journal of Materials Science Letters, 13*, 142-145.

Sivakumar, M., Suresh, K. D. K., Rajeswari, S., & Thulasiraman,V. (1995). Failures in stainless steel orthopaedic implant devices: A survey. *Journal of Materials Science Letters, 14*, 351-354.

Slack, S. M. (1997). Properties of biological fluids. In B. D. Ratner, A. S. Hoffman, F. J. Schoen, & J. E. Lemons, (Eds.). *In An introduction to materials in medicine* (469-471).USA: Academic Press.

Stan, G. E., & Ferreira, J. M. F. (2006). Sol - gel chemical routes for preparing bioactive fluorhydroxyapatite thin films and powders. *Digest Journal of Nanomaterials and Biostructures,1* (2), 37-42.

Stern, M., & Geary, A. L. (1957). Electrochemical polarization. a theoretical analysis of shape of polarization curves. *Journal of the Electrochemical Society, 104*, 56-.63.

Stoch, A., Jastrzebski, W., Brozek, A., Stoch, J., Szaraniec, J., Trybalska, B., et al. (2000). FTIR absorption–reflection study of biomimetic growth of phosphates on titanium implants. *Journal of Molecular Structure*, *555*, 375-382.

Sulzer, atmospheric plasma spray, (n.d). Retrieved August 20, 2008, from http://www.sulzermetco.com/desktopdefault.aspx/tabid-1741//3381_read-5289/

Syrett, B. C., & Wing, S. S. (1978). An electrochemical investigation of fretting corrosion of surgical implant materials. *Corrosion, 11*, 379-386.

Tanahashi, M., Kokubo, T., & Nakamura, T. (1996). Ultrastructural study of an apatite layer formed by a biomimetic process and its bonding to bone. *Biomaterials*, *17*, 47-51.

Tato, W., & Landolt, D. (1998). Electrochemical determination of the porosity of single and duplex PVD coatings of titanium and titanium nitride on brass. *Journal of Electrochemical Society*, *145* (12), 4173-4181.

Thamaraiselvi, T. V., & Rajeswari, S. (2005). Electrochemical behaviour of alkali treated and hydroxyapatite coated 316 LVM. *Trends in Biomaterials and Artificial Organs*, *18* (2), 242-246.

Thian, E. S., Huang, J., Best, S. M., Barber, Z. H., & Bonfield, W. (2006). Silicon-substituted hydroxyapatite thin films: Effect of annealing temperature on coating stability and bioactivity. *Journal of Biomedical Materials Research Part A*, *78* (1), 121-128.

Thomas, I. M. (1988). Multicomponent glasses from the sol-gel process. In L. C. Klein, (Ed.). *Sol-gel Technology for thin films, fibers, preforms, electronics, and specialty shapes* (2-13). USA: Noyes Publications.

Tüken, T., Yazıcı, B., & Erbil, M. (2006). Zinc modified polyailine coating for mild steel protection. *Materials Chemistry and Physics*, *99*, 459-464.

Vallet-Regia, M., & Gonzalez-Calbet, J. M. (2004). Calcium phosphates as substitution of bone tissues. *Progress in Solid State Chemistry, 32,* 1-31.

Vallet-Regia, M., Ramila, A., Padilla, S., & Munoz, B. (2003). Bioactive glasses as accelerators of apatite bioactivity. *Journal of Biomedical Materials, 66,* 580-585.

Van Dijk, K., Schaeken, H. G., Wolke, J. G. C., & Jansen, J. A. (1996). Influence of annealing temperature on RF magnetron sputtered calcium phosphate coatings. *Biomaterials*, *17*, 405-410.

Wainwright, S.A. (1995). What we can learn from soft biomaterials and structures. In M. Sarıkaya,. & I. Aksay. (Eds.) *Biomimetics. Design and processing of materials* (1-12). US: American Institute of Physics.

Wei, M., Ruys, A. J., Milthorpe, B. K., Sorrell, C. C., & Evans, J. H. (2001). Electrophoretic deposition of hydroxyapatite coatings on metal substrates: A nanoparticulate dual-coating approach. *Journal of Sol-Gel Science and Technology, 21*, 39–48.

Weiner, S., & Wagner, H. D. (1998). The material bone: Structure-mechanical function relations. *Annual Review of Materials Science, 28*, 271-298.

Wen, H. B., Wolke, J. G. C., De Wijn, J. R., Cui, F. Z., & Groot, K. (1997). Fast precipitation of calcium phosphate layers on titanium induced by simple chemical treatment. *Biomaterials, 18*, 1471-1478.

Weng, W., Zhang, S., Cheng, K., Piyi D. H., Shen, G., & Yuan, J. (2003). Sol-gel preparation of bioactive apatite films. *Surface and Coatings Technology*, *167*, 292-296.

Williams D. F. (1994). Titanium: epitome of biocompatibility or cause for concern. *The Journal of Bone and Joint Surgery, 76-B,* 348-349.

Williams, D. F. (1981). Electrochemical aspects of corrosion in the physiological environment. In Willams. D. F. (Ed.), *Fundamental aspects of biocompatibility, vol. 1* (11-20). Florida: CRC press.

Willmann, G. (1999). Coating of implants with hydroxyapatite: Material connections between bone and metal. *Advanced Engineering Materials, 1* (2), 95-105.

Wolke, J. G. C., Van der Waerden, J. P., Schaeken, H. G., & Jansen, J. A. (2003). In vivo dissolution behavior of various RF magnetron-sputtered Ca-P coatings on roughened titanium implants. *Biomaterials*, *24*, 2623–2629.

Wong, J. Y., & Bronzino, J. D. (2007). *Biomaterials*. New York: CRC Press.

Yamane, M., Inoue, S., & Nakazawa, K. (1982). Preparation of gels to obtain glasses of high homogeneity by low temperature synthesis. *Journal of Non-Crystalline Solids, 48* (1), 153-159.

Yoldas, B. E. (1984). Modification of polymer-gel structures. *Journal of Non-Crystalline Solids*, *63*, 145-154.

Yoldas, B. E., & Partlow, D. P. (1985). Formation of broad band antireflective coatings on fused silica for high power laser applications. *Thin Solid Films, 129*, 1-14.

You, C., Oh, S., & Kim, S. (2001). Influences of heating condition and substrate-surface roughness on the characteristics of sol-gel-derived hydroxyapatite coatings. *Journal of Sol-Gel Science and Technology, 21,* 49-54.

Yuan, H., & Groot, K. (2005). Calcium phosphate biomaterials: An Overview. In Reis, R. L., & Weiner, S. (Eds.), *NATO Science series 171: Learning from nature how to design new implantable biomaterials: From biomineralization fundamentals to biomimetic materials and processing* (37-57). New York: Kluwer Academic Publishers.

Zhang, X., Gubbels, G.H.M., Terpstra, R.A., & Metselaar, R. (1997). Toughening of calcium hydroxyapatite with silver particles. *Journal of Materials Science, 32*, 235-243.

Zhitomirsky, I. (1998). Cathodic electrosynthesis of titanium and ruthenium oxides. *Materials Letters, 33*, 305-310.

Zhitomirsky, I. (1998). Electrophoretic deposition of chemically bonded ceramics in the system CaO-SiO_2-P_2O_5. *Journal of Materials Science Letters, 17*, 2101-2104.

Zhitomirsky, I. (2000). Ceramic films using cathodic electrodeposition, *JOM-e, Journal of the Minerals, Metals & Materials Society, 52* (1). Retrieved June 25, 2008,from http://www.tms.org/pubs/journals/JOM/0001/Zhitomirsky/Zhitomirsky-0001.html.

Zhitomirsky, I. (2000). New developments in electrolytic deposition of ceramic films. *American Ceramic Society Bulletin, 79* (9), 57-63.

Zhitomirsky, I. (2002). Cathodic electrodeposition of ceramic and organoceramic materials: Fundamental aspects. *Advances in Colloid and Interface Science*, *97*, 279-317.

Zhitomirsky, I., & Gal-Or, L. (1997). Electrophoretic deposition of hydroxyapatite. *Journal of Materials Science: Materials in Medicine*, *8*, 213-219.

Zhitomirsky, I., Gal-Or, L., Kohn, A., & Hennicke, H. W. (1995). Electrodeposition of ceramic films from non-aqueous and mixed solutions. *Journal of Materials Science, 30*, 5307-5312.